A comparison of processing approaches for distributed radar sensing

Pier Francesco Sammartino

Supervisors:
Prof. H.D. Griffiths
Prof. C.J. Baker
Dr. K. Woodbridge

A thesis submitted for the degree of
Doctor of Philosophy
of
University College London

Department of Electronic and Electrical Engineering
University College London
27^{th} May 2009

In everlasting memory of
Candida, Edvige and Luigi.

I, Pier Francesco Sammartino, confirm that the work presented in this thesis is my own and has not been submitted in any form for another degree or diploma at any university or other institute of tertiary education. Information derived from other sources has been indicated in the thesis.

Abstract

Radar networks received increasing attention in recent years as they can outperform single monostatic or bistatic systems. Further attention is being dedicated to these systems as an application of the MIMO concept, well know in communications for increasing the capacity of the channel and improving the overall quality of the connection. However, it is here shown that radar network can take advantage not only from the angular diversity in observing the target, but also from a variety of ways of processing the received signals. The number of devices comprising the network has also been taken into the analysis. Detection and false alarm are evaluated in noise only and clutter from a theoretical and simulated point of view. Particular attention is dedicated to the statistics behind the processing. Experiments have been performed to evaluate practical applications of the proposed processing approaches and to validate assumptions made in the theoretical analysis. In particular, the radar network used for gathering real data is made up of two transmitters and three receivers. More than two transmitters are well known to generate mutual interference and therefore require additional efforts to mitigate the system self-interference. However, this allowed studying aspects of multistatic clutter, such as correlation, which represent a first and novel insight in this topic. Moreover, two approaches for localizing targets have been developed. Whilst the first is a graphic approach, the second is hybrid numerical (partially decentralized, partially centralized) which is clearly shown to improve dramatically the single radar accuracy. Finally the effects of exchanging angular with frequency diversity are shown as well in some particular cases. This led to develop the Frequency MIMO and the Frequency Diverse Array, according to the separation of two consecutive frequencies. The latter is a brand new topic in technical literature, which is attracting the interest of the technical community because of its potential to generate range-dependant patterns. Both the latter systems can be used in radar-designing to improve the agility and the efficiency of the radar.

Acknowledgements

I would like to acknowledge gratefully the help and the support provided by my supervisors Prof. Chris Baker, Prof. Hugh Griffiths and Dr. Karl Woodbridge throughout my time at UCL.

I also hereby express my utmost gratitude to my family and my friends (with special acknowledgements to Mr. Alessio Balleri and Ms. Emanuela Cerrone) for backing me up when I most needed it.

Dr. Anthony Zyweck (DSTO, Australia) and Dr. Paul Herselman (CSIR, South Africa) are here quoted for the interesting and enlightening discussions during their time at UCL.

AFRL and EOARD, in the persons of Dr. Muralidhar Rangaswamy and Dr. George York, respectively, are acknowledged for the given support and the demonstrated interest in this research.

Last, but not least, I would like to thank the support staff of the Electronic and Electrical Engineering Department for promptly solving any administrative and non-academic issues occurring in these years.

Publications arising from this research

The following publications have been derived from this work.

Books and contributions to books:

H.D. Griffiths, C.J. Baker, P.F. Sammartino, M. Rangaswamy – "MIMO as a radar network" – Chapter contribution for "MIMO Radar Signal Processing" edited By J. Li and P. Stoica, Wiley books, Nov 2008.

P.F. Sammartino, C.J. Baker, H.D. Griffiths – "A comparison of algorithms for MIMO and netted radar systems" – Accepted for "Principles of Waveform Diversity and Design", edited by V. Amuso, S. Blunt, E. Mokole, D. Schneible and M. Wicks, SciTech Publishing, Dec 2009 (expected).

Journal Publications:

P.F. Sammartino, C.J. Baker, H.D. Griffiths, M. Rangaswamy – "Processing in distributed radar networks" – Submitted to IEEE transactions on Aerospace and Electronic Systems.

Conference Publications:

1. P.F. Sammartino, C.J. Baker, H.D. Griffiths – "A comparison of algorithms for MIMO and netted radar systems" – 2^{nd} International Waveform Diversity & Design Conference, Lihue, Hi, 22^{th}–27^{th} Jan 2006,

2. P.F. Sammartino, C.J. Baker, H.D. Griffiths – "Target Model Effects On MIMO Radar Performance" – 2006 IEEE ICASSP, International Conference on Acoustic, Speech and Signal Processing, Toulouse, Fr, 14^{th}–19^{th} May 2006,

3. P.F. Sammartino, C.J. Baker, H.D. Griffiths – "MIMO performance in clutter environment" – CIE Rad 2006, International Conference, Shanghai, Ch, 16^{th}–19^{th} Oct 2006,

4. P.F. Sammartino, C.J. Baker, H.D. Griffiths – "A comparison of algorithms for MIMO and netted radar systems" – IEEE radar 2007, Waltham, Ma, 17^{th}–20^{th} Apr 2007,

5. P.F. Sammartino, C.J. Baker, H.D. Griffiths, M. Rangaswamy – "Effects of decentralized processing in networks of radars" – IET Radar 2007, International Conference on Radar Systems, Edinburgh, UK, 15^{th}–18^{th} Oct 2007,

6. P.F. Sammartino, C.J. Baker, M. Rangaswamy – "Coverage in radar networks" – 41^{st} Conference on Signals, Systems, and Computers, Asilomar, Pacific Grove, CA, 4^{th}-7^{th} Nov 2007,

7. P.F. Sammartino, C.J. Baker, M. Rangaswamy – "MIMO radar, theory and experiments" – CAMSAP 2007, St. Thomas, US Virgin Islands, 12^{th}-14^{th} Dec 2007.

8. P.F. Sammartino, C.J. Baker, M. Rangaswamy – "Moving target localization with multistatic radar systems" – Radarcon 2008, Rome, Italy, 26^{th} - 30^{th} May 2008,

9. P.F. Sammartino, C.J. Baker – "The Frequency Diverse Bistatic System" – Waveform Diversity and Design 2009, Orlando, FL, 8^{th} - 13^{th} Feb 2009,

10. P.F. Sammartino, C.J. Baker – "Development in the Frequency Diverse Bistatic System" – Radarcon 2009, Pasadena, CA, 4^{th} - 9^{th} May 2009.

Contents

List of Figures

List of Acronyms

CACFAR:	Cell Average Constant False Alarm Rate
CFAR:	Constant False Alarm Rate
CW:	Continuous Wave
DOA:	Direction of Arrival
DRN:	Decentralized Radar Network
ECCM:	Electronic Counter Counter Measures
ECM:	Electronic Counter Measures
ERP:	Effective Radiated Power
ESA:	Electronically Steered Array
FAR:	False Alarm Rate
FDA:	Frequency Diverse Array
FDBS:	Frequency Diverse Bistatic System
GLRT:	Generalized Likelihood Ratio Test
HH:	Horizontal (transmit) Horizontal (receive)
HV:	Horizontal (transmit) Vertical (receive)
I&Q:	Inphase and Quadrature
LPI:	Low Probability of Intercept
LRT:	Likelihood Ratio Test
MEP:	Minimum Error Probability
MIMO:	Multiple Input, Multiple Output
ML:	Minimum Losses (criterion)
NR:	Netted Radar
P_D:	Probability of Detection
PDF:	Probability Density Function
P_E:	Probability of Error
P_{FA}:	Probability of False Alarm
P_{MD}:	Probability of Missed Detection

PRF:	Pulse Repetition Frequency
PPI:	Planned Position Indicator
RCS:	Radar Cross Section
RPNR:	Re-Phased Netted Radar
RV:	Random Variable
SNR:	Signal to Noise Ratio
STAP:	Space Time Adaptive Processing
TOT:	Time On Target
VV:	Vertical (transmit) Vertical (receive)
WA:	Wavelength Array

Chapter 1

Introduction

The concept of using radiofrequency waves in order to detect metal and other objects was first developed at the beginning of the last century. The word RADAR (RAdio Detection And Ranging) itself was coined many years later, in 1941. However, since the 1930s there has been a high interest in investigating and improving the capabilities of these systems. The basic principle of a radar system is to transmit an electromagnetic signal and receive a copy after reflection from a target. The time to receive the echo determines the range of the target. The transmitter and the receiver can be co-located (monostatic radars) or separated (bistatic radars). The basic principles of radars are described in Chapter 3.

Radar systems have been developed constantly over time and nowadays are applied in a wide variety of ways. Applications include air traffic control, target recognition and tracking, weather monitoring, imaging, global navigation, automatic systems guidance, road speed control, through-the-wall imaging, etc. . . [1, 2, 3, 4, 5]. Originally designed, developed and built with analogue technology, in the past radar systems could generally perform one or two main tasks only. However, in recent years, they have been taking advantage of developments in digital technology. In particular, a combination of digital signal processing and array antennas has allowed radar systems to become much more versatile. As a consequence future generations of radar systems are being designed to perform

multiple tasks. These include detection, tracking and target classification performed in a variety of modes (area surveillance, volume search, etc.) and often simultaneously. These are the so-called 'multi-role' radars or 'multi-function' radars (although there is not a strict definition yet).

1.1 Overview and motivation

This thesis examines a relatively new concept in which the transmitters and receivers comprising the radar system are distributed in space. In this way they form a networked or distributed sensor. This provides new degrees of freedom in design. In this thesis these new freedoms are explored by evaluating the resulting performance compared to that of a monostatic system. In particular a concept termed MIMO (Multiple Input – Multiple Output) has received a lot of attention in literature, often with significant claims being made for detection performance. Thus in this thesis the MIMO concept is compared with other forms of processing applied to a distributed radar. In this way MIMO radar can be evaluated in comparison with other approaches.

1.1.1 The radar network concept

A radar network consists of transmitters and receivers distributed over a geographic area such that it is possible to view targets at different aspect angles. Transmitters and receivers can be co-located or not. A schematic example of such a network is shown in Figure 1.1. Signal processing techniques for radar networks has received considerable attention and this has spawned a wide variety of system structures and processing methods that can be employed [29, 36, 37].

In this case, the same data acquired by a radar network can be processed in a number of different ways, leading to a range of performance levels. In this thesis we describe and compare four different signal processing approaches. These vary from the processing of fully coherent signals to processing incoherent signals. The processing approaches can be 'cen-

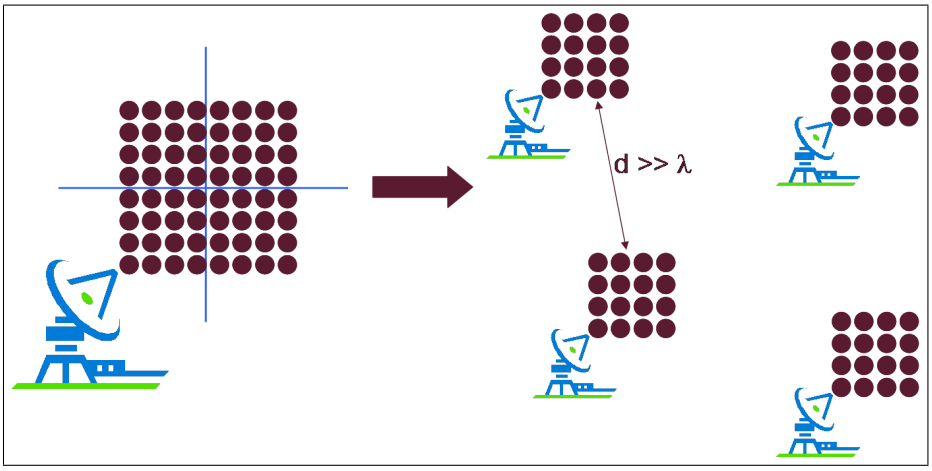

Figure 1.1: From the monostatic to the MIMO concept

tralized' (i.e. the detection decision is taken at a single processing unit) or 'decentralized' (decisions are taken at individual receivers in the radar network across all possible mono/bistatic pairs). The statistical properties of the signals resulting from the differing signal processing approaches lead to substantial differences in their performance in terms of FAR (False Alarm Rate) and even more so when subject to either accidental or deliberate interference (jamming). Such an analysis allows a detailed examination of the benefits and drawbacks associated with radar networks and the various possible processing schemes. This provides a simple but thorough interrogation enabling the potential of radar networks in terms of their false alarm performance to be assessed.

Results for monostatic systems are also reported to provide a well understood benchmark. The achievable detection performance is computed as a function of (*i*) processing method, (*ii*) Radar Cross Section (RCS) model of the target and (*iii*) the number of nodes comprising the radar network. Furthermore, the sensitivity of each system is calculated to show the extent of the range coverage that these differing systems could potentially achieve. In order to provide a fair comparison of the processing types, the total Effective Radiated Power (ERP) is maintained constant in transmission regardless of the number of nodes comprising the network. In other words, a monostatic radar with a fixed power in transmission P_t and

a specific antenna gain G is compared to a radar network comprised by a number of devices (say L) all able to transmit and receive, using a fraction of the power in transmission $\left(\frac{P_t}{L}\right)$ and with antennas with a fraction of the gain $\left(\frac{G}{L}\right)$. Such a decision has been taken in order to provide a fairer comparison between the radar network and the monostatic performance. Actually it would not be hard to demonstrate that, whenever each transmitter of the radar network is fed with as much power as the monostatic case and the tx/rx antennas have the same gain, the performance is expected to be higher, simply for the reason that an increased amount of total energy is injected into the system.

Figures 1.2 and 1.3 show an example of the antenna patterns when the original antenna is split in $L = 4$ smaller antennas. As is known, not only is the gain lower, but also the pattern or angular resolution is wider. Therefore two significant drawbacks of applying this approach when comparing with traditional monostatic radar, are: (*i*) the reduced *SNR* expected in every receiver and (*ii*) the smaller angular resolution of each antenna. However, as seen in Chapters 5 and 8, the increased number of processable signals together with the achieved angular diversity can recover performance. In Chapter 4 the considered processing approaches for this concept of radar systems are reported in detail.

1.1.2 The MIMO concept

MIMO is a recently developed concept that has attracted much interest in application to communication systems, e.g. [41] to [52]. This is because it allows enhanced performance of a communication channel in terms of data transfer (capacity) without requiring additional bandwidth or power in transmission. This technique employs a number of antennas, say M, in transmission and others, say N, in reception.

MIMO has recently been applied to radar systems, attracting much attention (e.g. [53] to [58]). Therefore the ideas behind MIMO and distributed radar are very similar and form a core part of the investigation

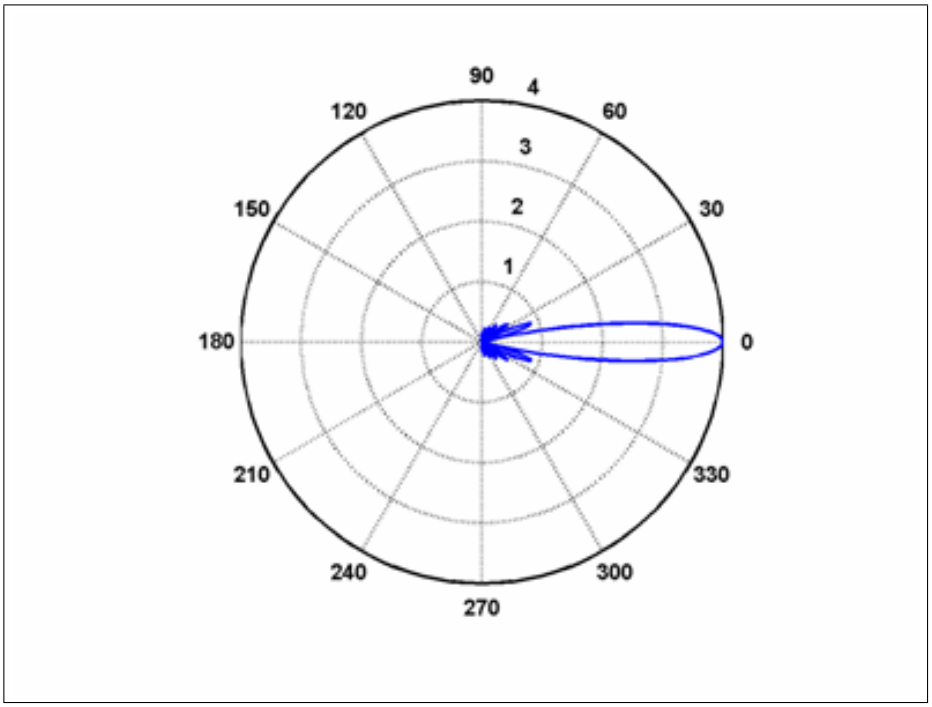

Figure 1.2: Monostatic beam

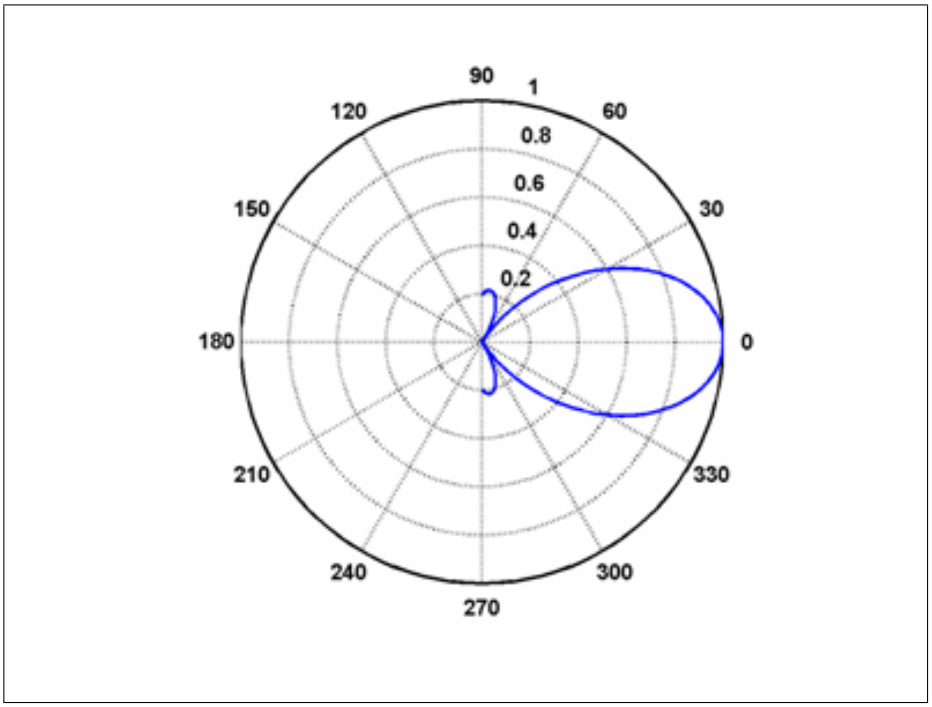

Figure 1.3: MIMO single antenna beam

of this thesis. A more complete discussion on the research on this topic is reported in Chapter 2. In the following Section an overview of the principles of the MIMO communication system is presented, as applied within this thesis. This allows a more fundamental understanding of the MIMO concept as applied to radar to be developed. However, it has to be pointed out clearly that a detailed description and evaluation of the MIMO communication systems is outside the scope of this thesis. In particular, this investigation aims to focus on the possible application of this concept to radar networks to allow new exploitation of sensor resources, increasing accuracy, parameter estimation, tolerance to jamming, etc. . . Overall, this thesis examines spatial diversity as a new degree of freedom.

MIMO concept as a communication system

As stated above, it has been extensively reported in the literature that MIMO systems show improvements in channel capacity and subsequent performance of communication systems in several ways (Chapter 2). They transmit and receive a number of signals (e.g. x_1, x_2, x_3, ...) on differing elements simultaneously. At the receiver a MIMO decoder operates on each of the antenna elements. MIMO antennas are spaced by multiple of wavelengths, usually between 1 and 10. This allows, in an indoor environment, independent samples of the interfering signals in reception. Each antenna element receives signals coming from any of the transmit elements, thus:

$$\begin{array}{rcl} r_1 & = & h_{11}x_1 + h_{12}x_2 + \ldots + h_{1M}x_M + n_1 \\ r_2 & = & h_{21}x_1 + h_{22}x_2 + \ldots + h_{2M}x_M + n_2 \\ \vdots & \vdots & \vdots \\ r_N & = & h_{N1}x_1 + h_{N2}x_2 + \ldots + h_{NM}x_M + n_N \end{array} \tag{1.1}$$

where h_{ij} are the channel weights and n_k the possible disturbances incoming in the receiver (noise, jammers, multipath, clutter). This can be written in a compact way as:

$$\mathbf{r} = \mathbf{H}\mathbf{x} + \mathbf{n}. \tag{1.2}$$

By treating the set of channels as a matrix the individual data streams x_i can be recovered. To do this the disturbance vector $\mathbf{n}$ and the channel matrix $\mathbf{H}$ must be estimated and respectively subtracted and inverted to recover the individual data streams from the vector $\mathbf{r}$. This is equivalent to solving N simultaneous equations with M unknowns. The matrix can only be inverted or pseudo-inverted if there are sufficient paths between the transmitter and receiver.

MIMO is currently widely used in indoor wireless applications, since it allows a dramatic increase of the capacity of the channel and reduces the limitations due to fading, multipath and other secondary effects. This technology is still being developed, with increasing potential, as MUltiuser MIMO (MU-MIMO), Network MIMO or Intelligent Antennas MIMO (IA-MIMO), [50, 51] with different applications.

MIMO: from communications to radar systems

MIMO basic principles are being applied to radar systems and a number of publications have recently begun to emerge, e.g. [53] to [70]. These suggest there are advantages to using this technique derived from spatial or other forms of diveristy. As much as in wireless communications, the spacing of antennas is crucial in the application to radar systems. Some authors, on the contrary, apply the MIMO technique to an array of antennas spacing the elements up to a few wavelengths as in wireless communications. Other authors point out that the distance d between antenna elements in a MIMO system, for achieving independent angular measurements of the RCS of a target and therefore independency of the received signals, is determined by

$$d \geq \frac{\lambda R}{D}, \tag{1.3}$$

where λ is the wavelength, R is the target range and D the target's main dimension. As a consequence, assuming for instance a 20-meter wide target at 100 km and a wavelength of 3 cm, the spacing d between the antenna elements should be 150 m. This allows the target to be seen under different aspect angles and, consequently, to gather diverse measurements of the RCS. In this scenario, it is also clear that the coherency between the antennas is lost.

In the migration from the MIMO communication concept to the MIMO radar concept, another point that requires stressing is that in radar systems it is not of interest to maximize the capacity of the channel. This may seem debatable, but it is extremely important because a number of concepts that characterize the MIMO communication system have to be understood in depth before applying them to radar systems. In fact, the maximization of the channel information is the core of MIMO as developed in communications. The channel capacity of radar is extremely low and is not of interest. This is due, of course, to the ultimate purpose of a radar system which is detecting, tracking and sometimes classifying targets in an unknown or non-cooperative environment, rather than transmitting and/or receiving data from cooperative devices.

Other authors (e.g. [67] to [69]) have been investigating MIMO as a technique based on two arrays of antennas transmitting and receiving different codes from different (sub)elements. Here the distance between the elements is kept relatively small, i.e. in the order of the wavelength, and therefore angular diversity cannot be achieved. However this application, exploiting either orthogonal or partially correlated codes (e.g. [59] to [68]), has been shown to overcome the standard array of antenna performance and to provide an extra degree of freedom, allowing formation of multiple beams at the same time which can be used for tracking or jammer rejection. This is not considered further in this thesis.

MIMO concept as a radar system

When evaluating the MIMO concept from a communication to a radar basis, equation (1.3) is crucial. This equation states clearly that it is not possible to achieve angular diversity and consequently independent measurements of the RCS of a target, when antennas are closely spaced. This is the real basis of MIMO radar as independent samples of a target can be combined to provide a more accurate estimate of the underlying RCS. This is also valid for clutter and multipath, since the proximity of the antennas does not allow decorrelation of all the received signals. Therefore in radar systems, the antennas should be separated by distances not comparable with the wavelength. This generates a number of secondary effects, which require at least a strong awareness, that have not been taken into account in the analysis of MIMO as a communication technique.

First of all, the coherency between the antenna elements is totally lost. This is due to the increased distance that scrambles the received phases from element to element. Secondly, whenever more than one code (waveform) is used in transmission, these cannot be considered as temporally 'orthogonal' anymore, even if they have been designed with this property. Actually, two codes, say $w_i(t)$ and $w_k(t)$ are called 'orthogonal' when the following property applies:

$$\int_{-\infty}^{+\infty} w_i^*(t) \cdot w_k(t)\, dt = 0, \tag{1.4}$$

where * is the conjugate operator.

In radar systems employing several waveforms, each received signal goes through a bank of matched filters performing all the possible cross-correlations between the received signal itself and the reference waveforms, as in equation (1.5)

$$R_{w_{i,k}}(\tau) = w_i(t) \times w_k(t) = \int_{-\infty}^{+\infty} w_i'(t)\, w_k(t+\tau)\, dt, \tag{1.5}$$

where $\times$ is the cross-correlation function and τ is a delay. If the transmitting antennas are closely spaced, the delay in the time of arrival of all

the waveforms, assumed transmitted at the same time, is negligible and equation (1.5) can be expressed as equation (1.4) which still holds. As a result, when a peak in the cross-correlation of a waveform with itself occurs, the cross-correlations with all the other used waveform is 0 and therefore there are no interferences (noise apart).

When the antennas are located far away from one another, transmission and reception are not synchronized anymore because the paths between the transmitters, the target and the receivers have different lengths, usually much more than a resolution cell. In this case the corresponding different times of arrival of the echoes generate delays mismatching the orthogonality of the codes. Being unaware of this issue may lead to detection of multiple targets which in fact can be generated by the echoes from one target only. Of course it is possible to estimate the peak of the auto-correlation of a waveform and cancel it in the other received signals, but it requires additional efforts in signal processing.

1.2 Aim

This research examines distributed radar concepts in terms of performance and system utility. The overall aim of the work described here is to compare the performance, under various practical operating conditions, of different ways of implementing a MIMO radar system and netted radar concept. Exploring the potential allowed by introducing extra degree of freedom as in the MIMO case, an overlook to the advantages of a couple of novel 'frequency MIMO' concepts are also taken into consideration. These are designed to provide alternative benefits to radar systems without requiring multiple distributed sensors, notwithstanding the possibilities of mutual integration of the two concepts.

1.3 Thesis layout

Chapter 2 reviews the literature produced so far for MIMO systems in communications and radar systems. Additional publications on mono/bistatic radars are reported as well.

In Chapter 3 basic features of the mono/bistatic radar systems are reported. This provides a platform to have a better understanding of the multistatic scenarios described later in this thesis.

In Chapters 4, 5 and 6 we discuss of the number of processing that it is possible to apply to a radar network. Their performance as a function of signal to noise ratio has been evaluated for various models of targets including the introduction of secondary effects such as clutter. Chapter 7 reports the achievable coverage.

The UCL radar network, i.e. the system used for acquiring experimental data, is described in Chapter 8. In Chapters 9 and 10 an analysis of the acquired multistatic data is performed for both validating the theoretical results achieved in the previous Chapters and introducing a way for localization and tracking with multistatic systems.

Chapter 11 describes a novel form of frequency MIMO as applied to an array of antennas.

Finally in Chapter 12 the conclusions of the work produced so far are reported with suggestions for further improvements and possible future developments.

1.4 Achievements of this work

In Chapters 5, 6 and 7 it is demonstrated that radar networks are not required to be made up of a number of nodes to outperform conventional monostatic systems. In particular, these Chapters demonstrate that it is possible to compromise on the complexity of the network, still allowing improved performance.

Few is known on correlation of multistatic clutter samples from a joint illuminated area. Chapter 9 shows first results on this topic. In particular

it is here demonstrated through real data processing that the statistics and the correlation of multistatic clutter signals from the same area can have different features. As a consequence, this is a starting point for further research.

Chapter 10 provides two different ways for localizing a moving target exploiting the information of six multistatic signals. The achieved accuracy is here demonstrated to be at least an order of magnitude greater than that of a monostatic system. In addition it is shown that it is possible to reconstruct the full Doppler vector reconstruction. Attention has been dedicated to a suboptimal algorithm which can speed up the processing time making it more suitable for online radar signal processing.

Finally, Chapter 11 reports a brand new concept for arrays of antennas. The results shown here are a first promising insight in the potential of these systems.

Chapter 2

Literature review

In this section a summary of the literature is presented, covering radar networks, MIMO systems, together with a brief survey on general radar systems.

The literature review is divided into four parts. The first part is made of general publications in radar. The second discusses clutter in monostatic and bistatic systems. The third is a comprehensive critique of the papers published on the netted radar concept. Finally the last part focuses specifically on MIMO as a radar system concept.

The theory underlying radar systems is reported in a number of publications. Because radar is a quite mature technology, a variety of books is currently on the market and no attempt is made here to review all the literature published on radar. However, among these, [1, 2, 3] are a significant survey of monostatic radar systems. As well, [4, 5] are a benchmark for the principles of bistatic systems. Chapter 3 reports an explanation of the most relevant concepts developed, as applied in this thesis, in order to improve the understanding of the results presented in the rest of this work. The principles of information theory and statistical signal processing, respectively, are covered comprehensively in [6, 7, 8].

Publications from [9] to [22] are significant with respect to clutter as utilized in this thesis. Whereas clutter is present in most of the radar applications, many studies have been carried out over the last 60 years.

As a consequence, robust theories and a number of models have been proposed to describe this phenomenon, although not all problems have been solved. Section 3.5 reports a brief survey of the principal models applied nowadays. Little is still known about the detailed pulse-to-pulse behaviour of bistatic clutter compared to monostatic measurements from the same area. Even less is known about the actual relationships between simultaneous measurements of monostatic and bistatic clutter from the same area and this is presented in Chapter 9. This is a very important issue for optimizing the processing of received echoes in a multistatic system. References [23] to [28] provide a basic survey of the most common detection approaches, which are presented in detail in Section 3.6. However, a thorough analysis of simulated mono-bistatic clutter is outside the scope of this thesis.

In recent times the concept of linking two or more radars together is finding new applications and therefore further stages of developments are ongoing. Whilst in the past radar networks were comprised of many receivers but one transmitter only, recent works on waveform diversity allow multiple sources of transmission at the same time.

"Multistatic systems" cover a broad range of radar systems, such as

(*i*) networks of monostatic radars (sometimes termed "netted radars" and already used in diverse applications),

(*ii*) systems comprised of multiple transmitters and receivers, each widely separated in space from one another and

(*iii*) single transmitter and multiple receivers.

The first and the third cases have already been investigated, at least partially. However, the capabilities of autonomous integrated systems of multiple transmitters and receivers are still to be fully evaluated. In [29] the author defines a Multisite Radar System as "a radar system including several spatially separated transmitting, receiving and (or) transmitting-receiving facilities where information of each target from all sensors are fused and jointly processed". When the system is comprised of more than

one transmitter, the requirement of using multiple waveforms can lead to an overall optimization of the resources, but can, on the other hand, provide additional problems in system design. Indeed, to make this work, it must be possible to distinguish the different signals in each receiver, avoiding cross-detection of targets. In addition, the difference in time of arrival must be adequately mitigated in the matched filtering to avoid the echo from the waveform "*a*" being recognized as a target after the matched filter applied to the waveform "*b*". This leads to the conclusion that with multiple and widely separated radar devices very low cross-correlation codes must be used. [30] and [31] focus on this issue, suggesting quasi-orthogonal codes so to allow multiple simultaneous transmission. Alternatively, transmitters may employ pseudo-random codes, such as in [32], mitigating this effect. However, it should be pointed out that whilst additional processing techniques may allow cross-interference cancellation, losses may arise from consistent differences in the measured RCS, reducing the low cross-correlation characteristic of the codes. An additional technique for separating signals after matched filtering is "frequency diversity", when each transmitter works on a different carrier frequency separated by more than the bandwidth of each carrier. In this case waveform diversity is not important anymore, as the separation is due to the multiple carriers. Unfortunately, the higher cost in terms of frequency occupation does not always make this solution easily feasible.

A good introduction to netted radars, including applications for tracking, is in [33, 34, 35] where basic concepts are introduced. However, they investigate, principally, the case of one transmitter and multiple bistatic receivers. More detailed studies on the topic of multistatic radar, e.g. from [36] to[40], provide an insight to scheduling, hardware, sensitivity and the ambiguity function.

Finally, multistatic collection and analysis of data is a concept that has been recently redeveloped in MIMO systems. It is recognized that a huge quantity of papers and publications has been produced in the literature about MIMO for communication systems. The improvements in performance (achievable in terms of capacity of the communication

channel) are shown to be very significant. Publications about MIMO as applied to radar systems have become relevant only in the last couple of years, as interest in this topic has developed only recently. For brevity and relevance to this research, we only examine the literature relevant to the MIMO and distributed radar concept.

Publications from [41] to [52] are representative of MIMO communication systems. These are of limited interest if applied directly to the topic discussed in this thesis. However, they provide a starting point to evaluate the migration from MIMO communication to MIMO radar systems. In particular, [41] describes in detail the background to MIMO wireless communications. The other publications focus on specific problems, such as multipath, spectral efficiency and interference cancellation. Whereas the MIMO concept has been developed for communication systems, most of these publications develop and investigate theoretical aspects which are not directly related to radar and have to be carefully interpreted if they are to be applied to radar systems.

Most relevant for the purposes of this thesis are the first papers on MIMO radar systems, e.g. from [53] to [58], in which the authors stress the point that a MIMO radar system operating in the "spatial diversity" mode manages to take advantage of effects, such as glint, that in conventional radar systems introduce a loss in achievable performance. This part will be reviewed in detail as it is the most relevant for this thesis.

So far it generally stands out that a distributed MIMO radar system makes use of "orthogonal" signals on transmit and has M transmitting and N receiving antennas in order to be able to distinguish between the signals with a bank of matched filters. Furthermore, the RCS responses of a common target are assumed to be independent and to have uncorrelated amplitudes and phases.

In [53], that is the starting point of the concept of MIMO radar systems, the authors develop a general approach to the problem together with a model for the received signal under the assumption of additional white Gaussian noise. Here the most relevant concept is that individual radars have to be far away from one another in order to exploit spatial diversity.

This is clearly stated when the authors demonstrate that the spacing d_t between the antennas should be

$$d_t \geq \frac{\lambda R}{D} \tag{2.1}$$

where R is the distance of the target, λ the wavelength, D the dimension of the target. Here the authors highlight in few paragraphs that with MIMO systems it is possible to distinguish more than one object within one resolution cell. This is an idea that should have been developed as the benefits that it might yield to the concept of MIMO as applied to radar systems are considerable. Unfortunately the background of this paper is in communications systems. This is made clear when the Cramer-Rao bound for the performance is developed under the hypothesis of a multistatic Swerling II-distributed RCS.

Publications [54] and [55], from the same authors, investigate further the MIMO application to radar systems. As [55] is a more complete work on spatially distributed MIMO radar systems, where the authors express the MIMO radar system they developed in full, also expanding concepts present in the previous works. It is worth giving a full and deep critique of this paper as it represents the starting point of this work.

In the paper it is assumed that there are M transmitters and N receivers and that the waveforms are distinguishable after matched filtering. The authors often refer to "orthogonal" waveforms, as in the communications system. In a radar system background it is more accurate to speak about "low-cross-correlation" waveforms, as every incoming signal is passed into one or more matched filters in parallel that perform a correlation with one or more waveforms. If the target is present, all the transmitted waveforms are received: the incoming signal is processed through a filter bank and M signals are available at its output. Then, considering this process for N receiving antennas, a total of MN signals can be processed by the entire system. In these papers all the outputs are packed into a vector $\mathbf{x}$, where the q^{th} element can be expressed as below:

$$x_q = r_k * s_h \tag{2.2}$$

where $*$ is the convolution operator, r_k is the signal received by the k^{th} antenna, s_h is the k^{th} transmitted waveform, $k = 1..N$, $h = 1..M$ and $q = (k-1)M + h$. Under these assumptions $\mathbf{x}$ is as follows:

$$\mathbf{x} = \begin{cases} \mathbf{n}, & H_0, \\ \sqrt{\frac{E}{M}}\boldsymbol{\alpha} + \mathbf{n}, & H_1, \end{cases} \tag{2.3}$$

where E is the total supplied power, $H_{1/0}$ is the hypothesis of target respectively present/not-present, $\mathbf{n}$ is Gaussian white complex noise, supposed to be $\sim CN\{0, \sigma_n^2 I_{MN}\}$, and $\boldsymbol{\alpha}$ a value taking into account all the parameters of the radar equation, including the phase-shift due to the path length and the transmitted energy of the signal and

$$\mathbf{x} = \begin{pmatrix} x_1 \\ x_2 \\ \cdots \\ x_{MN} \end{pmatrix}, \mathbf{n} = \begin{pmatrix} n_1 \\ n_2 \\ \cdots \\ n_{MN} \end{pmatrix}, \boldsymbol{\alpha} = \begin{pmatrix} \boldsymbol{\alpha_1} \\ \boldsymbol{\alpha_2} \\ \cdots \\ \boldsymbol{\alpha_{MN}} \end{pmatrix}. \tag{2.4}$$

In these papers, for the sake of simplicity, $\boldsymbol{\alpha}$ has been assumed as $\sim CN\{0, \sigma_n^2 I_{MN}\}$, i.e. normalization has been applied to the signal and noise powers.

Furthermore here the authors present a LRT (Likelihood Ratio Test) developed for this system and the analysis of its resulting performance. It is convenient here to report in more detail some achievements as they provide a background and a starting point for the results presented in this thesis. As is well known, the optimal detector in this sense is given by

$$\log \frac{p(\mathbf{r}|H_1)}{p(\mathbf{r}|H_0)} \underset{H_0}{\overset{H_1}{\gtrless}} \lambda, \tag{2.5}$$

where $p(\mathbf{r}|H_1/0)$ is the Probability Density Function (PDF) under the hypotheses of target respectively present/not-present, and λ is the threshold

set on the Probability of False Alarm (P_{FA}). Under the assumptions on $\mathbf{n}$ it is demonstrated that this structure for the detector is equivalent to the following:

$$\|\mathbf{x}\|^2 \underset{H_0}{\overset{H_1}{\gtrless}} \lambda, \tag{2.6}$$

From equation (2.3) it has been inferred that, under the assumption for $\mathbf{n}$ and $\boldsymbol{\alpha}$, $\mathbf{x}$ is the realization of a Gaussian random variable even when the target is present. This enables one to write in closed form the performance of spatial MIMO. From a mere statistical point of view the sum of the squared value of L Gaussian random variables generates a chi-square random variable with L degrees of freedom. In the specific case, the PDF of $\xi = \|\mathbf{x}\|^2$, where each element of $\mathbf{x}$ is a complex Gaussian random variable, will be a chi-squared PDF with $2MN$ degrees of freedom. This can be expressed as follows:

$$p(\xi) = p(\|\mathbf{x}\|^2) = \begin{cases} \frac{\sigma_n^2}{2}\chi^2_{2MN}(\xi), & H_0, \\ \left(\frac{E}{2M} + \frac{\sigma_n^2}{2}\right)\chi^2_{2MN}(\xi), & H_1, \end{cases} \tag{2.7}$$

where the variances have been divided by a factor 2 in order to consider both real and imaginary parts of the complex Gaussian variables. Then the P_{FA} (Probability of False Alarm) can be written as:

$$P_{FA}(\lambda) = \Pr\left\{\frac{\sigma_n^2}{2}\chi^2_{2MN}(\xi) \geq \lambda\right\} = \Pr\left\{\chi^2_{2MN}(\xi) \geq \frac{2\lambda}{\sigma_n^2}\right\}, \tag{2.8}$$

so, inverting this formula, the threshold guaranteeing a certain FAR is given by:

$$\lambda = \frac{\sigma_n^2}{2} F^{-1}_{\chi^2_{2MN}}(1 - P_{FA}), \tag{2.9}$$

where $F^{-1}_{\chi^2_{2MN}}(z)$ denotes the inverse cumulative distribution of the chi-squared PDF computed in z.

As **x** has a chi-squared distribution when the target is present (equation (2.7)), it is possible to achieve a closed form also for the P_D (Probability of Detection):

$$\begin{aligned} P_D(\lambda) &= \Pr\left\{\left(\frac{E}{2M}+\frac{\sigma_n^2}{2}\right)\chi^2_{2MN}(\xi) > \lambda\right\} = \\ &= \Pr\left\{\chi^2_{2MN}(\xi) > \frac{2\lambda}{\frac{E}{M}+\sigma_n^2}\right\} = \\ &= 1 - F_{\chi^2_{2MN}}\left(\frac{\sigma_n^2}{\frac{E}{M}+\sigma_n^2}F^{-1}_{\chi^2_{2MN}}(1-P_{FA})\right). \end{aligned} \tag{2.10}$$

This is the most preliminary result in [55].

Moreover, in these publications comparisons between MIMO system research work and an array of antennas and a MISO (Multiple Input, Single Output) system are reported. Although the results represent a first sight into the potential of MIMO radar, these publications are still written for a communication approach to the problem, as, for example, plots of P_D vs. P_{FA} are reported.

At a first stage a Gaussian model of the variables under observation is a reasonable choice, as a closed form can be very useful to compute and then to compare system performance. Unfortunately most targets do not have a noise-like scattering behaviour and the PDF associated with their RCS measurements can be complicated. As soon as secondary or additional non-Gaussian effects such as those of high resolution clutter are considered, it can be extremely hard, if not impossible, to achieve a closed form expression for the performance.

In [57, 58] a similar MIMO concept as examined in this thesis is developed. Here, the authors distinguish a MIMO system with widely separated antennas from a multistatic system through "the joint processing of signals for transmission and reception". At the same time they provide a quite precise description of their system. They refine the law for determining the minimum distance between the elements to allow angular diversity, they

also discuss the ambiguity function of such a system and finally provide a comparison of the detectors.

Papers [59, 60] stress the necessity of having a number of waveforms with particular low cross correlation properties in order to make MIMO work. Although authors here do not investigate the effects of having many antennas in transmission and reception, they develop particular polyphase codes, with a certain grade of tolerance to Doppler. As they point out, without low-cross-correlation codes, MIMO radar systems are not feasible unless it is possible to distinguish the several transmitted waveforms. This requirement is clearly necessary for merging and exploiting in a further processing all the multistatic and increased information gathered.

It has to be acknowledged that other authors, as from [61] to [70], used the MIMO as an array of antennas for beamforming using multiple orthogonal signals. [71] is a good book for understanding the basic principles of these electronic systems. These are vaguely or not at all related to the work proposed in these pages, so just a brief summary is given. Within these publications, a significant survey of MIMO radar systems with both co-located and separated antennas is provided in [61] by contributions from different authors. Of interest are also (*i*) the formalization in [62] of the model of the channel matrixes as function of time and of their effect on the final PDF of the received signal and (*ii*) the overall analysis of the MIMO communication channel in [63].

In [64] the authors develop an expression for the performance in case of a general coloured noise. This paper includes also a first study on performance in clutter, although it is still done from a communication perspective, expressing the Chernoff upper and lower bound limits for the probability of detection. A description of the mutual information exchangeable is provided as well. A limit of this paper is that it considers a fully known and constant channel matrix, while, especially in the radar field, it is well known that it may change in time. Thus in real systems it is necessary to trade this knowledge with an estimation of the real channel matrix that has to be appropriately updated. This publication provides a deeper overview of the capacities of the MIMO system and nonetheless a

better formulation of the system model.

As the MIMO radar is a relatively new concept in the scientific literature, most of the papers published at the beginning of this work did not take into account many fundamental aspects, such as the CFAR capabilities of the overall system, the performance achievable in most of the standard operative configurations, the response to different target models and the loss of performance due to mismatches in estimating most of the parameters involved in the several usages of a radar system.

Finally, it is worth mentioning the publication [70]. Here the authors provide a precise, concise and quite exhaustive description of MIMO with co-located antennas, addressing many of the issues described in previous publications through the search of eigenvalues and eigenvectors of a particular system. In particular, terming the multi-waveform transmitted signals as $\mathbf{s}$, the best configuration for such a system in terms of maximization of SNR and optimization of the resources in transmission and reception is given by the solution of the following constrained system

$$\begin{aligned} &\max_{\mathbf{s}} \left\{ \mathbf{s}' E\left\{ \mathbf{H}^H \mathbf{H} \right\} \mathbf{s} \right\} \\ &s.t. \begin{cases} E\left\{ \mathbf{H}^H \mathbf{H} \right\} \mathbf{s} = \lambda_{\max} \mathbf{s} & \text{(transmitter)} \\ \mathbf{H}_w = R^{-1} \mathbf{H}_T & \text{(receiver),} \\ \mathbf{H} = \mathbf{H}_T \mathbf{H}_w, \end{cases} \end{aligned} \tag{2.11}$$

where ^{H} is the Hermitian operator, $\mathbf{H}_T$ is the multi-waveform channel matrix and R is the multiwaveform nuisance correlation matrix, which can include clutter, multipath and jammerers, $E\{x\}$ is the expected value of x and finally $\lambda_{\max}$ is the maximum of the eigenvalues of $E\{\mathbf{H}^H \mathbf{H}\}$. Although this result comes directly from an extension of the single-waveform problem, the analysis provided by the authors suggests to use multiple orthogonal waveforms in a first moment where the environment is still unknown and therefore to switch to more conventional methods or reduce the number of transmitted waveforms to achieve the best results reducing the overall complexity of the system. However, whereas this topic is of marginal interest for this thesis, publications on MIMO radar systems with co-located antennas will not be discussed further.

In the existing literature, there is a lack of a complete and exhaustive comparison between the possible processing approaches of the information collected by a radar network. In particular, the achievable potential of these systems has never been reported as a function of the number of the devices comprising the network under the constraint of a constant ERP. This thesis attempts to fill this gap in Chapters 5, 6 and 7 where this topic is discussed under different scenarios. As well, whilst clutter in monostatic system has been widely investigated, the relationships between multistatic clutter have not been studied before. Chapter 9 is a first insight into this subject and it is a starting point for further research to come. Whilst a lot has been written about the concept of localization in radar networks, few publications report real data processing. For the last two purposes, real data collection has been necessary. As a consequence, a number of experiments has been planned and carried out. Finally, in this thesis the Frequency Diverse Array concept is introduced and developed. A lot is known about the employment of antenna arrays in radar system. As well, space diversity and frequency diversity are topic which have already been introduced and discussed in technical literature. However, the hybridization of frequency and space diversity within the same antenna array is a brand new topic with significant potential, which is here reported in Chapter 11.

Chapter 3

Fundamentals of monostatic and bistatic radars

In this Chapter the basic principles of monostatic and bistatic radars are described. This provides a well understood context in which multistatic systems can be subsequently introduced and examined.

The underlying concept of radar systems is to transmit an electromagnetic signal and receive the echo from objects that it intercepts, generally, in an unknown environment. The radar system then processes the signals appropriately to acquire as much information as possible. In most common applications, radar systems are applied to detect, locate and track targets. Alternatively another wide range of usage is in the field of imaging from aircraft or spacecraft systems. Radar systems can transmit Continuous Wave (CW) or pulses, i.e. transmitting for a relatively short time and receiving for the remaining time before another pulse is transmitted. In the rest of this work CW radars are not considered. In pulsed systems, therefore, it may appear convenient to transmit a pulse as short as possible to increase the resolution. However, a number of constraints limiting the lower duration of a single pulse are to be taken into account: the most common are (*i*) the frequency occupation of the signal, that can be considered at first as inversely proportional to its time duration (Section 3.2) and (*ii*) the peak and average power that the electronic physical devices

are capable of handle.

In this Chapter a survey of the most common issues of monostatic and bistatic systems and the trade-offs generally applied to compromise between the different requirements is reported. In particular, Section 3.1 introduces the matched filtering concept as in radar systems, in Section 3.2 the resolution as function of the bandwidth is described, in Section 3.3 the Doppler shift due to the velocity of a target is reported, Section 3.4 shows how the RCS of a target may change in multistatic systems, Section 3.5 presents the knowledge in modelling clutter and finally 3.6 gives an overview of the possible detection approaches that is possible to implement in a radar system.

3.1 The matched filter

After the transmission of a waveform $s(t)$, with duration T_s, the receiving antenna gathers all the returning echoes. As in all electronic devices, thermal noise is always present in reception. Therefore, a simple model of the incoming signal $r(t)$ can be written as follows:

$$r(t) = H_{0/1}\alpha s(t - T) + n(t), \tag{3.1}$$

α is an attenuating factor as in Section 3.4, $n(t)$ is the thermal noise and $s(t-T)$ is the echo of the target received at the time T after the transmission, with

$$T = \frac{2R}{c}, \tag{3.2}$$

where R is the target distance and c the speed of light.

It is widely recognized that 'matched' filtering the received signal is the best approach to maximize the Signal-to-Noise Ratio (SNR), under the hypothesis of white noise n. In this process the received signal $r(t)$ is processed through a filter $h(t)$ so to maximize the SNR. Therefore the matched filter is such that, if

$$\hat{r}(t) = \hat{s}(t) + \hat{n}(t), \tag{3.3}$$

where

$$\hat{s}(t) = \alpha s(t - T) * h(t) \tag{3.4}$$

and

$$\hat{n}(t) = n(t) * h(t), \tag{3.5}$$

the following applies:

$$h(t) = \arg\left\{\max_{h(t)} \frac{P_{\hat{s}}}{P_{\hat{n}}}\right\} = \arg\left\{\max_{h(t)} \frac{\int_{-\infty}^{\infty} |\hat{s}(t)|^2 \, dt}{\int_{-\infty}^{\infty} |\hat{n}(t)|^2 \, dt}\right\}. \tag{3.6}$$

Under the assumption of white Gaussian noise, it can be demonstrated [1] that the optimum matched filter can be expressed as

$$h(t) = s^*(-t). \tag{3.7}$$

Using a causality constraint, equation (3.7) can be written as

$$h(t) = s^*(T_s - t), \tag{3.8}$$

where T_s is the length of $s(t)$.

The matched filtering process is valid for both monostatic and bistatic systems.

3.2 Resolution

In pulsed radar the delay between the transmission and the reception of the backscattered waveform is directly dependent on the range of the target. For a non-compressed pulse of duration τ, the resolution Δr achievable for discriminating two targets relatively close can be expressed [1] as:

$$\Delta r = \frac{c\tau}{2\cos(\beta/2)} \tag{3.9}$$

where c is the speed of light, β is the bistatic angle between the transmitter, the target and the receiver and the bandwidth of the signal B can be expressed as

$$B = \frac{1}{\tau}, \tag{3.10}$$

that leads to the conclusion that the resolution is given by

$$\Delta r = \frac{c}{2B\cos(\beta/2)}. \tag{3.11}$$

In the monostatic case $\beta = 0$ and therefore the following well-known expression is achieved:

$$\Delta r = \frac{c}{2B}. \tag{3.12}$$

Thus the resolving power of any waveform depends on its frequency bandwidth, rather than its time duration. This cannot be of unlimited width for a number of technical and organizational reasons (e.g. available frequencies for transmission, maximum bandwidth of the amplifiers and the antennas comprising the system, other communication devices using contiguous frequencies, fractional band ratio, etc...).

Matched filtering is used to maximize the SNR by compressing long duration pulses that have been frequency modulated such that their bandwidth is greater than that implied by the inverse of their pulse length. Hence they achieve improved range resolution.

3.3 Doppler frequency

After receiving a number of echoes from a target, it is possible to process them coherently to gather information about its Doppler frequency, and

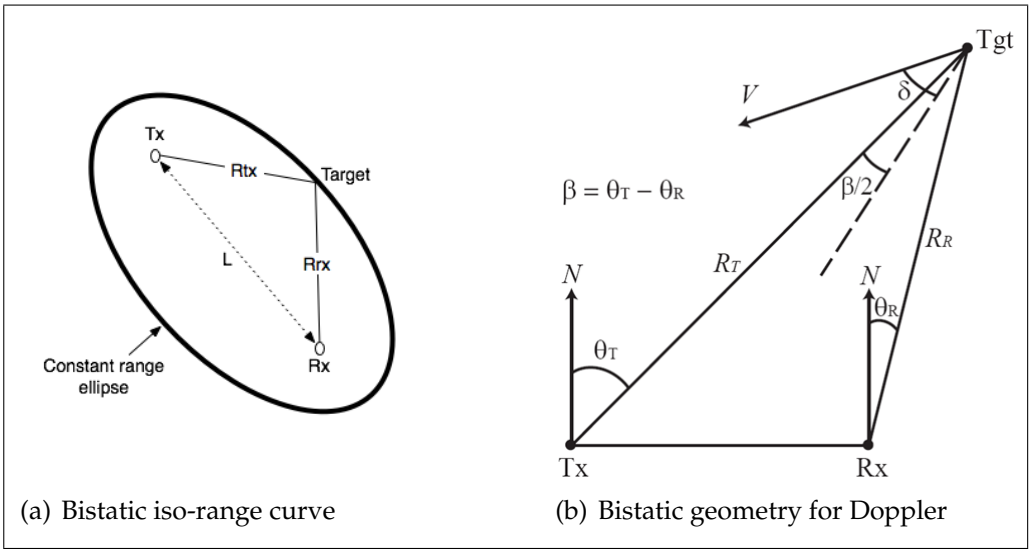

(a) Bistatic iso-range curve (b) Bistatic geometry for Doppler

Figure 3.1: Bistatic geometry

consequently its radial velocity. In general terms, the Doppler shift can be expressed as

$$f_D = \frac{1}{\lambda}\frac{\partial(R_{tx} + R_{rx})}{\partial t}. \tag{3.13}$$

Therefore, in a bistatic configuration a zero Doppler frequency is associated to targets moving on the iso-range curves which are well known to be ellipses [4]. Rearranging equation (3.13), the Doppler frequency can be expressed as

$$f_D = \frac{2V}{\lambda}\cos(\delta)\cos\left(\frac{\beta}{2}\right), \tag{3.14}$$

where δ is the angle between the velocity vector of the target and bisector of β, as in Figure 3.1. If $\beta = 0$,

$$f_D = \frac{2V}{\lambda}\cos(\delta), \tag{3.15}$$

that is the well known monostatic case.

3.4 Radar Cross Section

There are diverse reasons behind the different RCS responses of a target as a function of a number of the parameters of the radar and viewing geometry. In a monostatic system differences in aspect angles produce a variety of backscattering levels. Whilst for particular reflectors, such as a dihedral or a flat plate (Figures 3.2 and 3.3 respectively) the backscattering variation as a function of the aspect angle is deterministic, common targets, such as airplanes, helicopters, tanks, etc... are known to change rapidly, according to range and geometry. Even a change in the viewing angle of few milliradians can result in a severe impact on the measurable amplitude of the signal [1] due to fluctuation. Figure 3.4 provides a simplified example of this concept.

In concept, bistatic RCS has the same behaviour as the monostatic. In particular, it has to be pointed out that simultaneous monostatic and bistatic measurements usually provides significantly different levels in the echo of the signal. A simple example is the flat plate target [4] where the monostatic RCS achieves its maximum when the measurement is orthogonal to the plate. On the contrary, the bistatic measurements achieve its peak when the transmitter is specular to the receiver and the plate is in line with the baseline within the two.

3.5 Clutter

Clutter is unwanted echo from anything than the desired target. It has been deeply investigated in the past and is present in most radar applications. Being reflected from the environment in which the targets are present, clutter cannot usually be rejected easily. Actually the clutter is usually represented as the sum of the elemental scatterers. As a consequence of the movement of each single scatterer, a Doppler shift is generated in the received signal. The spectrogram of the clutter can be spread across multiple frequencies, because of the single scatterers' movement. In some applications, such as weather forecasting, the main Doppler shift can be used to estimate the speed of the wind. However, in most cases, the Doppler component due to clutter can mask real targets. Recently, new sophisticated ways for removing clutter, creating specific nulls in the pattern of the antenna at specific times, such as STAP (Space Time Adaptive Processing) [73, 74], have been developed. In the following sections, general model of clutter are presented, together with some approximation of the way in which Doppler and wind speed are linked.

In more general terms, it should be pointed out that, although the knowledge about monostatic clutter is quite exhaustive, little is known about bistatic clutter samples acquired from the same area and at the same time, i.e. as for the data presented here. For this purpose, Section 9 provides some initial insight to this topic.

3.5.1 Clutter models

Four main models for describing clutter analytically [9, 10, 22] can be considered. These models are widely adopted not only because they are a practical tool for describing clutter statistically, but also because they fit the reality quite well. These are: (*i*) Gaussian, generally used for ground clutter, (*ii*) K and (*iii*) Log-normal, usually describing sea clutter, and finally (*iv*) Weibull, which can model both in different conditions.

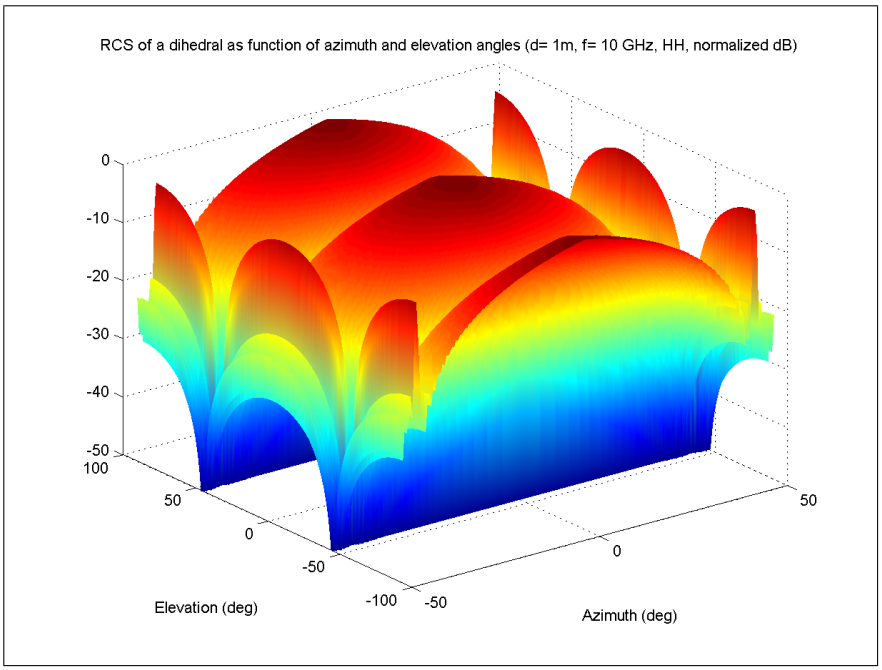

Figure 3.2: Monostatic RCS of a dihedral

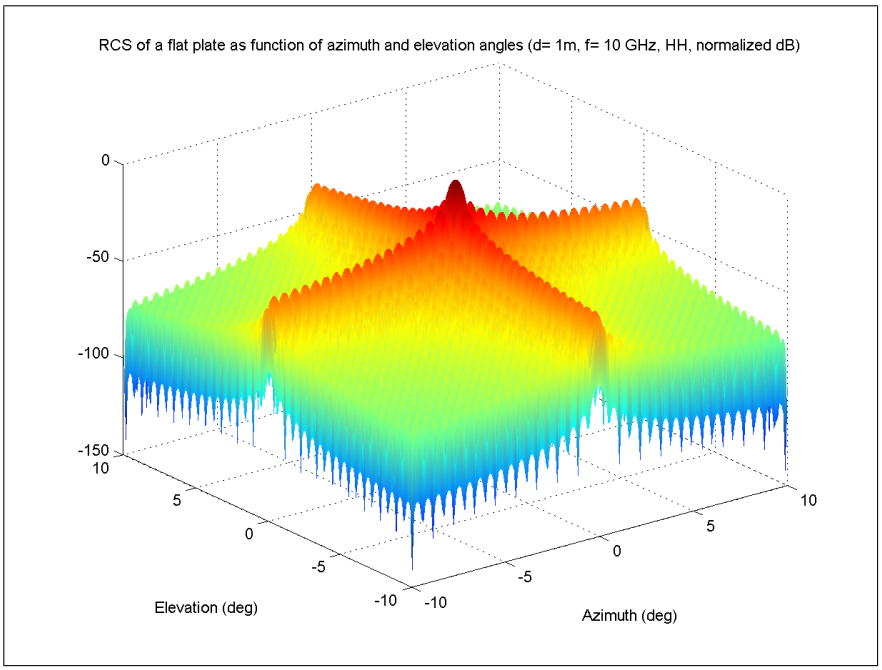

Figure 3.3: Monostatic RCS of a flat square plate

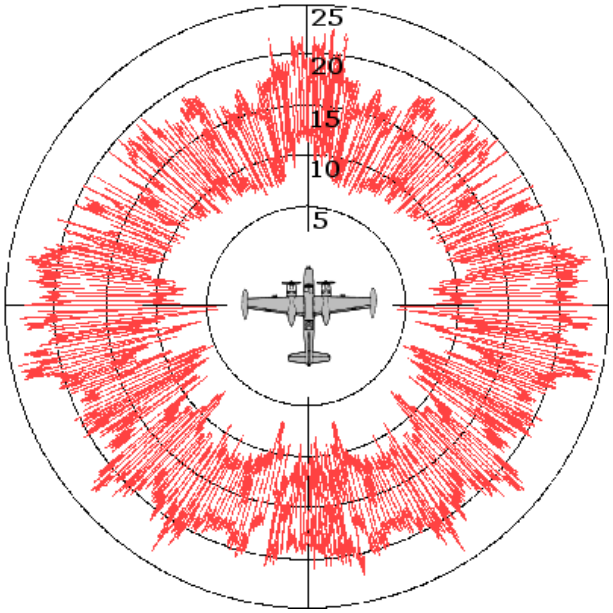

Figure 3.4: Monostatic RCS

It is widely accepted that echoes from the clutter can be written as the product of two independent random variables. Commonly it is written:

$$\mathbf{c} = \sqrt{\tau}\mathbf{x}, \tag{3.16}$$

where $\mathbf{x}$ is an m-dimensional complex Gaussian circular vector, termed 'speckle' and τ is the 'texture' and represents the power associated to the speckle. Statistically, $\mathbf{x}$ can be described as a 0-mean value vector with unit variance and correlation matrix $\mathbf{M}_x$, where clearly

$$\mathbf{M}_x = E\left\{\mathbf{x}\mathbf{x}^H\right\}. \tag{3.17}$$

Many authors use the compact writing

$$\mathbf{x} \sim CN\left\{0, \mathbf{M}_x\right\}. \tag{3.18}$$

It is worth pointing out that τ is a non-negative variable. The product

model as in equation (3.16) has been shown to describe accurately the scattering mechanism [9, 10, 11, 16, 22]. In addition, whilst for sea clutter the speckle **x** decorrelates in a short time, i.e. in the order of a few milliseconds, the texture τ decorrelates in a longer time, in the order of seconds, so within the Time On Target (TOT), τ can be considered constant [11, 22].

Therefore, the four models referred to at the beginning of this Section differ substantially. These are as in Table 3.1, where the mean value and the variance are as in the Table 3.2.

Distribution	Expression
Gaussian	$p(\tau) = \frac{\tau}{\sigma_\tau} \exp\left\{-\frac{\tau^2}{2\sigma_\tau}\right\}$
K	$p(\tau) = \frac{1}{\Gamma(\nu)} \left(\frac{\nu}{\mu}\right)^{\nu} \tau^{\nu-1} \exp\left\{-\frac{\nu}{\mu}\tau\right\}$
Weibull	$p(\tau) = \frac{\nu}{q} \left(\frac{\tau}{q}\right)^{\nu-1} \exp\left\{-\left(\frac{\tau}{q}\right)^{\nu}\right\}$
Log-Normal	$p(\tau) = \frac{1}{\sqrt{2\pi}\tau\sigma_{\log}} \exp\left\{-\frac{[\log(\tau) - T]^2}{2\sigma_{\log}^2}\right\}$

Table 3.1: Common probability density functions for the texture

Distribution	Mean	Variance
Gaussian	0	σ_τ
K	μ	$\frac{\mu^2}{\nu}$
Weibull	$q\Gamma\left(1 + \frac{1}{\nu}\right) = \mu$	$q^2\Gamma\left(1 + \frac{2}{\nu}\right) - \mu^2$
Log-Normal	$\exp\left\{T + \sigma_{\log}^2/2\right\} = \mu$	$\exp\left\{\sigma_{\log}^2 - 1\right\}\mu^2$

Table 3.2: Texture statistics

In these Tables, σ_τ and σ_{log} are the variances of the Gaussian and Log-Normal PDFs, respectively, ν is the shape parameter for both K and Weibull distributions, μ is the expected value of the K distribution, q is the scale parameter of the Weibull and finally T is the expected value of the Log-Normal PDF.

3.5.2 Spectral distribution

As reported at the beginning of this Section, clutter is generally comprised of the coherent sum of the echoes from a number of elemental scatterers. These includes leaves, drops of rain, snow flakes and/or sea waves. For the sake of simplicity, assume that the radar platform is not moving: whenever these single components move within the same range cell, they add a Doppler shifted reflection on the clutter echoes. Whereas the speed of the single elements can vary significantly, it is usually possible to describe statistically the spectrum of the clutter as a random variable with a mean value, which is dependent on the average speed of the elements, and a variance, which has been shown [3] to be a function not only of the type of clutter and its average speed, but also of a number of radar parameters such as the wavelength, the angular velocity of the antenna and its aperture. It is clear that fixed clutter, such as buildings or rocks, do not have a Doppler shift and therefore in this case the spectrum is concentrated at the frequency $f = 0$. However, in high reflectivity scenarios, the clutter sidelobes can be manifest in non-zero Doppler cells.

As a result, the spectrogram of the clutter can be spread over a number of frequencies. In addition it is possible that two or more kinds of clutter (e.g. ground and rain clutter) are present within the same range cell. In this case the spectrogram can be made up of two or more components, as in a bimodal distribution.

Typical models for describing the spectrum $S_c(f)$ of the clutter are (*i*) the Dirac function (fixed clutter), which is also the simplest and less realistic assumption, (*ii*) Gaussian, (*iii*) two-sided exponential, (*iv*) power law, (*v*) autoregressive, (*vi*) Lorentzian (i.e., autoregressive of order 1) and finally and (*vii*) Voigtian (convolution of the Gaussian and Lorentzian) [22], as reported in Table 3.3, where A is a general constant that takes into account the power of the clutter spectrum (in some formulas, for convenience, it groups other constants which are usually reported as separated), f_0 its the centroid of the spectrum, β is a constant linked to the decay of the clutter spectrum, λ is the wavelength, α is generally 2 or 3 in sea clutter modelling,

Dirac	$S_c(f) = A\delta(f)$
Gaussian	$S_c(f) = \frac{A}{\sigma_f} \exp\left\{-\frac{(f-f_0)^2}{2\sigma_f^2}\right\}$
2-sided exponential	$S_c(f) = \frac{\beta\lambda}{4} \exp\left\{-\frac{\beta\lambda}{2}\left\|f\right\|\right\}$
Power law	$S_c(f) = A/f^{\alpha}$
Autoregressive	$c[n] = \epsilon_n - \sum_{i=1}^{p} a_j c[n-j]$
Lorentzian	$S_c(f) = \frac{A}{(f-f_0)^2 + A}$
Voigtian	$S_c(f) = \frac{A}{\pi} \int_{-\infty}^{+\infty} \frac{e^{-x^2}}{\left(\frac{f-f_0}{f_V} - x\right)^2 + A^2} dx$

Table 3.3: Typical models for the clutter spectrum

p usually varies between 2 and 5, ϵ_n is white noise and finally f_V is a scale frequency for the Voigtian function.

Figure 3.5 shows an asymmetrical spectrum, which is in general typical of sea clutter, of real clutter data (HH and VV components) and the corresponding fittings with sums of a Gaussian and a Voigtian functions.

3.6 Detection approach

In reception two assumptions maybe usually considered in processing the signals: target present or target not present. This is commonly described as follows:

$$r(t) = \begin{cases} n(t), & H_0, \\ s(t-t_0) + n(t), & H_1, \end{cases} \tag{3.19}$$

where n groups all the possible non desired target signals. Under this assumption, the radar approach to signal processing consists of keeping the probability that a target is declared when it is not present as low as

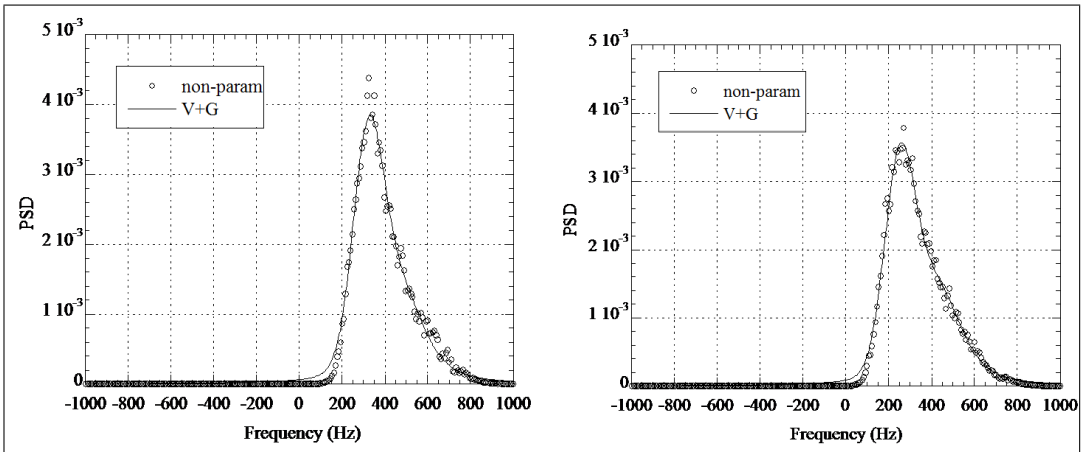

(a) HH spectrum and fitting (b) VV spectrum and fitting

Images courtesy of Prof. Maria Sabrina Greco, Università di Pisa

Figure 3.5: Clutter spectra and fittings

possible, i.e. within predetermined limits, allowing at the same time a reasonably high probability of detecting the target when it is present.

Let one assume that a detection is declared when received signal $\tilde{r}$, given by

$$\tilde{r} = r * h = (s + n) * h = \tilde{s} + \tilde{n}, \tag{3.20}$$

is greater than a given threshold θ. The symbol $*$ is representative of the convolution operator. The decision rule may be written as follows:

$$\begin{cases} |\tilde{r}|^2 \geq \theta & \Rightarrow \quad D_1 \\ |\tilde{r}|^2 < \theta & \Rightarrow \quad D_0. \end{cases} \tag{3.21}$$

Therefore in a decision process, four events are possible. These are as in Table 3.4.

Correct decisions are obviously desirable. However, as noise and the target echoes are random variables, rather than deterministic signals, incorrect decisions can be made and therefore the decision rule has to be designed to avoid them as much as possible. From a statistical point of view, then,

	H_0	H_1
D_0	Correct	Incorrect
D_1	Incorrect	Correct

Table 3.4: Decisions in the decision process

Table 3.4 can be written as Table 3.5 where the probabilities P of correct or wrong detection are expressed more explicitly.

	H_0	H_1
D_0	$P(\|\tilde{r}\|^2 < \theta \| H_0) = P(\|\tilde{n}\|^2 < \theta)$	$P(\|\tilde{r}\|^2 < \theta \| H_1) = P(\|\tilde{s} + \tilde{n}\|^2 < \theta)$
D_1	$P(\|\tilde{r}\|^2 < \theta \| H_0) = P(\|\tilde{n}\|^2 \geq \theta)$	$P(\|\tilde{r}\|^2 < \theta \| H_1) = P(\|\tilde{s} + \tilde{n}\|^2 \geq \theta)$

Table 3.5: Statistics in the decision process

Usually these probabilities are referred as:

(i) Probability of false alarm: $P_{FA} = P(|\tilde{n}|^2 \geq \theta)$ – This is the probability of declaring detection when no target is present;

(ii) Probability of detection: $P_D = P(|\tilde{s} + \tilde{n}|^2 \geq \theta)$ – This is the probability of a correct detection of a target;

(iii) Probability of missed detection: $P_{MD} = P(|\tilde{s} + \tilde{n}|^2 < \theta)$ – This is the probability of missing the detection of a target.

These probabilities can also be expressed as follows:

$$\begin{aligned} P_{FA} &= \int_{\theta}^{+\infty} p(y = |\tilde{n}|^2)\, dy, \\ P_D &= \int_{\theta}^{+\infty} p(y = |\tilde{s} + \tilde{n}|^2)\, dy, \\ P_{MD} &= \int_{0}^{\theta} p(y = |\tilde{s} + \tilde{n}|^2)\, dy \quad = \quad 1 - P_D. \end{aligned} \tag{3.22}$$

It is worth highlighting, clearly, the case of equation (3.22), the following two set of limits:

$$\begin{cases} \lim_{\theta \to 0} P_{FA} &= 1, \\ \lim_{\theta \to 0} P_D &= 1, \end{cases} \tag{3.23}$$

and

$$\begin{cases} \lim_{\theta \to +\infty} P_{FA} &= 0, \\ \lim_{\theta \to +\infty} P_D &= 0. \end{cases} \tag{3.24}$$

These limits are fundamental in radar systems, since they clearly demonstrate that it is not possible on average to achieve full detection of a target whilst keeping the number of false alarms moderate. Alternatively, it is not possible to avoid completely false alarms still being able to detect targets.

As a consequence, in radar systems it is common to use the Neyman-Pearson criterion, which consists of (*i*) fixing a threshold θ so to constrain the P_{FA} within a predetermined value and at the same time (*ii*) minimizing the P_{MD}, i.e. maximizing the P_D. Whereas

$$|\tilde{s} + \tilde{n}|^2 \leq (|\tilde{s}| + |\tilde{n}|)^2 = |\tilde{n}|^2 \left(\sqrt{SNR} + 1 \right)^2 \tag{3.25}$$

and

$$|s + n|^2 \geq (|\tilde{s}| - |\tilde{n}|)^2 = |\tilde{n}|^2 \left(\sqrt{SNR} - 1 \right)^2, \tag{3.26}$$

maximizing the SNR increases the P_D. For this purposes, a matched filter as described in 3.1 is usually employed. A detector with a limited P_{FA} is usually termed as guaranteeing the CFAR (Constant False Alarm Rate) condition. From a mathematical point of view, it can be shown that the Neyman Pearson approach is a problem of constrained optimization using a Lagrange multiplier, say ξ. The rule can be expressed as [3]

$$\max_{\theta} \left\{ P\left(|\tilde{r}|^2 \geq \theta | H_1 \right) - \xi \left[P\left(|\tilde{r}|^2 \geq \theta | H_0 \right) - P_{FA} \right] \right\}. \tag{3.27}$$

The most used CFAR techniques are the LRT (Likely Ratio Test), its more general version GLRT (Generalized LRT) and the CA-CFAR (Cell

Average CFAR). The first two rules decide according to

$$\frac{p\left(\tilde{r}|H_1\right)}{p\left(\tilde{r}|H_0\right)} \underset{H_0}{\overset{H_1}{\gtrless}} \theta_{LRT} \tag{3.28}$$

in the LRT case or to

$$\frac{\max\limits_{P}\left\{p\left(\tilde{r}|H_1\right)\right\}}{\max\limits_{P}\left\{p\left(\tilde{r}|H_0\right)\right\}} \underset{H_0}{\overset{H_1}{\gtrless}} \theta_{GLRT} \tag{3.29}$$

in the GLRT case, where each pdf is maximized using the parameters on which P depends. The CA-CFAR will be described and used in Chapter 6.

Other decision rules, such as the MEP (Minimum Error Probability) and the Bayes minimum risk, are widely described in literature of decision theory, but are rarely applied in radar systems. In particular, the MEP minimizes the following total error probability of error P_E:

$$P_e = P\left(H_0\right)P\left(D_1|H_0\right) + P\left(H_1\right)P\left(D_0|H_1\right), \tag{3.30}$$

i.e. the sum of P_{FA} and P_{MD}, weighted with the probability of the events H_0 and H_1, respectively. Whereas

$$P\left(D_0|H_1\right) = P_{MD} = 1 - P_D = 1 - P\left(D_1|H_1\right), \tag{3.31}$$

equation (3.30) can be rewritten as

$$\begin{aligned} P_E &= P\left(H_0\right)P\left(D_1|H_0\right) + P\left(H_1\right)\left(1 - P\left(D_1|H_1\right)\right) = \\ &= P\left(H_1\right) + \left\{P\left(H_0\right)P\left(D_1|H_0\right) + P\left(H_1\right)P\left(D_1|H_1\right)\right\} = \\ &= P\left(H_1\right) + \left\{P\left(H_0\right)P_{FA} + P\left(H_1\right)P_D\right\}. \end{aligned} \tag{3.32}$$

By minimizing the part in curly brackets, this criterion is equivalent to the Neyman-Pearson's when $P\left(H_0\right)$ and $P\left(H_1\right)$ are known and equal to $\frac{1}{2}$. However, since this is not always the case in radar system and the two

latter probabilities are unknown, this detector, although efficient, is not commonly used.

Similarly The Bayer minimum risk is uncommon. This detector tries to minimize the following cost function C:

$$C = \sum_{i=0}^{1} \sum_{j=0}^{1} C_{i,j} P\left(H_j\right) P\left(D_i | H_j\right). \tag{3.33}$$

Whereas the costs of correct decisions cannot be different from 0, i.e. $C_{0,0} = C_{1,1} = 0$, the cost function can be reduced to

$$\begin{aligned} C &= C_{1,0} P\left(H_0\right) P\left(D_1 | H_0\right) + C_{0,1} P\left(H_1\right) P\left(D_0 | H_1\right) = \\ &= C_{1,0} P\left(H_0\right) P_{FA} + C_{0,1} P\left(H_1\right) P_{MD}, \end{aligned} \tag{3.34}$$

which is a generalized version of the MEP detector.

Finally, it has to be pointed out that in more general terms the decision rule can be more complicated. A generalized expression can be

$$\begin{aligned} f\left(\tilde{\mathbf{r}}\right) \geq \theta\left(\tilde{\mathbf{r}}\right) &\Rightarrow D_1 \\ f\left(\tilde{\mathbf{r}}\right) < \theta\left(\tilde{\mathbf{r}}\right) &\Rightarrow D_0, \end{aligned} \tag{3.35}$$

where $\mathbf{r}$ is a vector or a matrix comprised of either a number of received signals at different pulses, ranges or elementary antennas (the latter within the same array) and $f(\mathbf{x})$ and $\theta(\mathbf{x})$ are arbitrary (but appropriate) functions of $\mathbf{x}$.

This Chapter the elementary concepts of radar systems have been presented. The information presented is a starting point to understand the basic concepts of the investigation of the rest of this work.

Chapter 4

Systems types

Recently the idea that a radar network can offer improved and more versatile performance has been progressively developed (e.g. from [29] to [40]). A radar network usually consists of a number of transmitters and receivers that can be co-located or not. Although a robust synchronization has to be performed and an increased quantity of data has to be jointly processed, the potential achievable benefits can be worth these efforts. These are, for example, (*i*) an improved detection capability due to multistatic scintillation of the target, that enhance the possibilities of getting one or more sharp echoes from the target, (*ii*) joint estimation of the target position and DOA (Direction Of Arrival), that increases the accuracy of location over a single nodes and, consequently, (*iii*) the potential capability of resolving multiple targets within a single resolution cell compared to a single node, (*iv*) increased information using the same bandwidth occupation and (*v*) increased ECCM (Electronic Counter Counter Measures) capabilities due to the physical and electronic vulnerability.

In this Chapter the processing approaches considered in this thesis are reported. These are:

(*i*) MIMO approach, which operates incoherently,

(*ii*) Netted Radar approaches (NR and RPNR), operating coherently and finally

(*iii*) Decentralized Radar Network (DRN) approach, operating as the sum of single devices.

These concepts are to be described as in Sections 4.1, 4.2 and 4.3. To provide a well-known benchmark, these systems will be compared throughout this thesis against a monostatic radar. As a result the same total amount of ERP (Effective Radiated Power) has been assigned to the transmitting antennas, regardless of their number. Unless specified, the reference setup can be schematically represented as in Figure 4.1. Here it is possible to see that radars are scattered in space and transmit their own waveform, so that it would be possible to distinguish signals after receive. Sections 4.4 and 4.5 describe an alternative way of exploiting diversity: here the spatial diversity is exchanged with frequency diversity. As seen in the following Chapter, the results when bandwidths do and do not overlap will be only briefly examined in this work. However, this will lead to further considerations about the achievable improvements when any kind of diversity is introduced in the system.

Each antenna points at the target from a different aspect angle, so that the measurement of RCS into a certain receiver can differ from the other measurements by several dB or more, i.e. independent spatial samples of the scattering from the target are obtained. In previous work, e.g. [1, 3] the target RCS model has been assumed to be noise-like. This is a questionable assumption but provides a useful jump off point from previously published research.

The mathematical description for Sections 4.1, 4.2 and 4.3 is formulated as follows. The received signal $r_k(t)$ can be expressed as:

$$r_k(t) = \sum_{m=1}^{M} \alpha_{k,m}(t)\, s_m\left(t - \frac{R_{m,k}}{c}\right) + n_k(t), \tag{4.1}$$

supposing $s_m(t)$ is the m^{th} transmitted signal, $n_k(t)$ is white Gaussian noise, $R_{m,k}$ the distance covered by the signal, and

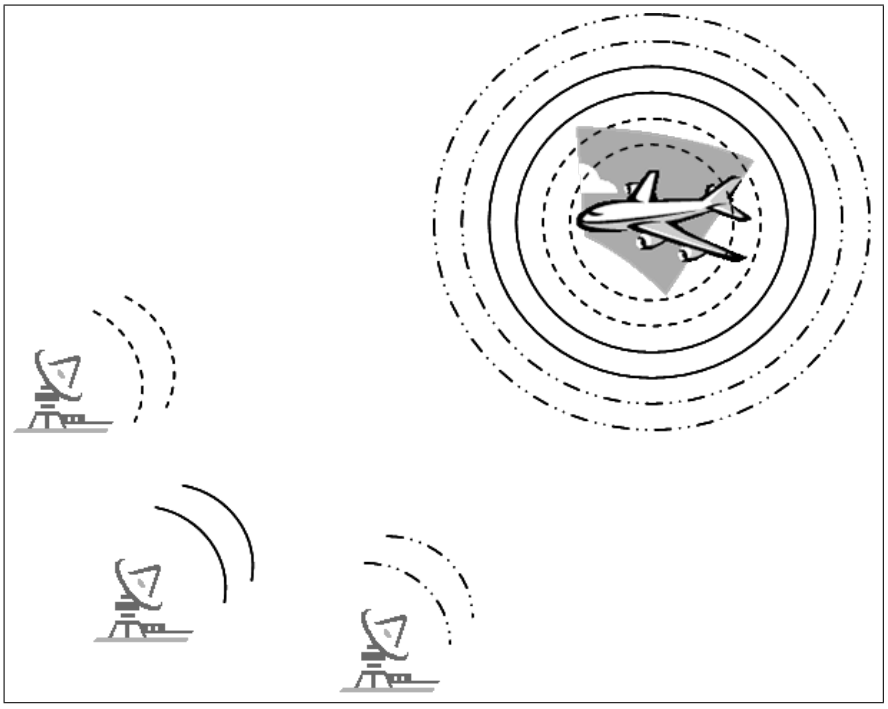

Figure 4.1: MIMO spatial diversity, NR and DRN configuration

$$\alpha_{k,m}(\sigma) = \sqrt{\frac{P_t}{M}} \sqrt{\frac{G_{tx} G_{rx} \lambda^2 \sigma}{(4\pi)^3 R_{m-ta}^2 R_{ta-k}^2}} \exp\left\{-j \frac{2\pi R_{m,k}}{\lambda}\right\} \tag{4.2}$$

is a coefficient including the amplitude and the phase of the received signal, where G_{tx} and G_{rx} are respectively the gains of the transmitting and receiving antennas, σ the RCS of the target, P_t the transmitted power, R_{m-ta} and R_{ta-k} the distance tx-target and target-rx respectively. From equation (4.1) it is clear that the autocorrelation of the received signal will be made up of four terms, these are:

1. sum of the auto-correlations $R_{s,m}(\tau)$ of the transmitted waveforms, where *s,m* stands for the m^{th} signal, i.e. $\sum_{m=1}^{M} \|\alpha_{k,m}(\sigma)\|^2 R_{s,m}(\tau)$,
2. the sum of the cross-correlation between two of the transmitted waveforms, i.e. $\sum_{m=1}^{M} \sum_{\substack{n=1 \\ n \neq m}}^{M} \alpha_{k,m} \alpha_{k,n}^{*} R_{m,n}(\tau + \tau_{m,n,k})$, where $\tau_{m,n,k}$ takes into

account the difference in the paths,

3. the sum of the cross-correlation between the transmitted waveforms and the noise, i.e. $\sum_{m=1}^{M} \alpha_{k,m}(\sigma)\, s_m\left(t - \frac{R_{m,k}}{c}\right) \times n_k(t)$, and finally
4. the auto-correlation of the noise, i.e. $\sigma_n^2 \delta(\tau)$, where $\delta(\tau)$ is 1 for $\tau = 0$, 0 otherwise.

So, all together, it is possible to write the auto-correlation of the received signal as

$$\begin{aligned} R_k(\tau) &= r_k(t) \times r_k(t) = \\ &= \sum_{m=1}^{M} \|\alpha_{k,m}(\sigma)\|^2 R_{s,m}(\tau) + \sum_{m=1}^{M} \sum_{\substack{n=1 \\ n \neq m}}^{M} \alpha_{k,m} \alpha_{k,n}^{*} R_{m,n}(\tau + \tau_{m,n,k}) + \\ &+ \sum_{m=1}^{M} \alpha_{k,m}(\sigma)\, s_m\left(t - \frac{R_{m,k}}{c}\right) \times n_k(t) + \sigma_n^2 \delta(\tau), \end{aligned} \tag{4.3}$$

where $\times$ is the correlation operator, function of the time delay τ . As the received signal is processed in each receiver through a bank of filters that are matched to the different waveforms, it makes more sense to express the result of the cross-correlation of the received signal with one, say the m^{th}, of the transmitted waveforms. This is:

$$\begin{aligned} r_k(t) \otimes s_m(t) &= \\ = \alpha_{k,m} R_m(t) + \alpha_{k,m} R_{m,n}(t + \tau_{m,n,k}) + n_k(t) \otimes s_m\left(t - \frac{R_{m,k}}{c}\right) \end{aligned} \tag{4.4}$$

The two latter elements in equation (4.4) represent the noise in the processing scheme. Apart from the term directly dependant from the noise/jamming present in reception, this equation highlights how the use of low-cross-correlation codes is vital for the system concept in order not to affect the discrimination of the transmitted waveforms and therefore

to lose all the benefits of multistatic data collection. This aspect has been treated in [30, 32]

4.1 Spatial MIMO system

MIMO radar does not have a strict definition. The MIMO spatial diversity model that will be described is a form of MIMO that has appeared in the literature [53, 54, 55] and hence provides a useful start point for these studies. This form of MIMO radar system exploits measurements of independent samples of target scattering as the basis for improving the probability of detection. Data are processed incoherently and in a centralized architecture, i.e. there is a central processing unit collecting the receiver outputs from all the nodes and returning a decision about the presence or absence of a target.

4.2 Netted radar systems

Two other models that have been developed have the same physical layout as the spatial diversity MIMO but instead use conventional coherent processing.

In these systems the received signals are processed coherently. As the model of the received signal is the same as in equation (4.1), the results of processing after filtering are the same as those in equation (4.4). In this research, two different kinds of netted radar are considered: the first one is termed "coherent Netted Radar", while the second one is the "Re-Phased coherent Netted Radar".

4.2.1 The coherent netted radar

This system obtains the same samples of the spatial MIMO radar system, but sums them coherently. We examine this not as a MIMO concept but to provide a means of comparison. The phases of the incoming signals are

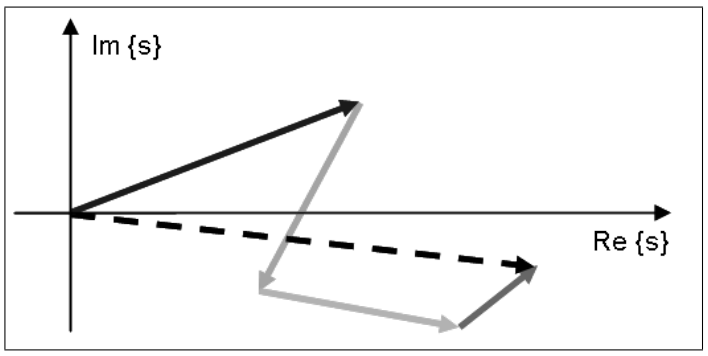

Figure 4.2: The coherent netted radar integration

in this case highly correlated, as they depend from the target's position and the geometry of the system. Yet it is well known that the phase wraps every half wavelength, so, given that the position of the target cannot be measured with this accuracy, the signals apparently have uncorrelated phases uniformly distributed between $-\pi$ and π . In Figure 4.2 it is shown what happens if 4 signals are coherently summed without processing the phases. In this case the phases results to be uniformly distributed and the overall coherent sum is a signal whose amplitude is much smaller than the sum of the amplitudes of the single elements. In the extreme case, when the amplitude is constant and the sum of the phases is 2π, it is possible to cancel the signal completely. As shown in the next sections, in such conditions this processing will provide us with the lower bound limit for the performance, as its SNR after integration will be statistically the same as in a single pulse case.

4.2.2 The re-phased coherent netted radar

This system gets the same samples as the previous one, but it performs a re-phasing of the vectors according to the exact position of the target in order to maximize the signal-to-noise ratio (Figure 4.3) and subsequently the achieved performance. This assumes perfect knowledge of the 3-D location of the target and that it has a single phase centre, which are conditions unlikely to be found in practice. However, if the phases of

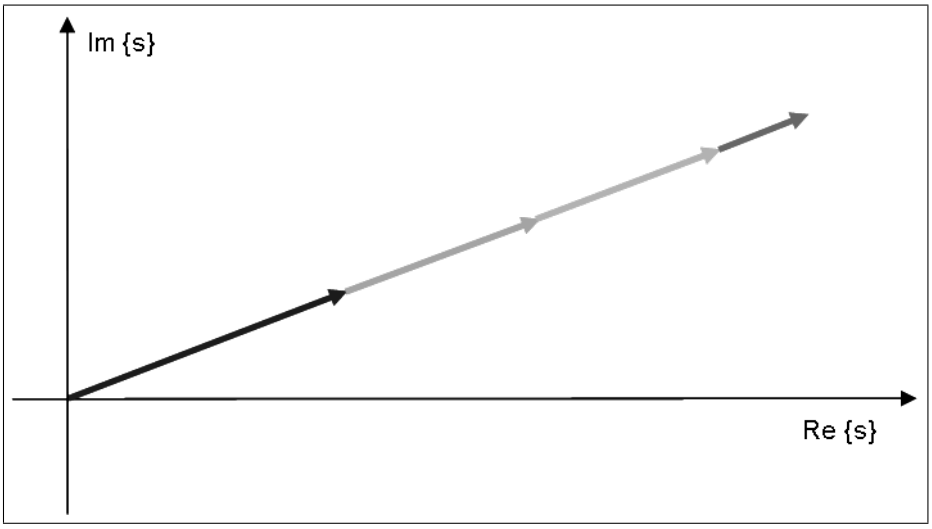

Figure 4.3: The re-phased coherent netted radar integration

the signals in Figure 4.2 can be opportunely re-aligned, the amplitude of their sum is the biggest possible. This system therefore provides the upper bound limit for the performance as it maximizes the signal to noise ratio. It is considered in order to see what the losses of the MIMO processing are.

4.3 Decentralized radar Network

In this Section a different sub-optimum strategy is applied to a radar network. This represents another possible alternative to MIMO and NR processing for radar networks. Whilst the radar network operates in the same geometry of MIMO and NR systems, it is here considered as being made of all the possible mono/bistatic radars working separately in a first stage and consequently fusing the results together. The processing therefore consists of two parts. Firstly, detection is extracted from the signals for each of the mono/bistatic cases, i.e. in a decentralized pre-processing. Secondly all the decisions are jointly fused, so the system can provide a final output.

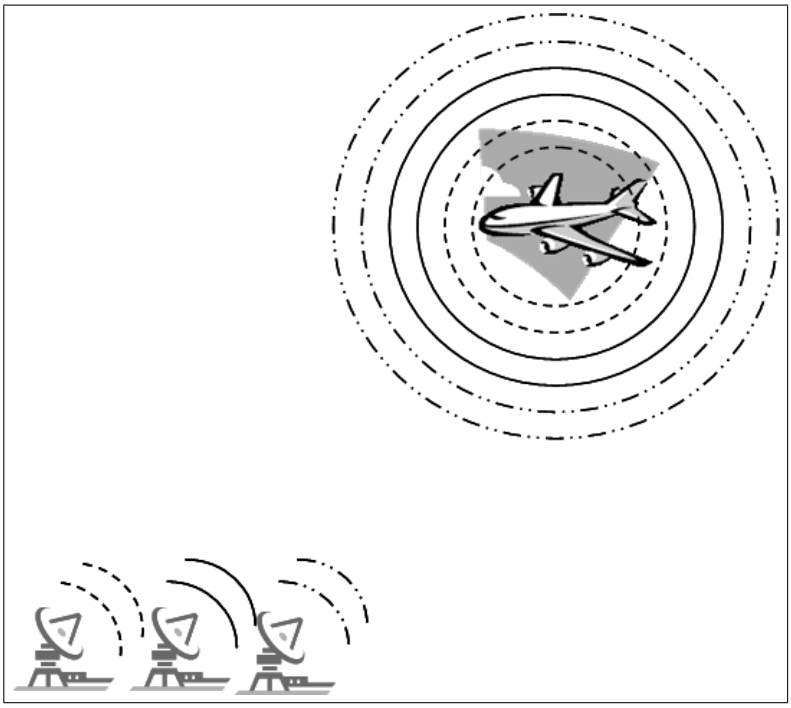

Figure 4.4: Frequency MIMO diversity and configuration

4.4 Frequency MIMO system

Here we introduce a different form of MIMO radar that attempts to exploit frequency rather than spatial diversity. The principle relies on the simultaneous transmission of multiple independent frequencies from each element of an array antenna as shown schematically in Figure 4.4. This has the advantage of being able to use the MIMO technique in a compact single radar site form.

The bands and the carrier frequencies of the M transmitted signals have to be chosen such that they do not overlap and are not adjacent, in order to (*i*) get independent measurements of the RCS of the target after an appropriate matched filtering and to (*ii*) avoid the Doppler-shifted spectra of the received signals to overlap. Clearly, this will be dependent on the complete target scattering function (i.e. over all angles, frequencies and polarizations). This concept is not too different from the 'frequency diversity' [75]. Mathematically we have:

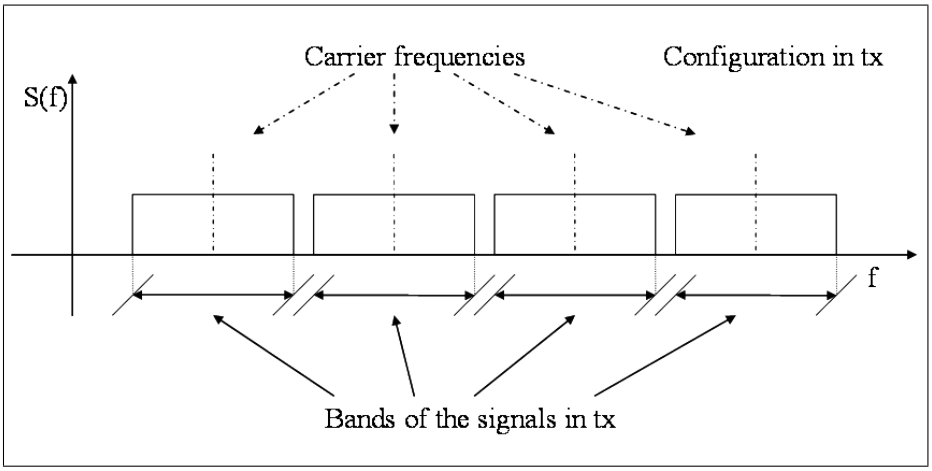

Figure 4.5: frequency MIMO diversity model

$$r_k(t) = \sum_{m=1}^{M} \alpha_k(\sigma, f_m)\, s_m\left(t - \frac{R_{m,k}}{c}\right) + n_k(t), \tag{4.5}$$

supposing f_m to be the carrier frequency of the m^{th} signal,

$$\alpha_{k,m}(\sigma, f_m) = \sqrt{\frac{P_t}{M}} \sqrt{\frac{G_{tx} G_{rx} \lambda_m^2 \sigma(f_m)}{(4\pi)^3 R_{m-ta}^2 R_{ta-k}^2}} \exp\left\{-j\frac{2\pi R_{m,k}}{\lambda_m}\right\} \tag{4.6}$$

a coefficient including the amplitude and the phase of the received signal, (σ, f_m) the RCS of the target at f_m and all the other symbols meaning as in equation (4.1). Due to the separability in frequency, signals can therefore be distinguished through M adequate band-pass filters, after which standard matched filtering can be applied.

4.5 Frequency Diverse Array

The Frequency Diverse Array (FDA) concept has been developed starting from the Frequency MIMO. As in the previous Section, the effects of transmitting the same signal on different frequencies are investigated. It is well known that the use of different frequencies in transmission can improve the detection and the classification of targets, as it decorrelates

clutter, provides a better estimate of a target's mean echo strength and provides a sampling of the frequency response of the target. In these examples the carrier frequencies are far from one another such that the bandwidths of the signals do not overlap.

Here, although each element still transmits at a different frequency, the frequencies are set extremely close with one another. In fact, the difference between two consecutive frequencies is in the order of a few kHz, whilst the carrier is in the order of GHz. As a result, here it is not expected to have an increase of the performance due to the exploitation of frequency diversity, whereas the frequency response is assumed to be the same for each transmitted antenna, due to the negligible difference in the wavelengths.

In other words, manipulating the concept of the Frequency MIMO, through this system the effects in transmission and propagation of a transmitted signal consisting of equally-spaced frequencies relatively close to one another are investigated. This concept has been explored from [76] to [81] only and it is a brand new topic which is attracting interest from the technical community.

It is here anticipated that the results of this concept are completely different from those presented in the rest of the thesis. As a consequence, these are reported in a separate Chapter (Chapter 11), together with a formalization of the concept and possible developments of this technique. Figures 4.6 and 4.7 are a first schematic outline of this concept. In its most simple form one can envisage an array antenna [71] where the different elements comprising the array carry signals with differing frequencies as in Figure 4.7. In particular, in the latter Figure it has to be pointed out that the distance from the target of the k^{th} element, i.e. $R_0 + kd \sin\theta$ (where d is the distance between 2 consecutive elements) generates a phase shift which is function of the k^{th} frequency. As shown in Chapter 11, this in turns generates a range-angle dependant pattern.

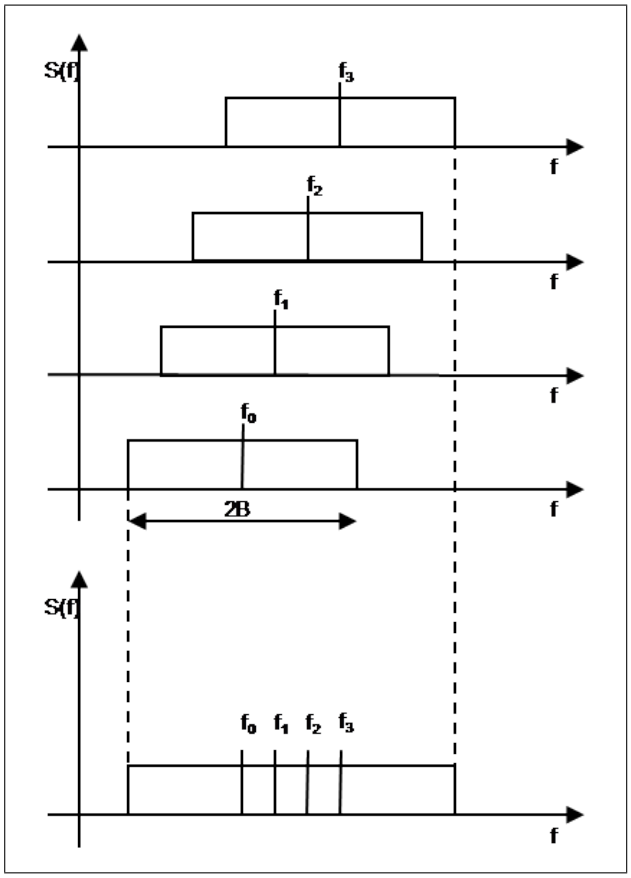

Figure 4.6: The FDA concept

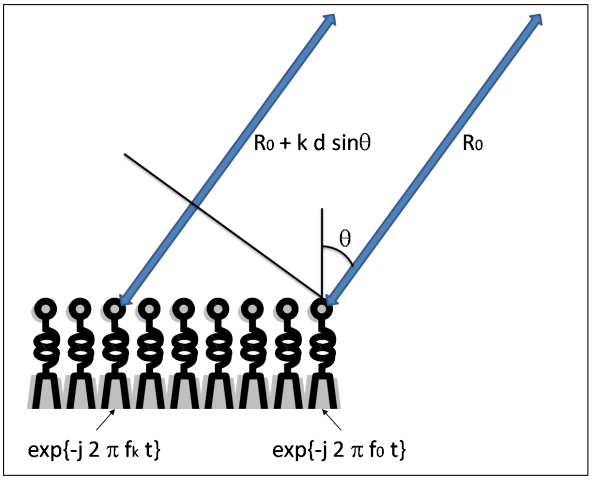

Figure 4.7: An example of FDA

Chapter 5

Detection performance

In this Chapter the performance of the first four radar system concepts described previously are reported. In order to get a fair comparison, the same power in transmission is provided to the system. This means that systems with a lower number of nodes[1] have an increased available power per node. In other terms, if the total power available is P, each of the M transmitters is provided with a power $\frac{P}{M}$. Furthermore, in comparing the frequency MIMO to the other systems, the same number of transmitters has been considered. Thus, in approaching the frequency MIMO performance, the same configuration of the spatial MIMO has been taken into account, relocating all the nodes in the same position and trading spatial diversity with frequency diversity.

5.1 False Alarm Rate

Here the P_{FA} against threshold is investigated in the case where only white Gaussian noise with zero mean value and normalized variance is input to the receivers.

[1] In this thesis any path between a transmitter and a receiver is termed "node". This implies that, for instance, a network made up of 2 transceivers is considered as formed of 4 nodes. As well, 1 transmitter and 4 netted receivers comprise a network of 4 nodes. Unless otherwise specified, transmitters, receivers and transceivers are in this thesis called "devices".

5.1.1 MIMO

When only white noise comes into the receivers, spatial MIMO performs the incoherent summation of a number of samples and compares them with a threshold. The same process is made by frequency MIMO. Here the only difference is that the noise affecting the spatial MIMO system has an equivalent bandwidth centered on the only carrier frequency, while the one affecting the frequency MIMO system is centered on the many carrier frequency used. When the equivalent noise bandwidth and the spectrum of the noise (here supposed white) are the same for both spatial and frequency MIMO cases and the same number of signals are processed, the overall incoming noise power is statistically the same and consequently spatial and frequency MIMO perform equally.

From a mathematical point of view, given the complex noise n_k at the output of any of the matched filters and when no target is present, the overall noise power[2] can be written as

$$\begin{aligned} \sigma^2_{n,MIMO} &= \|\mathbf{n}\|^2 = \mathbf{n}^H\mathbf{n} = \\ &= \sum_{k=1}^{MN} |n_k|^2 = \sum_{k=1}^{MN} \sigma_k^2, \end{aligned} \tag{5.1}$$

where MN is the number of processed signals.

In addition, we term x_k and y_k the I&Q noises each one independently Gaussian-distributed with mean value 0 and standard deviation σ. Consequently the PDF of n_k can be expressed as the joint PDF $p(x_k, y_k)$ and it is:

[2]It seems appropriate to highlight here that in this thesis the radar convention of expressing the power of a vector/signal applies. In particular, this implies that the energy and the power are defined in the same way, assuming an implicit normalization of 1Ω (Ohm) in the latter case.

$$p(n_k) = p(x_k, y_k) = p(x_k)p(y_k) = \\ = \frac{1}{\sqrt{2\pi\sigma_k^2}} \exp\left\{-\frac{x_k^2 + y_k^2}{2\sigma_k^2}\right\}. \tag{5.2}$$

Thus in amplitude this results in a Rayleigh distribution $\rho_k = \sqrt{x_k^2 + y_k^2}$ with PDF:

$$p(\rho_k) = \frac{\rho_k}{\sigma_k^2} \exp\left\{-\frac{\rho_k^2}{2\sigma_k^2}\right\}, \tag{5.3}$$

that in power $w = \rho_k^2$ becomes an exponential:

$$p(w_k) = \frac{1}{2\sigma_k^2} \exp\left\{-\frac{w_k}{2\sigma_k^2}\right\}, w_k \geq 0 \tag{5.4}$$

For the sake of simplicity, this expression is modified in

$$p(t_k) = \exp\{-t_k\}\, u(t_k), \tag{5.5}$$

i.e. the following transformation is applied

$$t_k = \frac{w_k}{2\sigma_k^2} \tag{5.6}$$

to equation (5.4) and the function

$$u(t) = \begin{cases} 0, & t < 0 \\ 1, & t \geq 1 \end{cases} \tag{5.7}$$

is introduced. This is equivalent to considering each noise having unit power.

When MIMO processing is applied, the sum of the random variables is in power and not in amplitude and phase. This means that the PDF of the power of 2 signals, say $\tau = |n_1|^2 + |n_2|^2$, can be expressed from equation (5.5) as

$$
\begin{aligned}
p(\tau) = p(t) * p(t) = \\
&= \int_{-\infty}^{+\infty} p(t)p(\tau - t)\, dt = \\
&= \int_{-\infty}^{+\infty} \exp\{-t\}u(t) \exp\{-(\tau - t)\}u(\tau - t)\, dt = \\
&= \int_{0}^{\tau} \exp\{-t\} \exp\{t - \tau\}\, dt = \\
&= \int_{0}^{\tau} \exp\{-\tau\}\, dt = \\
&= \exp\{-\tau\} \int_{0}^{\tau} dt = \\
&= \tau \exp\{-\tau\}u(\tau).
\end{aligned} \tag{5.8}
$$

Therefore the distribution resulting from the sum of the power of two noise signals is a Rayleigh. Applying this process MN times, the PDF of the sum of MN noise power $\tau = \sum_{k=1}^{MN} |n_k|^2$ is distributed as follows:

$$
p(\tau) = \frac{\tau^{MN-1}}{(MN-1)!} \exp\{-\tau\}\, u(\tau), \tag{5.9}
$$

i.e. with a Poisson distribution. This distribution of power, as in many works published so far [82], can be represented as a chi-squared with $2MN$ degrees of freedom:

$$
p(\zeta) = \frac{\zeta^{n/2-1}}{2^{n/2}\Gamma(n/2)} \exp\left\{-\frac{\zeta}{2}\right\} u(\zeta), \tag{5.10}
$$

with $n = 2MN$. Introducing this value in equation (5.10), it becomes

$$
\begin{aligned}
p(\zeta) = \frac{\zeta^{MN-1}}{2^{MN}\Gamma(MN)} \exp\left\{-\frac{\zeta}{2}\right\} u(\zeta) = \\
= \frac{\zeta^{MN-1}}{2^{MN}(MN-1)!} \exp\left\{-\frac{\zeta}{2}\right\} u(\zeta).
\end{aligned} \tag{5.11}
$$

Finally the two expressions in equations (5.9) and (5.10) are exactly the same when the change of variables $\tau = \frac{\zeta}{2}$ is applied. This transformation is necessary in order to reduce the mean value of the equations (5.11) from $2MN$ to MN that is the expected value, since we sum MN noise samples with unit variance (power).

Figure 5.1 show the threshold required to achieve a chosen FAR for a variety of numbers of overall processed signals. In particular, it shows that the more the nodes, the more the signals, the bigger the noise power added up and, as a consequence the higher the threshold required to guarantee a fixed FAR. As seen in the next Section, this is a common characteristic of centralized systems.

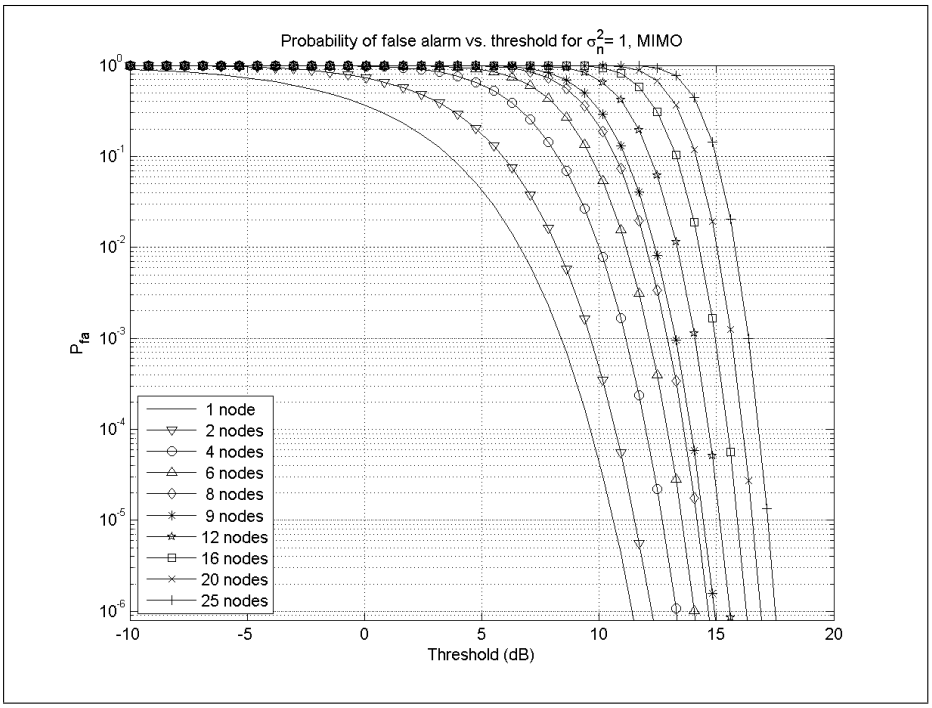

Figure 5.1: The MIMO diversity P_{FA} performances

5.1.2 NR and RPNR

When no target is present, the processing of NR and RPNR is the same. The coherent netted radar cannot align the phases of the signals coming from

the target, so the two systems achieve the same results. As consequence of these, only the NR is examined here.

The overall noise affecting the NR processing can be written as

$$\begin{aligned}\sigma^2_{n,NR} &= \left|\sum_{k=1}^{MN} n_k\right|^2 = \sum_{k=1}^{MN} n_k^H \sum_{k=1}^{MN} n_k = \\ &= \sum_{k=1}^{MN} |n_k|^2 + \sum_{k=1}^{MN} n_k^H \sum_{k=1}^{MN} n_k = \\ &= \sum_{k=1}^{MN} \sigma_k^2 + 2\mathrm{Re}\left\{\sum_{k=1}^{MN-1}\sum_{h=k+1}^{MN} n_k^H n_h\right\} = \\ &= \sigma^2_{n,MIMO} + 2\mathrm{Re}\left\{\sum_{k=1}^{MN-1}\sum_{h=k+1}^{MN} n_k^H n_h\right\}. \end{aligned} \tag{5.12}$$

It is then clear that, even when the NR's noise samples are statistically independent and the mean values of noise are the same in both systems, an extra variance has to be considered in the PDF of the noise power of the NR when comparing equation (5.1) with (5.12). This extra variance leads to an increased probability that noise is detected as a target for a given threshold.

Looking at the problem from a statistical point of view, an even deeper understanding can be provided. Proceeding as in the previous Section and using the same symbols, when NR processing is applied, it can be easily shown that the PDF resulting from the coherent summation of MN noise-variables is a complex Gaussian with variance MN times bigger than the original one. Consequently the PDF of the resulting power can be expressed as:

$$p(\hat{t}) = \frac{1}{MN}\exp\left\{-\frac{t}{MN}\right\}u(t), \tag{5.13}$$

where $\hat{t} = \left|\sum_{k=1}^{MN} n_k\right|^2$.

Figure 5.2 shows the FAR as a function of the threshold for a variety of numbers of overall processed signals. Fixing the FAR to a certain value and comparing this Figure with 5.1, say 10^{-6}, it is shown here that MIMO systems have a performance advantage over coherent networks as a smaller threshold is required to achieve the same rate. The advantage achieved by the MIMO system is due to the incoherent processing of the signals effectively reducing the variability in the total received signal hence enabling a lower threshold to be set, i.e. the total noise power contributing to the detection decision is lower in the MIMO systems than in the netted ones: the coherent netted case requires a threshold of some 3 to 8 dB more to achieve an equivalent level of performance. The reduced threshold set with incoherent processing gives, as seen in this Chapter, an increased sensitivity to MIMO systems when used for detection.

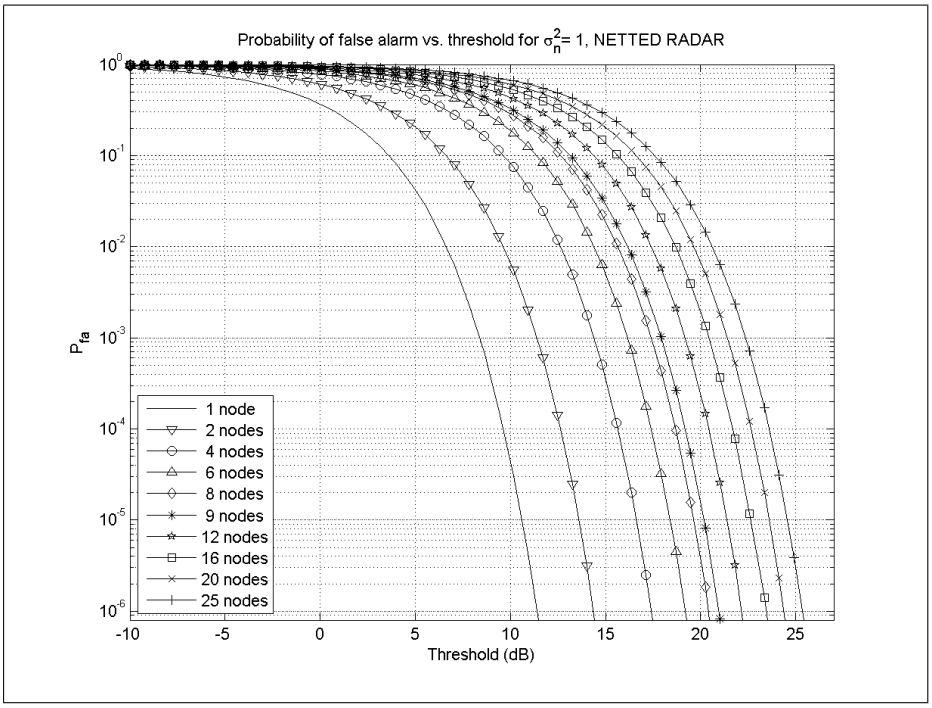

Figure 5.2: The NR diversity P_{FA} performances

In addition, equation (5.13) explains why the curves in Figure 5.2 have exactly the same shape and the only difference is a shift on the x-axis. Actually they are the realization of the same PDF apart from a different

variance. Furthermore the distance, measured on the x-axis, between a certain curve and the monostatic one is exactly MN converted to dB.

Comparing equations (5.9) and (5.13), it is clear that asymptotically whilst the distribution of the power in a MIMO system decays with an exponential coefficient, the distribution of the power in NR systems decays with the same coefficient divided by the number of nodes, i.e. more slowly. In evaluating the FAR, this allows a lower threshold to be set for the incoherent case. As known, in turns lower thresholds allow to discriminate a target also for reduced SNR, which obviously impacts on the detection capability of the system. Therefore fixing a certain threshold for both systems, say λ, the NR's and the MIMO P_{FA} can be expressed respectively as:

$$\begin{aligned} p_{FA_{NR}} &= \int_{\lambda}^{+\infty} \frac{1}{MN} \exp\left\{-\frac{t}{MN}\right\} dt = \\ &= \exp\left\{-\frac{\lambda}{MN}\right\}, \end{aligned} \tag{5.14}$$

and

$$\begin{aligned} p_{FA_{MIMO}} &= \int_{\lambda}^{+\infty} \frac{t^{MN-1}}{(MN-1)!} \exp\{-t\} = \\ &= \exp\{-\lambda\} \sum_{k=0}^{MN-1} . \frac{\lambda^k}{k!} \end{aligned} \tag{5.15}$$

Figures 5.3 and 5.4 show the distributions in equations (5.9) and (5.13) for 4 and 25 nodes. As it can be seen here, the PDFs differ considerably in the two cases.

5.1.3 DRN

In a DRN, assuming as usual and for the sake of simplicity that the noise after every matched filter has the same statistics, the thresholds for all

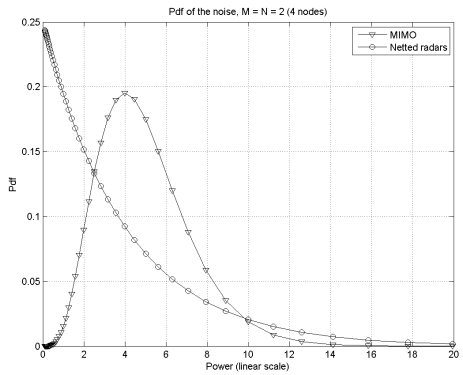

(a) 4 nodes, linear scale

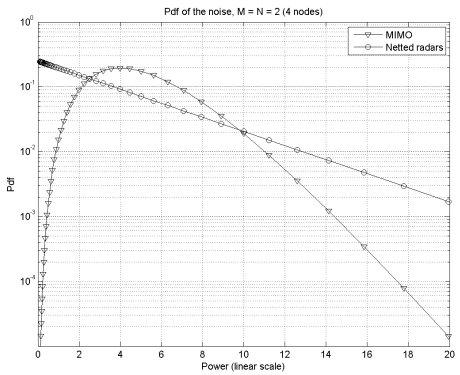

(b) 4 nodes, logarithmic scale

Figure 5.3: PDF of the noise power in MIMO and NR

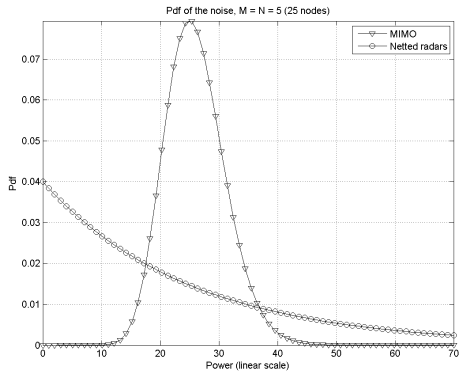

(a) 25 nodes, linear scale

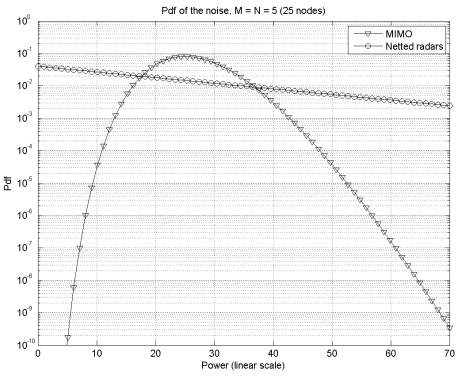

(b) 25 nodes, logarithmic scale

Figure 5.4: PDF of the noise power in MIMO and NR

the nodes are set to the same value in order to guarantee the same FAR. After each mono/bistatic decision has been taken, a vector **v**, containing the detection results from all the nodes is available for the second stage of processing. Obviously, each element of **v** is either 0 or 1. At this point the decision rule assumes that the target is present when L elements of the vector are set at 1. The number of L can vary according to the specifications of the system. Thus the decision rule is as follows:

$$\sum_{k=1}^{MN} v[k] \geq L. \tag{5.16}$$

From a statistical point of view, if each element of **v** is independent from the others and each value '1' occurs with a probability P, the overall probability that equation (5.16) is verified is given by the following binomial function:

$$P\left(\sum_{k=1}^{MN} v[k] \geq L\right) = \sum_{k=L}^{MN} \binom{MN}{k} P^k (1-P)^{MN-k} \tag{5.17}$$

where

$$\binom{h}{k} = \frac{h!}{k!\,(h-k)!} \tag{5.18}$$

is the binomial coefficient that takes into account all the permutations of the possible positions of '1' in **v**.

From a radar point of view the P_{FA} of the overall system can be expressed as

$$P_{FA_{global}} = \sum_{k=L}^{MN} \binom{MN}{k} P_{FA}^k (1-P_{FA})^{MN-k}. \tag{5.19}$$

It is worth noting that, when the FAR of each single node is relatively small (i.e. $1 - P_{FA} \approx 1$), equation (5.19) can be written as:

$$P_{FA_{global}} = \sum_{k=L}^{MN} \binom{MN}{k} P_{FA}^{k} (1 - P_{FA})^{MN-k} \approx$$
$$\approx \sum_{k=L}^{MN} \binom{MN}{k} P_{FA}^{k} \approx \binom{MN}{L} P_{FA}^{L}. \tag{5.20}$$

This concept is therefore very close to the 'Moving Window' concept that is well known in monostatic radar systems [28]. However an important difference between this and the Moving Window algorithm is that here we gather samples in a space-diversity context only and consequently there is no sliding window in time; in other words we collect in one instant of time all the signals from different aspect angles and we apply a criterion as in equation (5.16).

After this stage a number L of minimum detections that minimizes the losses is used. This has been heuristically estimated in [28]

$$L \approx 1.5 \sqrt{MN}. \tag{5.21}$$

This means that overall detection is assumed when respectively 1, 3, 5, 6 and 8 single detections occur.

In Section 5.6 it is shown that by introducing a different criterion, it is possible to achieve similar performance and at the same time to have an increased tolerance to Electronic Counter Measures (ECM). In particular, the attention is focused on the case

$$L = \left\lceil \frac{MN}{2} \right\rceil, \tag{5.22}$$

where $\lceil x \rceil$ is the greater nearest integer of x, i.e. it is assumed that a target is present if at least the 50% of nodes detect the target in a mono/bistatic configuration. This is to increase the interference rejection of the overall system, as shown in Section 5.6. Given the number of co-located transmitters and receivers, a target is detected when 1, 3, 5, 9 and 13 thresholds of the single nodes are passed. The first three numbers are the same for both

the decision rules, so there will be no difference in their results. However this indicates that for a reduced number of nodes the two reported criteria are equivalent. On the contrary, when the radar network is made of an increased number of nodes, the two decision rules differ considerably, since there is a difference of roughly 20% of nodes in assuming detection.

Figures 5.5 and 5.6 show the results of the overall FAR achievable by the network of radar against the FAR of a single node respectively using the two criteria in equation (5.21), i.e. the minimum losses case, and in equation (5.22), i.e. the 50% + 1 single detections case. In these cases it is evident that the false alarm generated in one node is compensated by all the double-threshold processing. Actually, as it can be seen from these plots, to global FAR (y-axis) is lower than that of the single nodes comprising the system (x-axis). It can be also evidenced that the FAR achieved by the minimum losses criterion is higher than that of the other case. In particular it can be observed that the latter criterion allows the curves of networks made up of a greater numbers of nodes to have an advantage over those of the first criterion. Moreover, whilst in the second case the more the nodes, the better the performance, the first criterion does not necessarily guarantee increased performance when the number of nodes grows up. This is clear in the plots related to networks made up of 9 and 16 nodes. Here, the levels of the second thresholding are such that these curves differ not as much as for the latter criterion.

Figure 5.7 shows the FAR achieved by this system against the single node threshold. If compared to Figures 5.1 and 5.2, it is evident that, whilst for MIMO and NR systems the higher the number of nodes, the higher the threshold, the opposite happens when using a decentralized algorithm. This peculiarity is explained by the fact that in the DRN case the threshold is set at the single node, while in centralized systems it was determined for the overall set of received signals. For this purpose, Figures 5.8 and 5.9 allow a direct comparison of FAR as a function of the threshold in MIMO, NR and DRN systems. In particular they report the P_{FA} for all the examined systems fixing the number of nodes. As it can be seen, the difference in the threshold levels can be in the order of up to 20 dB. For instance, fixing

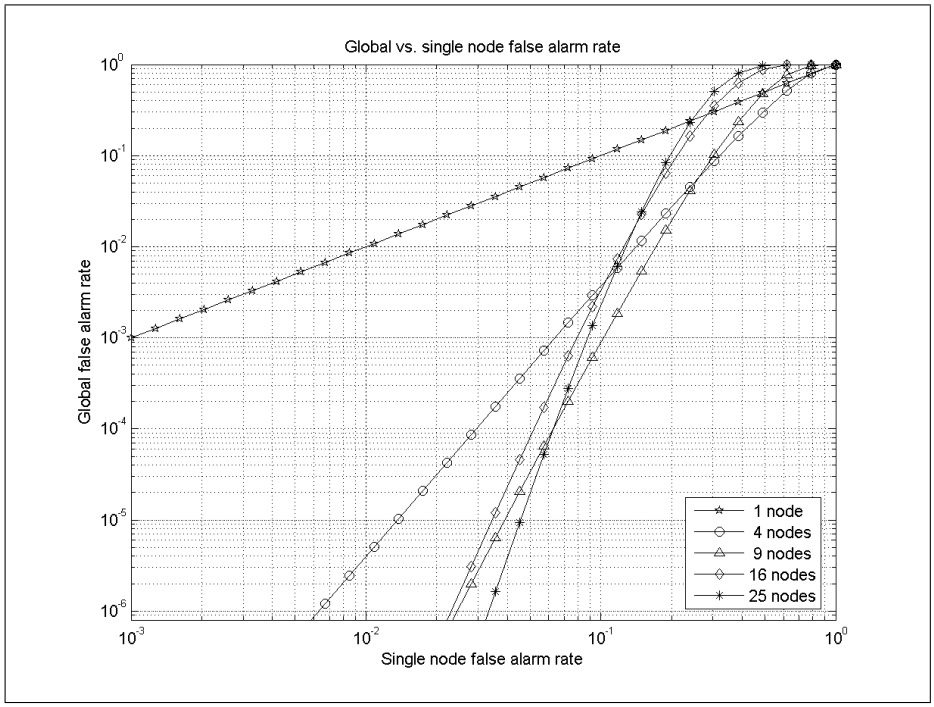

Figure 5.5: Global FAR against single node FAR, minimum losses criterion

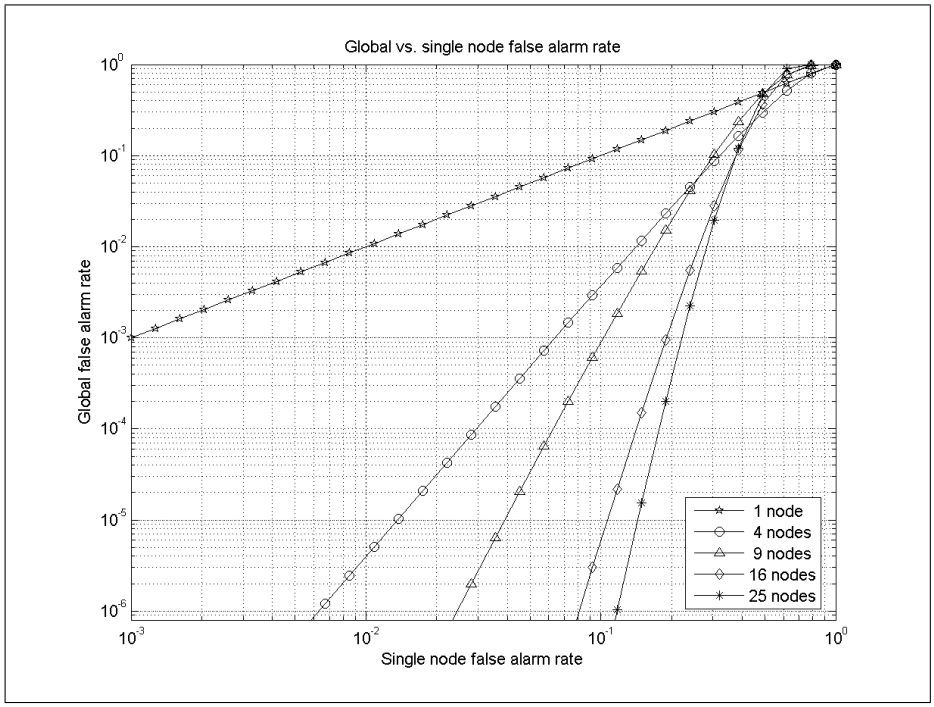

Figure 5.6: Global FAR against single node FAR, 50% criterion

the P_{FA} to 10^{-6} and the number of nodes to 4, it can be observed that whilst a MIMO system requires a threshold of approximately 14 dB, the NR requires approximately a threshold of 18 dB and the single node of a DRN 7 dB only. Difference are remarkable when the number of the nodes increases to 25. In this case these are 4 dB for the DRN approach, 17 for the MIMO and approximately 25 for the NR.

5.2 Detection of Swerling I targets

In this Section a target model is introduced so that detection performance can be evaluated.

Here a Swerling I, i.e. noise-like distributed, target model is considered when networks made up of two to five radars are assumed to transmit and receive ($M = N = 2 \dots 5$), with co-located devices. The system concepts described in Chapter 4 are here reported. The detection of a monostatic radar is reported as well, in order to have a clear mean of comparison ($M = N = 1$) to a meaningful benchmark. Frequency MIMO is not explicitly reported in this section as the results are identical to those of the spatial MIMO case, given that the RCS of the target has a noise-like response in space as well as in frequency. The total transmitted power is a constant in all the cases as before.

Figures from 5.10 to 5.14 show detection performance for the systems examined so far, i.e. the NR, RPNR, MIMO, DRN 50% and DRN ML, as a function of signal to noise ratio and the number of devices comprising for a P_{FA} of 10^{-6}. As it can be seen, the MIMO and the DRN systems have performance in between those of the netted radars, which represents the upper and lower bound limit for performance. In these Figures the losses for incoherent processing, compared to the RPNR, can be estimated from 1 to 5 dB, when respectively from 4 to 25 signals are taken into account for $P_D = 80\%$. Even if the RPNR performs best, as it maximizes the signal-to-noise ratio, MIMO and DRN achieve good results without requiring additional information about the effective position of the target.

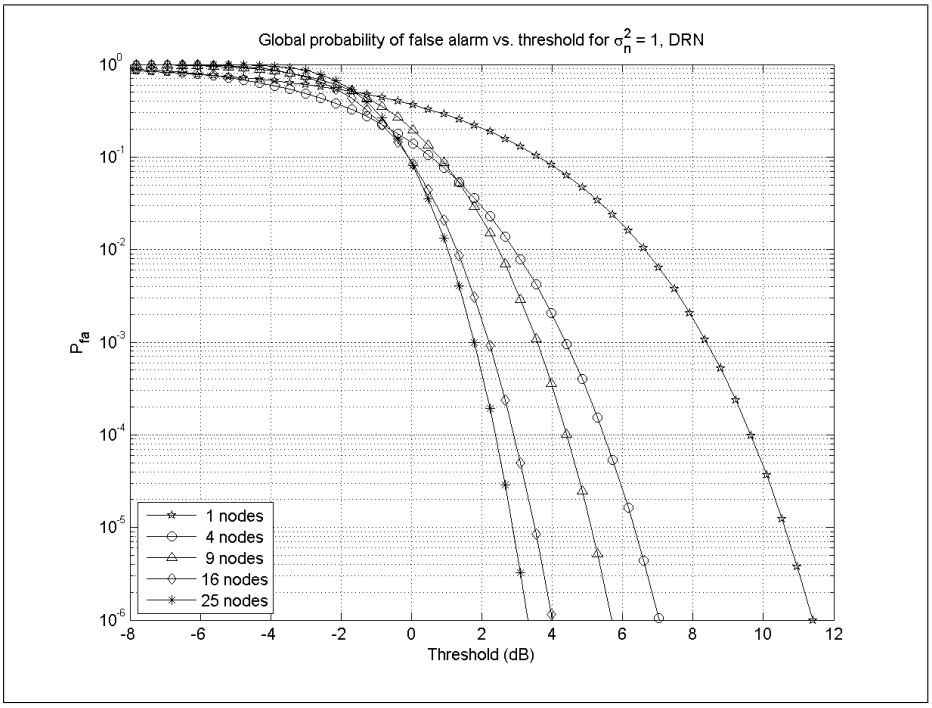

Figure 5.7: Global FAR against single node threshold, 50% criterion

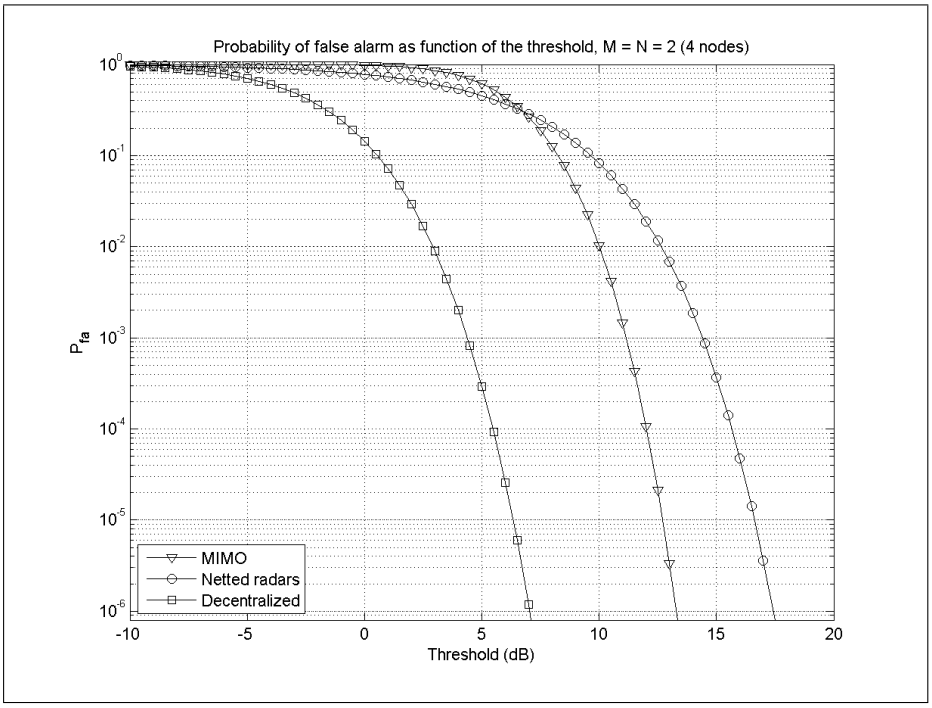

Figure 5.8: P_{FA} in MIMO, NR and DRN, 4 nodes

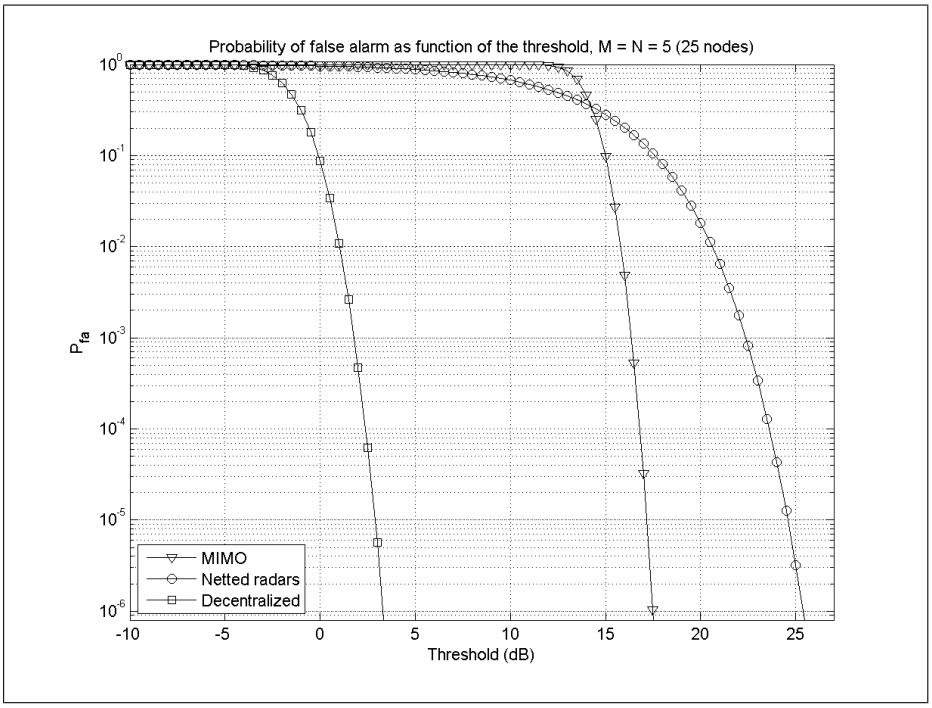

Figure 5.9: P_{FA} in MIMO, NR and DRN, 25 nodes

This good performance is due to the acquisition of independent samples effectively reducing the noise variance and to the lower threshold that has been possible to set as shown in the previous section. Finally, it may seem peculiar that the NR is the only case where the performance decreases as the number of nodes increases. This may seem contrary to expectation but is explained by the increasing randomizing of the received signal phases with increasing number of independent looks.

For incoherent systems, the higher the number of processed signals the higher the performance. However, over a certain number, e.g. 3, increasing the number of nodes does not guarantee the same improvement in detection. This suggests that, from a practical point of view, it is possible to improve the capacity of detection of a radar system by adding just a few devices at different aspect angles. However, this assumes that independent samples can always be taken. Although this is common with most targets, the opposite case is partly examined by considering, for example, the sphere target (Section 5.5).

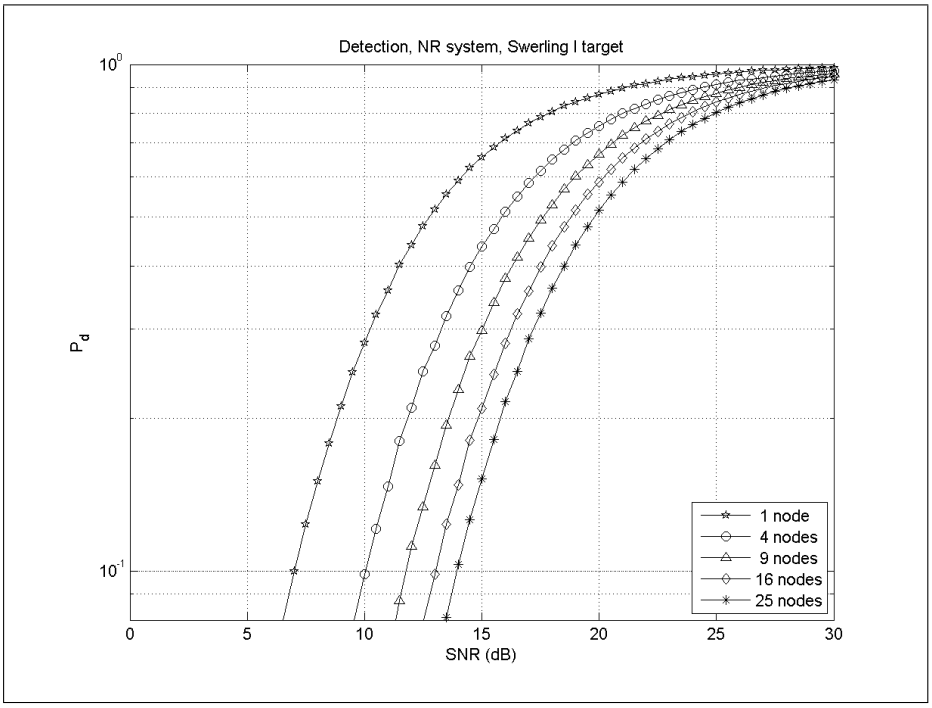

Figure 5.10: NR, Swerling I P_D performances

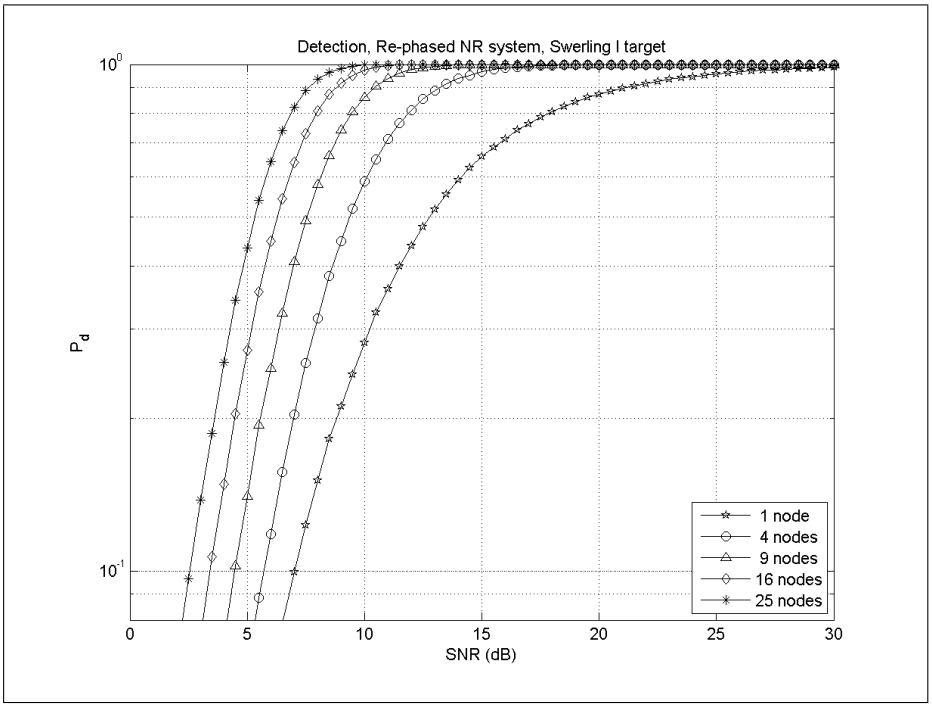

Figure 5.11: RPNR, Swerling I P_D performances

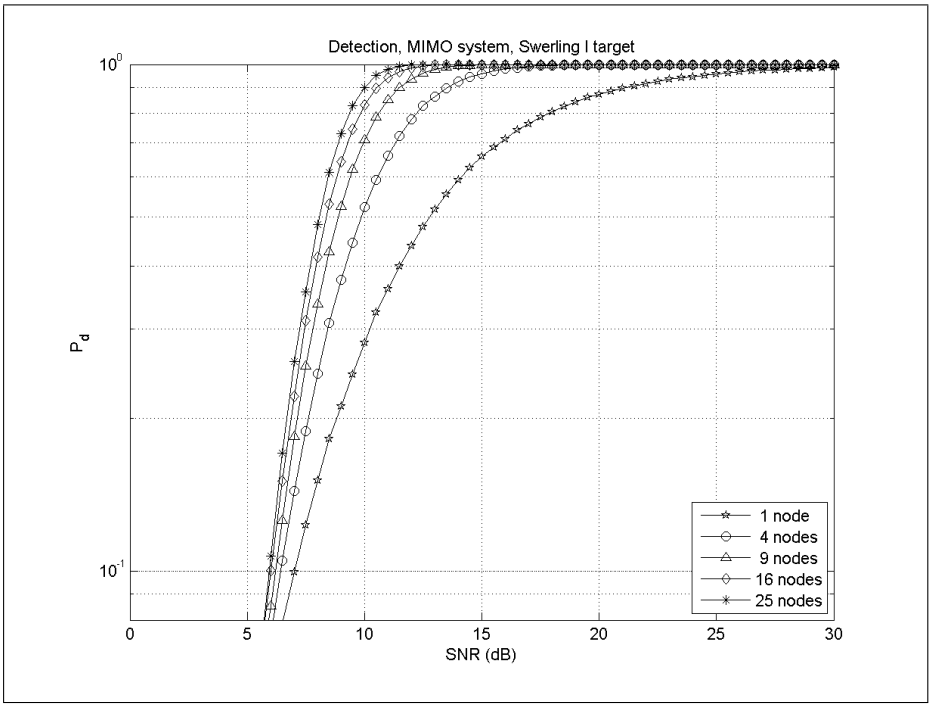

Figure 5.12: MIMO, Swerling I P_D performances

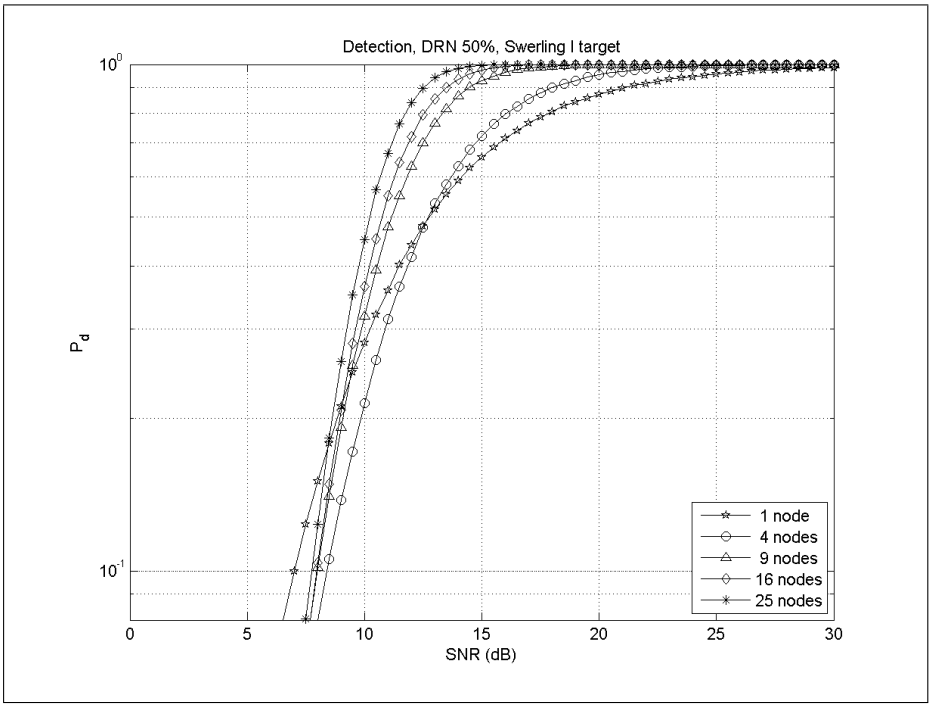

Figure 5.13: DRN 50%, Swerling I P_D performances

For completeness, Figure 5.15 reports the detection results for a single node of a DRN 50% before merging all the detections. As it can be seen from a comparison of this and Figure 5.13, the improvement in detection in the global system is considerable and can be explained by the compensation of the missed detections performed by the nodes of the network. In addition it is worth noting that in this case, due to the constraints on the transmitted power, the monostatic detection overcomes that of a single node.

In general, it can be observed that losses in SNR at $P_D = 80\%$ of MIMO and DRN systems, compared to RPNR, are relatively small and can be estimated in roughly 1 to 5 dB for 4 to 25 signals. It can be observed that, notwithstanding the constraints on the power, the more spatial samples taken the better the resulting detection performance. However, it stands out clearly that the implementation of a MIMO or a DRN system is much simpler than the RPNR due to the greatly reduced tolerance required for the re-phasing. Indeed this may prove impossible for distributed targets, i.e. the synchronization and data communication requirements are much less severe than for the fully coherent network.

In turn, the poorer performance of a decentralized systems, compared to the centralized, can be explained as follows:

1. In DRN systems the received power is a function of the measured RCS, here this system is not able to detect a target when just a few echoes are large and the others relatively small. This is a drawback of this algorithm that is mitigated in centralized processing algorithms.

2. Furthermore, for relatively low SNR, while MIMO and NR systems sum up every signal coming into the receiver, this sub-optimum algorithm considers only the signals with a power greater than the first threshold. So, whilst in centralized processing every received signal contributes to the output power, here only a number of them are taken into account. This can be considered as a loss of power or sensitivity introduced into the second stage of processing and consequently in a loss of performance.

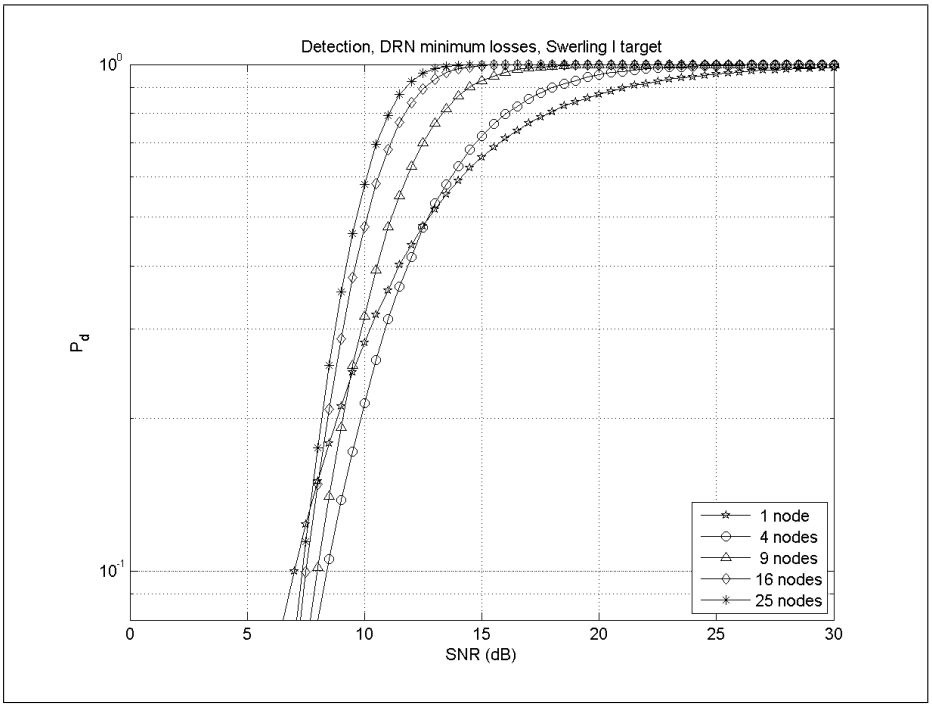

Figure 5.14: DRN ML, Swerling I P_D performances

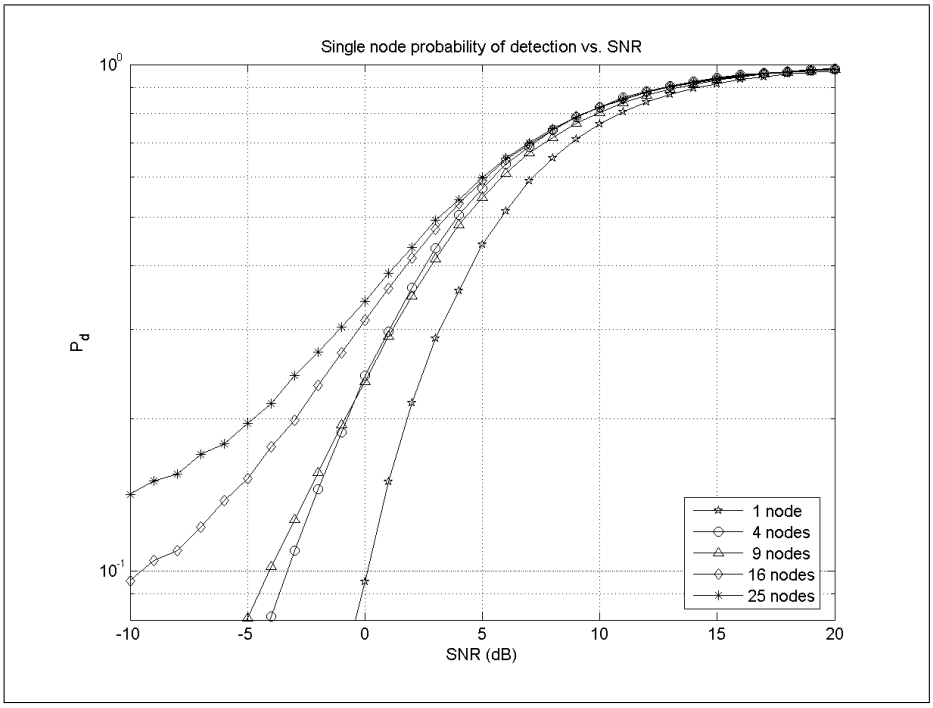

Figure 5.15: Single node P_D against SNR, global FAR= 10^{-6}, 50% criterion

5.3 Detection of Swerling III targets

A Swerling III model corresponds to a target consisting of one dominant scatterer plus a number of smaller ones. The resulting PDF can be expressed as in equation (5.23) and it is representative of a chi square distribution with 4 degrees of freedom or, equivalently, with 2 complex degrees of freedom [82]:

$$p(\sigma) = \frac{4\sigma}{\bar{\sigma}^2} \exp\left\{-\frac{2\sigma}{\bar{\sigma}}\right\}, \tag{5.23}$$

where $\bar{\sigma}^2$ is the variance of the RCS of the target.

Figure 5.16 shows the results for spatial MIMO, NR, DRN and RPNR against a Swerling III target for a network made up of 5 devices, which provides the biggest difference in dB among the systems. Again, frequency MIMO is not reported as the RCS model is independent of the carrier frequency. The results of other numbers of nodes are not reported for brevity, as they have smaller distances between the curves and, overall, it would be a variation of the Figures of the previous Section. As in the previous Section, MIMO and DRN fall between the two netted cases. The difference in performance with respect to the netted cases is greater here than a Swerling I target.

5.4 Detection of Rician targets

Both spherical target and Swerling III RCS model can be considered a particular realization of this distribution as it is made of a deterministic and a random parts. Under this assumption, a more realistic statistical model of the RCS of a target is expected to be described in this way. As known, the PDF of the RCS σ can be written as follows:

$$p(\sigma) = \frac{\sigma}{\bar{\sigma}^2} \exp\left\{-\frac{\sigma^2 + m^2}{2\bar{\sigma}^2}\right\} I_0\left(\frac{\sigma m}{\bar{\sigma}^2}\right), \tag{5.24}$$

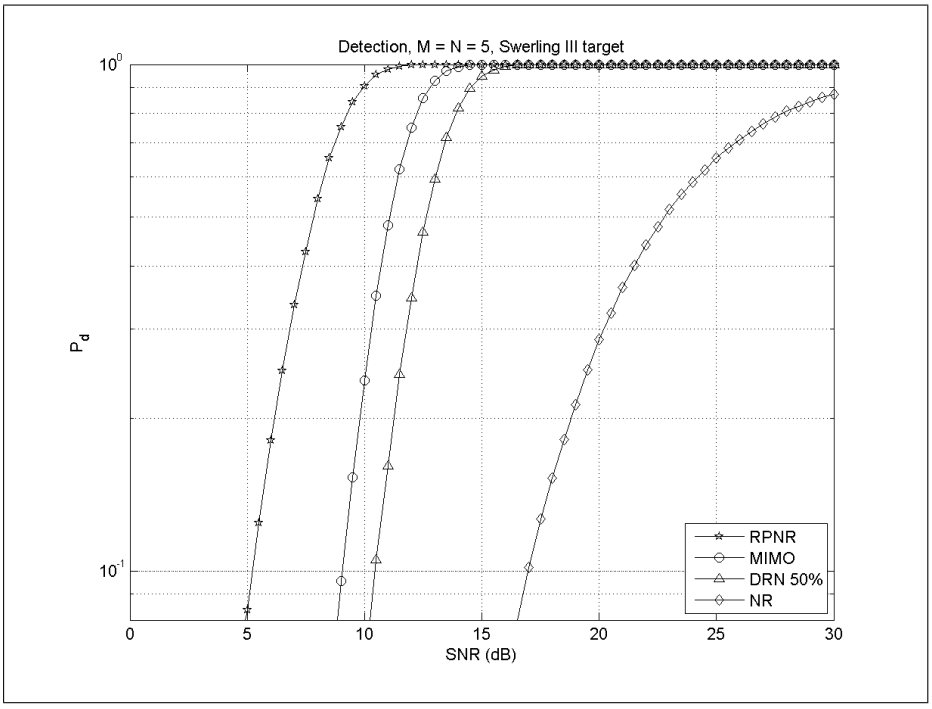

Figure 5.16: Comparison of P_D for a Swerling III target, with $M = N = 5$

where $\bar{\sigma}$ is the 2^{nd} not centered moment of the RCS distribution, m is a parameter controlling its moments and I_0 is the modified Bessel function of first kind and order 0. Figure 5.17 shows the results for such distribution. As in the previous two cases, the ranking of performance is here confirmed with negligible differences.

In general therefore, for Swerling and Rician distributed targets incoherent performance is much better than the NR's one. This is mainly due to the coherent processing realized by this system that, without a-priori information and an algorithm for re-phasing the incoming signals, is not able to exploit all its potential.

5.5 Detection of spherical targets

A further comparison of the performances has been considered for the case of a spherical target as its RCS exhibits a simple frequency dependence

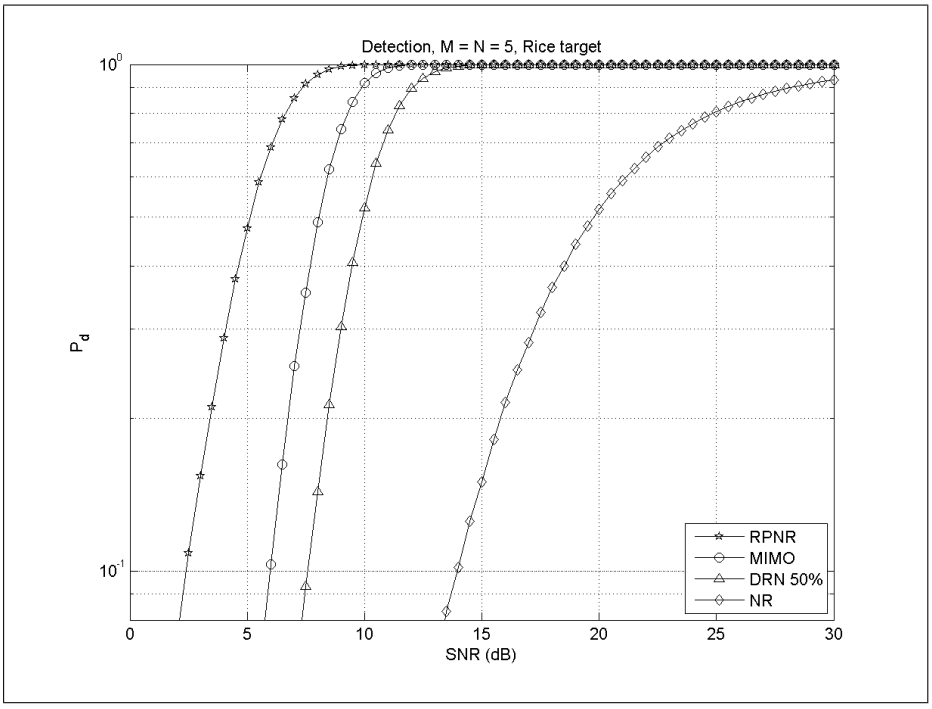

Figure 5.17: Comparison of P_D for a Rician target, with $M = N = 5$

with radius. This case exhibits a highly correlated RCS, so it provides a first view of the MIMO performance when the target is not noise-like. It is here acknowledged that this is an extreme case for a target, as its RCS is deterministic and therefore can provide a benchmark for the detection performance for other directional targets such as flat plates, dihedrals and trihedrals. Several values of the radius of the sphere r have been considered, in order to get the related performances of the systems. A frequency $f_0 = 3$ GHz has been chosen as the carrier frequency of the spatial MIMO and the netted radar, while, as in this case a frequency model for the RCS of the target was available, the carrier frequencies of the frequency MIMO vary in the range of $1 - 5$ GHz, with bandwidths that do not overlap each other. The RCS of a sphere as a function of the ratio $\frac{2\pi r}{\lambda}$ is plotted in Figure 5.18 to illustrate frequency dependence.

The results are shown in Figures from 5.19 to 5.22 for a variety of ratios $\frac{r}{\lambda_0}$. The received SNR, shown in the x-axis, is computed at the

wavelength $\lambda_0 = \frac{c}{f_0}$ (10 cm). When a frequency MIMO radar system has been considered, the reported performance is affected by the different responses of the RCS of a sphere to different wavelengths that modify the effective SNR value, according to the following:

$$SNR\,|_{\lambda} = SNR\,|_{\lambda_0}\,\frac{\sigma(r,\lambda)}{\sigma(r,\lambda_0)}, \tag{5.25}$$

where it is assumed $G_T(\lambda)G_R(\lambda)\lambda^2 = G_T(\lambda_0)G_R(\lambda_0)\lambda_0^2$ (in the expression of the SNR). This is done to provide a comparison between the systems where the values of the SNR change according to the differences of the measured RCS only and not the differences of gains of the transmitting/receiving antennas to different wavelengths.

The performances achieved in this case are extremely interesting as they show differences when comparing spatial and frequency MIMO systems. The spherical target does not yield independent samples for spatial MIMO but it does to a certain extent when the frequency variant is employed. Figures from 5.19 to 5.22 indicate that it is not possible to predict the best performer a priori between the frequency and the spatial MIMO cases and might be more indicative when considering real targets.

In Figure 5.19 the performance achieved by frequency MIMO approaches that of the RPNR. This is due to the frequency diversity permitting at least one measurement of the target's RCS in the resonance zone of the curve in Figure 5.18 $0.5 \leq \frac{2\pi r}{\lambda} \leq 1.5$ that introduces some extra signal strength into the signal power, hence enhancing detection. It is then evident that the frequency MIMO's performances are affected by the ratio $\frac{r}{\lambda}$, as theoretically expected. For a small number of transmitted signals, the frequency MIMO seems to perform better than the corresponding spatial MIMO; on the contrary the higher the number of processed signals, the more similar the achieved results.

The loss of performance of frequency MIMO for $\frac{2\pi r}{\lambda} = 1$ is significant. In this case all the spatial MIMO's and NR's signals operate in peak of the resonance zone of Figure 5.18; on the contrary, the frequency diversity of

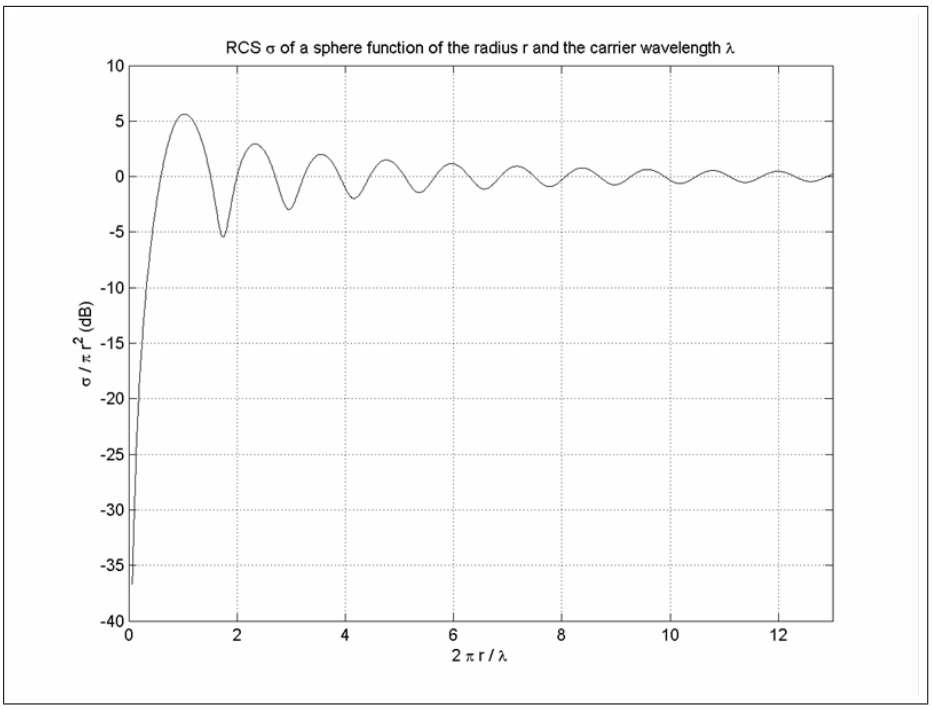

Figure 5.18: RCS of a sphere

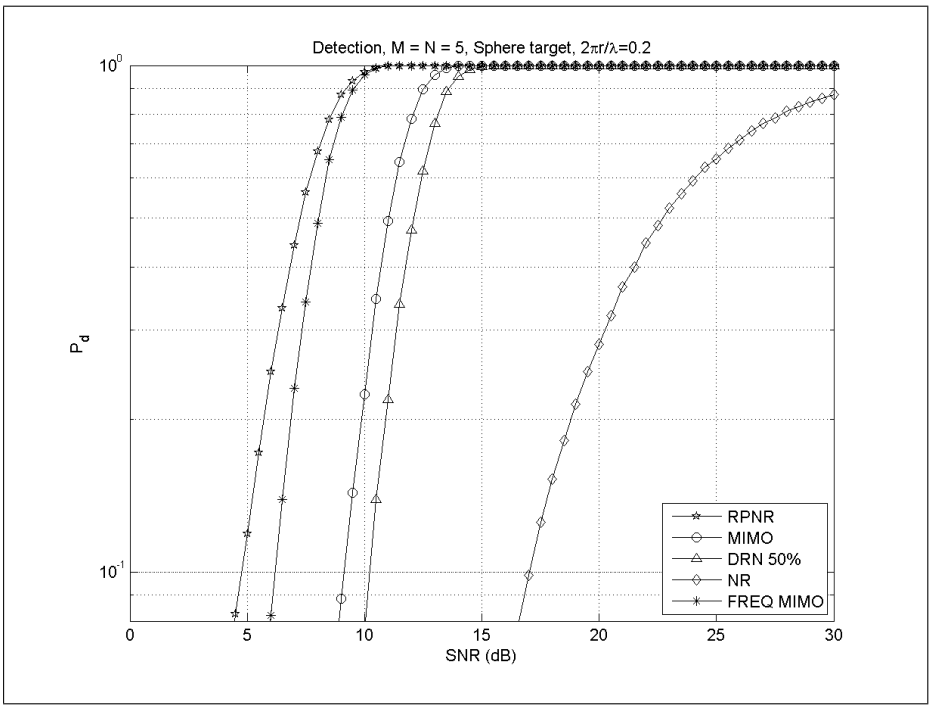

Figure 5.19: Compared P_D for spherical target, $M = N = 5$, $2\pi\frac{r}{\lambda} = 0.2$

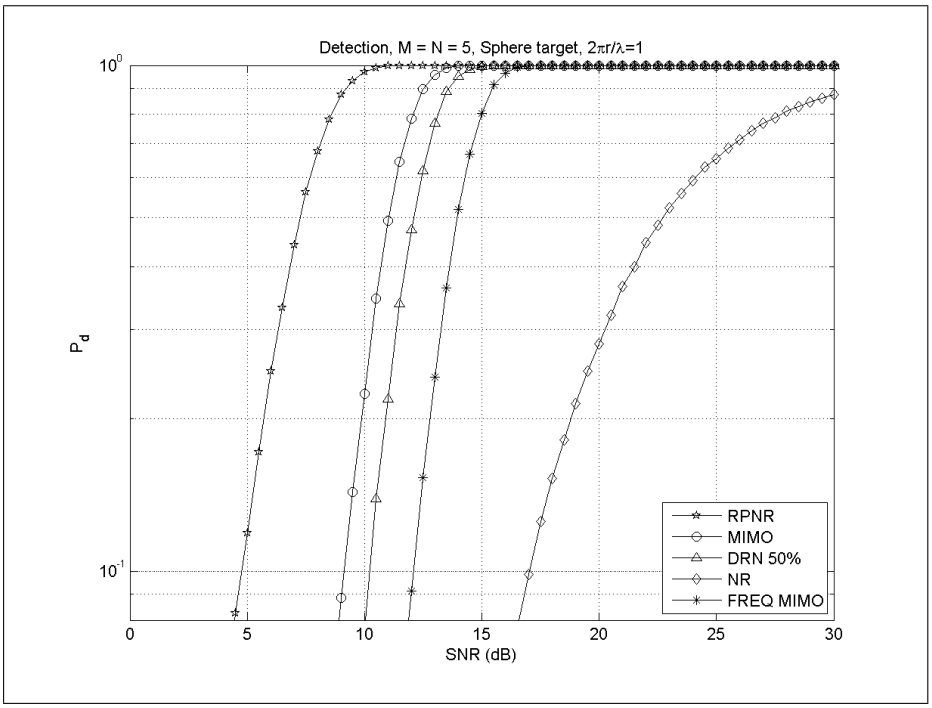

Figure 5.20: Compared P_D for spherical target, $M = N = 5$, $2\pi\frac{r}{\lambda} = 1$

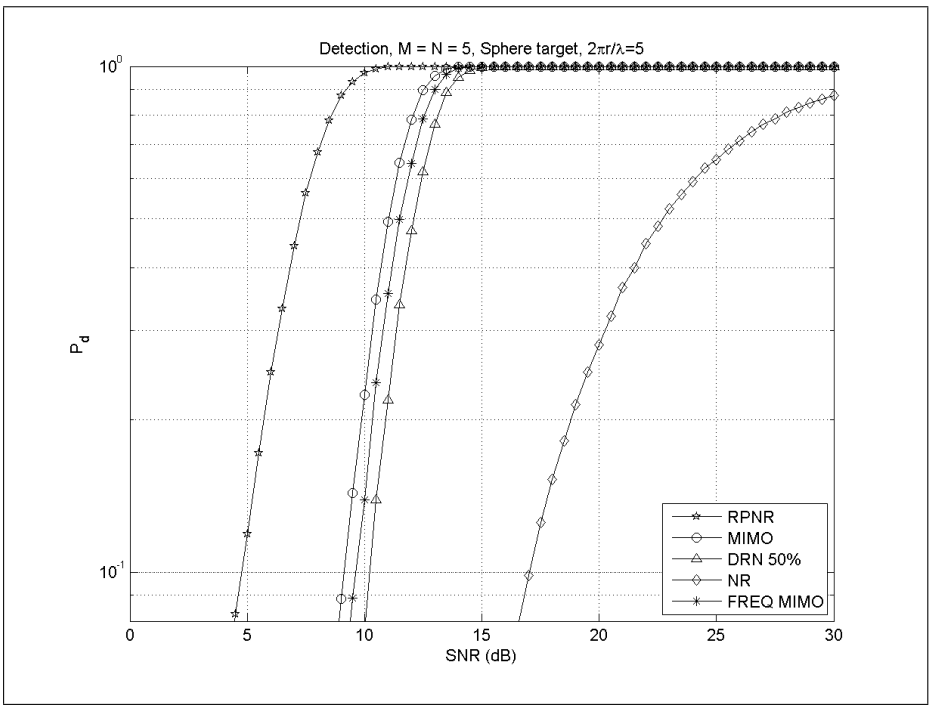

Figure 5.21: Compared P_D for spherical target, $M = N = 5$, $2\pi\frac{r}{\lambda} = 5$

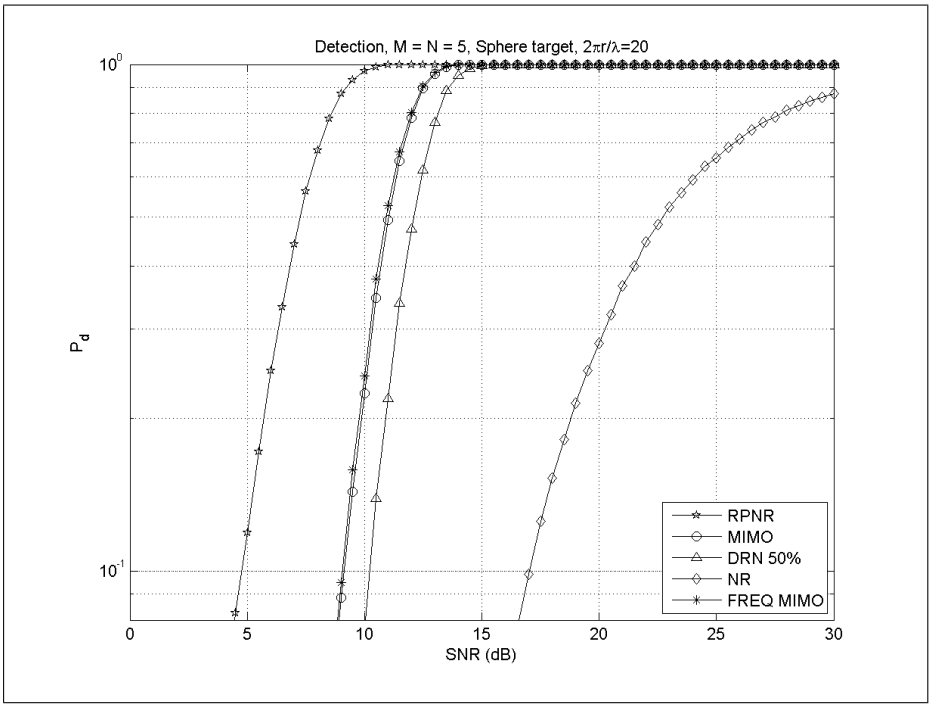

Figure 5.22: Compared P_D for spherical target, $M = N = 5$, $2\pi\frac{r}{\lambda} = 20$

the other MIMO system allows at least one signal to operate in that zone, while all the others are in the Rayleigh or optical regions[3].

As soon as the ratio $\frac{2\pi r}{\lambda}$ reaches the optical zone of Figure 5.18, the frequency MIMO cannot exploit the extra signal strength so it performs worse than the RPNR. As expected, the spatial MIMO P_D curve always performs worse than the RPNR as the phase-shifting maximizes the received SNR.

The detection performance here examined are a benchmark for the detection of real targets. These are generally made of deterministic and random contributions giving a backscattered radiation which cannot be predicted. In addition the assumption of a point target with one phase

[3]With regards to the normalized RCS of a sphere as a function of the ratio $\frac{2\pi r}{\lambda}$, as in Figure 5.18, the part of the plot where the radius of the sphere is comparable with the wavelength $2\pi r \approx \lambda$ is usually referred as "Rayleigh region" . On the contrary, the case $2\pi r >> \lambda$ is usually referred as the "optical region". In particular, the last region is characterized by reduced fluctuations of the normalized RCS, as seen in the right part of the plot in Figure 5.18.

centre only is not realistic in most of the cases. However, notwithstanding the complexity of the backscattering process, it has here been presented that the behaviour of the different approaches to detection is similar in all the examined cases.

5.6 DRN tolerance to jamming

In this Section the effect on performance is considered when one of the receivers of the network is jammed with a fully matched transmission, i.e. when the received signal at the q^{th} receiver is expressed as

$$r_q(t) = H_{0/1} \sum_{m=1}^{M} \alpha_{q,m}(\sigma) s_m \left(t - \frac{R_{m,q}}{c} \right) + n_q(t) + \sum_{m=1}^{M} \beta_{q,m}(\sigma) s_m \left(t - \tau_m \right), \quad (5.26)$$

with symbols as in Chapter 4 and

$$\begin{cases} |\beta|^2 \gg |\alpha_{q,m}|^2 \\ |\beta|^2 \gg \sigma_n^2 \\ |\beta|^2 \gg \lambda_{q,m} \end{cases} \quad (5.27)$$

and $\lambda_{q,m}$ is the threshold after matched filtering of for the m^{th} waveform at the q^{th} receiver.

Figures 5.23 and 5.24 show the performance of the FAR when one of the N receivers is jammed. This means that, due to the co-location of transmitters and receivers, M nodes (from 1 to 5 respectively) are being jammed. As expected there is a significant loss in FAR for all the systems. In this scenario the monostatic radar system totally loses its capacity for detection and it is evident that the higher the number of nodes, the lower the losses. No ECCM has been considered and thresholds are kept fixed at nodes, so applying any sort of ECCM algorithm will provide an additional tolerance. Here it is evident the minimum losses criterion has much worse performance when jammed. That is the reason why a criterion as the

50% + 1 one, that introduces roughly just one dB of extra losses, should be preferred to the other for a decentralized processing in a radar network.

In this Chapter it has been shown that incoherent systems provide a good trade-off between fully coherent systems and coherent systems under the assumption of white Gaussian noise only in receive. This has been confirmed for noise-like targets and more deterministic targets, such as the sphere. In general terms, a loss of only few dB in terms of SNR has been observed, compared to the RPNR. In addition, incoherent systems and the RPNR outperform the conventional monostatic radar, also under the constraint of providing constant ERP to the system. DRN has the great asset to allow an increased tolerance to jamming. The Frequency MIMO concept has been shown to be able to achieve the same benefits as spatial diversity under the reported assumptions. The analysis presented here is going to be extended in more details and under different background assumptions in the next Chapter.

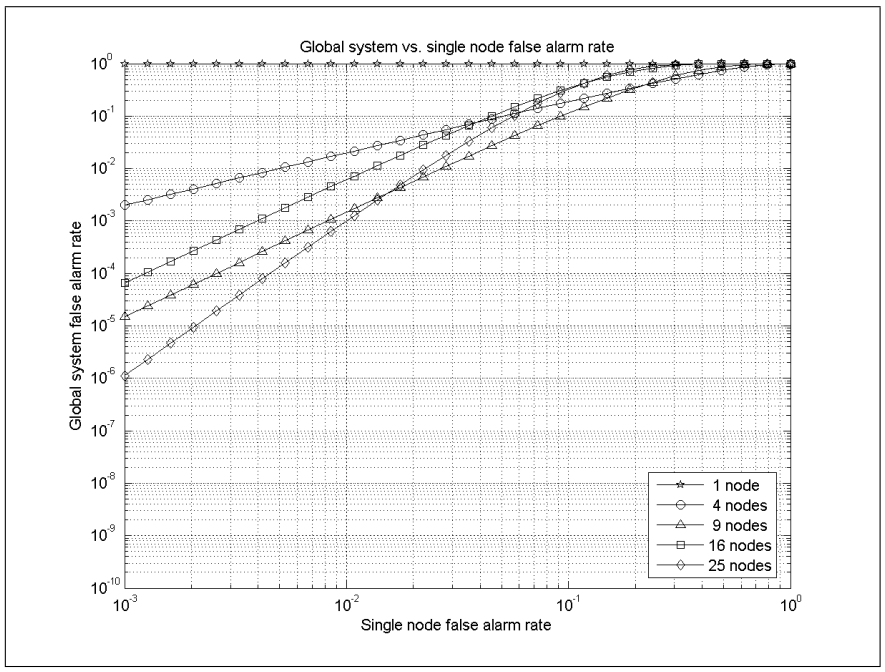

Figure 5.23: Global FAR against single node FAR, 1 jammed receiver, ML criterion

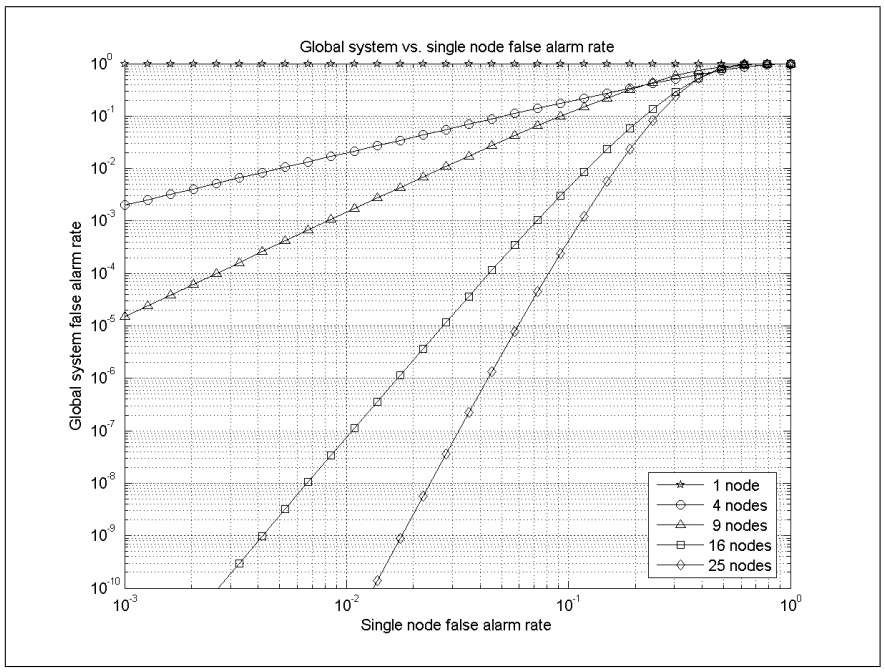

Figure 5.24: Global FAR against single node FAR, 1 jammed receiver, 50% criterion

Chapter 6

Performance in clutter

So far different target models under noise limited conditions have only been investigated. However, it is more realistic to also include the effects of the environment such as clutter. Here the effects of clutter on the performance of the various distributed radar concepts are investigated.

The issues in investigating multistatic clutter, together with the characteristics of the K-distributed clutter, have been introduced in Section 3.5. Here the effects of K-distributed clutter on multistatic performance are investigated on a single carrier frequency. The processing of the received echoes has to take into account the extra information provided and the environment that the radars are in. The PDF of the total disturbance has obviously changed and the change in performance in terms of FAR and P_D is reported.

Because of the lack of works and solid background on the multistatic aspects of clutter, in this Chapter a first analysis is developed starting on some assumptions, for instance on the clutter correlation. However, this topic has been investigated in a second time of this work through an analysis of real data (Chapter 9).

6.1 Signal models and statistical approach

In this Section the characteristics of the incoming signals are described. First of all, the k^{th} received signal is modelled as:

$$r_k = \sum_{m=1}^{M} (H_{0/1}\alpha_{m,k}s_m + c_{m,k}) + n_k, \tag{6.1}$$

where $c_{m,k}$ is the clutter, $m = 1..M$ is the number of transmitters, $k = 1..N$ is the number of receivers and the other symbols as in the previous Chapters.

For the sake of simplicity the RCS of the target has been assumed Swerling II[1] distributed for both the monostatic and the bistatic case. The clutter has been modelled as a K-distribution (from [12] to [16]). This means that the amplitude has a Rayleigh distribution with a Γ-distributed variance. For echoes incoming from adjacent range cells, a correlation between the powers received has to been taken into account. Thus the following model for the amplitude of the clutter $\mathbf{c}$[2] can be introduced:

$$\mathbf{c} = \sqrt{\tau}\mathbf{x}, \tag{6.2}$$

where $\mathbf{x}$ is the complex vector of the received echoes from different range cells and its PDF is given by

$$p(\mathbf{x}|\tau) = \frac{1}{(2\pi\tau)^L \sqrt{|\mathbf{M}_x|}} \exp\left\{\frac{1}{2\tau}\mathbf{x}^H\mathbf{M}_x^{-1}\mathbf{x}\right\}, \tag{6.3}$$

where $\mathbf{M}_x$ is the covariance matrix of $\mathbf{x}$ given τ, i.e.

$$\mathbf{M}_x = E\left\{\mathbf{x}\mathbf{x}^H|\tau\right\}, \tag{6.4}$$

[1] When processing the returns from more than one pulse, the Swerling I and III models assume a degree of correlation from pulse to pulse. On the contrary the Swerling II and IV imply uncorrelated echoes from the same set of pulses. However, for a single pulse the Swerling I and Swerling II models are equivalent as well as the Swerling III and the Swerling IV. In this Chapter the analysis is performed as if the echoes change on a pulse to pulse basis, so a Swerling II model has been assumed for the target.

[2] In this thesis c (*italics*) refers to the speed of light, whilst $\mathbf{c}$ (**bold**) to the vector made up of clutter samples

and the texture τ follows a Γ-distribution of shape parameter ν and expected value μ:

$$p(\tau) = \frac{1}{\Gamma(\nu)} \left(\frac{\nu}{\mu}\right)^{\nu} \tau^{\nu-1} \exp\left\{-\frac{\nu}{\mu}\tau\right\}, \quad \tau > 0. \tag{6.5}$$

The general element $m_x(h,k)$ of $\mathbf{M}_x$ has been taken equal to

$$m_x(h,k) = \rho_x^{|h-k|} \tag{6.6}$$

where ρ_x is the correlation coefficient between two adjacent elements of the vector $\mathbf{x}$. As usual the thermal noise has been modelled as a white complex Gaussian Random Variable (RV) with zero mean value and variance σ_n^2.

So, considering clutter and noise to be mutually independent, it is possible to express the resulting PDF of the L-long vector of the disturbance as a complex Gaussian with zero mean value and covariance matrix equal to $\tau\mathbf{M}_x + \sigma_n^2\mathbf{I}_L$, where τ is distributed as in equation (6.5) and $\mathbf{I}_L$ is the LxL identity matrix.

In this analysis a certain number (Q) of echoes received during the TOT has been taken into account. When integration in time is performed, the clutter plus noise statistics change significantly. If in time the clutter echoes have textures τ_i, $i = 1..Q$, after the integration process the vector of the total disturbance can still be expressed as a complex Gaussian with zero mean value and covariance matrix given by

$$\sum_{i=1}^{Q} \left(\tau_i \mathbf{M}_x + \sigma_n^2 \mathbf{I}_L\right) = Q\sigma_n^2 \mathbf{I}_L + \mathbf{M}_x \sum_{i=1}^{Q} \tau_i. \tag{6.7}$$

The PDF of the RV $\tilde{\tau} = \sum_{i=1}^{Q} \tau_i$, that is the texture of the vector with the integrated contribution of clutter, can be expressed as a Γ RV with shape parameter ν and mean value $Q\mu$ if the textures are uncorrelated with each other in the time domain. In this case it is clear that the higher Q, the better the approximation $\sum_{i=1}^{Q} \tilde{\tau}_i \approx Q\mu$, so the overall PDF of the disturbance approaches asymptotically a Gaussian with mean value 0 and covariance

matrix equal to $Q(\mu\mathbf{M}_x + \sigma_n^2\mathbf{I}_L) = Q\sigma_n^2(CNR\mathbf{M}_x + \mathbf{I}_L)$. Unfortunately from this approximation it can be difficult to evaluate the threshold for the FAR in a closed form. In practice, in real systems, the number Q of integrated samples is directly dependent on TOT, so in most cases it is too small to approximate the overall PDF and thus to compute accurately thresholds for low and very low FAR.

In addition, if the textures are correlated in time a more complex expression for the PDF of the disturbance vector can be found. If, for instance, a first order Markov structure is assumed to describe the texture component on Q elements, then we can write (as in [13]):

$$p(\bar{\tau}) = p(\tau_1)\prod_{i=1}^{Q-1} p(\tau_{i+1}|\tau_i), \tag{6.8}$$

where

$$\begin{aligned} p(\tau_{i+1}|\tau_i) =& \frac{\nu}{\mu}\frac{1}{\rho^{\nu-1}(1-\rho^2)}\left(\frac{\tau_{i+1}}{\tau_i}\right)^{\frac{\nu-1}{2}} \\ & \exp\left\{-\frac{\nu}{\mu}\frac{\tau_{i+1}+\rho^2\tau_i}{1-\rho^2}\right\} I_{\nu-1}\left[\frac{\nu}{\mu}\frac{2\rho\sqrt{\tau_i}\tau_{i+1}}{1-\rho^2}\right], \end{aligned} \tag{6.9}$$

and I_z is the modified Bessel function of first kind and order z. The covariance matrix $\mathbf{M}_T$ in time has been assumed of the same kind as $\mathbf{M}_x$ with a different correlation coefficient.

6.2 Multistatic information and correlation

In multistatic systems it is now assumed that each transmitter-receiver couple provides a set of data of the form previously described. Thus the total data incoming into the system and suitable for processing should be organized in a three-dimensional matrix as shown in Figure 6.1. Clutter echoes from the same area generated by one of the M transmitted wave-

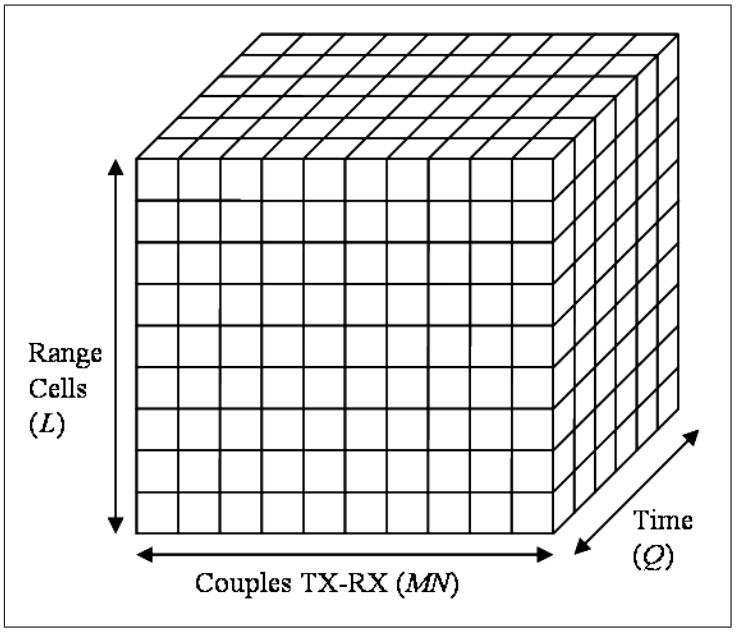

Figure 6.1: Multistatic data organization

forms can have correlated values of the textures as observed in practice (from [12] to [16]).

As already pointed out, whilst correlation in time and range has been largely investigated, there is a lack of knowledge about a possible correlation of the data in a multistatic configuration. Here it is assumed that echoes scattered by the same clutter can be partially correlated, especially under the hypothesis of narrowband due the relatively high number of elementary scatterers [19, 20]. Thus a third correlation matrix $\mathbf{M}_{t-r}$ can be introduced. At this stage two clutter samples from the corresponding range cell $c_{m,k}(p)$ and $c_{n,h}(p)$, $n, m = 1..M, k, h = 1..N, p = 1..L$ are assumed to have a correlation coefficient 1 if $n = m$ and $k = h$, ρ_{tx-rx} if $n = m$ but $k \neq h$, with $0 < \rho_{tx-rx} < 1$, and otherwise 0. The choice of 0 in the latter case can be explained due to the slightly (for far targets) different orientation of the range cells: when transmitters far away each other illuminate different-shaped range cells, although in the same area, the coherent sums of all the backscattered contributions of the clutter are not expected to be correlated with each other.

An additional hypothesis is that multistatic clutter is not correlated either: ideally many cases should be considered and examined as currently insufficient knowledge exists about target and clutter scattering under bi- and multi-static conditions. The examined cases show a reasonable range of performance variation.

Clutter and its correlation properties in multistatic systems have still to be measured and analyzed via experimental results.

6.3 Signal processing and performance

Once data are collected, there is more than one way of processing them in order to obtain a detection. In this Section three ways are considered. These are: (*i*) a fixed threshold algorithm applied to the raw data, (*ii*) a fixed threshold algorithm whitening the incoming data, assuming that the exact correlation matrixes are known and (*iii*) finally an adaptive threshold algorithm applied to the raw data. These are reported in the following sub-sections, together with the corresponding results. Here a multistatic Swerling II target has been assumed, in analogy to the previous Chapter.

6.3.1 Fixed threshold on correlated and whitened data

Correlated data

A first method is to process data as it arrives at the receiver. This is not be the best case, but it avoids estimating the correlation matrixes: after initial processing, the data is available to the detectors; the two corresponding thresholds (one for MIMO systems, the other for netted radars) ensuring FAR have been recomputed due to the non-gaussian distribution of the total disturbance. These results have been reported in Figures from 6.2 to 6.9 in pairs P_{FA} (top figure) – P_D (bottom figure). From the plots of the top figure the FAR is set to 10^{-4}. Fixing this value, the P_D performance as a function of CNR, SNR and number of nodes is reported in the bottom figure. As in the previous Chapter, NR performs the worst and RPNR

the best, with the other two systems in the middle. Covariance matrixes have been considered as described in sections 6.1 and 6.2 with coefficients equal to 0.9 (range), 0.7 (pulses) and 0.2 (nodes). Results of FAR against threshold for CNR equal to 0 and 15 dB and for 1, the monostatic case, 4 and 25 signals are shown.

As in the simple case, where only thermal noise had been considered, MIMO and DRN radar systems allows a lower threshold to be set in any configuration, if compared to the NR system. This means that a lower noise power is introduced into the detector. Data whitening produces the best performance as processing of raw data requires a threshold of 5 to 10 dB higher.

Whitened data

Firstly, given the covariance matrix in time, $\tau\mathbf{M}_T + \sigma_n^2\mathbf{I}_L$, it is possible to whiten the data in this domain, which is the best way to remove or reduce the correlation, given a fully known correlation matrix. In so doing it is also possible to achieve, after integration, a simpler expression for the PDF of clutter plus noise, as can be inferred from equation (6.7).

As the detectors for both the MIMO and the NR system work on the row of the matrix in Figure 6.1, it is convenient to whiten data in this dimension as well as it decorrelates the samples and consequently allows lowering the threshold. In fact, especially for netted radar systems, it is better to avoid clutter correlation as the coherent sum processed into the detector may enhance the disturb power, thus increasing false alarms. However, in real systems clutter will be correlated and thus may mean that the analysis here leads to a "best case" result.

A second method of processing is to remove the correlation in the 3^{rd} (or just 2^{nd}, if range is not taken into account) dimension. It is clear that, as detectors will work on the row of the matrix, a certain amount of correlation on the columns of the 3D matrix in Figure 6.1 does not affect the decision process. After this operation it will be possible to write down a decision rule (threshold for CFAR condition) using the properties of the

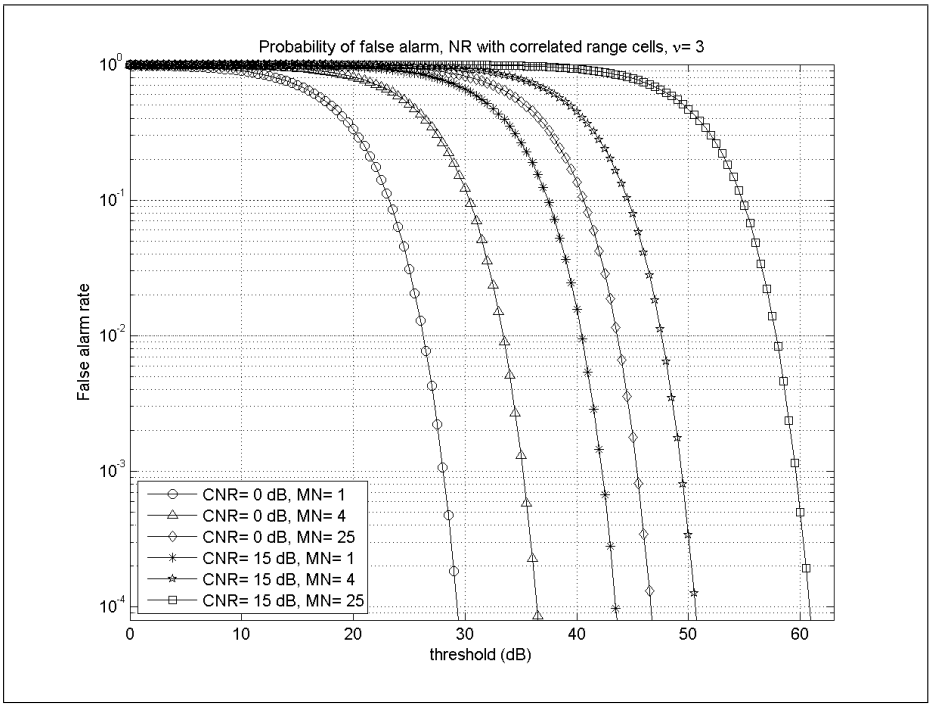

Figure 6.2: FAR, NR, correlated clutter, L= 16

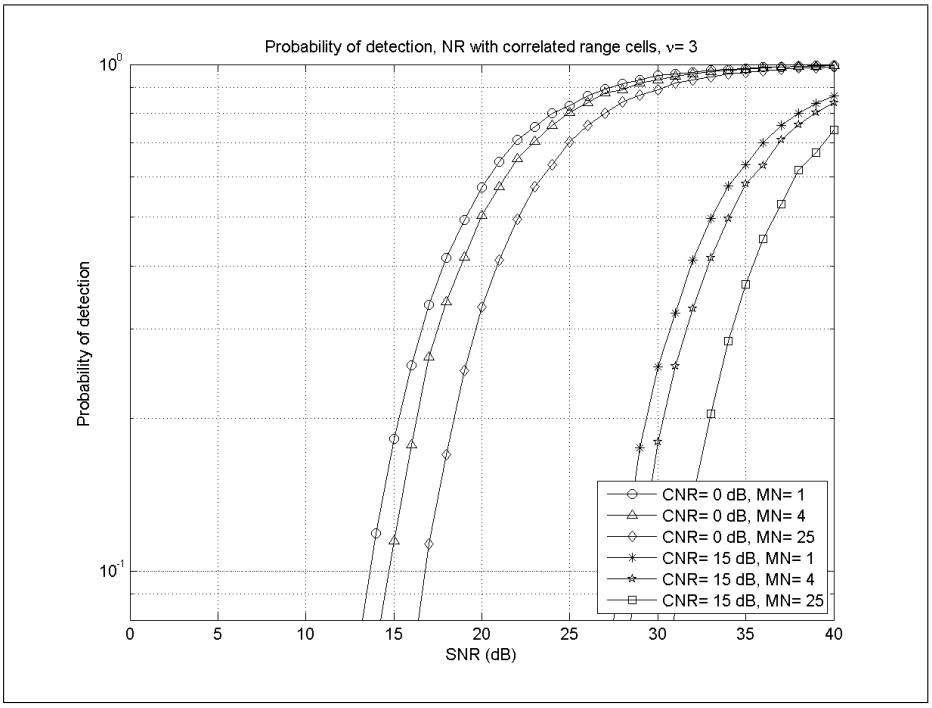

Figure 6.3: P_D, NR, correlated clutter, L= 16

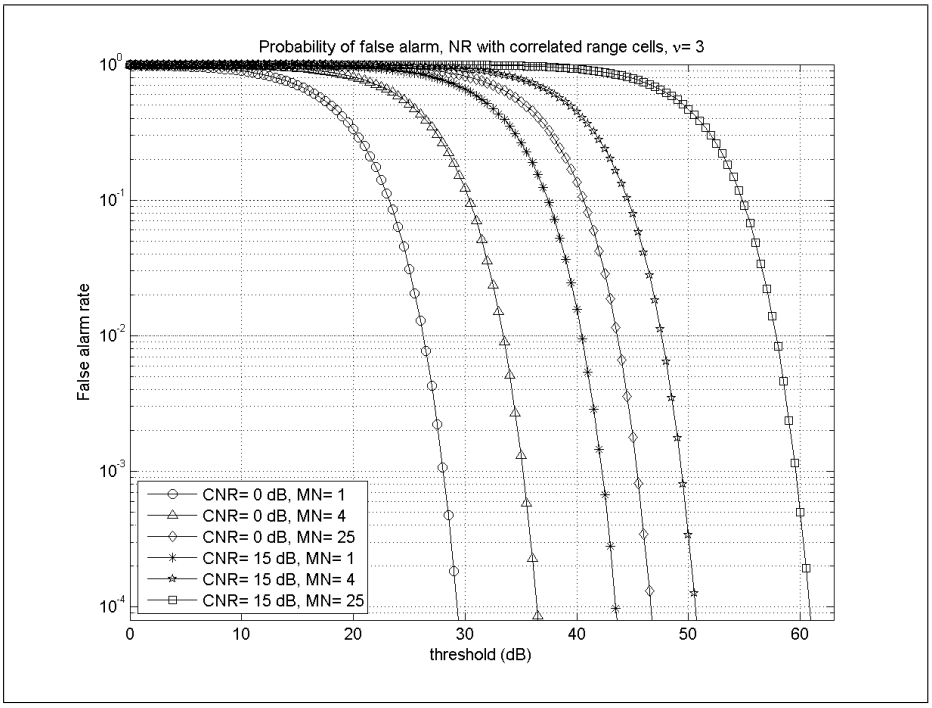

Figure 6.4: FAR, RPNR, correlated clutter, L= 16

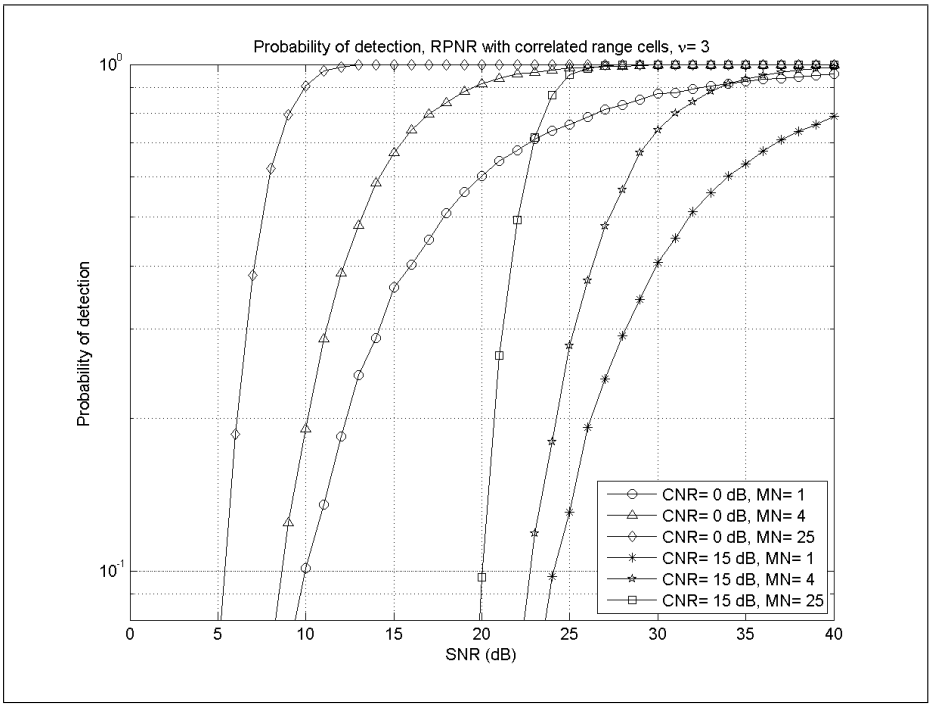

Figure 6.5: P_D, RPNR, correlated clutter, L= 16

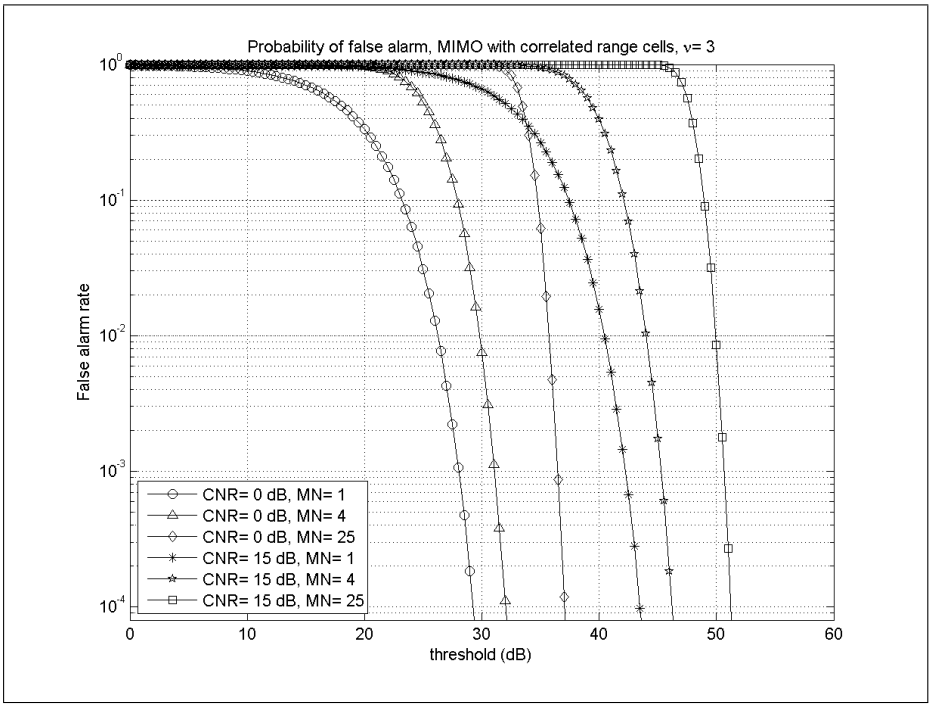

Figure 6.6: FAR, MIMO, correlated clutter, L= 16

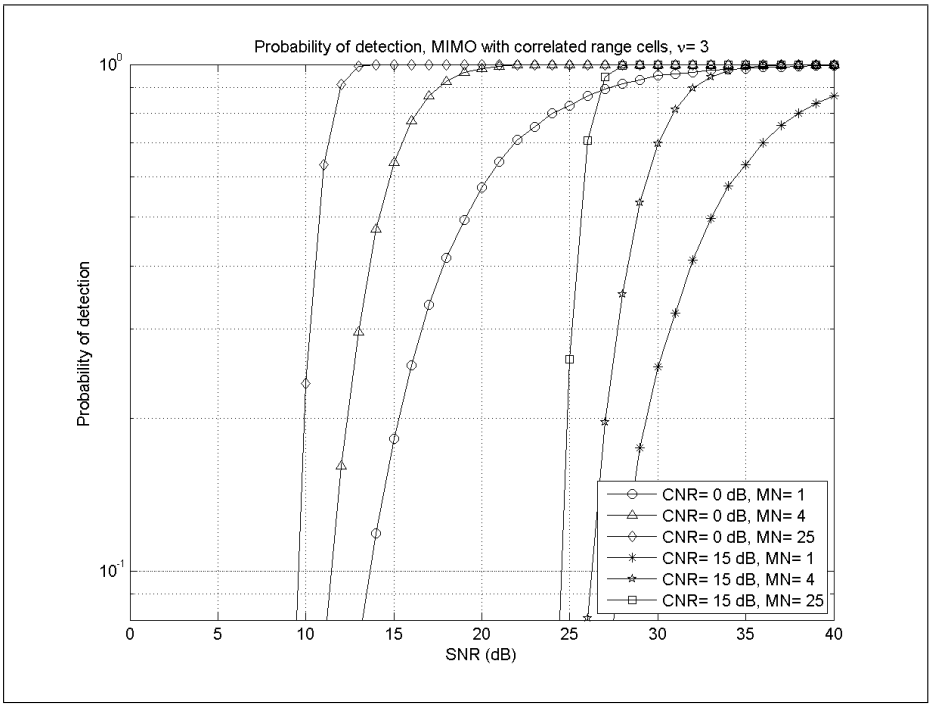

Figure 6.7: P_D, MIMO, correlated clutter, L= 16

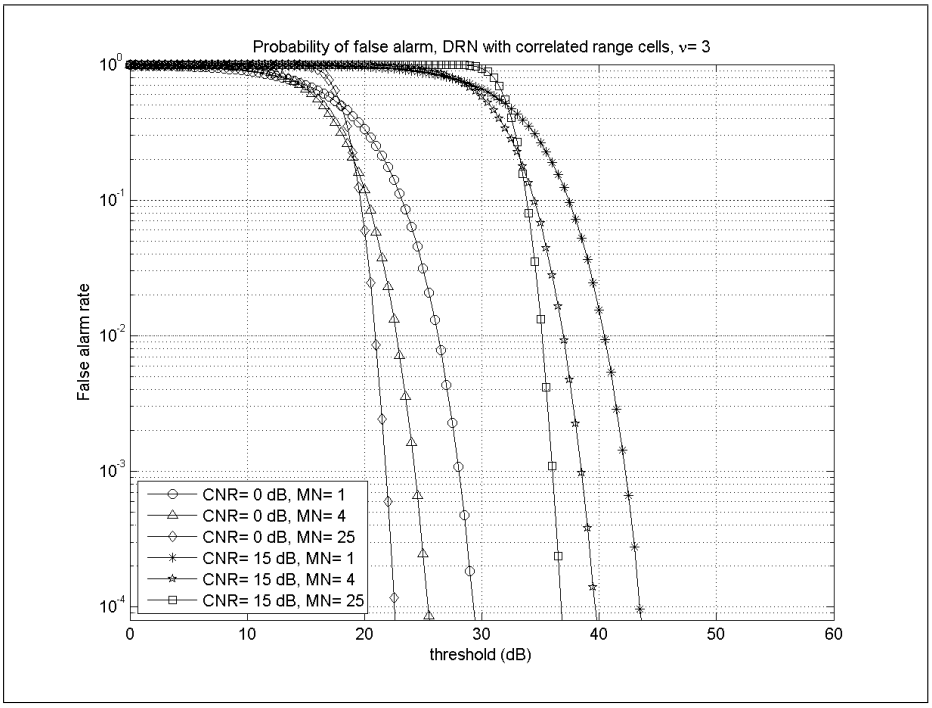

Figure 6.8: FAR, DRN, correlated clutter, L= 16

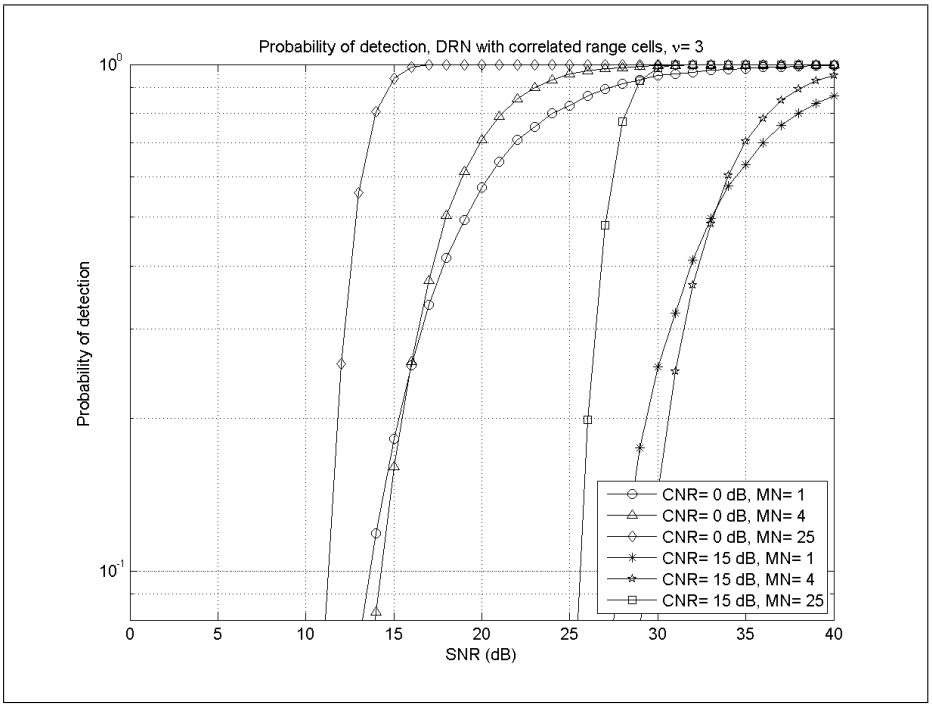

Figure 6.9: P_D, DRN, correlated clutter, L= 16

PDF of the disturbance (noise and clutter). It is worth highlighting that this solution cannot be performed without estimating the clutter texture on a limited number of cells, thus it is reasonable that practical errors in estimates produce mismatches in the data. The improved performance (roughly from 5 to 10 dB compared to the previous set) with whitened data highlights the importance of the effects of correlation.

Statistical considerations

Theoretically, the threshold of the NR system processing MN data, after whitening, can be computed as follows: the sum of MNQ independent complex Gaussian RV with variance $\tau_{i,q} + \sigma_n^2$ is, again, a complex Gaussian RV, say w, with variance

$$\sigma_w^2 = MNQ\sigma_n^2 + \sum_{i=1}^{MN}\sum_{q=1}^{Q}\tau_{i,q} = \hat{\sigma}_n^2 + \hat{\tau}, \tag{6.10}$$

where $\hat{\tau}$ is Γ-distributed with shape parameter ν and mean value $MNQ\mu$. Thus, given a threshold λ_{NR}, the probability of false alarm will be given by

$$P_{FA} = \int_{\lambda_{NR}}^{+\infty}\int_{0}^{+\infty} p\left(r|\hat{\tau},\hat{\sigma}_n^2\right)p(\hat{\tau})\,d\hat{\tau}\,dr, \tag{6.11}$$

where $r = |w|^2$, so $p\left(r|\hat{\tau},\hat{\sigma}_n^2\right)$ is an exponential PDF. Thus

$$\begin{aligned} P_{FA} &= \int_{0}^{+\infty} p(\hat{\tau})\left[\int_{\lambda_{NR}}^{+\infty} p\left(r|\hat{\tau},\hat{\sigma}_n^2\right)dr\right]d\hat{\tau} = \\ &= \int_{0}^{+\infty} p(\hat{\tau})\left[\int_{\lambda_{NR}}^{+\infty}\frac{1}{2\left(\hat{\tau}+\hat{\sigma}_n^2\right)}\exp\left\{-\frac{r}{2\left(\hat{\tau}+\hat{\sigma}_n^2\right)}\right\}dr\right]d\hat{\tau} = \\ &= \int_{0}^{+\infty}\exp\left\{-\frac{\lambda_{NR}}{2\left(\hat{\tau}+\hat{\sigma}_n^2\right)}\right\}p(\hat{\tau})\,d\hat{\tau}. \end{aligned} \tag{6.12}$$

Under the same hypothesis, the PDF of the received power of clutter and noise, when processing data in MIMO systems, can be expressed as the convolution of MN identical PDFs $p(r)$ where

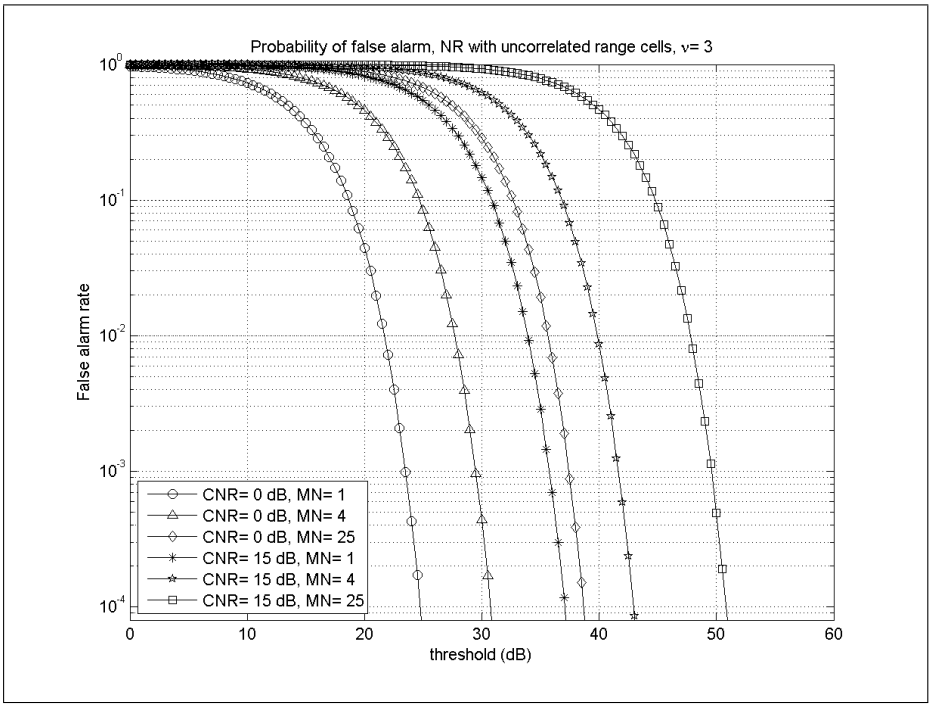

Figure 6.10: FAR, NR, whitened clutter, L= 16

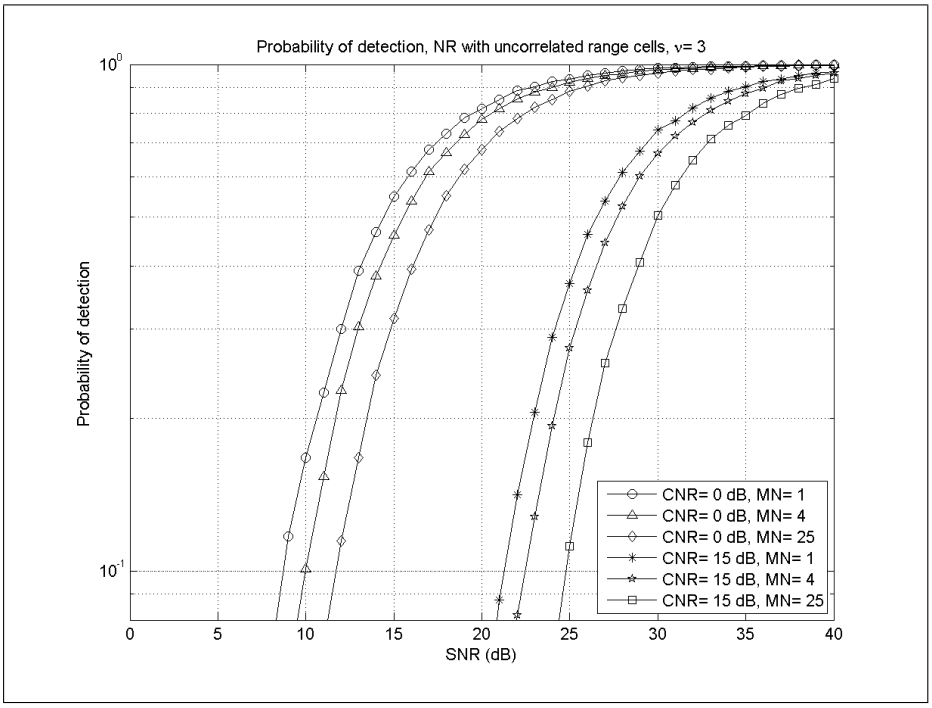

Figure 6.11: P_D, NR, whitened clutter, L= 16

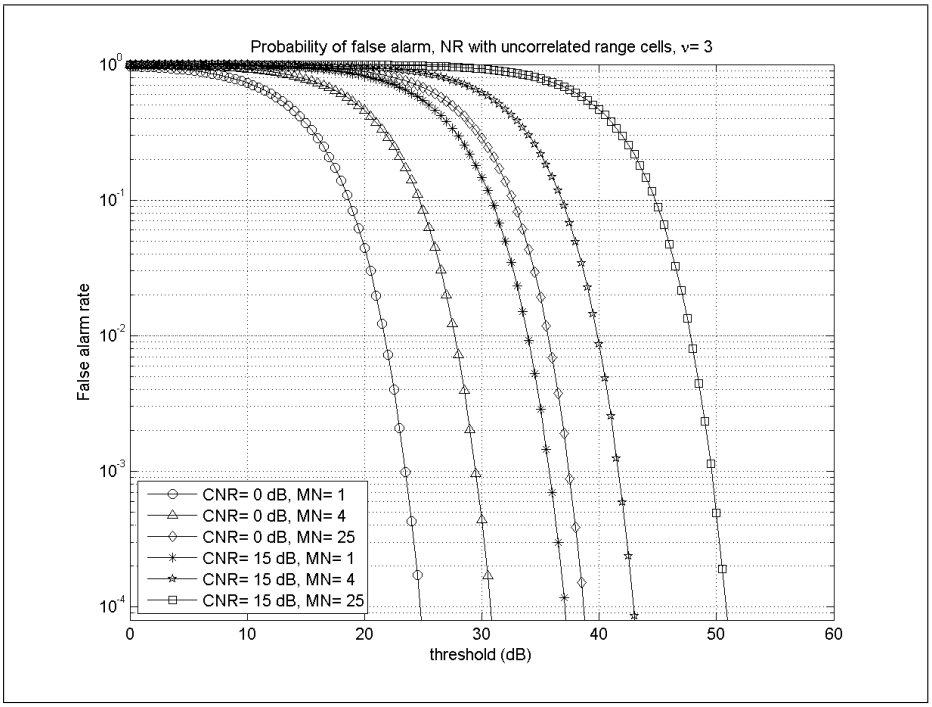

Figure 6.12: FAR, RPNR, whitened clutter, L= 16

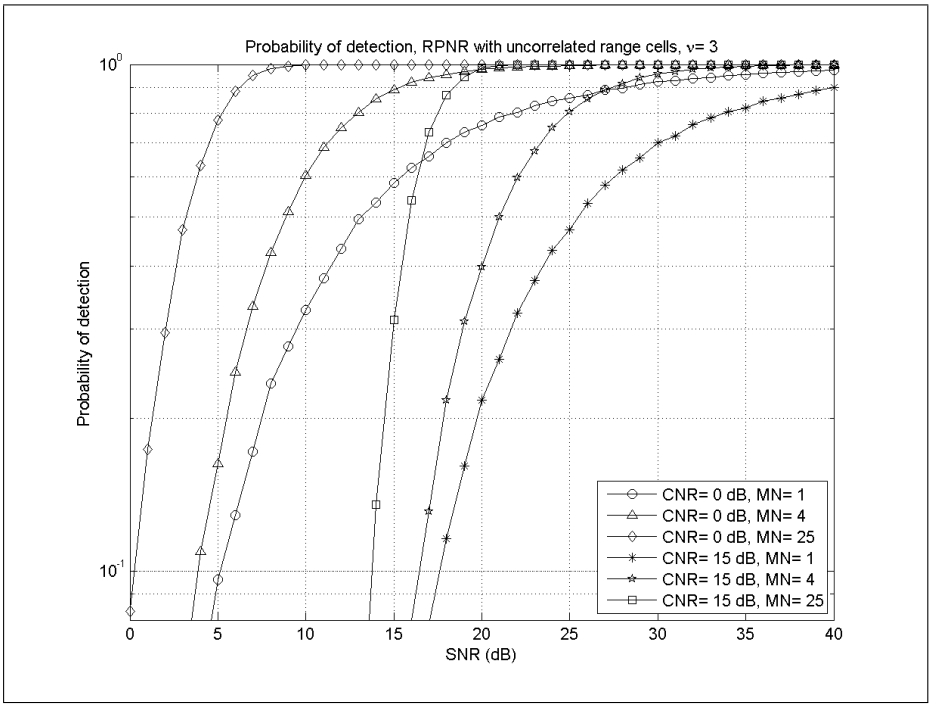

Figure 6.13: P_D, RPNR, whitened clutter, L= 16

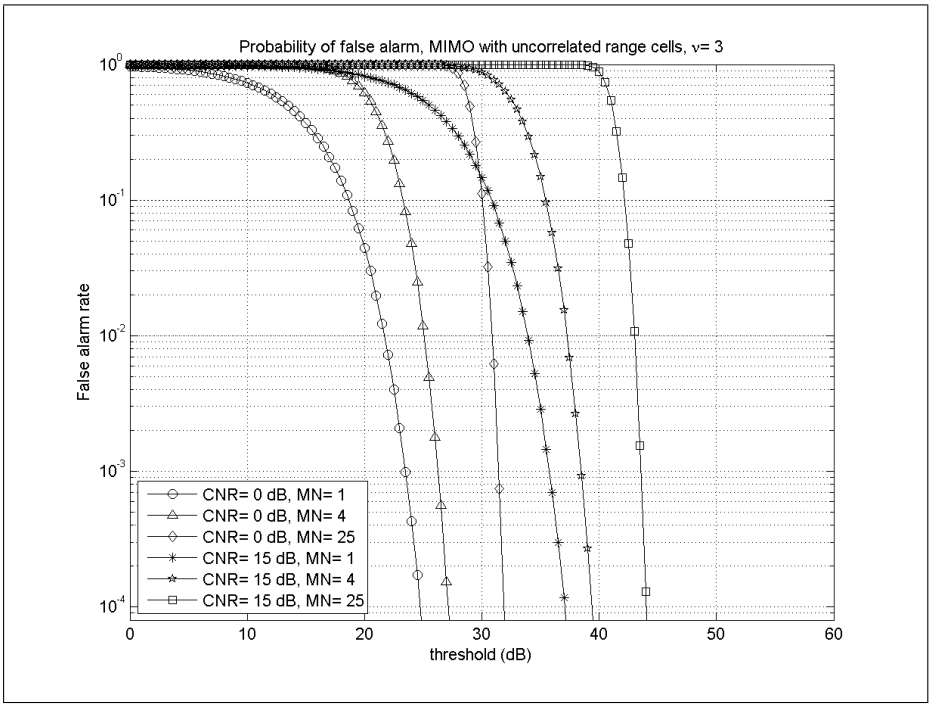

Figure 6.14: FAR, MIMO, whitened clutter, L= 16

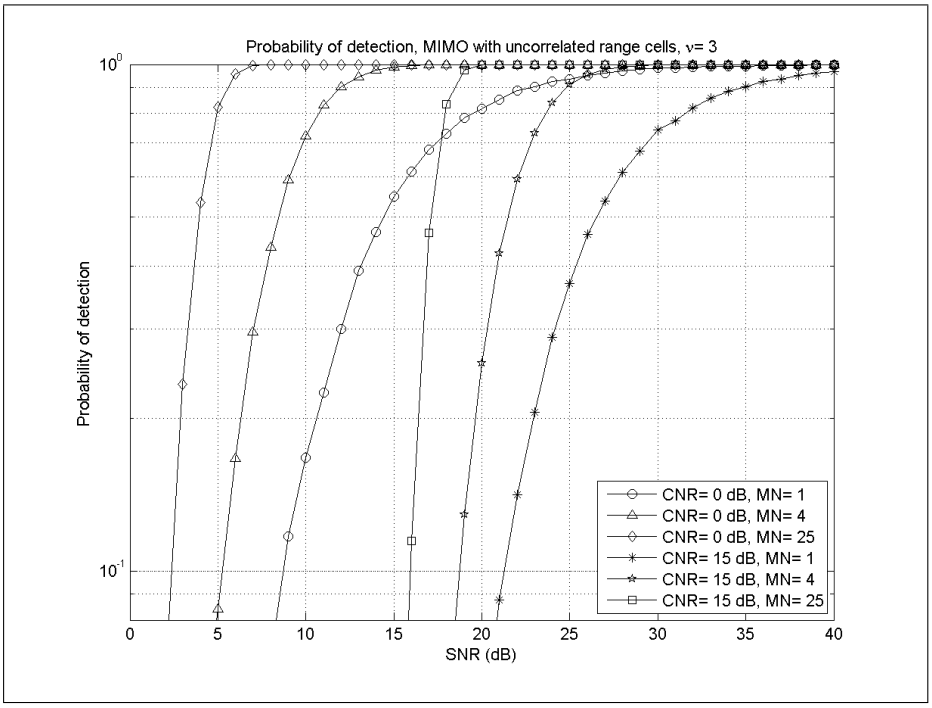

Figure 6.15: P_D, MIMO, whitened clutter, L= 16

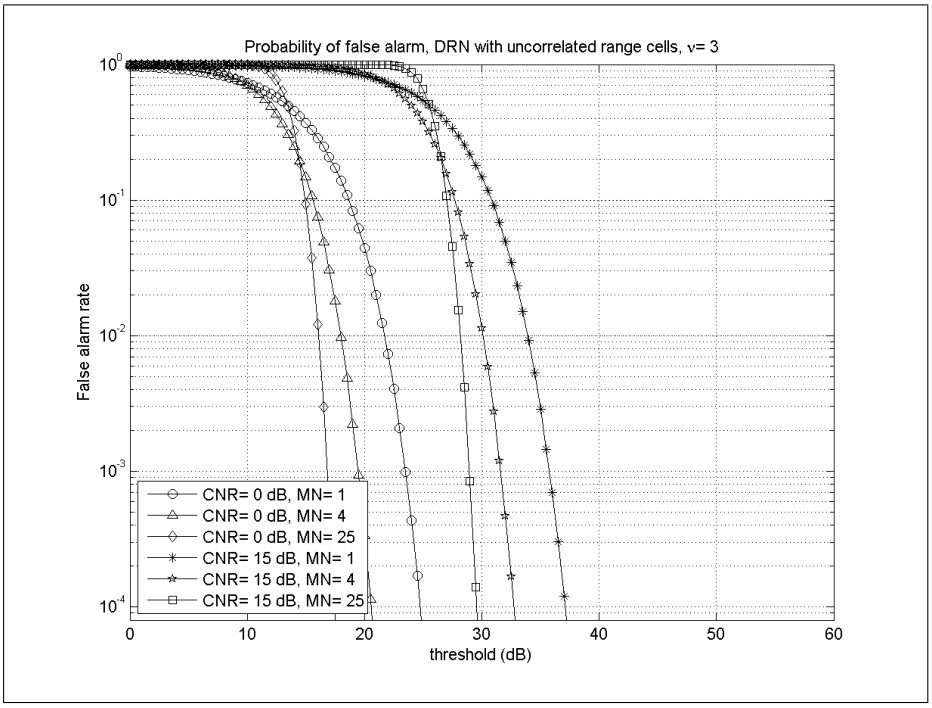

Figure 6.16: FAR, DRN, whitened clutter, L= 16

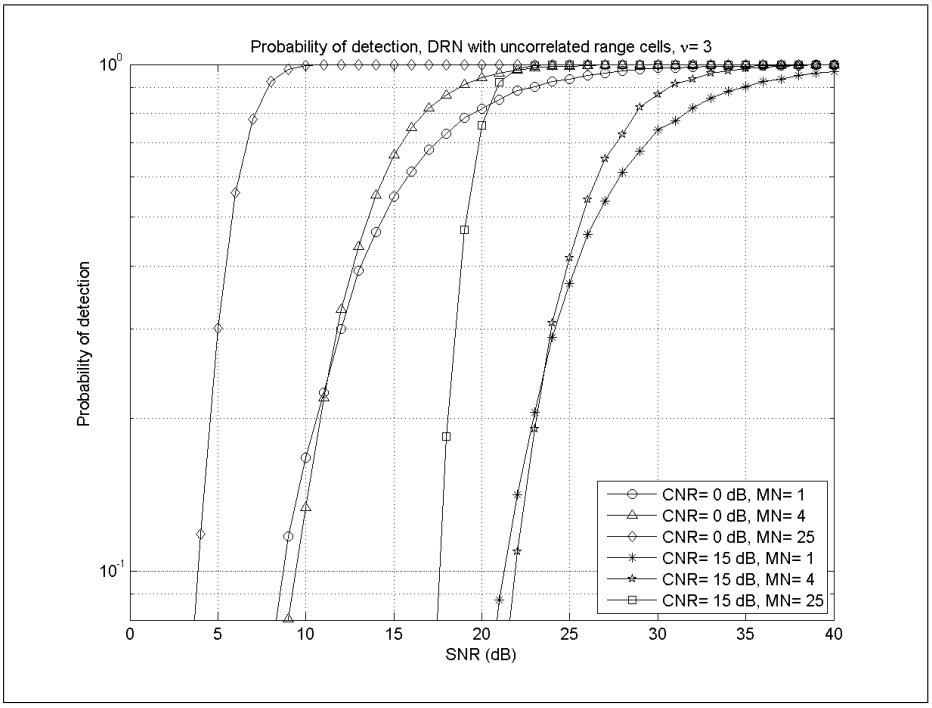

Figure 6.17: P_D, DRN, whitened clutter, L= 16

$$p(r) = \frac{1}{2\left(\sigma'^2_n + \tau'\right)} \exp\left\{-\frac{1}{2\left(\sigma'^2_n + \tau'\right)}\right\} p(\tau') \tag{6.13}$$

and σ'^2_n and τ' are RV generated as in equation (6.10) but performing the summation only on the time domain. It is clear then that expressing the FAR in a closed form is hard. Prediction in a closed form of the results in detection is not possible for both netted radar and MIMO systems as well.

The overall results achieved show a loss of performance for both NR and MIMO systems when the correlation is present. This is consistent with the results of monostatic systems.

6.3.2 Adaptive threshold (CA CFAR) on raw data

In this Section an adaptive CFAR algorithm for detection in MIMO radar and RPNR systems operating in the same clutter conditions is considered. As before, a statistical description of the signal processing is reported and thus the results in FAR and detection. Moreover the incoherent algorithm is compared with a coherent way of processing the same data in order to provide a deeper understanding.

In particular an adaptive Cell Averaging Constant FAR (CA CFAR) incoherent algorithm is applied to provide an increased tolerance to high power peaks that might occur when clutter is present. The CA CFAR is a well known algorithm [17, 27]. Two possible implementations of this algorithm are considered here. In both the clutter power is estimated by averaging L range cells adjacent to the Cell Under Test (CUT). The only difference is in the choice of the cells used for this estimation. In the first case the two adjacent cells to the CUT are taken into account and in the second they are disregarded. In the latter case the presence of these two 'guard cells' can be justified since a target may occupy more than one resolution cell, so its backscattering power can take part in the adaptive threshold estimation, decreasing the overall P_D. However, in the rest of the Section the target is assumed to be within one resolution cell only. Figure 6.18 shows a schematic representation of a CA CFAR detector. The grey

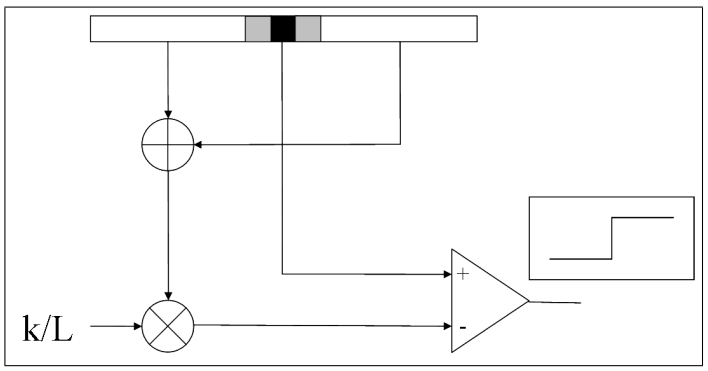

Figure 6.18: CA CFAR scheme for a monostatic radar

cells represent the 'guard cells' that in the second version of the algorithm are not been taken into account in estimating the detection threshold. The black cell is the CUT.

In the monostatic case the CA CFAR algorithm compares the power of the CUT with the average power of L adjacent cells. So, terming x_m^2 the content of the CUT, the average power $|y_m|^2$ of the L adjacent cells can be expressed as (in the case of guard cells the indexes should be appropriately shifted):

$$|y_m|^2 = \sum_{h=m-L/2}^{m-1} |x_h|^2 + \sum_{h=m+1}^{m+L/2} |x_h|^2. \tag{6.14}$$

The decision rule is therefore:

$$|x_m|^2 - \frac{k}{L}|y_m|^2 \underset{H_0}{\overset{H_1}{\gtrless}} 0, \tag{6.15}$$

where $\frac{k}{L}$ is an averaging parameter guaranteeing a certain FAR.

In this case, from all the nodes, a vector X made up of all the measurements from the CUT and a vector Y with the measurements from all the secondary data are gathered. The overall decision rule in the MIMO case can therefore be written as follows:

$$\sum_{q=1}^{MN} |x_m(q)|^2 - \frac{k}{L} \sum_{q=1}^{MN} |y_m(q)|^2 \underset{H_0}{\overset{H_1}{\gtrless}} 0, \tag{6.16}$$

When a RPNR system is considered, in the event of the presence of a target in the CUT, the algorithm is applied coherently, assuming full knowledge of the geometry and the target's position, in order to achieve the maximum SNR. Clearly, once again, this is not possible in practice so here it is used to represent an upper performance bound. As consequence, a coherent summation, aligning the phases of the echoes from the target, is performed and a CA CFAR decision is applied. Mathematically, in this case the decision rule is:

$$\left| \sum_{q=1}^{MN} \hat{x}_m(q) \right|^2 - \frac{k}{L} \left| \sum_{q=1}^{MN} \hat{y}_m(q) \right|^2 \underset{H_0}{\overset{H_1}{\gtrless}} 0, \tag{6.17}$$

where $\hat{x}_m(q)$ and $\hat{y}_m(q)$ are respectively $x_m(q)$ and $y_m(q)$ after aligning the phases of the target only, when present. Similarly for the NR case, with the only exception of the phase-aligning.

As expected, for the DRN case, a decision rule on the single node is considered as in equation (6.14). Detections are then fused together using the 50% + 1 rule used before.

Figures from 6.19 to 6.34 show the performance in FAR and P_D for different values of CNR, when the multiplicative factor k varies (L is set to 16 as in the previous Sections). All these results have been generated for clutter with shape parameter $\nu = 3$. Other values of this parameter have been taken into account. However, whereas the overall behaviour of the curves is not modified in concepts as a function of this parameter, results for different ν are not reported.

As in previous results, the higher the number of nodes, the smaller the ratio $\frac{k}{L}$ guaranteeing the performance in terms of FAR. Moreover, a comparison of these figures highlights the loss of performance due to

discarding the guard cells in the CA CFAR algorithm. This is evident particularly in the monostatic systems: with spiky and highly correlated clutter, discarding the closest cells can lead to a considerable underestimation that has to be compensated with a bigger value of $\frac{k}{L}$.

However, it is worth noting that multistatic systems manage to make this loss much smaller: with 4 nodes (2 tx, 2 rx), but especially with 25 nodes (5 tx, 5 rx) this is almost negligible. This is due to the increased information carried by the radar network and to the diverse aspect angle of the clutter that allow a better estimation of the characteristics of the area under observation and mitigates the loss of knowledge occurring in disregarding the most meaningful cells. Small differences between curves with the same numbers of nodes, but different CNR, are due to some residuals of thermal noise affecting the processing. The noise samples are in fact independent and therefore its response to the CA algorithm has similar effects to removing the adjacent range cells of a CUT: it decreases the algorithm's accuracy in averaging. Of course the lower the CNR, the higher the thermal noise effect.

A common feature observed in coherent processing is that increasing the number of nodes and processing data coherently do not modify the shape of the original distribution of the interference and therefore the behavior of the performance is similar to the monostatic case. On the contrary the incoherent processing realized by the MIMO radar systems modifies this distribution. In those Figures, as well as in the work produced so far, this modification allows setting a lower threshold, when compared to the coherent case, for the FAR.

From the detection point of view, there are minor differences between the reported results of the two versions of the CA CFAR implementation. Once again MIMO systems loose a few dB against the RPNR and DRN a few dB against MIMO. This is due to the lower threshold set for FAR that allows recovering most of the losses due of sub-optimal processing. As previously, NR apart, here multistatic systems overcome the monostatic one also when constant power is transmitted.

The relatively high values of SINR necessary to yield an adequate

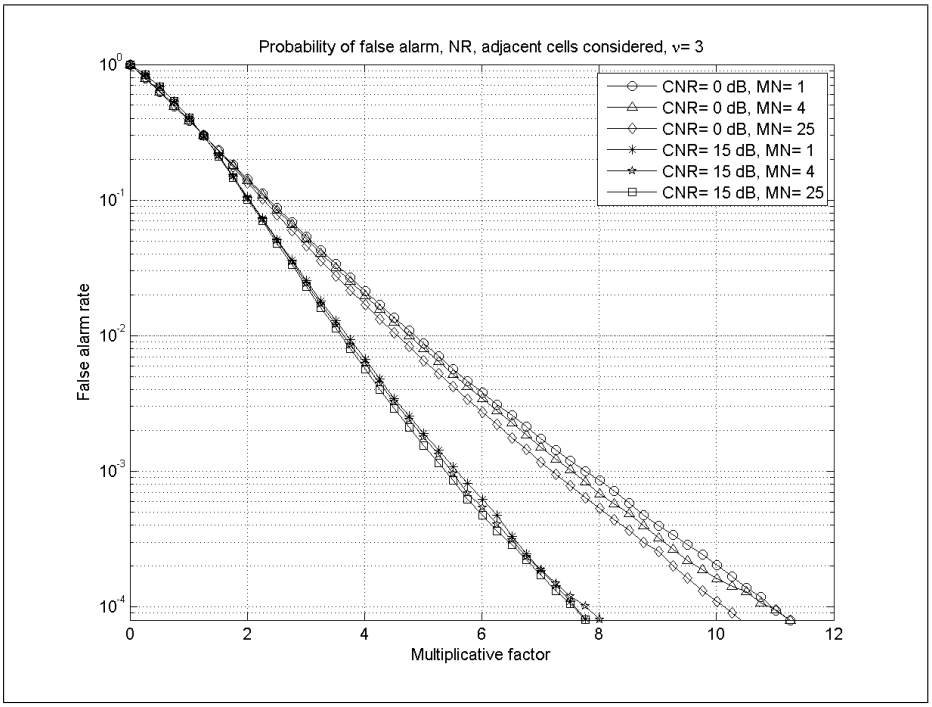

Figure 6.19: FAR, NR, guard cells considered, L= 16

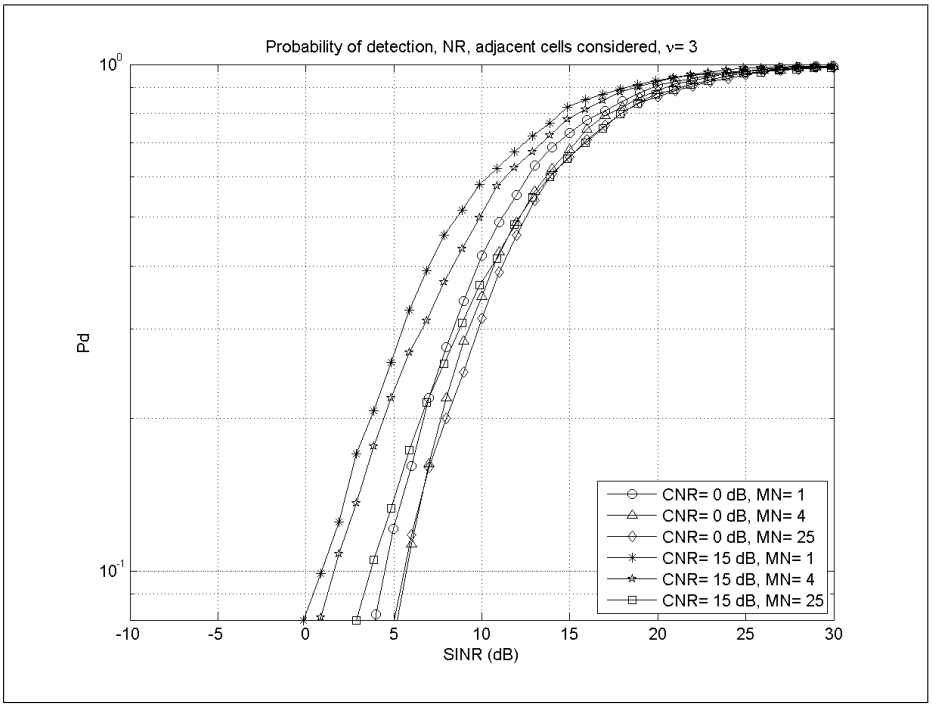

Figure 6.20: P_D, NR, guard cells considered, L= 16

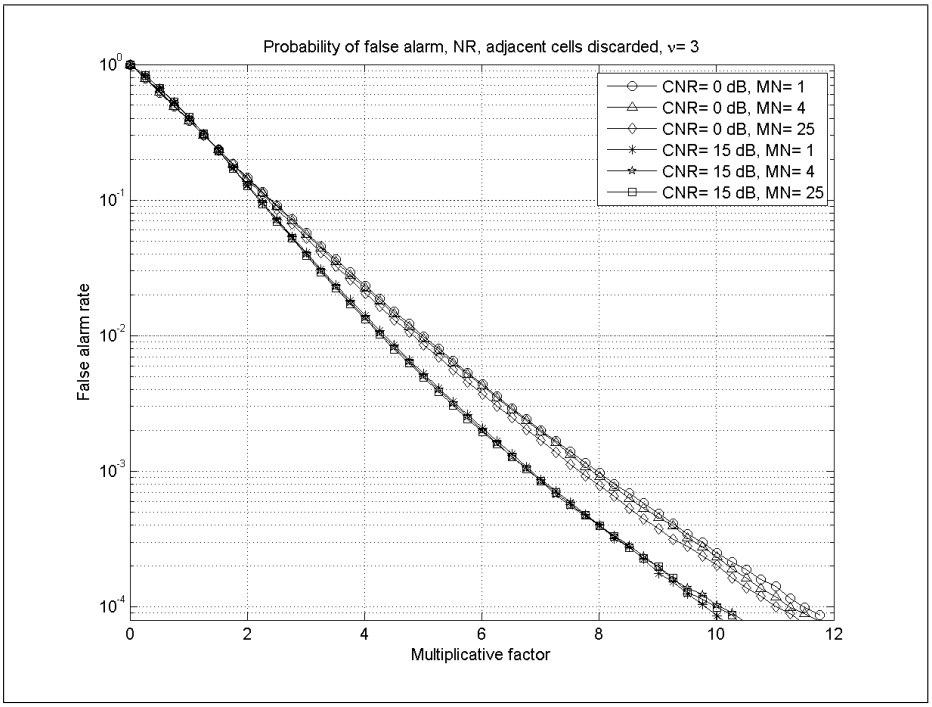

Figure 6.21: FAR, NR, guard cells discarded, L= 16

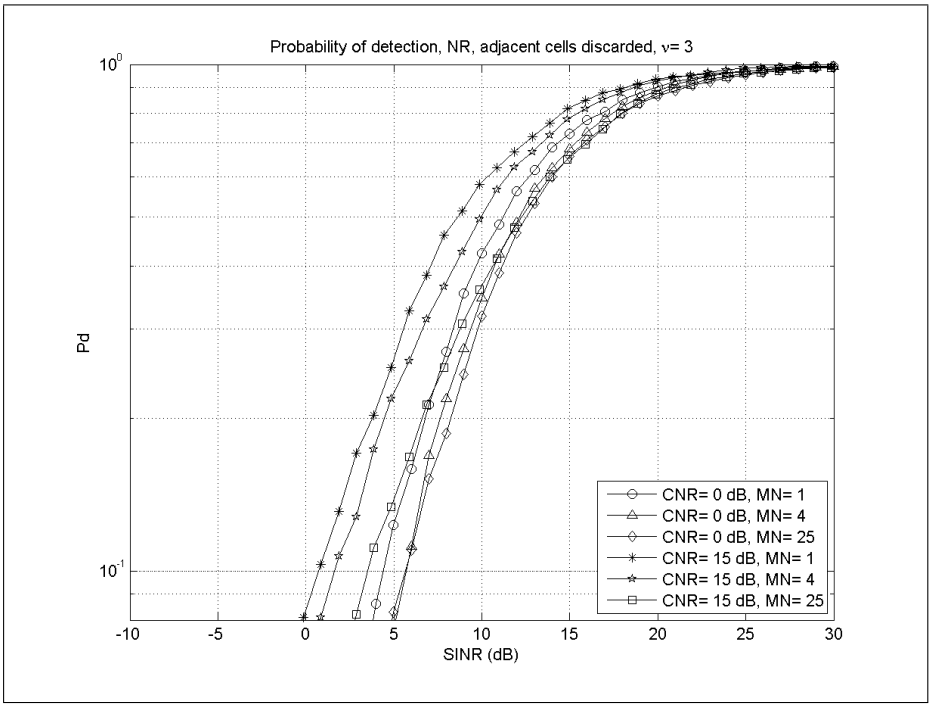

Figure 6.22: P_D, NR, guard cells discarded, L= 16

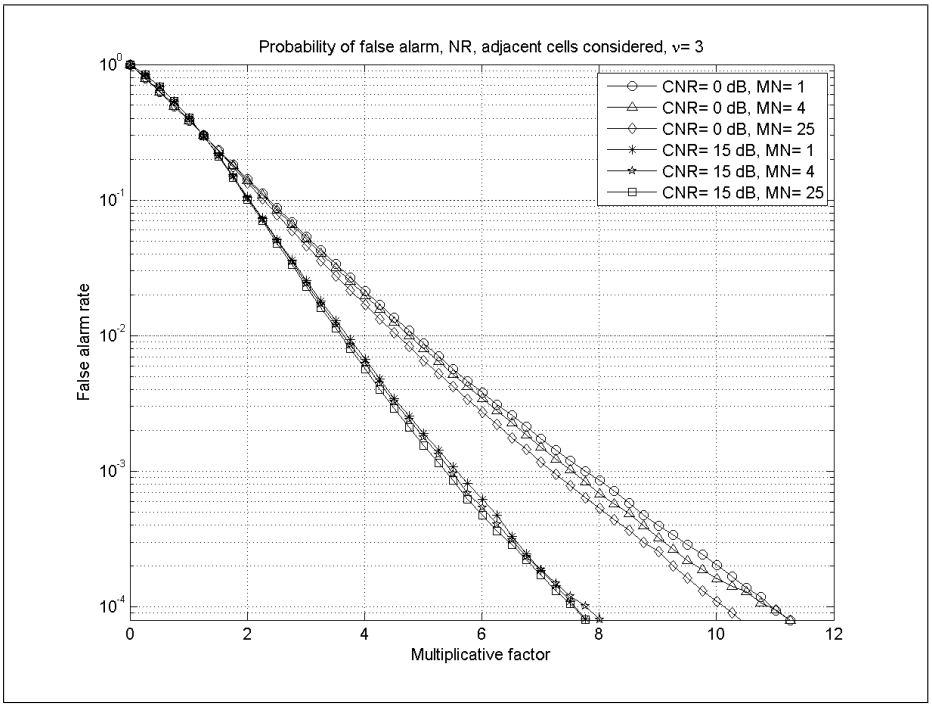

Figure 6.23: FAR, RPNR, guard cells considered, L= 16

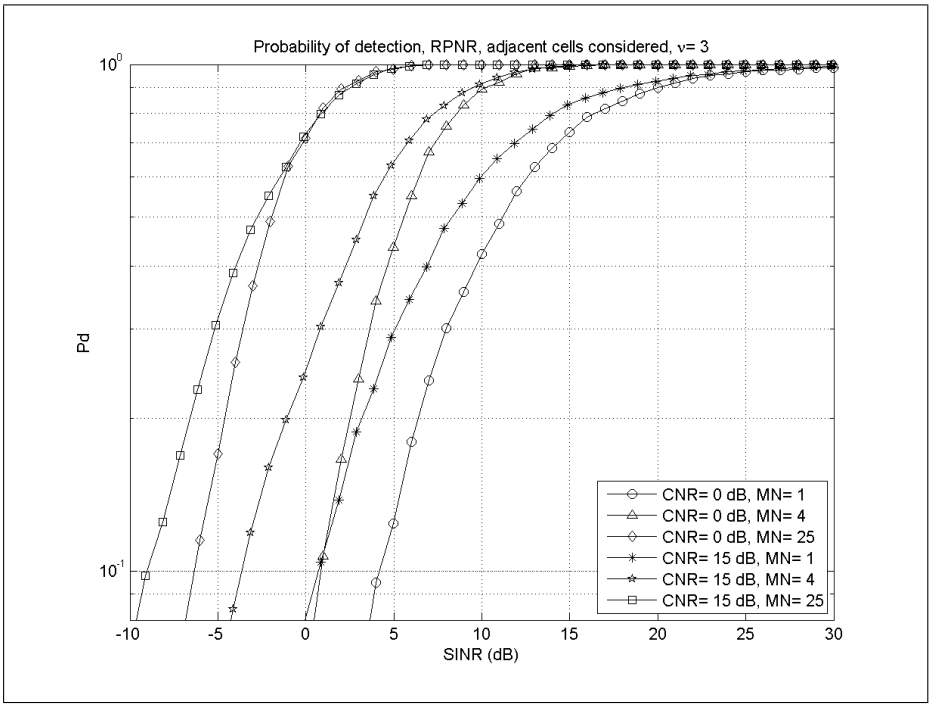

Figure 6.24: P_D, RPNR, guard cells considered, L= 16

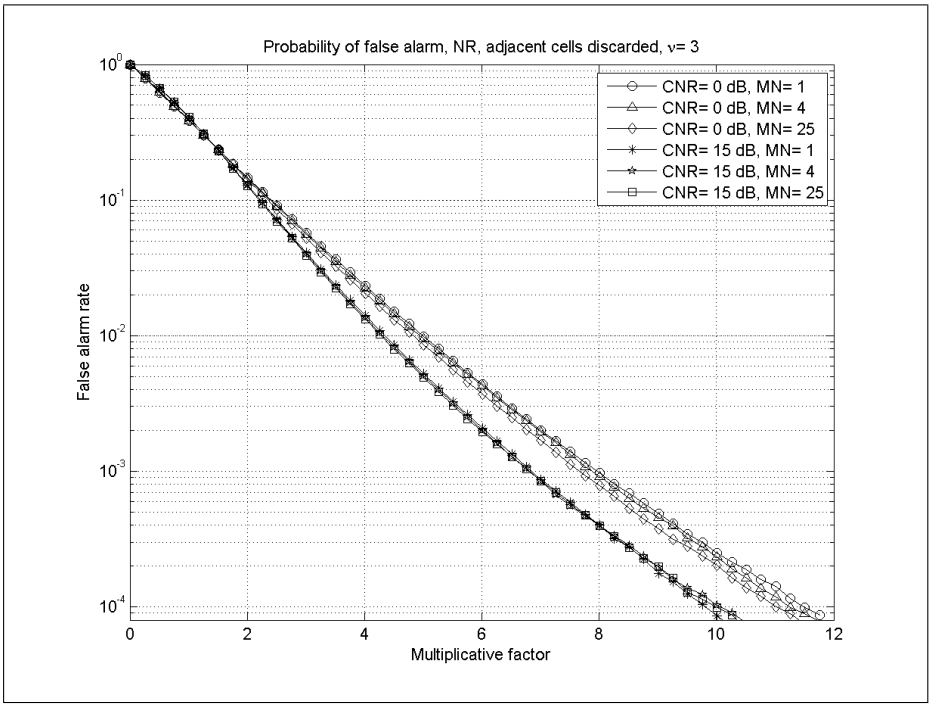

Figure 6.25: FAR, RPNR, guard cells discarded, L= 16

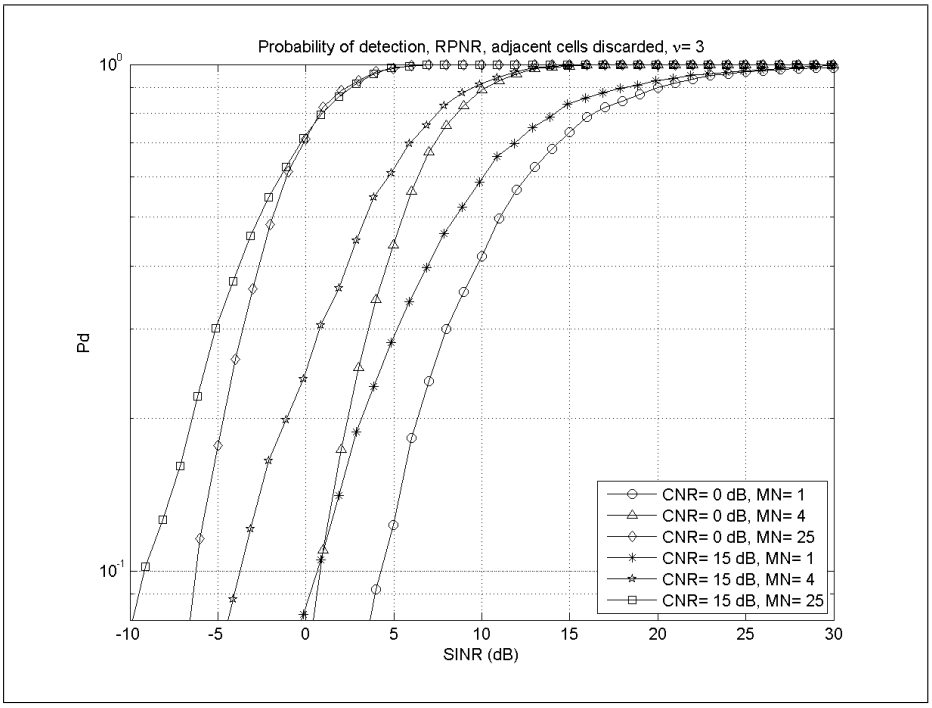

Figure 6.26: P_D, RPNR, guard cells discarded, L= 16

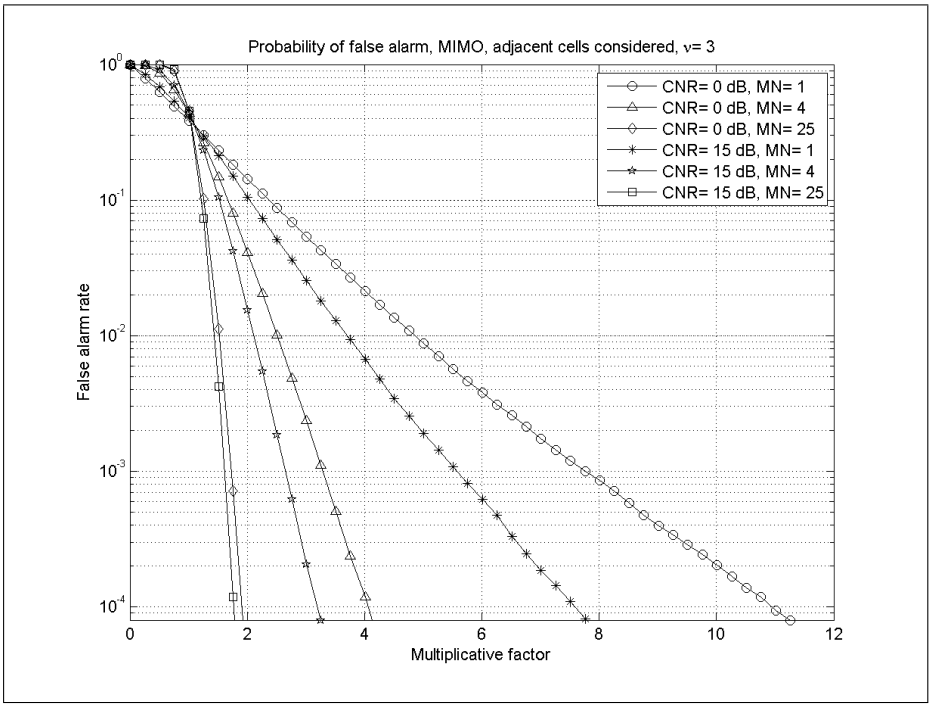

Figure 6.27: FAR, MIMO, guard cells considered, L= 16

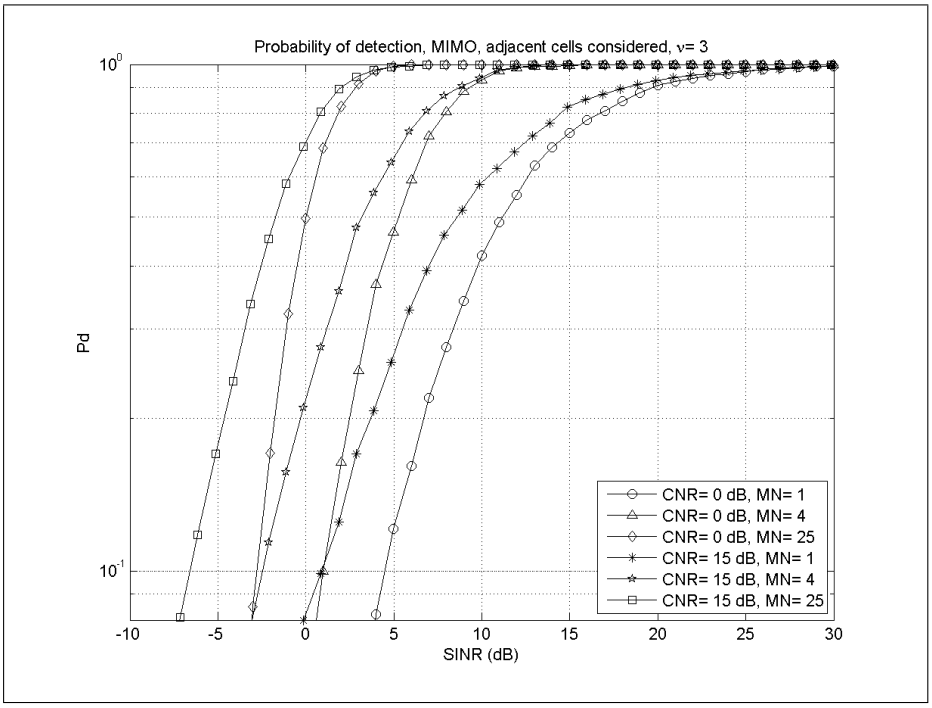

Figure 6.28: P_D, MIMO, guard cells considered, L= 16

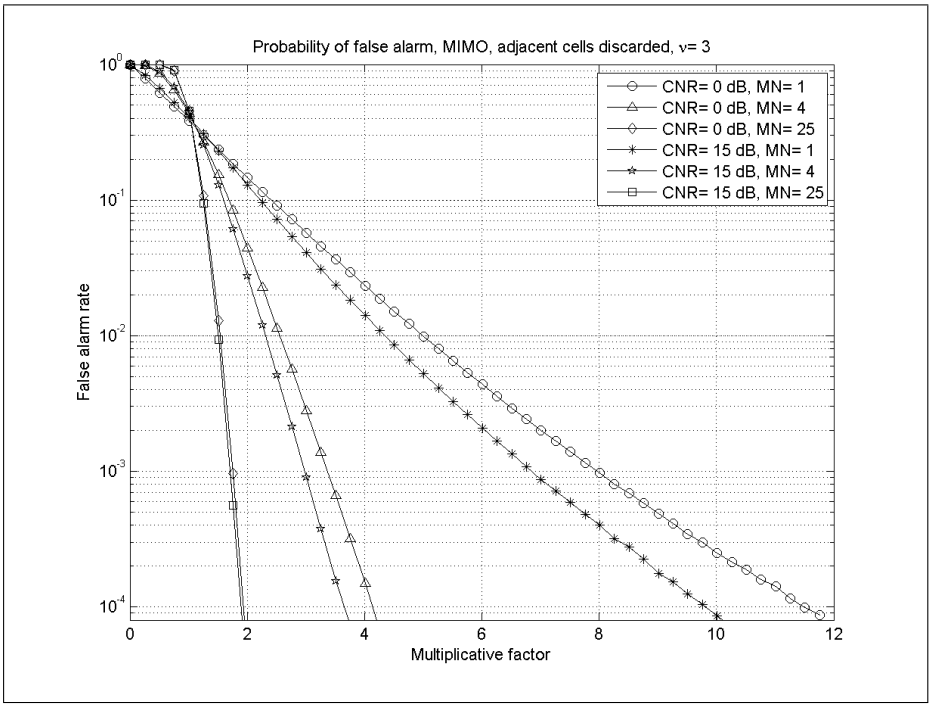

Figure 6.29: FAR, MIMO, guard cells discarded, L= 16

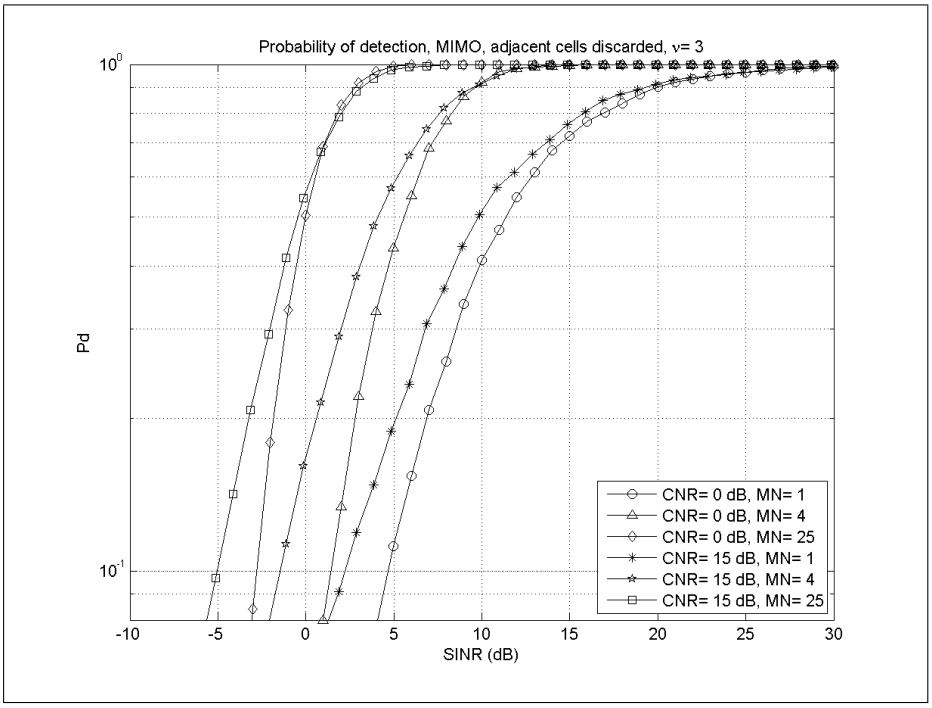

Figure 6.30: P_D, MIMO, guard cells discarded, L= 16

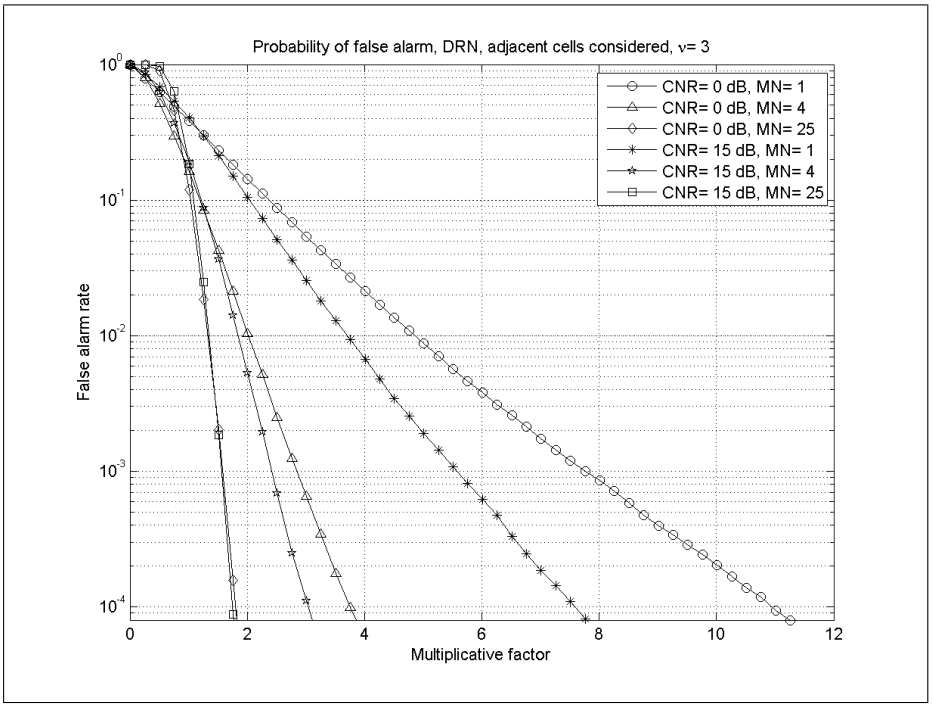

Figure 6.31: FAR, DRN, guard cells considered, L= 16

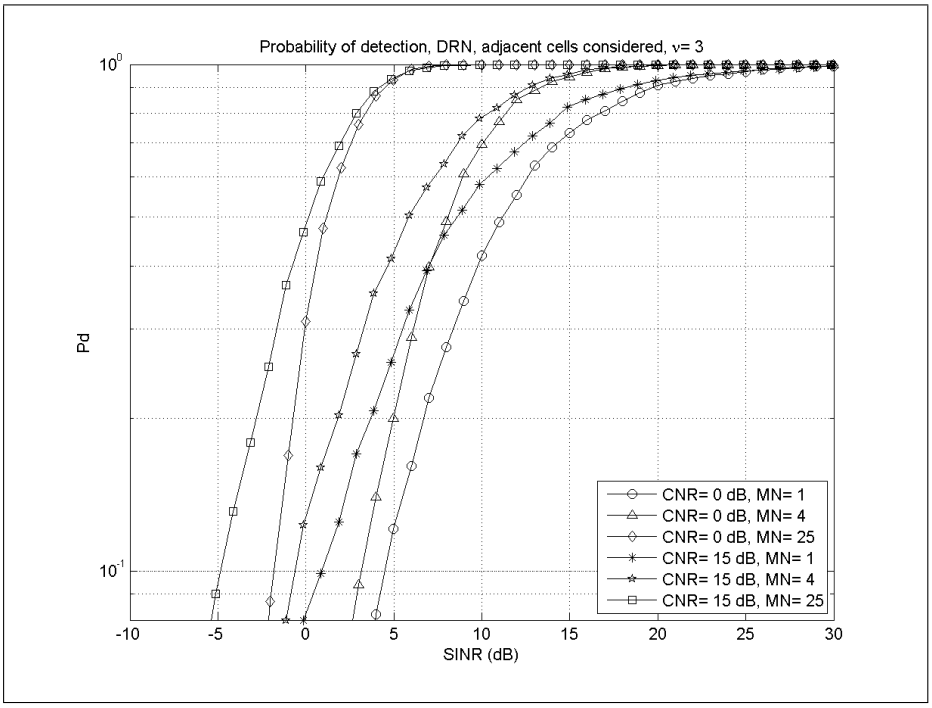

Figure 6.32: P_D, DRN, guard cells considered, L= 16

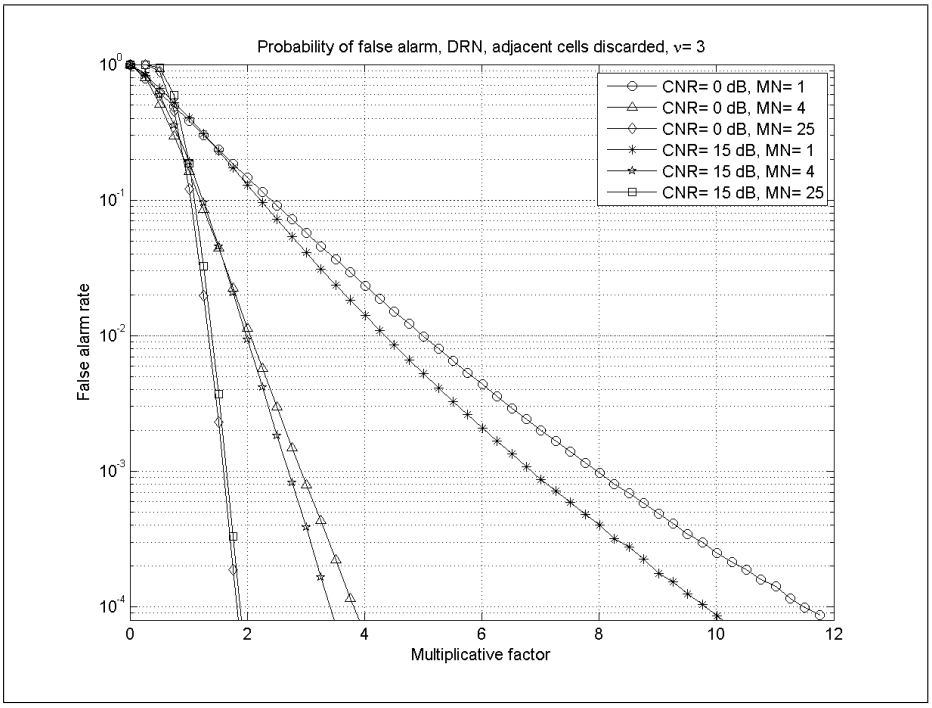

Figure 6.33: FAR, DRN, guard cells discarded, L= 16

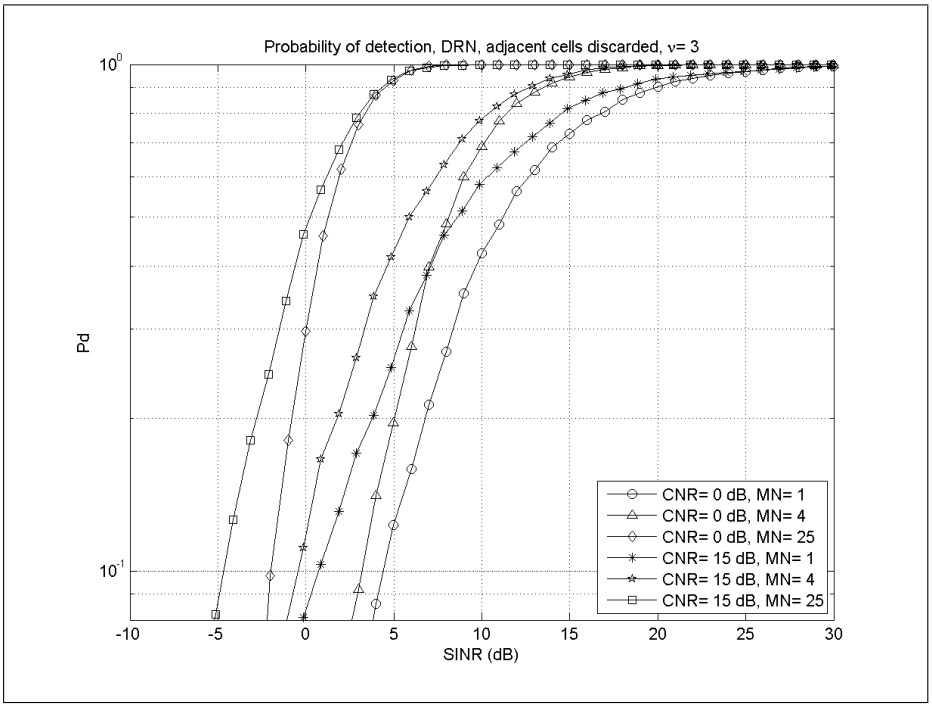

Figure 6.34: P_D, DRN, guard cells discarded, L= 16

detection rate can be justified by taking into account the distributions used in the models and the integration time ($Q = 16$ pulses) before processing: actually in the time-integration process, whilst the noise and signal's power achieve a gain of Q only, because they are uncorrelated, the power of the clutter, that is highly correlated, is magnified by a much higher factor.

Statistical considerations

In this Section the modification of the statistics of the received signals during the processing are briefly discussed. From a statistical point of view, in a monostatic system using a CA CFAR algorithm as in equation (6.15) the random variable z_m, given τ is considered:

$$z_m = |x_m|^2 - \frac{k}{L}|y_m|^2. \tag{6.18}$$

Detection occurs when $z_m \geq 0$. This infers that, given its PDF $p_z(z_m|\tau)$, the system yields detection with a rate equal to

$$\int_0^{+\infty} p_z(z_m|\tau)\, dz_m. \tag{6.19}$$

Therefore $p_z(z_m|\tau)$ can be written as function of x_m and y_m:

$$p(z_m|\tau) = p\left(|x_m|^2 - \frac{k}{L}|y_m|^2|\tau\right). \tag{6.20}$$

This expression is also a function of the noise power and of the correlation properties of the clutter.

If the samples x_m in equation (6.15) are statistically independent and they have constant texture, the final expression of the PDF is much simpler and clearer. Whilst the second assumption can be considered fairly close to reality, as the texture is almost constant in the interval of few range cells, the first assumption is usually not realistic, unless a pre-processing of data is realized in order to remove the correlation between range cells. In any case, the statistical modifications that follow and their consequences are useful to improve understanding especially when the correlation between

the samples of clutter is reintroduced. Under the hypotheses above, it is possible to write:

$$p(z_m|\tau) = p_{x^2}(|x_m|^2|\tau) * p_{y^2}\left(-\frac{k}{L}|y_m|^2|\tau\right) = \\ = p_{x^2}(|x_m|^2|\tau) \times p_{y^2}\left(\frac{k}{L}|y_m|^2|\tau\right). \tag{6.21}$$

When no target is present, $p_{x^2}(|x_m|^2|\tau)$ is an exponential PDF function of power $w|\tau$, i.e.

$$p_{x^2}(|x_m|^2|\tau) = p_{wx}(w|\tau) = \\ = \frac{1}{\tau + \sigma_n^2}\exp\left\{-\frac{w}{\tau + \sigma_n^2}\right\}, \tag{6.22}$$

and $p_{y^2}(|y_m|^2|\tau)$ is a gamma, as a result of L convolutions of the distribution in equation (6.22) with itself:

$$p_{y^2}(|y_m|^2|\tau) = p_{wy}(w|\tau) = \\ = p_{wy}(w|\tau) * p_{wy}(w|\tau) * \cdots * p_{wy}(w|\tau) = \\ = \frac{1}{(L-1)!}\frac{1}{\tau + \sigma_n^2}\left(-\frac{L}{k}\frac{w}{\tau + \sigma_n^2}\right)^{L-1}\exp\left\{-\frac{L}{k}\frac{w}{\tau + \sigma_n^2}\right\}, \tag{6.23}$$

Considering $p_{y^2}\left(\frac{k}{L}|y_m|^2|\tau\right)$, as in equation (6.23), the factor $\frac{k}{L}$ has to be taken into account. Consequently this PDF can be expressed as:

$$p_{y^2}(|y_m|^2|\tau) = \\ = \frac{L}{k}\frac{1}{(L-1)!}\frac{1}{\tau + \sigma_n^2}\left(-\frac{L}{k}\frac{w}{\tau + \sigma_n^2}\right)^{L-1}\exp\left\{-\frac{L}{k}\frac{w}{\tau + \sigma_n^2}\right\}, \tag{6.24}$$

Figure 6.35 shows the PDF in equation (6.20) (in a logarithmic scale on

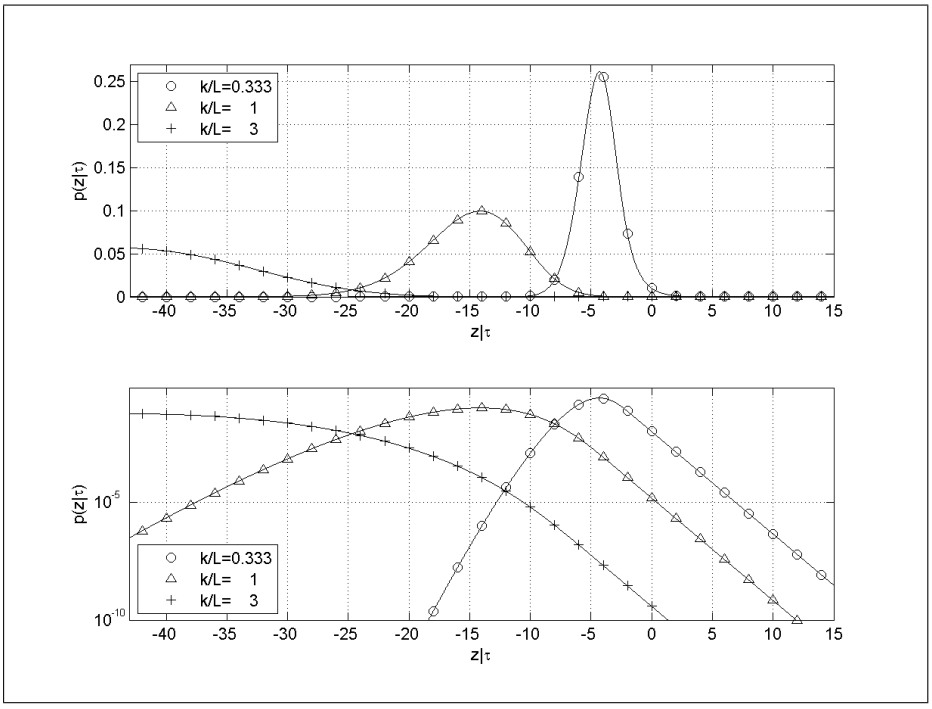

Figure 6.35: PDF of $z_m|\tau$, monostatic case

the vertical axis) for several values of $k\left(\frac{16}{3}, 16, 48\right)$, $L = 16$ and $\tau + \sigma_n^2 = 1$. Since no target is present, the area of the curves for $z \geq 0$ represents the P_{FA}. As expected, the lower the ratio $\frac{k}{L}$ (i.e. the lower averaging coefficient of the power from the all the secondary data), the bigger the FAR.

In a multistatic incoherent radar system, such as a MIMO, we have to develop the distribution descriptions starting from the decision rule, equation (6.16), and the mono/bistatic distributions, as in equations (6.23) and (6.24). Working in analogy with the monostatic case, the curves for $p(z_m|\tau)$ are as in Figure 6.36.

These curves have been obtained considering a multistatic system made of 2 tx and 2 rx and they confirm that, also in this case, the lower the ratio $\frac{k}{L}$, the bigger the FAR. From a comparison with Figure 6.35 a modification of the PDF is observed. In particular, it is worth mentioning that the FAR increases for small values of $\frac{k}{L}$, whilst it decreases for greater values of this ratio.

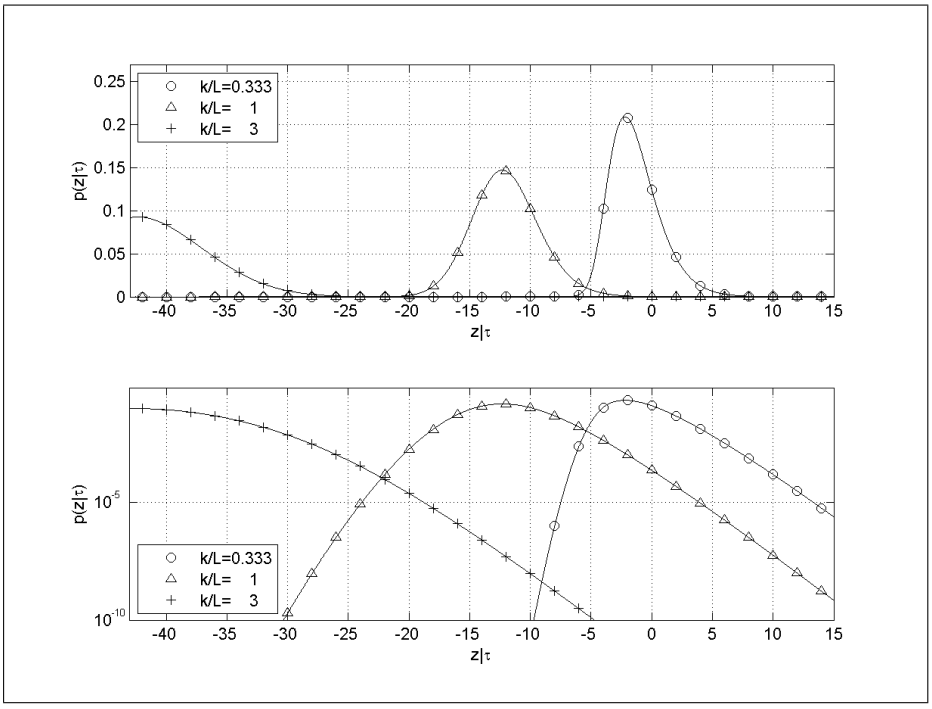

Figure 6.36: PDF of $z_m|\tau$, multistatic case (MN= 4)

Statistics in the coherent case (RPNR) are similar to the monostatic case since one CA CFAR is present at the end of coherent summation of all the components, as in equation (6.17). In this case, and under the same assumptions of the MIMO case (i.e. uncorrelated samples of clutter and constant texture in range), the only difference with the monostatic case is that the coherent pre-summation of all the contributes originates two distributions identical to equations (6.23) and (6.24) apart from a multiplicative factor for the variance $\tau + \sigma_n^2$: this is due to the effects of summing coherently *MN* independent random variables. For brevity the corresponding curves are not reported.

In this Chapter it has been confirmed that MIMO and DRN approach the performance of the best coherent system also under the assumption of clutter. They both have superior detection performance to (not-re-phased)

NR. A decentralized approach has also been shown to have a simplest structure of detector with moderate losses in SNR. Most of the results of the previous Chapter have also been confirmed.

Chapter 7

Coverage

Radar sensitivity and coverage are fundamental attributes of system performance and hence are here considered as a means of comparison of the different processing approaches. Therefore here the sensitivity of each processing approach and subsequent coverage capacity are computed as a function of the number of nodes in the radar network. This allows the received power and the SNR levels for a target in a particular geometry to be examined. It is recalled that a constant transmit power is supplied to the radar network regardless of the number of transmitters as has been used previously. This allows for a more straightforward comparison of performance.

7.1 Sensitivity

From the bistatic radar equation [4] the power received $P_r(m,k)$ from a target at a distance R_m from the transmitter and R_k from the receiver is given by

$$SNR(m,k) = \frac{P_0}{M}\frac{G_T(m)G_R(k)\lambda^2\sigma(\theta_{m,k},\phi_{m,k})}{(4\pi)^3 R_m^2 R_k^2 LKTBF} = \frac{P_r(m,k)}{KTBF} \tag{7.1}$$

where $P_r(m,k)$ is the received power of the useful signal, K is Boltzmann's constant, T is the receiver temperature in Kelvins, B is the bandwidth of

the system and F is the noise figure and the rest of the symbols are defined in Section 4. This reduces to the monostatic case when $R_m = R_k$.

All the parameters with no dependency on distance, number of nodes or RCS are grouped and give the symbol $\rho_{m,k}$ (where m refers to the transmitter and k to the receiver). Thus:

$$\rho_{m,k} = P_0 \frac{G_T(m) G_R(k) \lambda^2}{(4\pi)^3 L}. \tag{7.2}$$

Therefore the dependency of the power at a single node of the network system on the range and on the number of transmitters is:

$$SNR(m,k) = \frac{1}{M} \frac{\rho_{m,k} \sigma(\theta_{m,k}, \phi_{m,k})}{R_m^2 R_k^2} \frac{1}{KTBF}. \tag{7.3}$$

In the rest of this section, for simplicity and to allow an immediate comparison, it is assumed that $P_0 = 5$ kW (peak), $G_T(m) = G_R(k) = 30$ dB, $\lambda = 12.5$ cm, $L = 1$, $T = 290°K$, $F = 2$, $B = 10$ MHz, $M = 5$, i.e. $\rho_{m,k}$ is a constant, say ρ_0. For the sake of simplicity, the pulse is assumed not to be compressed and therefore its duration τ is equal to $\frac{1}{B}$. It is still assumed that the RCS $\sigma(\theta_{m,k}, \phi_{m,k})$ is Swerling I distributed with zero mean value and variance $\sigma_0 = 10$ m^2.

7.2 Covered area

The coverage resulting from the differing processing approaches is evaluated via the average SNR as a function of range. A value of SNR is chosen so that the overall detection rate, for each system, is 80% with a FAR equal to 10^{-6}. This means, given the differences in the underlying statistics of the overall incoming noise, the chosen SNR value for a single pulse at each node is different in every system. As it can be inferred by inspection of the FAR and detection plots in Sections 5.1 and 5.2, the required SNR levels are (approximately) 18 dB in the monostatic case, 7 dB in the RPNR case, 25 dB in the simple NR case, 9.5 dB in the MIMO system and finally 11.75 dB in the DRN one (Figure 5.2 and 5.9 for the monostatic case).

7.2.1 Monostatic case

In the monostatic case the coverage (in two dimensional space) is circular and the maximum covered radius can be recovered inverting equation 7.3 and setting $R_m = R_k = R$ and $M = 1$:

$$\max\{R\} = \sqrt[4]{\frac{\rho_0\sigma_0}{KTBF}\frac{1}{\min\{SNR_{mono}\}}}. \tag{7.4}$$

With $\frac{\rho_0\sigma_0}{KTBF} = 186.9$ dB $\cdot$ m^4 and $\text{SNR}_{mono} \approx 18$ dB, $R_{max} \approx 16.7$ Km. Figure 7.1 shows the coverage under these assumptions.

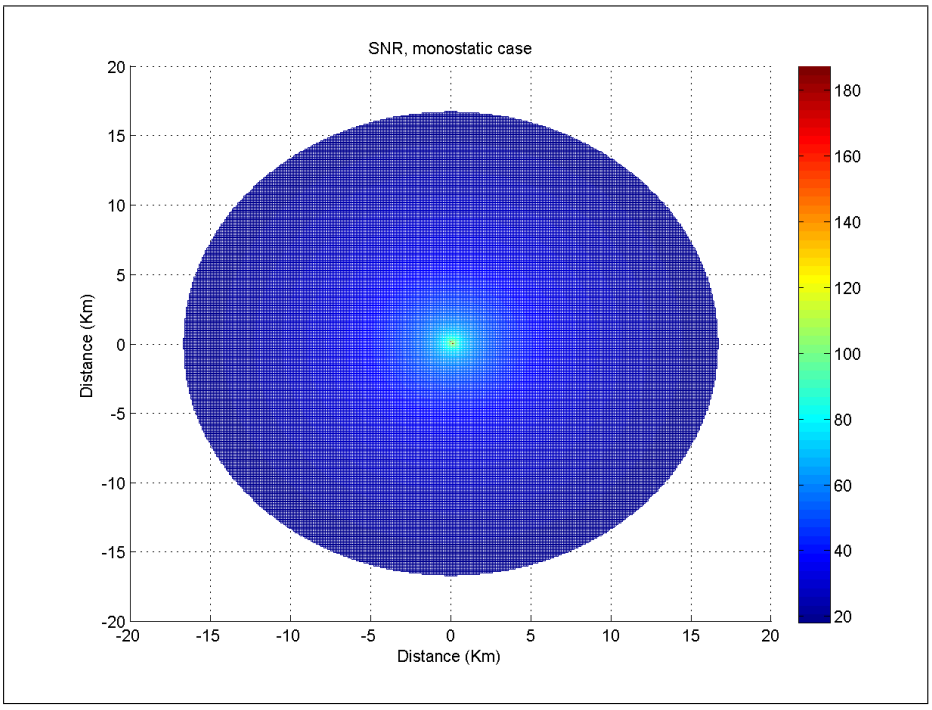

Figure 7.1: SNR and coverage, monostatic case

7.2.2 RPNR

Here the RPNR is examined. In this case it is convenient not to focus on power at a first stage as these systems operate coherently, but on amplitude and phase of all incoming signals. The global received power, after the

appropriate alignment of the phases from all the signals, can be expressed as

$$P_r = \left| \sum_{m=1}^{M} \sum_{k=1}^{N} \frac{1}{R_m^2 R_k^2} \sqrt{\frac{\rho_{m,k}\sigma(\theta_{m,k}, \phi_{m,k})}{M}} \exp\left\{ j\phi_0 \right\} \right|^2, \tag{7.5}$$

where the phases of all the signals have been realigned to ϕ_0. On average and in the far field, where $R_m \approx R_k = R$, the received power can be expressed as

$$\begin{aligned} P_r &\approx \frac{1}{R^4} E\left\{ \left| \sum_{m=1}^{M} \sum_{k=1}^{N} \sqrt{\frac{\rho_{m,k}\sigma(\theta_{m,k}, \phi_{m,k})}{M}} \exp\left\{ j\phi_0 \right\} \right|^2 \right\} = \\ &= \frac{\rho_0}{MR^4} E\left\{ \left| \sum_{m=1}^{M} \sum_{k=1}^{N} \sqrt{\sigma(\theta_{m,k}, \phi_{m,k})} \right|^2 \right\}, \end{aligned} \tag{7.6}$$

where $\sqrt{\sigma(\theta_{m,k}, \phi_{m,k})}$ is Rayleigh distributed.

From a statistical point of view, if x_k and y_k are Gaussian RV with 0 mean value and σ^2 and $\xi_k = |x_k + jy_k|$ is their corresponding Rayleigh-distributed envelop, the following applies:

$$\begin{aligned} &E\left\{ \left| \sum_{k=1}^{L} \xi_k \right|^2 \right\} = E\left\{ \sum_{k=1}^{L} \xi_k^2 + \sum_{k=1}^{L} \sum_{\substack{h=1 \\ h\neq k}}^{L} \xi_h \xi_k \right\} = \\ &= E\left\{ \sum_{k=1}^{L} \xi_k^2 \right\} + E\left\{ \sum_{k=1}^{L} \sum_{\substack{h=1 \\ h\neq k}}^{L} \xi_h \xi_k \right\} = 2L\sigma^2 + \sum_{k=1}^{L} \sum_{\substack{h=1 \\ h\neq k}}^{L} E\left\{ \xi_h \xi_k \right\} = \\ &= 2L\sigma^2 + \sum_{k=1}^{L} \sum_{\substack{h=1 \\ h\neq k}}^{L} E\left\{ \xi_h \right\} E\left\{ \xi_k \right\} = 2L\sigma^2 + \sum_{k=1}^{L} \sum_{\substack{h=1 \\ h\neq k}}^{L} \frac{\pi}{2}\sigma^2 = \\ &= 2\sigma^2 L\left[1 + (L-1)\frac{\pi}{4} \right]. \end{aligned} \tag{7.7}$$

Therefore, as a consequence of equation (7.7) equation (7.6) can be reduced to:

$$P_r \approx \frac{\rho}{MR^4} MN \left[1 + (MN-1)\frac{\pi}{4}\right] \sigma_0. \tag{7.8}$$

The computation of the average SNR after re-phased coherent summation of all the signals is therefore:

$$\begin{aligned} SNR_{RPNR} &= \frac{\frac{\rho_0}{MR^4} MN \left[1 + (MN-1)\frac{\pi}{4}\right] \sigma_0}{MNKTBF} = \\ &= \frac{\rho_0}{MR^4} \frac{\sigma_0}{KTBF} \left[1 + (MN-1)\frac{\pi}{4}\right], \end{aligned} \tag{7.9}$$

where it is convenient to point out clearly that the white Gaussian noise power is increased by a factor MN because of the coherent summation of all the noise samples.

Here, compared to the monostatic case, there is a gain $\left[1 + (MN-1)\frac{\pi}{4}\right]$ in the global SNR. This can be approximated to $\frac{N\pi}{4}$ as the number of nodes increases. The coverage from the centre of each device is approximately 45 Km. The increase of coverage is huge when compared to the monostatic case and this is due to the increased global SNR after processing and the reduced minimum SNR required at each single node (from 18 to 7 dB). Again, when compared to MIMO and the DRN processing, this gives us the upper bound limit for performance. Figure 7.2 shows the coverage for this kind of radar when devices are spaced 0.5 km away from the original position in the monostatic case when the system is made of 5 transmitters and 5 receivers (co-located devices). This network configuration will be the same for the other processing approaches. As shown, in both cases the coverage is increased and can be further improved by locating the nodes further away from each other (at least until the limit on sensitivity starts to be exceeded).

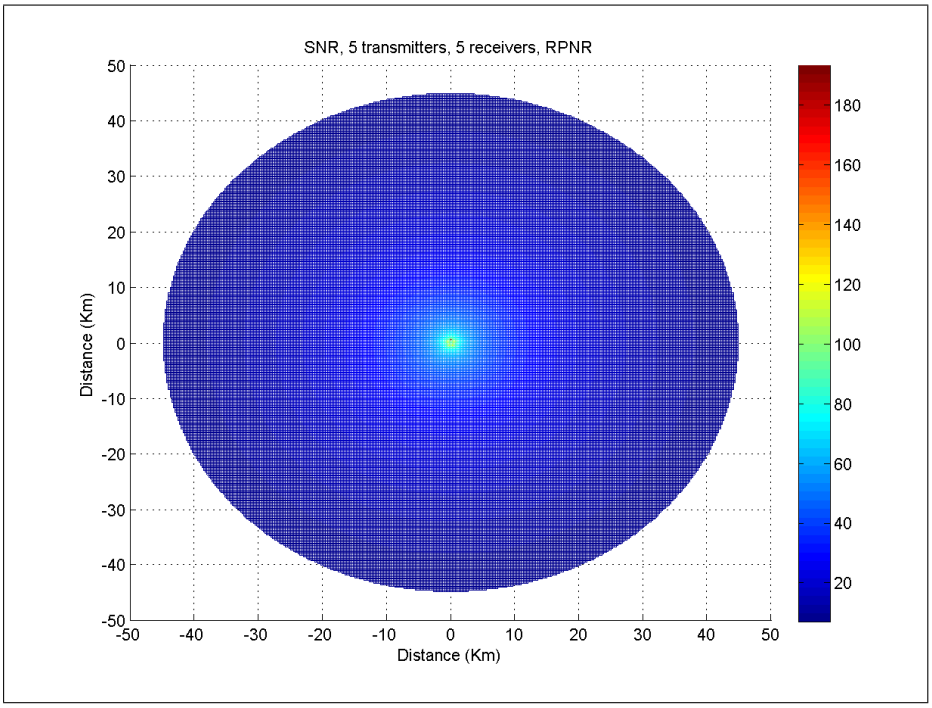

Figure 7.2: SNR and coverage, RPNR case, d= 500 m

7.2.3 NR

For the same conditions as used previously the received power is given by:

$$P_r = \frac{1}{R^4}\left|\sum_{m=1}^{M}\sum_{k=1}^{N}\sqrt{\frac{\rho_{m,k}\sigma(\theta_{m,k},\phi_{m,k})}{M}}\exp\{j\phi_0\}\right|^2 \approx$$
$$\approx \frac{1}{M}\frac{\rho_0}{R^4}\left|\sum_{m=1}^{M}\sum_{k=1}^{N}\sqrt{\sigma(\theta_{m,k},\phi_{m,k})}\exp\{j\varphi_{m,k}\}\right|^2, \tag{7.10}$$

where $\varphi_{m,k}$ takes into account the phase-shift due to the path. On average this quantity can be expressed as

$$P_r \approx \frac{1}{M}\frac{\rho_0}{R^4}\left|E\left\{\sum_{m=1}^{M}\sum_{k=1}^{N}\sqrt{\sigma(\theta_{m,k},\phi_{m,k})}\exp\{j\varphi_{m,k}\}\right\}\right|^2. \tag{7.11}$$

It is well known that the coherent sum of Gaussian distributed white RV

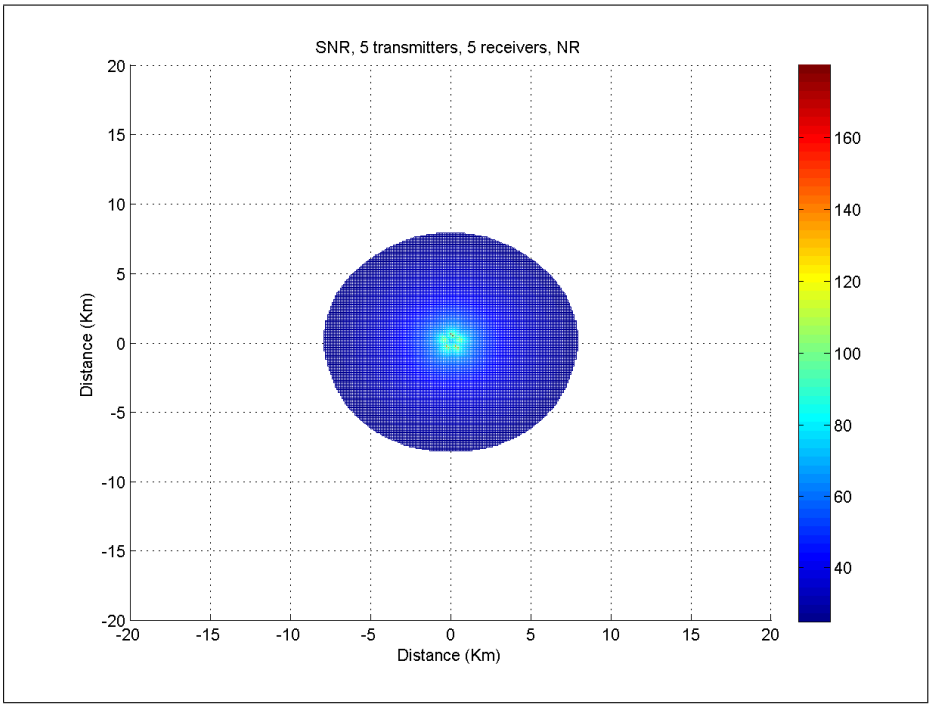

Figure 7.3: SNR and coverage, NR case, d= 500 m

achieves a gain equal to MN in power, therefore the global SNR on the far field can be written as:

$$SNR_{NR} \approx \frac{1}{M}\frac{\rho_0}{R^4}\frac{MN\sigma_0}{MNKTBF} = \frac{1}{M}\frac{\rho_0}{R^4}\frac{\sigma_0}{KTBF}. \tag{7.12}$$

As a consequence in this system the overall SNR is of a factor M smaller than the monostatic case and in addiction the threshold on the single node is bigger (from 18 to 25 dB). This explains the reduced coverage in Figure 7.3.

7.2.4 Spatial MIMO

When spatial MIMO processing is applied, the received power is computed from the signals as

$$P_r \approx \frac{1}{M}\frac{\rho_0}{R^4}\left|E\left\{\sum_{m=1}^{M}\sum_{k=1}^{N}\sqrt{\sigma(\theta_{m,k},\phi_{m,k})}\exp\{j\varphi_{m,k}\}\right\}\right|^2. \tag{7.13}$$

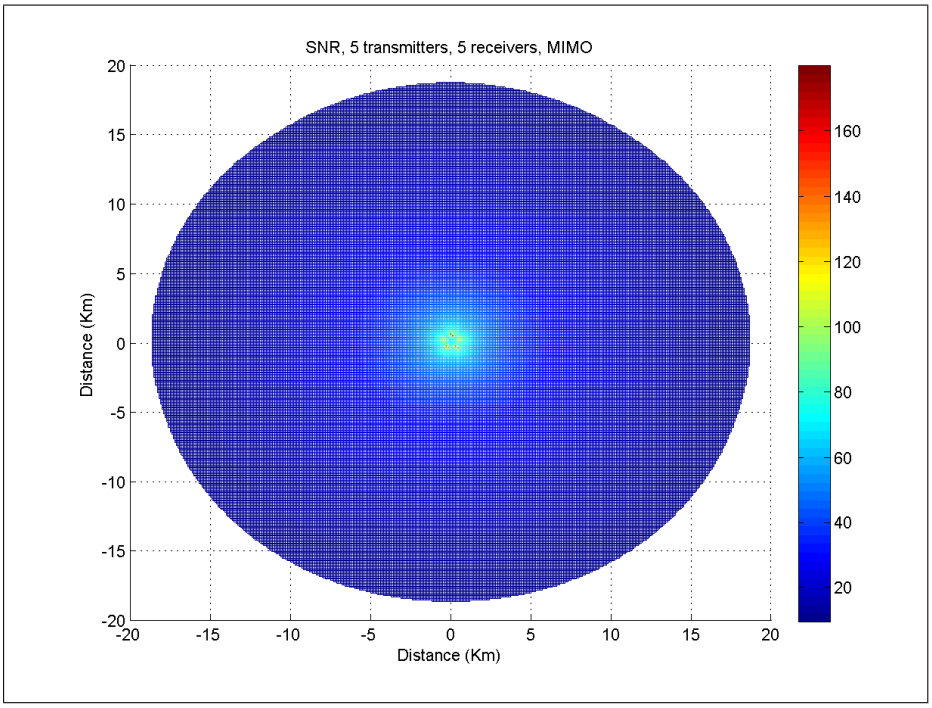

Figure 7.4: SNR and coverage, MIMO case, d= 500 m

On average and in the far field this can be approximated by

$$SNR_{MIMO} \approx \frac{MN\frac{1}{M}\frac{\rho_0}{R^4}}{MNKTBF} = \frac{1}{M}\frac{\rho_0}{R^4}\frac{1}{KTBF} = \frac{1}{M}SNR_{MONO}. \tag{7.14}$$

Therefore in the MIMO case decreased SNR and hence reduced coverage might be expected when compared to the re-phased case. Figure 7.4 show the coverage for MIMO processing. Here the maximum covered distance is approximately 18 Km. However it is worth noting that in this case the coverage is still more extensive than in the monostatic case. This reinforces the hypothesis that in real cases, when the RCS has a complex multistatic behaviour, the angular diversity provided by MIMO radar systems can exploit scintillation of the target to outperform a monostatic system.

7.2.5 DRN

In DRN processing each node of the system operates as a single mono/bistatic radar system and in a second stage the gathered information is fused together. Under this assumption, when each device works in a monostatic configuration, it can assumed that the SNR is M times smaller than the monostatic case (due to the reduced transmitted power), thus the maximum area covered can be obtained from equation (7.4). In the far field this assumption is valid including when the receivers work in a bistatic configuration.

Figure 7.5 shows that with this form of processing the minimum SNR required at 80% of P_D is approximately 11.75 dB, against 18 dB for the monostatic case (i.e. with a gain of approximately 6 dB), but has a loss of M (= 5, i.e. $\approx$ 7 dB) due to the bound on the total transmitted power. Therefore the actual loss of this system in SNR, compared to the monostatic case is approximately 0.75 dB and the subsequent loss on the covered distance is $\approx$ 4.2%. However this loss in coverage could be fully recovered by spacing the devices in a more optimum fashion. Indeed, in realistic scenarios this will be dictated by the terrain.

In this Chapter the coverage of all the systems under analysis have been examined. It has been shown that the incoherent systems achieve a coverage comparable with the monostatic radar. RPNR is reported, once again, to achieve the optimal performance. However, the analysis here takes into account transceiver distant 500 meters from one another. In real systems the devices are placed according to the geographical configuration and this can improve the joint coverage further.

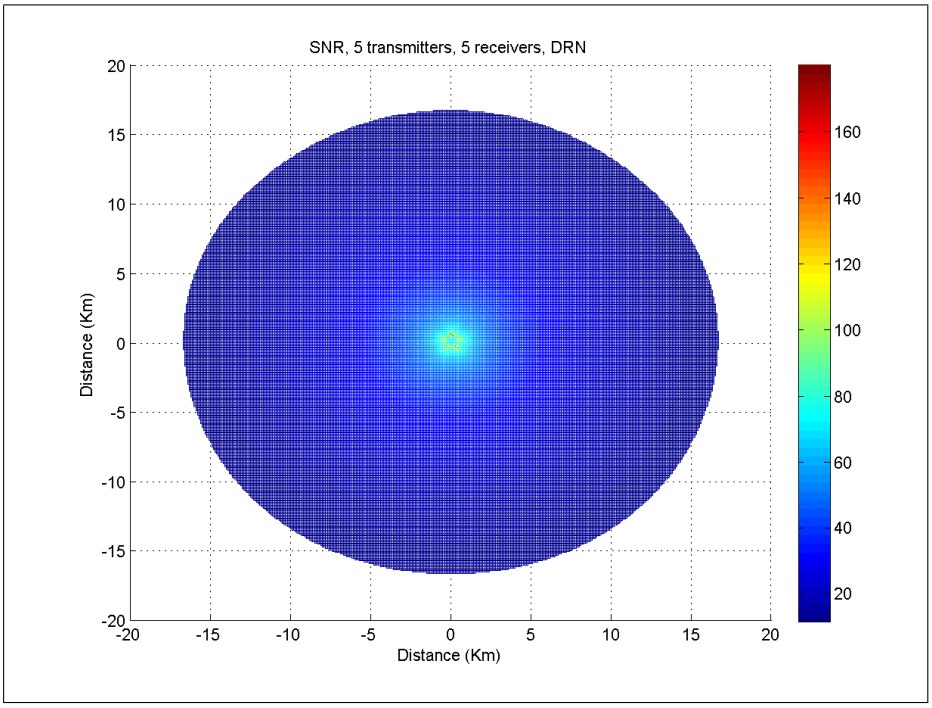

Figure 7.5: SNR and coverage, DRN case, d= 500 m

Chapter 8

Experimentation

In order to examine the theoretical results achieved in the previous part of this thesis, a small number of experiments were conducted. This does not allow a exhaustive tests of all arguments of performance for each of the distributed concepts but not all arguments can be examined.

In this Chapter the radar system used for acquiring data is introduced and consequently the experiment setup and the processing of the data are described. Through the acquired data the aim is to validate the concepts developed so far and provide a more realistic scenario of the potential of a radar network.

In particular, the following are reported:

(*i*) the hardware configuration,

(*ii*) the experiment setup,

(*iii*) the noise and clutter characteristics.

These are introductory to show in the following Chapters:

(*i*) the multistatic data characteristics for a moving target (person) and clutter,

(*ii*) a range-Doppler analysis of the acquired data,

(*iii*) ways for localizing a target.

8.1 Hardware

Figures 8.1 and 8.2 show one pair tx-rx used for the experiment.

The beamwidth of each tx or rx antenna has been chosen to be quite wide (20° el. ×30° az. one way beamwidth, as in Figure 8.6). Such a beam pattern has been chosen in order to illuminate an area wide enough to allow for the target movements, even though the clutter component in the received signal is greater.

The one-way gain of each antenna is ≈ 15 dB. The two transmitters have been set to a *PRF* of 10 kHz each. In a real system a couple of low cross-correlation codes would be employed for this purpose. However, due to hardware limitations, this was not possible when acquiring data. As a consequence an interleaved transmission has been used to emulate the separability allowed by the codes and consequently to enable full recovery of each of the tx-rx signals. The transmitted waveform is an up-chirp with 40 MHz effective bandwidth and duration $T = 0.6$ μs. The carrier frequency has been set at 2.4 GHz and the *IF* at 20 MHz. The A/D converter emits 100 MSamples/s, each one quantized to 14 bits. The nominal transmitted power for the data presented here is ≈ 23 dBm (≈ 0.2 W). The crosscorrelation of the transmitted waveform is reported in Figure 8.3. As it can be seen, the transmitted waveform has the properties of a chirp with first sidelobes at -13.3 dB.

8.2 Experimental setup

The experiment configuration is shown schematically in Figure 8.4. The experiment was conducted at the UCL Shenley Sports Ground, London, Colney in Hertfordshire (UK). The experimental site was chosen for its expected low clutter background. The system was comprised of 2 devices able to transmit and receive and one silent receiver. As a consequence, with $M = 2$ transmitters and $N = 3$ receivers, the system's output O is comprised of 6 multistatic signals, that can be schematically represented as

Figure 8.1: tx-rx external view

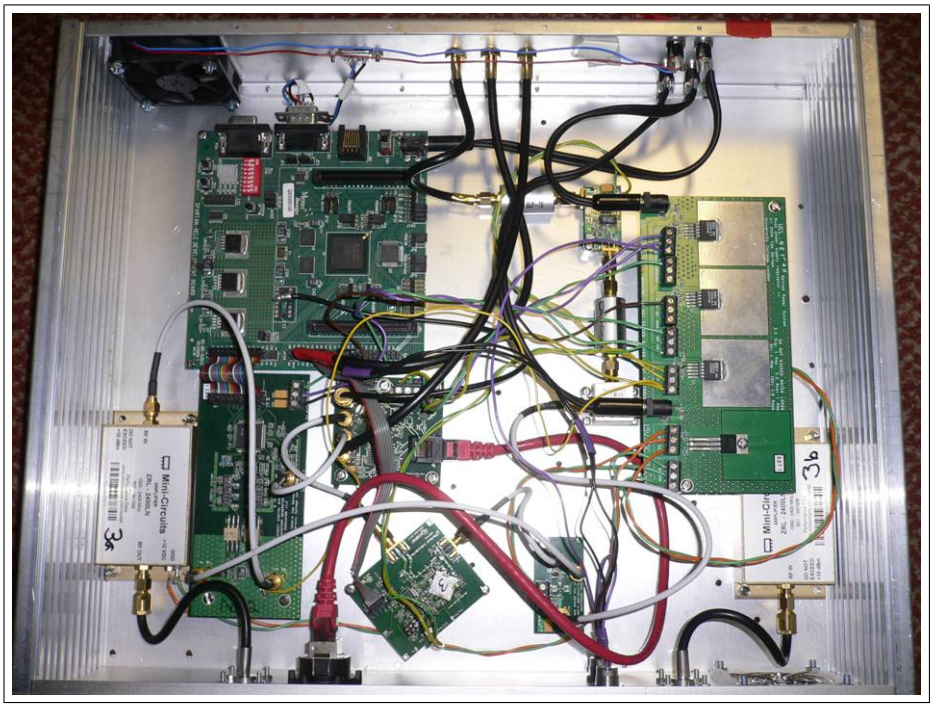

Figure 8.2: tx-rx internal view

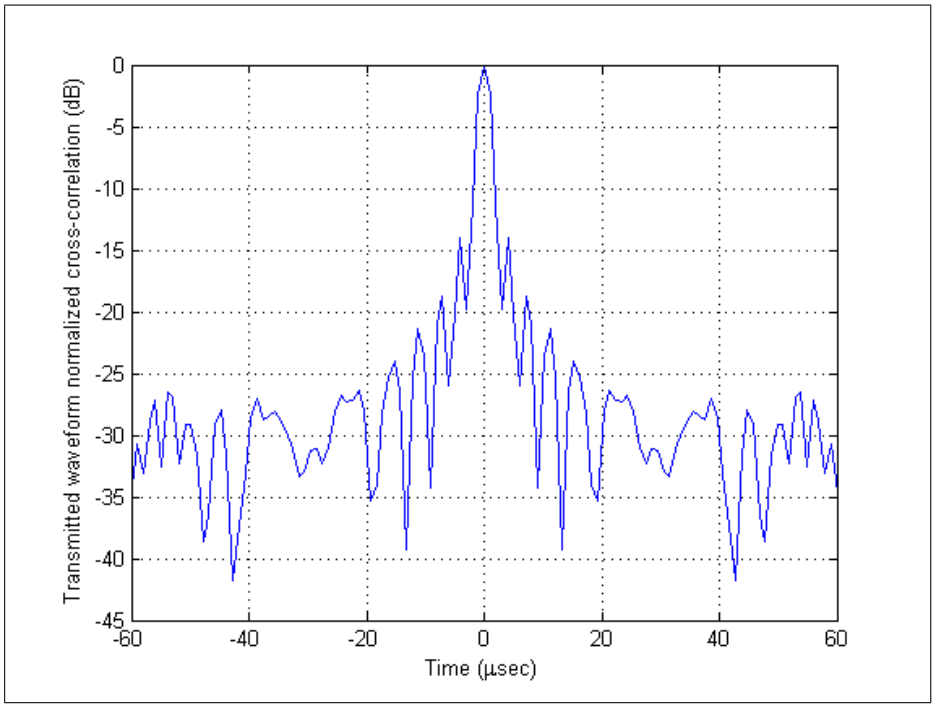

Figure 8.3: cross-correlation of the transmitted waveform

$$O = \begin{bmatrix} tx1 - rx1, & tx1 - rx2, & tx1 - rx3 \\ tx3 - rx1, & tx3 - rx2, & tx3 - rx3 \end{bmatrix}. \tag{8.1}$$

The antennas were fixed, i.e. during the acquisition of the data they were not scanning, and pointed to the initial position of the target. The transmitting and the receiving antennas of the first and third devices were separated by a small distance ($\approx$ 90 cm), although for simplicity they have been represented as one in Figure 8.4. Here this is referred to as either "monostatic signals" or "monostatic configuration" or "quasi-monostatic". In Chapter 9 it is seen that the different location of the tx and rx antennas affects the observations.

It is worth highlighting that there is a symmetry between the bistatic signals of the first and the third devices and therefore a very high correlation is expected between $r_{1,3}$ and $r_{3,1}$, where $r_{h,k}$ is the signal after matched filtering when the h-th device transmits and the k-th receives. This acts also a simple test of the system and the experimental method. The target

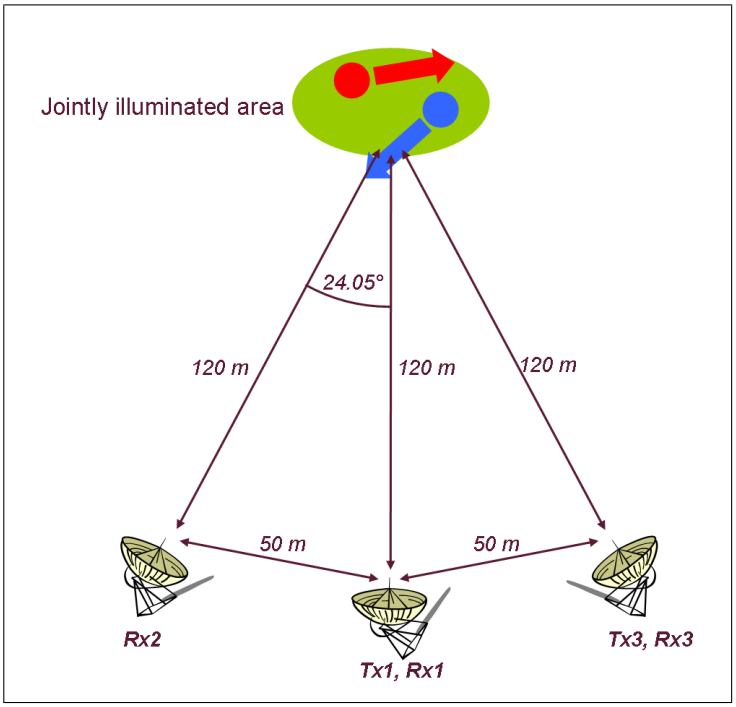

Figure 8.4: Schematics of the radar network configuration

Figure 8.5: Actual radar network configuration

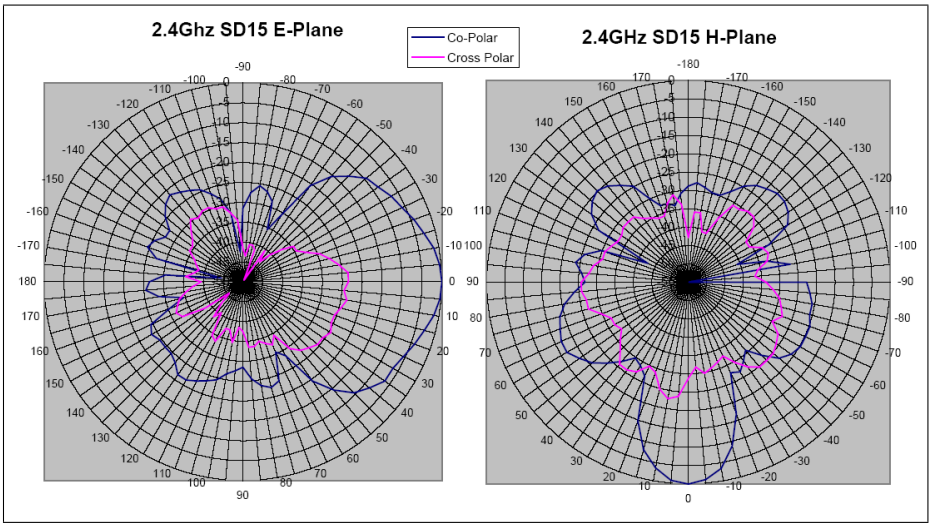

Figure 8.6: Antenna patterns in elevation and azimuth – images provided by the producer

presented in the following figures is a person walking radially towards the first device starting from a range of (approximately) 120 m.

8.3 Received signals and clutter removal

The signal to each receiver after matched filtering is expected to be made of (*i*) target (when present), (*ii*) clutter, (*iii*) multipath and (*iv*) thermal noise, i.e.

$$r_{k,m}(t) = \sum_{m=1}^{M} H_{0/1}\left[\alpha_{k,m} s_m\left(t-\tau_s\right) + \beta_{k,m} s_m\left(t-\tau_s-\Delta\tau_s\right)\right] + \\ + c_{k,m}\left(t-\tau_c\right) + n_k\left(t\right), \tag{8.2}$$

where $k = 1..N$, $m = 1..M$ and $\alpha_{k,m}$ and $\beta_{k,m}$ are the backscatter coefficients, inclusive of the phase terms determined by the parameters of the radar equation and due, respectively, to the direct path and the multipath. The other symbols are as in previous Chapters. The dependency of the delays $\tau_{s/c}$ and $\Delta\tau_s$ on the indexes k and m have been omitted for brevity.

In the acquisitions completed, the time between two interleaved transmissions of the reference chirp and the distance of the target allows the echoes from the target to be separated in time. Thus it is possible to write equation (8.2) in a simplified form as:

$$r_{k,m}(t) = H_{0/1}\left[\alpha_{k,m} s_m\left(t-\tau_s\right) + \beta_{k,m} s_m\left(t-\tau_s-\Delta\tau_s\right)\right] + \\ + n_k\left(t\right) + c_{k,m}\left(t-\tau_c\right). \tag{8.3}$$

In more complex systems, covering greater distances, it will be necessary to exploit code diversity or other properties to minimize the mutual interference between the transmitted signals. This argument is not considered in this thesis.

8.3.1 Clutter removal

In this Section a brief description of the processing adopted to remove the clutter is reported, together with its effects on the received signals. Figures 8.7 and 8.8 show a snapshot of the signals arriving at all the receivers, after matched filtering and integration but before clutter suppression, when tx1 and tx3 are transmitting. From the a-priori knowledge of the experiment, the moving target is expected to be at a mono/bistatic range of 120 m. Whilst in Figures 8.7 and 8.8 a visual analysis cannot confirm the presence of the target at this distance, after clutter removal, i.e. in Figures 8.9 and 8.10, the target stands out much clearly than before.

As the clutter was expected to be due to the backscattering from the stationary ground, and consequently without a significant Doppler spread, it has therefore been cancelled using a high-pass filter with a cutoff frequency of 10 Hz. Figure 8.12 shows its amplitude response. The filter cutoff has been designed to attenuate the stationary clutter as much as possible while preserving the Doppler response of slow-moving targets such as a walking person. The effectiveness of filtering in saving the Doppler information of a walking person is also shown in Figure 8.11. Here a range-Doppler plot of the monostatic signal tx1-rx1 is reported

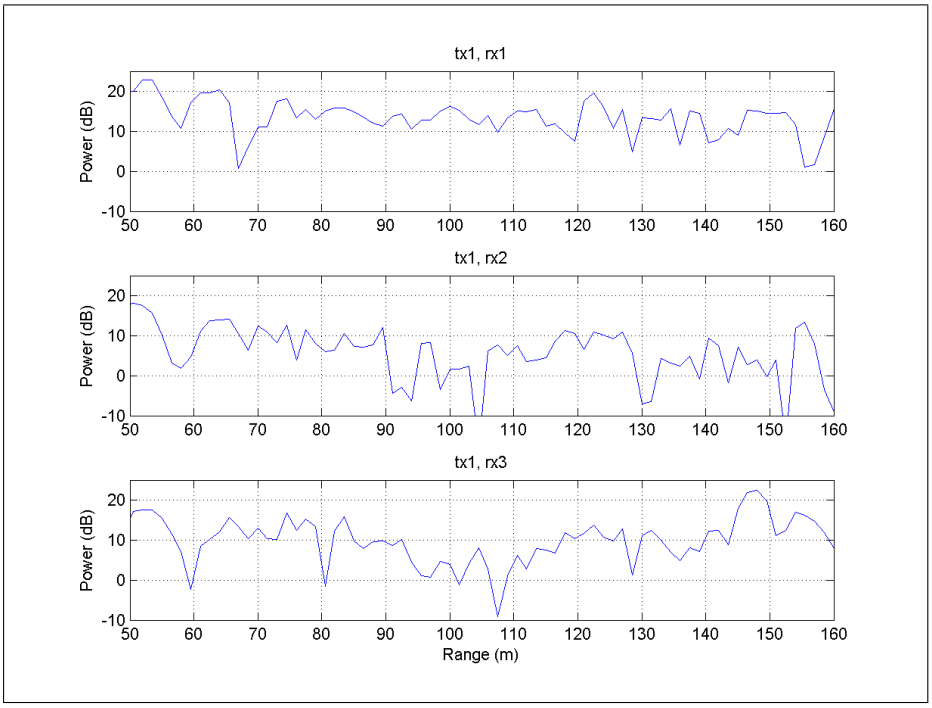

Figure 8.7: Signals from tx1 to all receivers

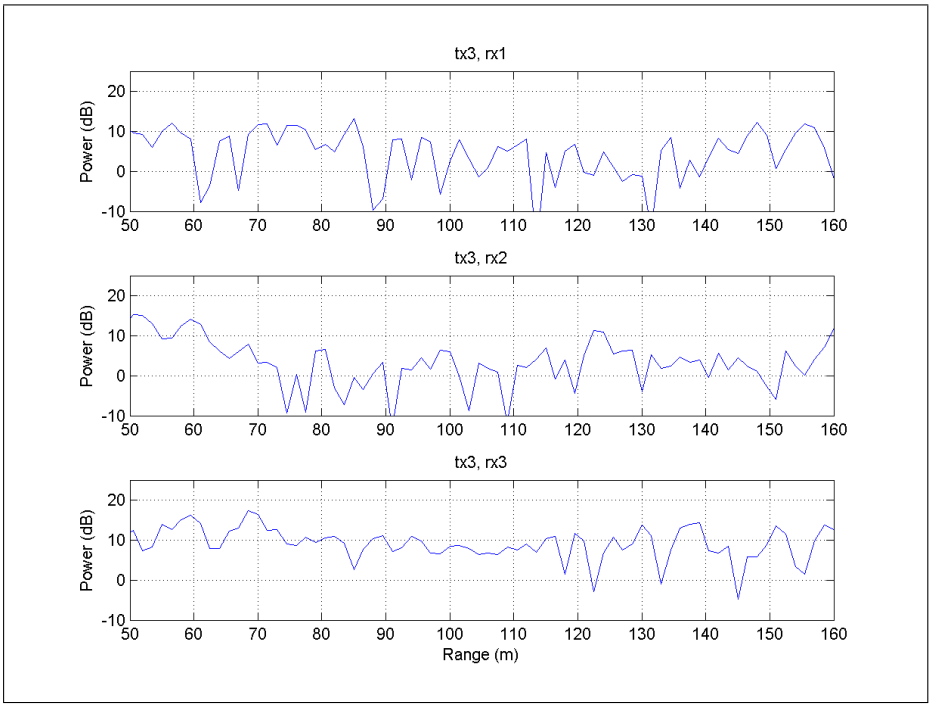

Figure 8.8: Signals from tx3 to all receivers

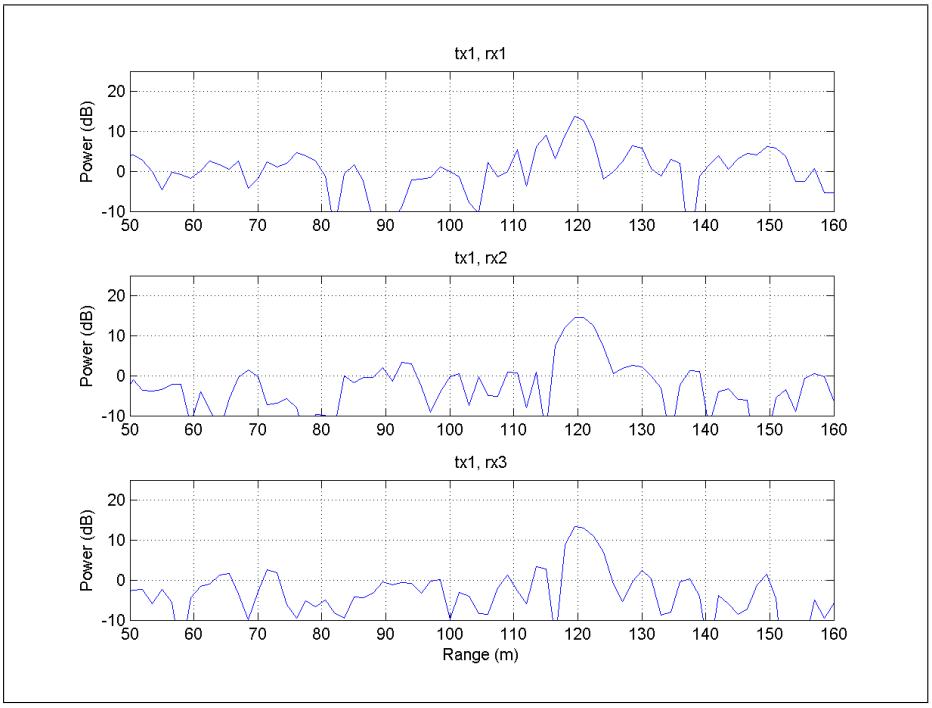

Figure 8.9: Signals received from tx1 after clutter removal

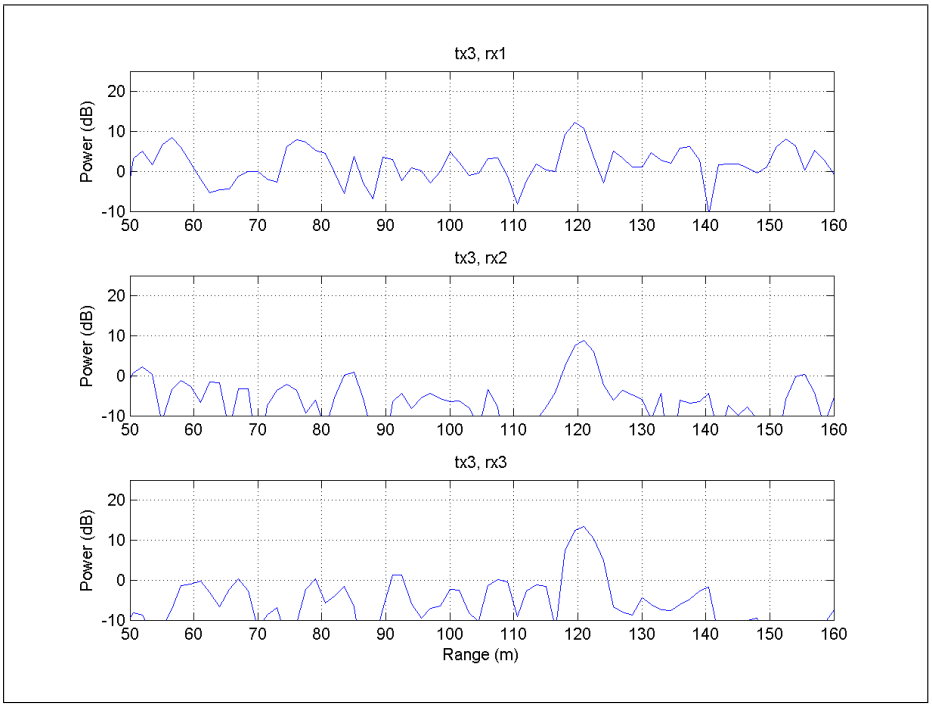

Figure 8.10: Signals received from tx3 after clutter removal

before and after clutter removal. The integration time is here 1 second. This is too high as range cell migration of the target occurs. However, as also discussed in Section 10.2.2, it allows a better evaluation of the clutter removal.

Finally, further considerations on the geometry of the experiment concern the direct feeding of the receivers, due to the presence of sidelobes in the pattern of the tx/rx antennas. An attempt to mitigate this interference was setting rx2 and rx3 in the first null of the azimuth pattern of tx1, according to the information shown in Figure 8.6. In turn, rx1 and rx2 have been placed, respectively, in the first and second null of tx3. As the antennas in tx and rx were of the same kind, this turned out to place the transmitters in nulls of the receiving patterns as well. As Figures 8.7 and 8.8 show, this has avoided the saturation of the receivers. The residual direct feeding has then been cancelled in a second stage of processing by the same filter used for the clutter, as it had a zero Doppler component.

8.3.2 Target, noise and clutter signals

This Section describes in more detail the signals introduced in the previous Section. Particular attention is given to the echoes from two different range cells: the first is the target's and the second contains only clutter and noise. For the sake of simplicity, only echoes related to the pair tx1-rx1 only are here examined: the signals from the remaining pairs have similar behaviours and therefore for brevity are not reported.

Figure 8.13 shows the power (in dB) and the phase (in degrees) of the received signal for a series of pulses for the range cell where the target is present. One second of acquired data at a PRF of 10 kHz are reported here (i.e. 10000 pulses). After removing the clutter by filtering, the signal appears as shown in Figure 8.14. It is worth highlighting that for relatively high SNR the linear (after filtering) behaviour of the phases is clearly evident, whilst it is partially or totally lost for low SNR, e.g. between pulses 6000 and 7000, as it is expected. In other words, for high SNR a quite strong correlation of the phases from pulse to pulse for the target is

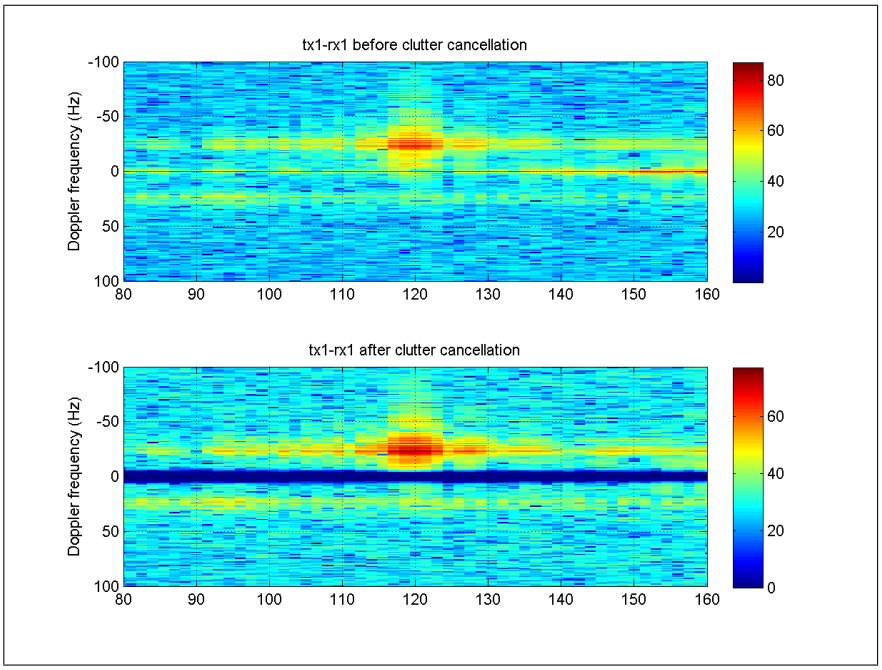

Figure 8.11: Range-Doppler plots before and after clutter removal

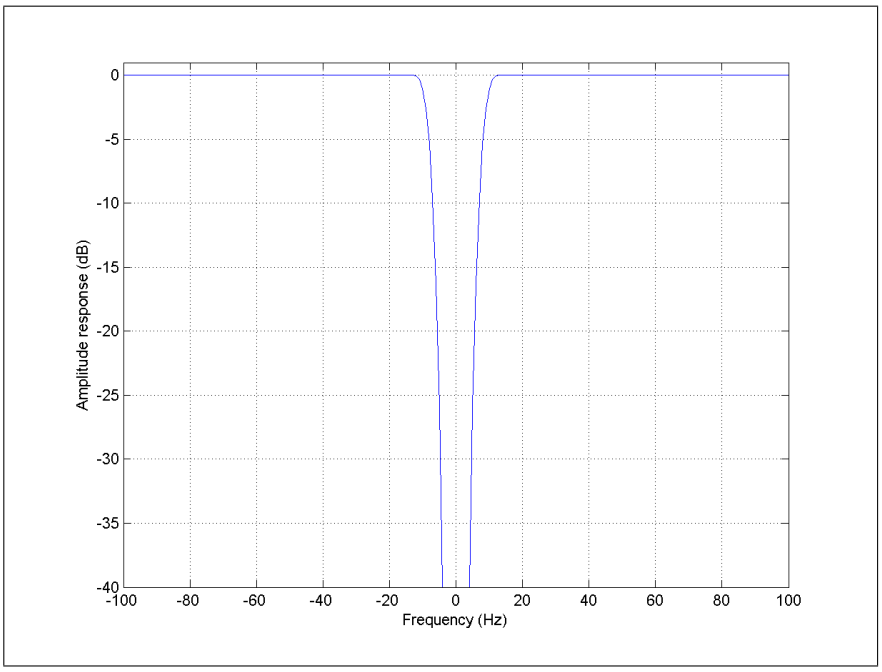

Figure 8.12: Amplitude response of the high-pass filter used for clutter removal

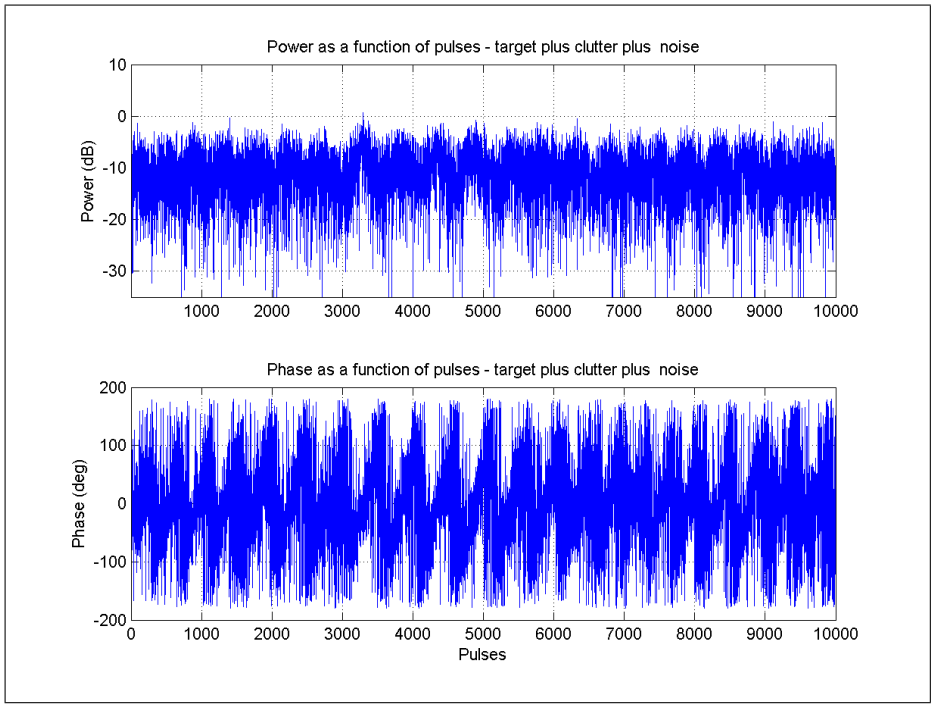

Figure 8.13: Signal and interference as a function of pulses – tx1-rx1

observed. This might be expected considering that the target is a walking person (therefore with a modest velocity) and the radar has a relatively high PRF and hence there is little change from pulse to pulse.

Figures from 8.15 to 8.17 refer to the a range cell at 187.5 m where clutter and noise only are present. Here the power and phase of (*i*) clutter and noise, (*ii*) noise only after filtering as in the previous Sections and finally (*iii*) clutter only, as the difference of the received signals and the filtered noise. As it is possible to observe, whilst the noise has an uncorrelated phase, when the clutter is present, its phase has a degree of correlation. However, since a visual analysis cannot describe exhaustively the statistical description of clutter, the following Chapter is dedicated to a more detailed analysis which includes considerations on the multistatic statistics of the clutter together with an introductory study of the correlation of the interference as function of the nodes.

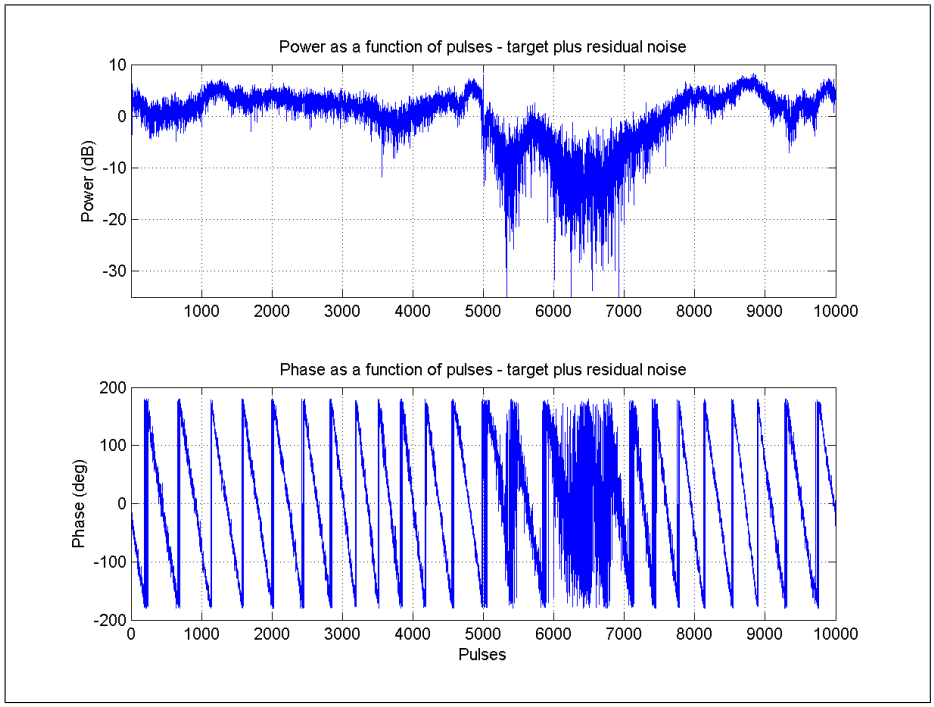

Figure 8.14: Signal and residual noise as a function of pulses – tx1-rx1

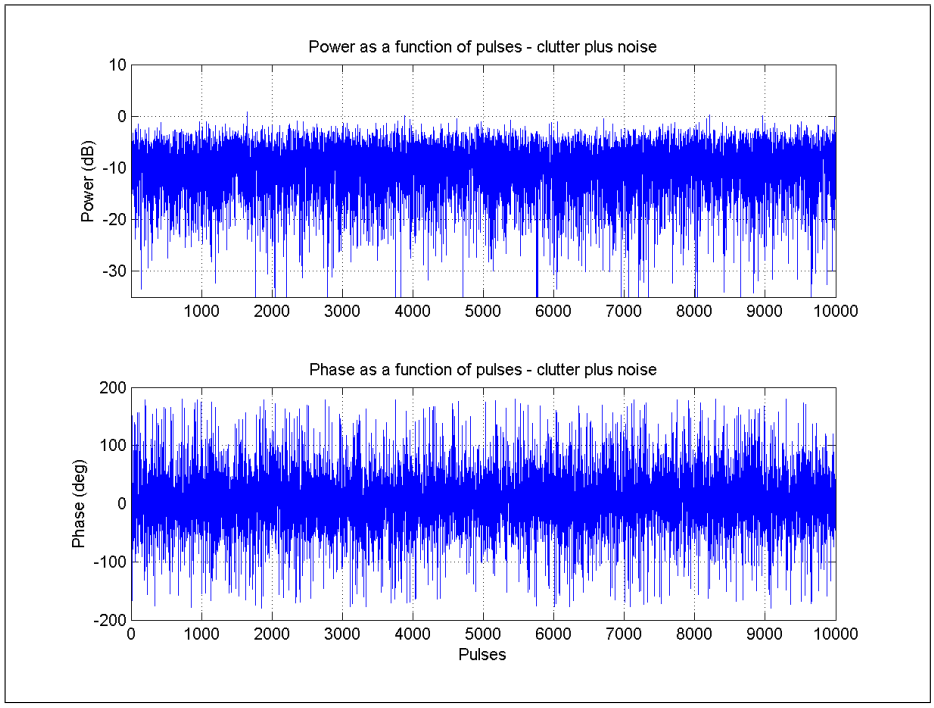

Figure 8.15: Clutter and noise as a function of pulses – tx1-rx1

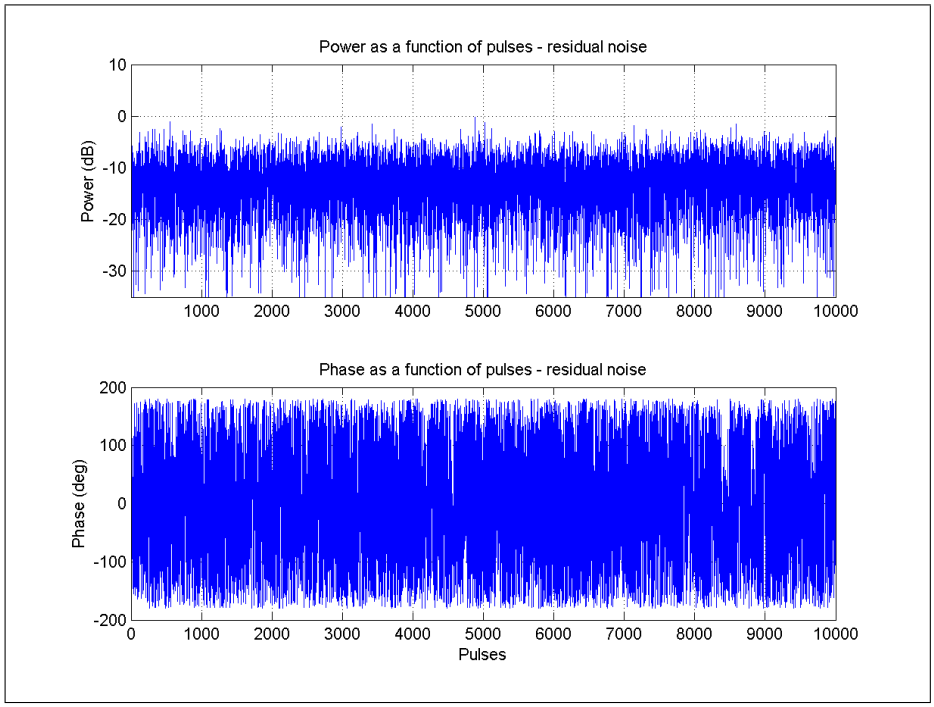

Figure 8.16: Noise as a function of pulses – tx1-rx1

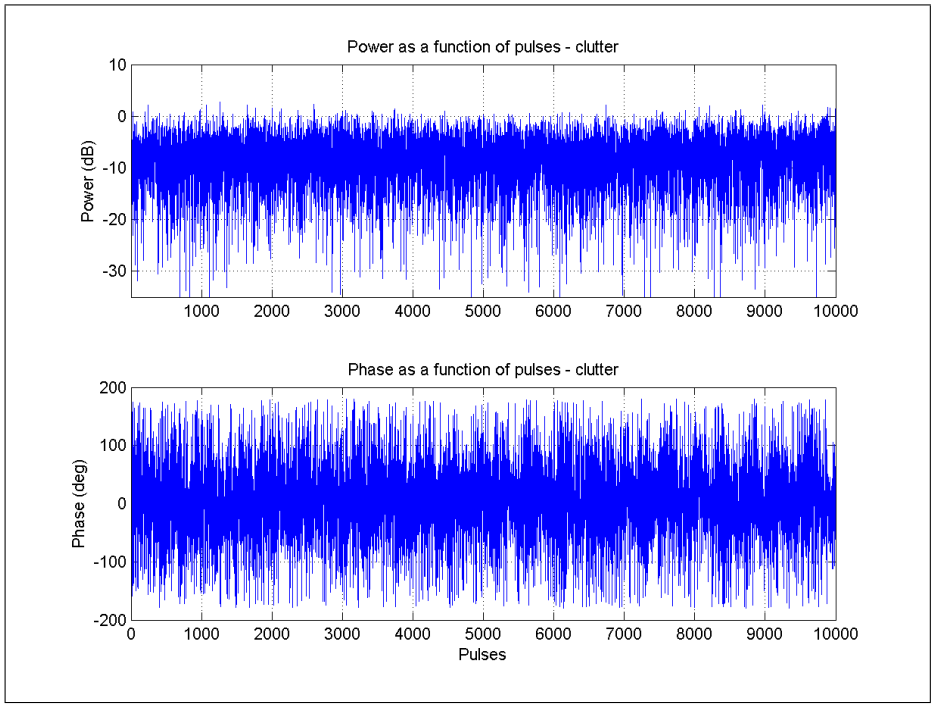

Figure 8.17: Clutter as a function of pulses – tx1-rx1

Chapter 9

Multistatic data characteristics

In this Section some properties of the set of the acquired signals are investigated. This is a merely preliminary analysis to examine properties of multistatic data and an experimental means of evaluating the assumptions of previous chapters, such as Chapter 6. In particular, the attention here is focused on the cross-correlation characteristics of the received signals and their relationship as a function of the nodes.

In general, throughout this chapter the correlations have been computed taking into account the data either in (*i*) their complex format, (*ii*) their amplitude alone and finally (*iii*) their phase alone, in order to best understand all the possible existing relationships. Correlations have been computed on single pulses and then averaged over a period of 1 second.

9.1 Clutter and noise only

In this Section the average correlation and the PDF of clutter as function of nodes are reported.

Figure 9.1 shows, on the same plot, the average correlation properties of the signals from tx1 to rx1 with all the others in the network. In particular complex data correlation is reported in blue, amplitude correlation in green and finally phase correlation in red. It appears convenient now to describe

in more details the procedure applied here to get such plots. In general terms, the k^{th} received signal from the i^{th} receiver can be written as

$$r_{i,k}(t) = H_{0/1} s_i(t) + c_{i,k}(t) + n_k(t), \tag{9.1}$$

with symbols as in Chapter 6. Nonetheless, $r_{i,k}(t)$ can be written in terms of its amplitude an phase, i.e.

$$r_{i,k}(t) = |r_{i,k}(t)| \exp\left\{j\phi_{i,k}(t)\right\}. \tag{9.2}$$

Therefore in the following Figures the correlation coefficient between $r_{i,k}(t)$ and $r_{m,q}(t)$ are reported. In addition, in a first instance, the reader can assume that signals have been collected from one range cell only[1]. Moreover, echoes have been acquired for 1 second at a *PRF* of 10 KHz, so it would be more correct to write equation 9.2 as

$$\begin{aligned} r^p_{i,k}(mT) &= |r^p_{i,k}(mT)| \exp\left\{j\phi^p_{i,k}(mT)\right\} = \\ &= |r^p_{i,k}[m]| \exp\left\{j\phi^p_{i,k}[m]\right\} = r^p_{i,k}[m], \end{aligned} \tag{9.3}$$

where $m = 1 \ldots 10000$, $T = \frac{1}{PRF}$ and finally ^{p} refers to the p^{th} range cell. The correlations coefficients $\rho_{\xi,\eta}$ reported in Figure 9.1 (and following) are evaluated as follows:

$$\rho_{\xi,\eta} = \frac{\sum_{l=1}^{L} \xi^*[l]\eta[l]}{\sqrt{\left(\sum_{l=1}^{L} \xi^*[l]\xi[l]\right)\left(\sum_{l=1}^{L} \eta^*[l]\eta[l]\right)}} \tag{9.4}$$

where $L = 10000$ and * is the conjugate operator. The variables ξ and η are defined as

[1] In a multistatic system, range cells cannot match perfectly, due to the difference in geometry. However, range cells have been chosen to have most of the illumination in common. For the sake of simplicity in the rest of this Chapter it is referred as if signals come from one range cell only, notwithstanding the difference in geometry.

(i) $\xi = r^p_{i,k}$, $\eta = r^p_{m,q}$ when complex data are analyzed (blue plot),

(ii) $\xi = |r^p_{i,k}|$, $\eta = |r^p_{m,q}|$ when amplitude data are analyzed (green plot) and

(iii) $\xi = \phi^p_{i,k}$, $\eta = \phi^p_{m,q}$ when phase data are analyzed (red plot).

In Figure 9.1 (and following) the paths are reported on the x-axis and the correlation values on the y-axis. The distance of the cell taken into consideration is 187.5 m from the first node. As it is possible to see, when the signal is correlated with itself, all the correlation levels are 1. Although this is expected and therefore redundant, these values have been plotted anyway to (*i*) provide an immediate understanding of the reference signal and to (*ii*) allow uniform axes of the Figures for an easier comparison. However, when describing the Figures, these values will not be analyzed. On the contrary the attention is focused on the correlation values with the rest of the paths, which can vary more or less significantly, according to the nodes and the kind of data examined (complex data, amplitude only, phase only).

In Figures from 9.1 to 9.4, although the amplitudes are shown to be statistically dependent from one another, the phases can be considered almost independent. Also the overall correlation of complex data correlation is quite low. There are still exceptions to this general behaviour that stand out clearly: first of all, Figures 9.1 and 9.2 show a remarkable correlation between the monostatic measurements. This is quite unexpected, given the different aspect angles of illumination of the clutter patch, which is confirmed from the low correlation of the phases, therefore this relatively high level of correlation may be explained by a similarity of monostatic clutter backscattering from the same area. It is also true that in this particular case the clutter is made of terrain that can have a more homogeneous behaviour than other kinds of clutter, such as that from the sea surface, that is characterized by a spiky echoes rapidly varying in time. Figure 9.3 shows a quite high correlation between tx1-rx3 and rx3-tx1. This has to be expected if considering that this is originated by the symmetrical configuration of these devices, as described in the previous

Chapter. However, a possible argument can be that, notwithstanding the high degree of redundancy, the cross-correlation of the complex data of symmetrical signals falls to 61%, the amplitude correlation to 87% and the phase correlation as low as 20%. It has to be pointed out clearly that, as also shown in the next Section for the target, the noise effects here are such to decorrelate the clutter properties and therefore to lessen the its correlation. In particular for this set of data the CNR was quite low, i.e. in the order of 5 dB. Finally Figure 9.4 does not show any particular correlation for the clutter and noise case.

Figures from 9.5 to 9.7 show the distribution of the amplitude of the clutter. Most of these distributions have a Gaussian texture in common, which is reflected in the Rayleigh-shaped PDFs. As seen in Section 3.5, the Gaussian distribution is quite common for the texture in the case of ground clutter. In particular Figure 9.5 shows that the two monostatic measurements have two Rayleigh-distributed PDF with different standard deviations. As expected, the two symmetrical signals tx1-rx3 and tx3-rx1 have similar distributions (Figure 9.6). As it will be seen at the end of this Chapter, the difference here can be explained by the extra noise of the first receiver. Finally Figure 9.7 reports the clutter distribution of the remaining two bistatic signals. Whilst the one from tx3 to rx2 has an expected Gaussian shape, that from tx1 to rx2 has a tail which does not match the expectations. At this point, it is worth recalling that the relationships between multistatic clutter returns from the same area have received limited attention in the past and this is a first insight in this topic. In particular, the long tail of the distribution in the latter Figure might be an indicator of a change in the clutter distribution, not only in its statistics. Therefore, the complex backscattering from even a fairly simple kind of clutter, i.e. from a flat grass field (as in this case), seems to be able to provide a variety of reflected signals with different properties, as much as happens in more structured targets.

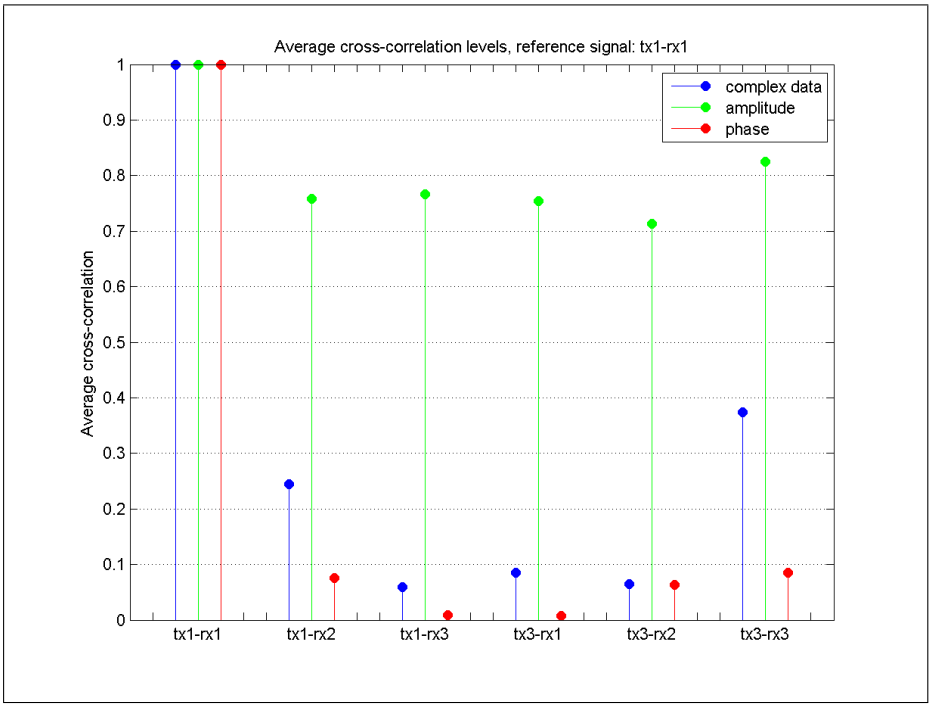

Figure 9.1: Cross-correlation levels with tx1-rx1 – clutter

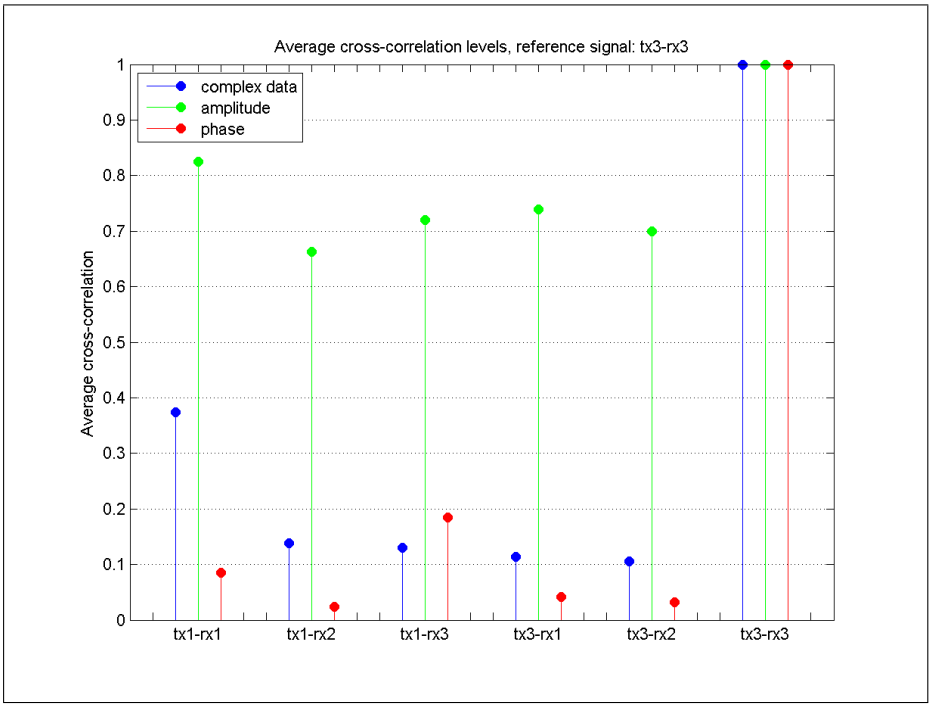

Figure 9.2: Cross-correlation levels with tx3-rx3 – clutter

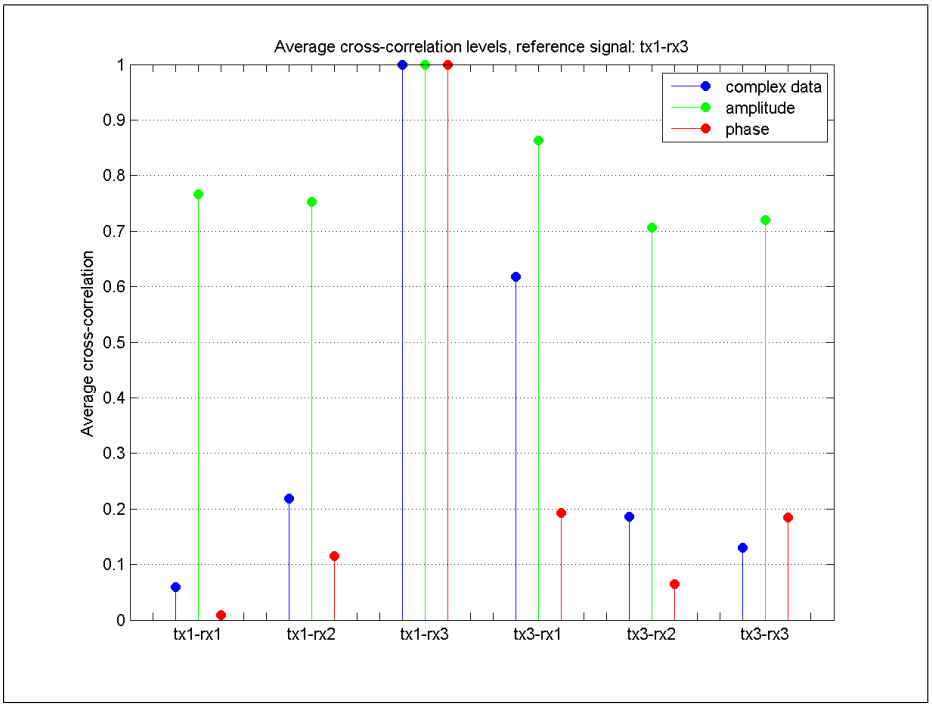

Figure 9.3: Cross-correlation levels with tx1-rx3 – clutter

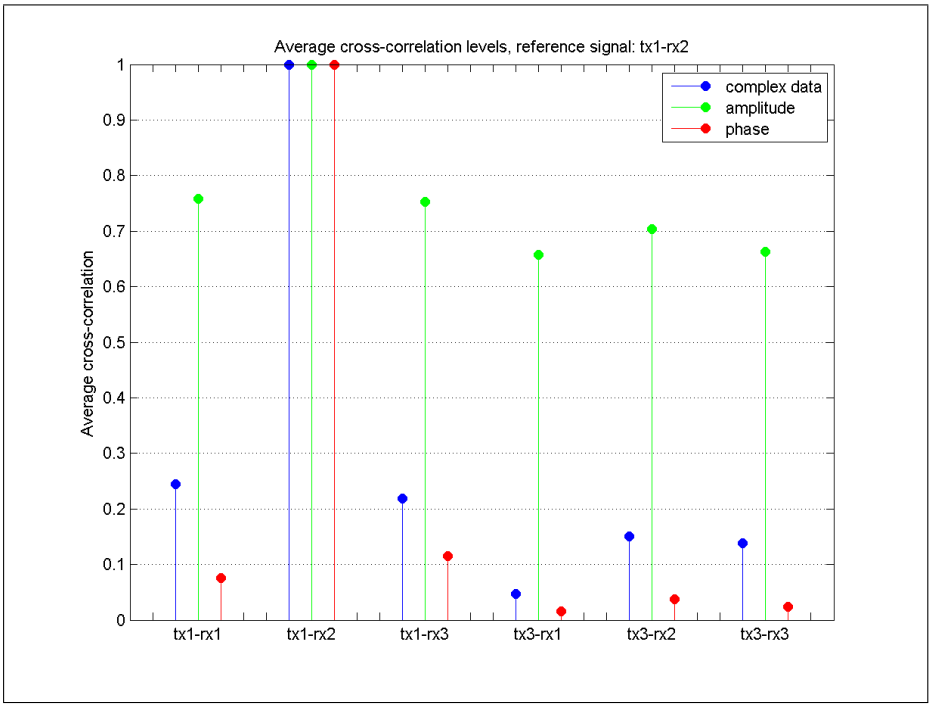

Figure 9.4: Cross-correlation levels with tx1-rx2 – clutter

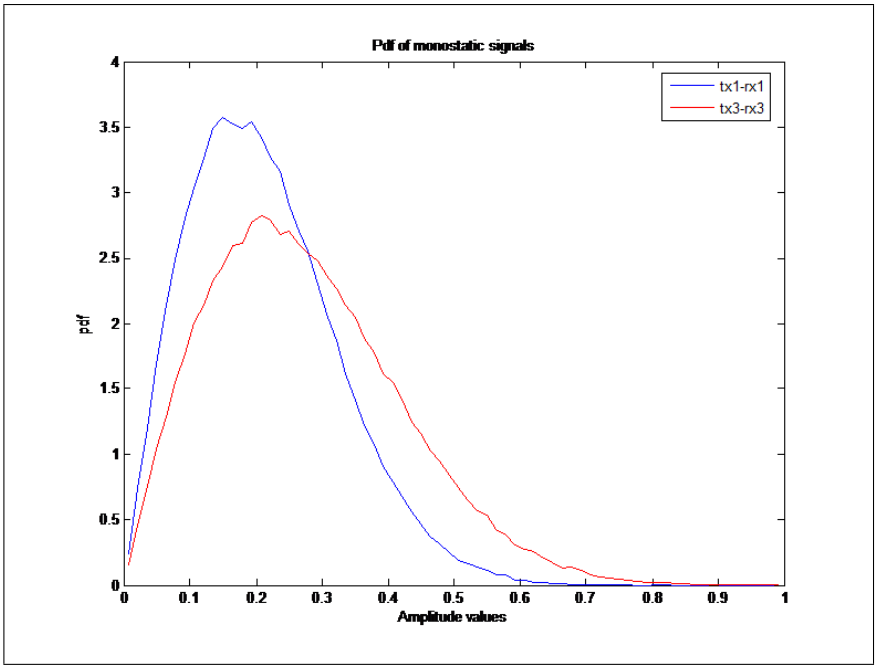

Figure 9.5: Multistatic PDF of the amplitude of the clutter, monostatic signals

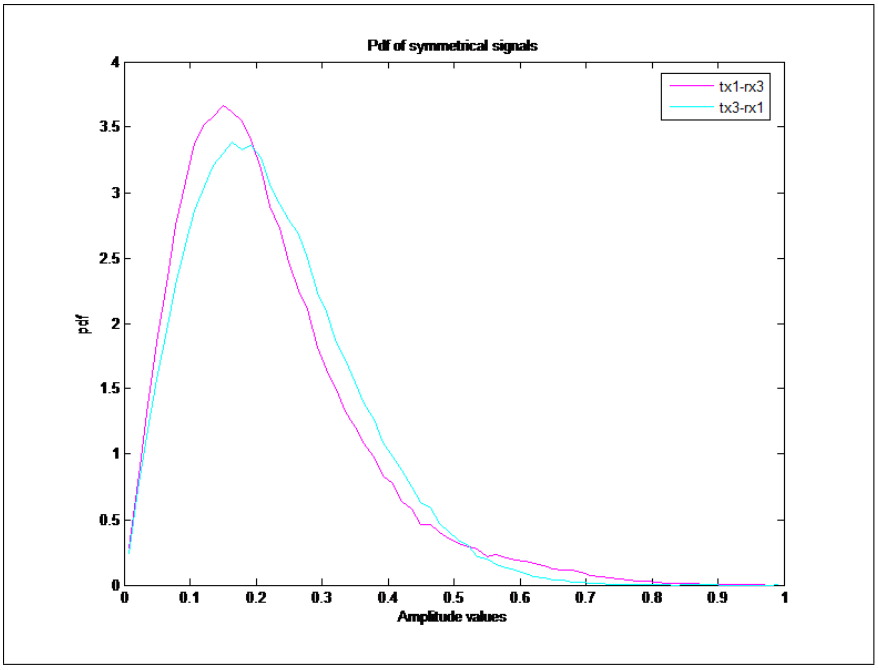

Figure 9.6: Multistatic PDF of the amplitude of the clutter, symmetrical signals

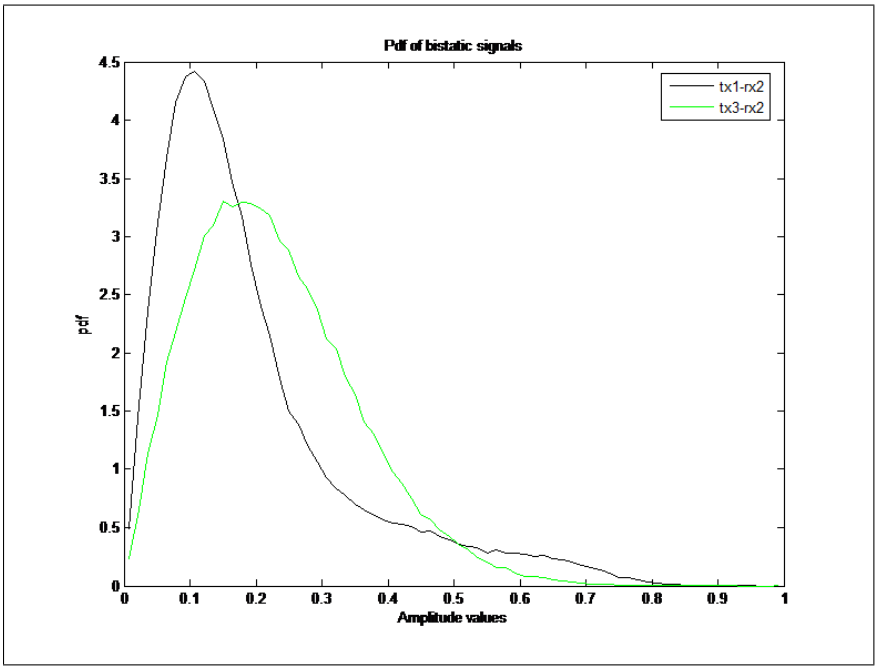

Figure 9.7: Multistatic PDF of the amplitude of the clutter, bistatic signals

9.2 Moving target - person

In this Section the correlation properties are studied when a moving target is present. In particular a window of 3 range cells around the target is taken into account. These 2 guard range cells around the nominal cell of the target have been introduced to take account the oversampled data rate and a possible migration of the moving target

The examination of Figures from 9.8 to 9.11 highlights a different correlation behaviour from that observed in Section 9.1 when a target is present. In these cases the amplitudes are extremely correlated in all the results shown. This is due to the characteristics of the target (a person) whose RCS does not scintillate as conventional targets and exhibits a longer correlation from pulse to pulse, due to the slow velocity (and the high PRF used). However, when considering the correlation between the phases and the entire complex data, different characteristics from those in Figures from 9.1 to 9.4 arise. In Figure 9.8 it is quite evident that the monostatic measurements are less similar to one another. On the

contrary the monostatic measurements from tx3 to rx3 (Figure 9.9) are quite similar to the one from tx1 to tx2. This is quite unexpected and does not match what found in the clutter cases and may be explained by the back scattering properties of the target. Figure 9.10 shows an interesting result that validates the a-priori expectations about the experiment: here the properties of the symmetrical configuration are extremely clear. There is a similarity at all levels between tx1-rx3 and tx3-rx1 highlights (the average cross-correlation on complex data is $\approx 88\%$) and also a quite high correlation is observed between tx1-rx3 and tx1-rx2, as it might be expected since the target is a person moving towards the central node. This due, again, to the symmetry in carrying out the experiment. Even the phases, which are extremely sensitive to minor mismatches and to low SNR, have a correlation up to almost 50% in one case and 40% in the other. These considerations are basically confirmed by Figure 9.11.

Figures 9.12 and 9.13 shows the signals received from pairs tx1-rx3 and tx3-rx1 respectively. As it can be seen, the overall shape of the signals is very similar, although the signal in Figure 9.13 has a greater contribution of noise, as it can be confirmed as well from an analysis of the phases.

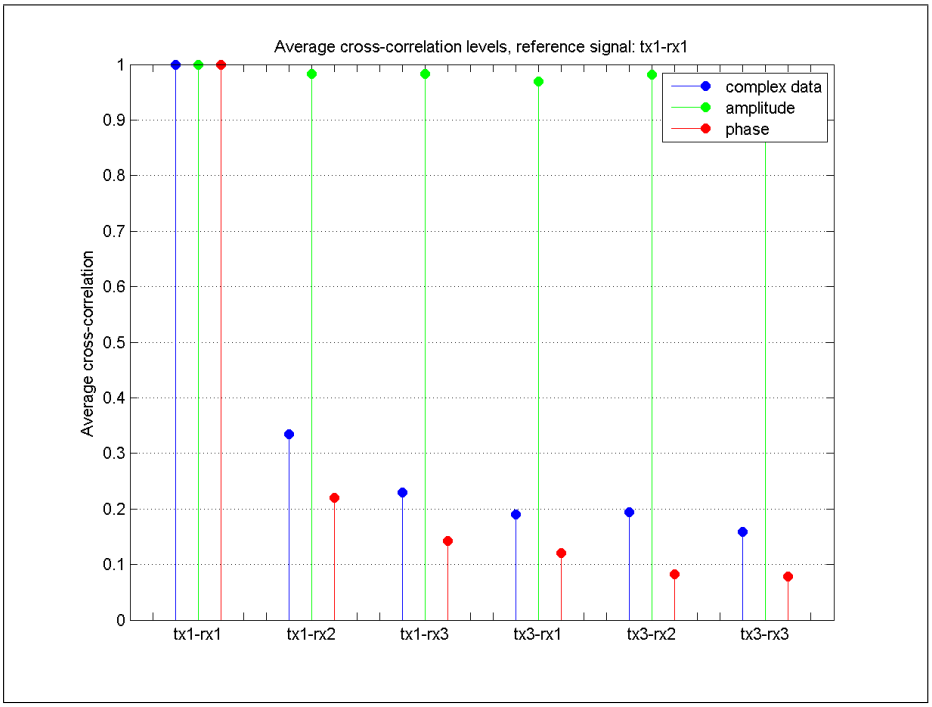

Figure 9.8: Cross-correlation levels with tx1-rx1 – target

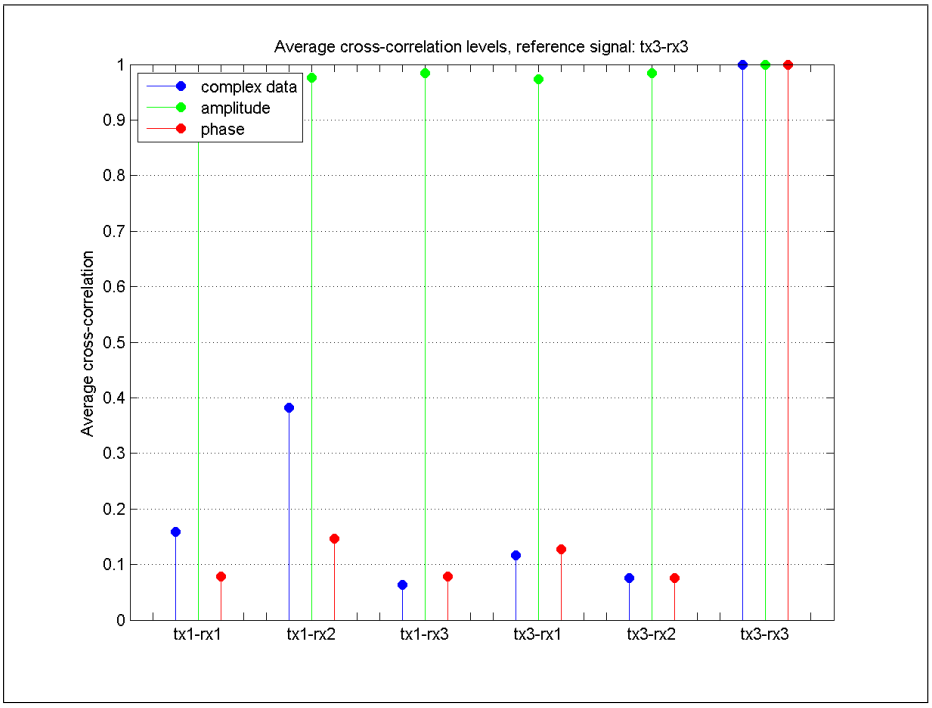

Figure 9.9: Cross-correlation levels with tx3-rx3 – target

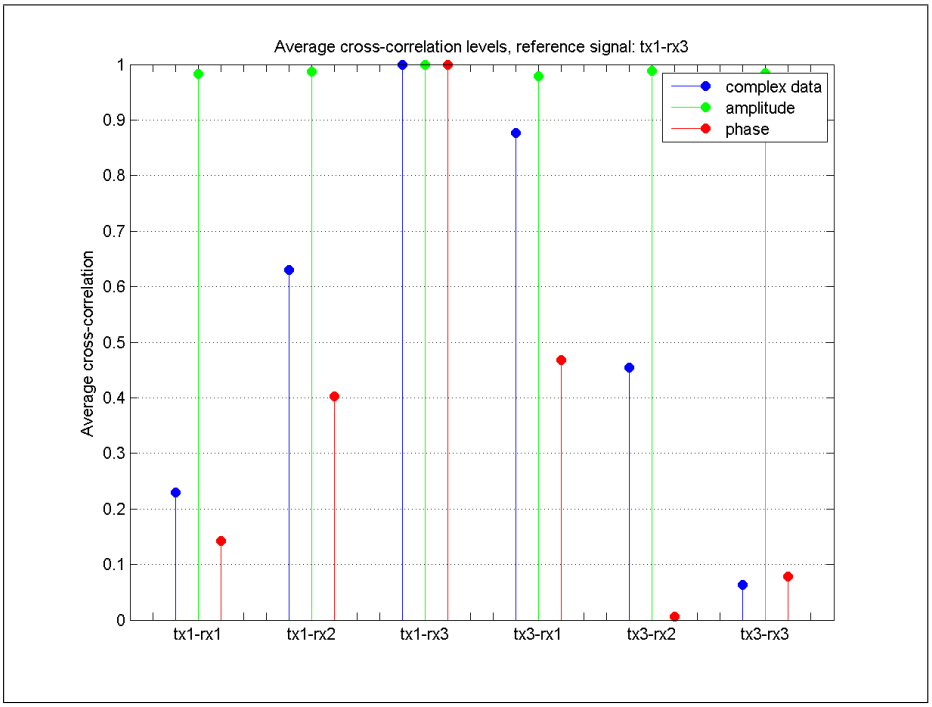

Figure 9.10: Cross-correlation levels with tx1-rx3 – target

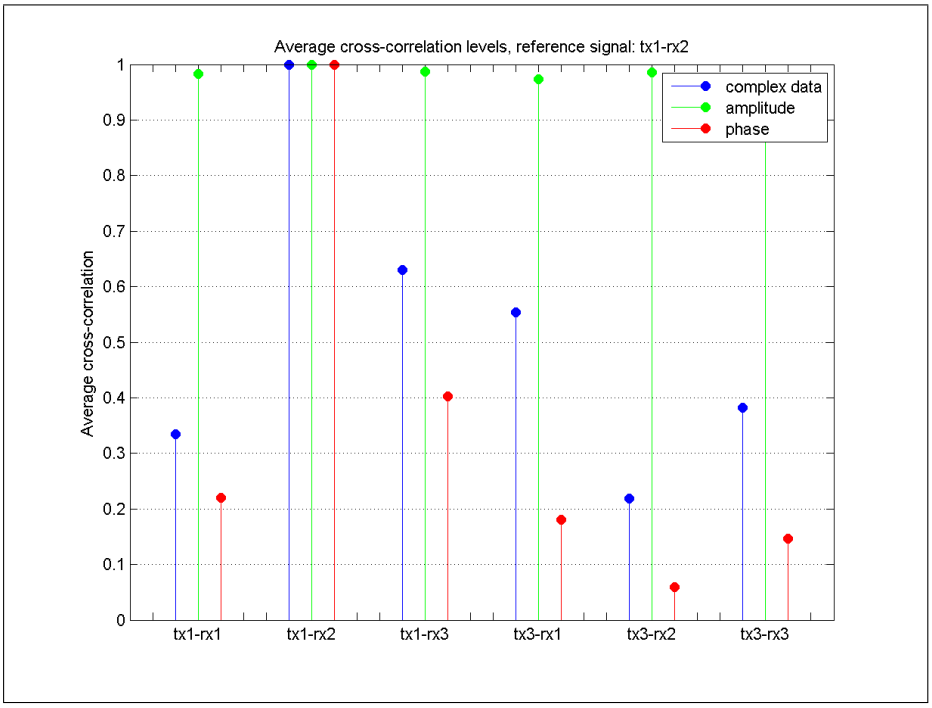

Figure 9.11: Cross-correlation levels with tx1-rx2 – target

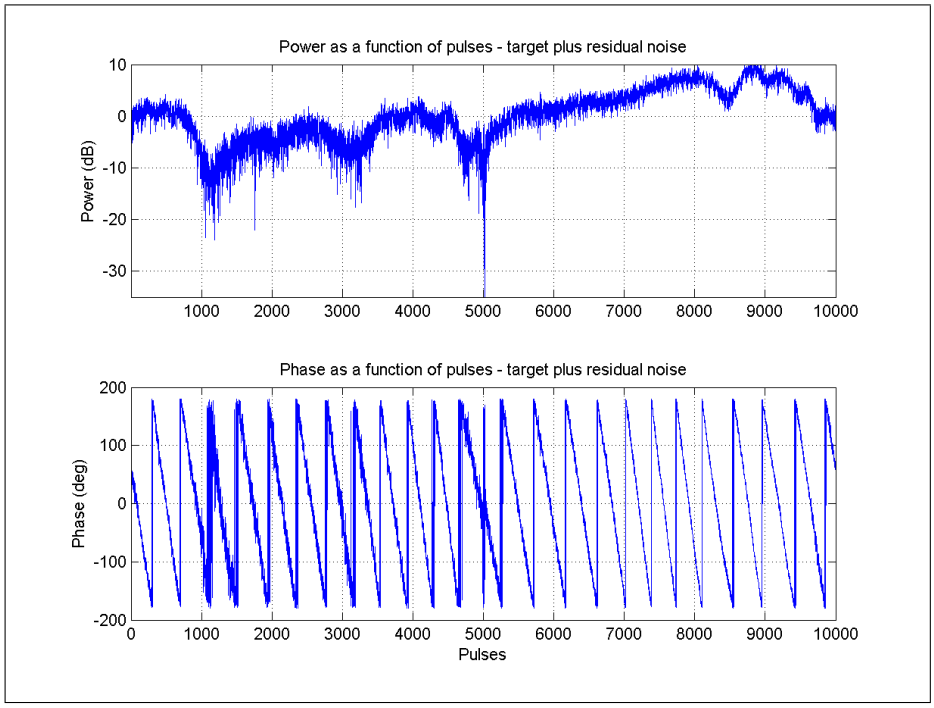

Figure 9.12: tx1-rx3

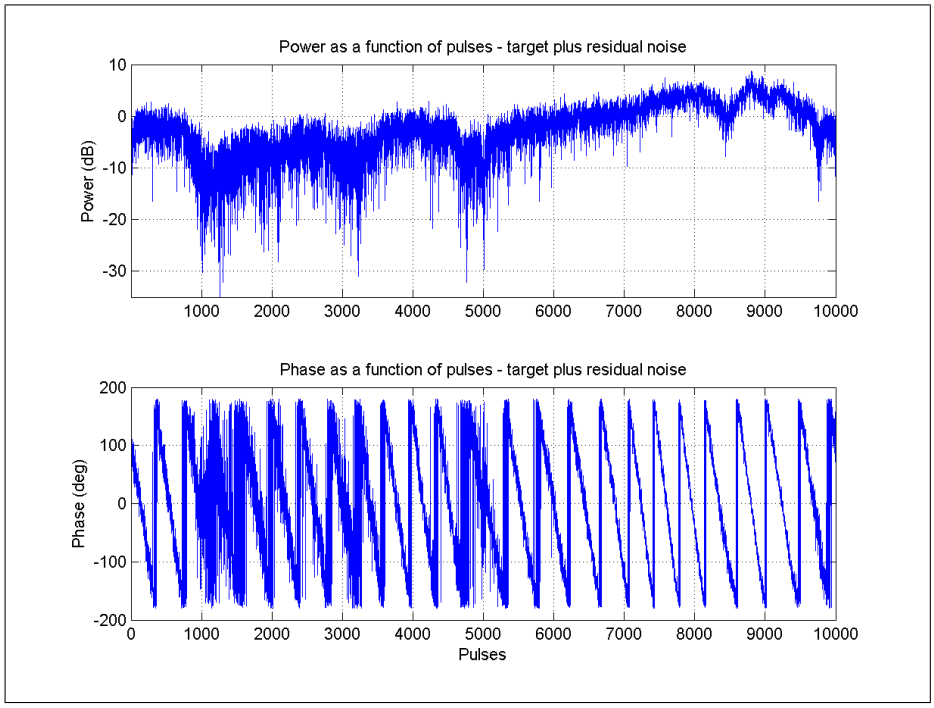

Figure 9.13: tx3-rx1

Chapter 10

Localization

In this Chapter a method for processing data from a chosen area as surveyed by a multistatic system for the localization of a target is presented. Experiment description and pre-processing of the signals have already been discussed in Chapter 8. In particular, two ways for localization are reported. The first is a graphical method, in which data are processed according to the strategies so far examined (MIMO, NR, RPNR, DRN). The second is an hybrid numerical approach in which the system works in part as decentralized and in part centralized. It is clear that numerical minimization of specific functions has to be applied when the estimated target location is used in a tracking algorithm, so an easy and immediate method to locate one (or more) target is also reported. This expands the domain of potential application. For this purpose, an easy and very fast sub-optimal algorithm is applied to the received data so to improve the estimation of the measures of the Doppler shifts and the range positions of the target.

Figure 10.1 shows a representation of 25 integrated received pulses, as a function of range. In particular, each subplot shows one path from a transmitter to a receiver. It has been chosen to integrate 25 pulses for (*i*) avoiding range cell migration and (*ii*) emulating the TOT as if the antennas were scanning. In this Figure, the shown signals are a representation on the (x, y) plane of the received echoes for each path. The first transceiver has

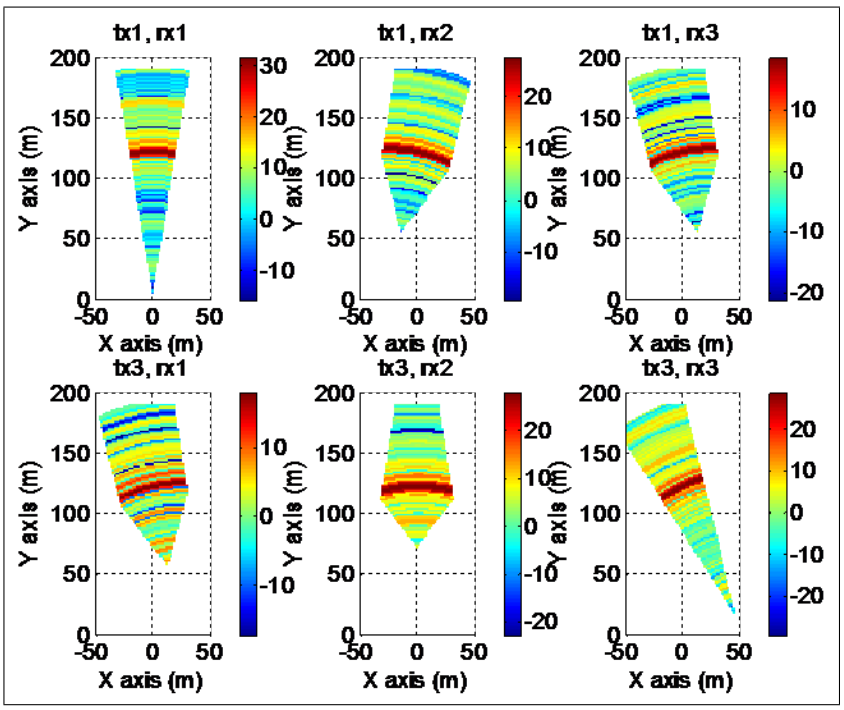

Figure 10.1: Graphical representation of acquired signals

been taken as the origin of the grid ($x = 0$ m, $y = 0$ m) and consequentially the other two devices are located at ($x = -48.96$ m, $y = 10.28$ m) and ($x = 48.96$ m, $y = 10.28$ m), respectively. In addition, the pattern of the antennas are here represented as if they are limited to the -3dB width. Bistatic paths in the subplots have been represented evaluating the patterns as the superimposition of the transmitter and receiver 1-way patterns. As it can be seen from this Figure, the *SNR* is expected to vary roughly from 15 to 30 dB, which is a fairly high SNR. However, as also seen in Section 8, these levels can be subject to a considerable fading. From the a-priori knowledge of the experiment, the moving target is expected to be ≈ 120 m far from the first device and walking away from it radially.

10.1 Visual localization

In this Section the diagrams in Figure 10.1 are summed up together into a single plot only, according to different strategies. These are, in order, in analogy with the concepts examined in the previous Chapters: (*i*) coherent centralized summation (NR), (*ii*) coherent centralized summation with phase correction (RPNR), (*iii*) incoherent centralized summation (MIMO) and (*iv*) incoherent decentralized summation (DRN). In other words in the NR case the diagrams in Figure 10.1 are summed in amplitude and phase, without re-aligning the phase from the target, in the MIMO case they are summed up in power, in the DRN after a first thresholding, in the RPNR after re-aligning the phases according to the position of the target. For the sake of simplicity, given the high SNR, in the RPNR it has been assumed that

$$\angle\left(s_{ta}\left(t_{ta}\right)\right) \approx \angle\left(s_{ta}\left(t_{ta}\right) + n_{ta}\left(t_{ta}\right)\right) \tag{10.1}$$

where $\angle x$ is the phase of x, and t_{ta} is the time of reception of the echo from the target. This is not the same as re-aligning the phases according to the real position of the target, but still gives a good approximation of the best performance available. However, as in the rest of this work, the first two systems are reported as a means of comparison.

Figures 10.2 and 10.3 show the graphical approach to localization in the area around the target at the beginning and at the end of the acquisition, respectively, i.e. at $t = 0$ sec and $t = 1$ sec. Here all the approaches described throughout this thesis are applied. The integration time was 2.5 msec, i.e. equal to 25 pulses. The subplots have been achieved by summing up, according to the different strategies, the signals as in Figure 10.1. Generally, the coherent uncorrected summation performs worst, as expected, whereas coherency is not achieved in the location of the target, but in other regions, whilst as expected, the re-phased coherent system performs at the best, whereas it exploits a-priori information. As it can be seen, the MIMO approach results in some uncertainty as to the position of the target, because of the wide beamwidth of the antenna patterns. On

the contrary the DRN approach manages to locate the target with higher accuracy, although it has to be pointed out that this approach requires a thresholding on the output of each pair tx-rx. In particular, the approach to thresholding for this set of results is a standard CA-CFAR, with one guard cell and two secondary cells per side, around the cell under test. The single-pair FAR has been set in this case to 10^{-1}, which is a fairly high value, but still allows to compare the systems limiting the advantage that the DRN can take from the double-thresholding. In addition it has to be pointed out that the graphical approach does not allow a clear discrimination of the movements of the target, as the plots at the beginning and the end of the acquisition (respectively Figures 10.2 and 10.3) differ by small differences. This scenario can be therefore of interest if the signals are to be plotted jointly on a screen or on a Planned Position Indicator (PPI), but it is not adequate for automatic applications. In the following Section a solution for addressing this issue is presented.

10.2 Numerical localization and Doppler reconstruction

In this Section a numerical approach to the problem of localization is reported. In addition, Section 10.2.2 and Section 10.2.3 describe some issues related to the range-Doppler measurements of the analyzed data and their solution. Finally Section 10.2.5 shows a convenient way of extracting further information on the movement of the target.

10.2.1 Algorithm

Numerically, the position of one or more targets can be computed by solving the following equations

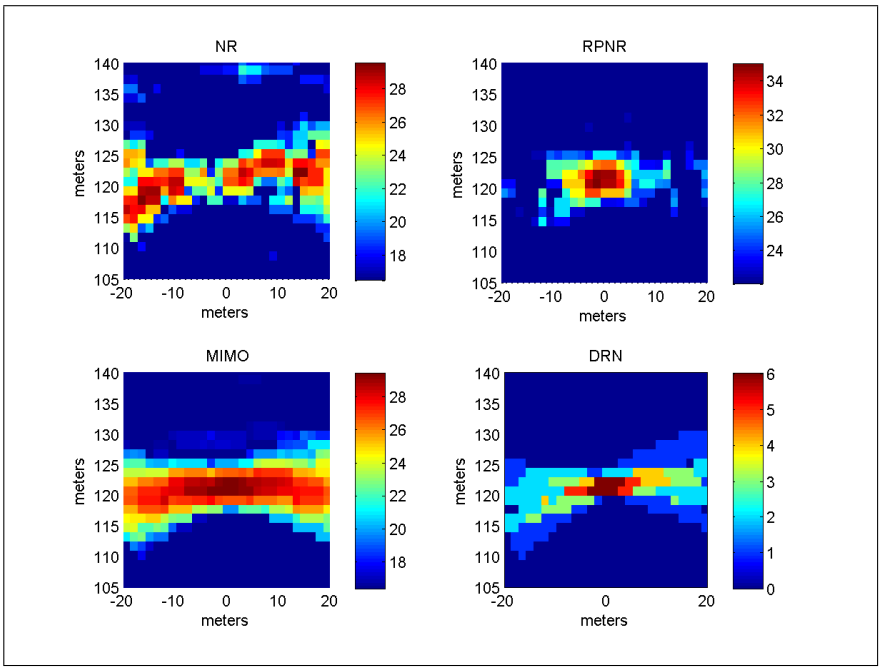

Figure 10.2: Graphical approach to localization, start of acquisition ($t = 0$ sec)

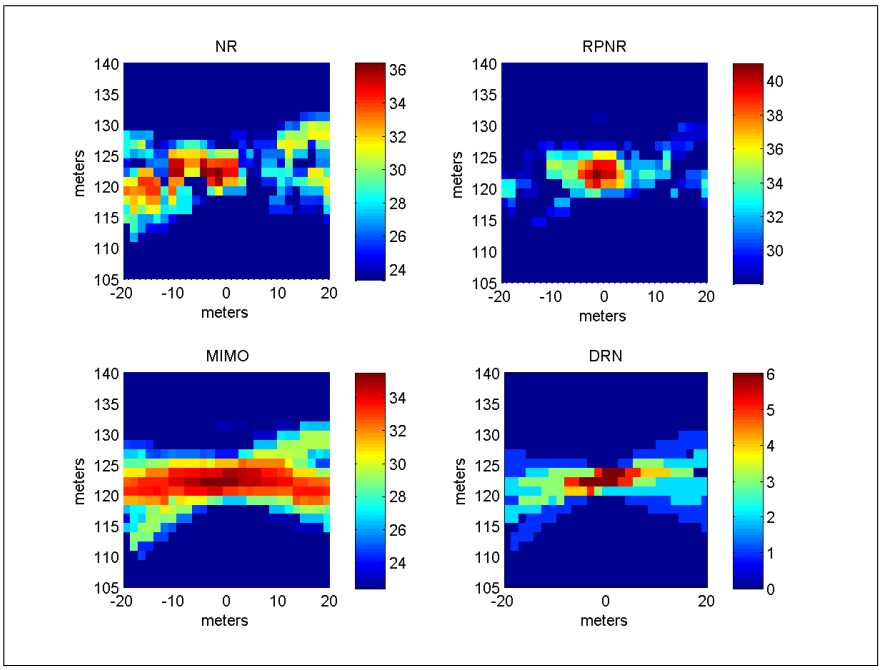

Figure 10.3: Graphical approach to localization, end of acquisition ($t = 1$ sec)

$$\begin{cases} \|\mathbf{v}_T - \mathbf{v}_{tx,1}\| & + & \|\mathbf{v}_T - \mathbf{v}_{rx,1}\| = & r_{1,1} \\ \vdots & & \vdots & \vdots \\ \|\mathbf{v}_T - \mathbf{v}_{tx,i}\| & + & \|\mathbf{v}_T - \mathbf{v}_{rx,k}\| = & r_{i,k} \\ \vdots & & \vdots & \vdots \\ \|\mathbf{v}_T - \mathbf{v}_{tx,M}\| & + & \|\mathbf{v}_T - \mathbf{v}_{rx,N}\| = & r_{M,N} \end{cases} \tag{10.2}$$

with respect to vector of the coordinates of the target $\mathbf{v}_T$, where $\mathbf{v}_{tx,i}$ is the vector of the coordinates of the i^{th} transmitter, $\mathbf{v}_{rx,k}$ is the vector of the coordinates of the k^{th} receiver and $r_{i,k}$ is the two-way estimated distance. Alternatively, it is possible to minimize a function such as

$$\epsilon(\mathbf{v}_T, \mathbf{V}_{tx}, \mathbf{V}_{rx}, \mathbf{r}) = \sum_{i=1}^{M} \sum_{k=1}^{N} \left(\|\mathbf{v}_T - \mathbf{v}_{tx,i}\| + \|\mathbf{v}_T - \mathbf{v}_{rx,k}\| - r_{i,k} \right)^2 , \tag{10.3}$$

where $\mathbf{V}_{tx}$ is the matrix comprised by the vectors of the coordinates of the transmitters, $\mathbf{V}_{rx}$ is the matrix comprised by the vectors of the coordinates of the receivers and $\mathbf{r}$ is the vector comprised by the measured 2-way distances. Under this assumptions, the solution of the system in equation (10.3) can be written as

$$\hat{\mathbf{v}}_T = \arg \left\{ \min_{\mathbf{v}_T} \{\epsilon(\mathbf{v}_T, \mathbf{V}_{tx}, \mathbf{V}_{rx}, \mathbf{r})\} \right\} , \tag{10.4}$$

since it is more robust when the set of distances $\mathbf{r}$ is not exact but affected by errors (thermal noise, residual clutter and range-estimation errors), as occurs generally in radar systems. However such minimization can be complicated and the complexity grows with the number of all the possible paths between the transmitters, the target and the receivers.

Alternatively, this problem can be slightly simplified by determining at a first stage an evaluation of the distance $\hat{d}_h = \|\mathbf{v}_t - \mathbf{v}_h\|$ between the target and the h^{th} device (either tx or rx) and in a second stage finding the minimum of a function such as:

$$\epsilon(v_T, \mathbf{V}, \mathbf{d}) = \sum_h \left(\|\mathbf{v}_T - \mathbf{v}_h\| - \hat{d}_h \right)^2 \tag{10.5}$$

where $\mathbf{V}$ is the matrix comprised by the vectors of the coordinates of all the devices. Consequently the solution of the function in equation (10.5) can be written as follows:

$$\hat{\mathbf{v}}_T = \arg \left\{ \min_{\mathbf{v}_T} \left\{ \epsilon(\mathbf{v}_T, \mathbf{V}, \hat{\mathbf{d}}) \right\} \right\}, \tag{10.6}$$

In other words, the minimum least square (MLS) optimization of equation (10.3) is divided in two sub-MLS-optimizations. In the first, starting from all the range estimations (as will be seen in Section 10.2.3), the distances between the devices (either tx or rx or both) and the target are computed and then the minimum of the function in equation (10.5) is searched.

In particular, the distances $\hat{d}_h$, can be found as the MLS solution of the following system:

$$\mathbf{A}\mathbf{d} = \begin{pmatrix} 2 & 0 & 0 \\ 1 & 1 & 0 \\ 1 & 0 & 1 \\ 1 & 0 & 1 \\ 0 & 1 & 1 \\ 0 & 0 & 2 \end{pmatrix} \begin{pmatrix} d_1 \\ d_2 \\ d_3 \end{pmatrix} = \begin{pmatrix} r_{11} \\ r_{12} \\ r_{13} \\ r_{31} \\ r_{32} \\ r_{33} \end{pmatrix} = \mathbf{r}, \tag{10.7}$$

i.e. as

$$\hat{\mathbf{d}}_{MLS} = \left(\mathbf{A}^T \mathbf{A} \right)^{-1} \mathbf{A}^T \mathbf{r}. \tag{10.8}$$

It has to be pointed out that many equations in (10.7) would be redundant if it was possible to measure distances without errors. In fact, this system states that the generic measured range $r_{i,k}$ is the sum of the distance d_i from the i^{th} transmitter to the target and the distance d_k from the target to the k^{th} receiver. Nevertheless, the inaccuracy of the measurements due to disturbance and limited resolution provides a reason for the inversion

of the system in (10.7) as in (10.8). However, it is particularly worth noting that (*i*) this MLS optimization is basically costless, whereas the matrix $\left(\mathbf{A}^T\mathbf{A}\right)^{-1}\mathbf{A}^T$ can be pre-computed and does not need to be updated, and (*ii*) the optimization of the function in equation (10.5) presents a much lower level of complexity than the one in equation (10.3).

For completeness, in the analysis of the localization, two further functions have been examined. These take into account the noise of the channel and are as follows:

$$\epsilon(\mathbf{v}_T, \mathbf{V}_{tx}, \mathbf{V}_{rx}, \mathbf{r}) = \sum_{i=1}^{M}\sum_{k=1}^{N}\frac{1}{\sigma_{i,k}^2}\left(\|\mathbf{v}_T - \mathbf{v}_{tx,i}\| + \|\mathbf{v}_T - \mathbf{v}_{rx,k}\| - r_{i,k}\right)^2, \tag{10.9}$$

and

$$\epsilon(\mathbf{v}_T, \mathbf{V}, \hat{\mathbf{d}}) = \sum_{h}\frac{1}{\hat{\sigma}_h^2}\left(\|\mathbf{v}_T - \mathbf{v}_h\| - \hat{d}_h\right)^2, \tag{10.10}$$

where $\sigma_{i,k}^2$ is an estimate of the noise present in the path from the i^{th} transmitter to the k^{th} receiver and

$$\begin{pmatrix}\hat{\sigma_1^2}\\ \hat{\sigma_2^2}\\ \hat{\sigma_3^2}\end{pmatrix} = \begin{pmatrix}\frac{1}{5} & 0 & 0\\ 0 & \frac{1}{2} & 0\\ 0 & 0 & \frac{1}{5}\end{pmatrix}\mathbf{A}^T\begin{pmatrix}\sigma_{1,1}^2\\ \sigma_{1,2}^2\\ \sigma_{1,3}^2\\ \sigma_{3,1}^2\\ \sigma_{3,2}^2\\ \sigma_{3,3}^2\end{pmatrix}, \tag{10.11}$$

where ^{T} is the transpose operator. In other words σ_h^2 is an average of the noise of the channels, when the h^{th} device is active as a transmitter and/or as a receiver. The matrix before $\mathbf{A}^T$ provides an averaging proportionally inverse to the sum of the columns of $\mathbf{A}$.

10.2.2 Range-Doppler analysis

In this Section the range-Doppler diagrams for the acquired signals are reported. The aims are (*i*) to validate that the clutter cancellation does not affect the Doppler-shift of the signal, (*ii*) to provide a starting point for an algorithm for improving the range and Doppler estimations and therefore (*iii*) to allow, in a second stage of processing (Section 10.2.5), better localization of the target and reconstruction of the Doppler vector of the target.

Although the acquisition time is 1 second, in a real-time scenario the precessing unit is capable of performing a range-Doppler analysis within a much shorter time interval. As a consequence, the TOT is assumed to be 50 msec only for producing the range-Doppler plots. Under this assumption and after the clutter removal, the range-Doppler plots for each pair tx-rx become as in Figure 10.4. As seen here, not only the clutter cancellation of the low frequencies is less effective, due to the coarse frequency resolution, but also the target's Doppler frequencies fall into the same bin, regardless from the pairs tx-rx. At the same time, because of the geometrical and iso-range configuration of the experiment, also the range bin of the target is the same for any pair of devices.

10.2.3 Range-Doppler estimation

To partially solve the ambiguity in Range and Doppler described in the previous Section, Doppler frequency and range estimation in a single pair tx-rx has been improved through an interpolation method based on fitting a parabolic curve to the logarithm of the absolute value of the peak of the range-Doppler function [72]. Here the method is applied to range estimation only, for brevity, since it is the same as for frequency.

Assuming that the maximum power P_0 (dB) occurs at the range R_0, the parabolic curve passing through the points $(R_{-1} - R_0, P_{-1})$, $(0, P_0)$ and $(R_1 - R_0, P_1)$ is considered, where R_{-1} and R_1 are respectively the range bins respectively before and after R_0 and P_{-1} and P_1 the corresponding power measured (in dB) and a translation from R_0 to the origin has been

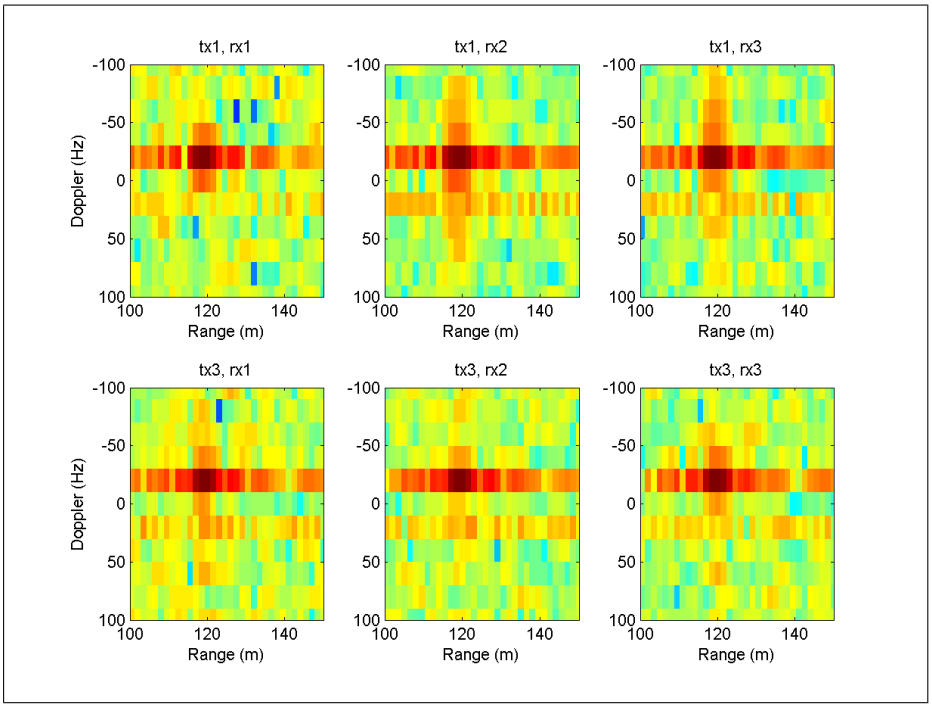

Figure 10.4: Range-Doppler plots over 50 ms

applied to the range domain. Therefore the power as function of the range is interpolated as

$$P(r) = ar^2 + br + c, \tag{10.12}$$

where a, b and c are unknown coefficients that can be recovered from the information

$$\begin{cases} P_{-1} = P(-\Delta R) = a(\Delta R)^2 - b\Delta R + c \\ P_0 = P(0) = c \\ P_1 = P(\Delta R) = a(\Delta R)^2 + b\Delta R + c \end{cases} \tag{10.13}$$

where

$$\Delta R = R_0 - R_{-1} = R_1 - R_0. \tag{10.14}$$

Under these assumptions, after solving the system, the range $\hat{r}_{max}$ of maximum power is

$$\hat{r}_{max} = \frac{1}{2}\frac{P_{-1} - P_1}{P_{-1} - 2P_0 + P_1}\Delta R, \tag{10.15}$$

which gives, translating the origin back to R_0:

$$r_{max} = R_0 + \hat{r}_{max} = R_0 + \frac{1}{2}\frac{P_{-1} - P_1}{P_{-1} - 2P_0 + P_1}\Delta R, \tag{10.16}$$

Exactly the same procedure applies to the Doppler frequency and therefore it is not reported for brevity. It is important to highlight that, after these processing, the new measurements in range-Doppler will also allow an improved cancellation of the target [72] and therefore a recursive application of the detection algorithm so to detect multiple targets (if present) with RCS smaller in the area.

10.2.4 Localization results

The optimizations of the functions in equations (10.3), (10.5), (10.9) and (10.10) have been computed with Nelder-Mead simplex method, that is known to be quite robust even if relatively slow. The starting point provided to the algorithm at the q^{th} iteration is the $(q-1)^{th}$ output. For the first iteration the starting point was deliberately set to $(0, 100)$, so to verify the convergence in just a few steps.

Figure 10.5 shows the series of the localizations after the optimization processes when pulses are processed at bursts of 25, i.e. over 2.5 msec. Figures 10.5(a) and 10.5(b) show the Y-axis and X-axis positions after the 1-stage minimization respectively without and with noise as in equations (10.3) (above) and (10.9) (below). Figures 10.5(c) and 10.5(d) show the Y-axis and X-axis positions after the 2-stage minimization respectively without and with noise as in equations (10.5) (above) and (10.10) (below). The average time for achieving the results in the following pictures varied between 2 seconds (2-step MLS algorithm) and 2.75 seconds (original 1-step version). Although the time of processing is greater than the time of acquisition, it has to be pointed out that it has been achieved using a

2 GHz processor and standard commercial minimization macros over an unoptimized hardware.

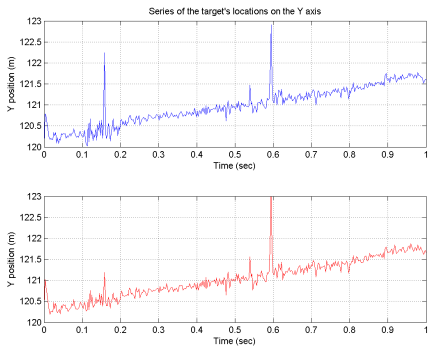

(a) 1-stage algorithm, Y axis, unweighed (up), weighed (down)

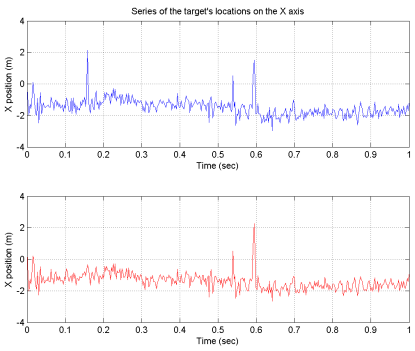

(b) 1-stage algorithm, X axis, unweighed (up), weighed (down)

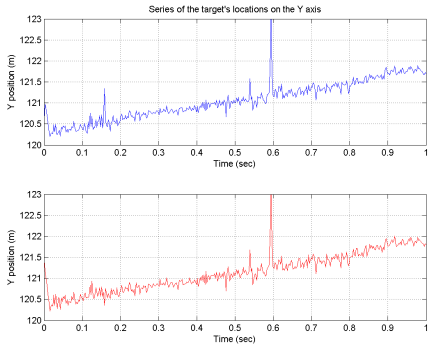

(c) 2-stage algorithm, Y axis, unweighed (up), weighed (down)

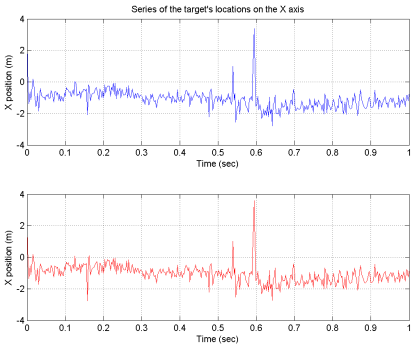

(d) 2-stage algorithm, X axis, unweighed (up), weighed (down)

Figure 10.5: Localization results on buffers of 2.5 msec

In particular, it is observed that:

(*i*) The series of localizations, in all cases, is a good representation of the actual path of the target, with a resolution that is dramatically improved compared to the nominal one (3.75 m),

(*ii*) The 2-stage process performs better than the single-stage one for low SNR. This can be seen from the absence of a couple of noise-affected localizations at approximately 0.16 sec.

(*iii*) The standard deviation of the errors in these Figures are between 15 and 17 cm on the Y axis and between 35 and 45 cm on the X axis.

(*iv*) For low SNR the weighted versions perform better than the non-weighted, as might be expected. However a higher standard deviation overall (approximately 5% more) has been observed in the latter cases.

Figure 10.6 shows the plots of the localization on the Y and X axis when buffers of 50 msec are processed. In this Figure the results of the minimization according to equation (10.3) only is reported. This is because the differences between the four minimization functions described previously are negligible. In addition, as it can be expected with a longer integration period, here the measurements are averaged, if compared to those in Figure 10.5, and therefore the overall movement of the target appears smoother. The increased length of the data-buffer had also the effect of reducing the measurements in input to any minimization function, leading to a dramatic reduction in the processing time: in this case, for each function taken into account, the time required to provide the output was approximately 0.1 sec, i.e. in the order of $\frac{1}{10}$ of the acquisition time, using unoptimized macros and hardware. This is of course of much greater interest for real systems applications.

10.2.5 Doppler vector reconstruction

Finally, in this Section the reconstruction of the full velocity vector $\mathbf{W}$ is performed, starting from the measurements of the single radars. The following system of equations describes the relationship between the real Doppler vector $\mathbf{W}$ and the Doppler measurements $\mathbf{F}_D$. The Doppler measurements are as after the process described in Section 10.2.3.

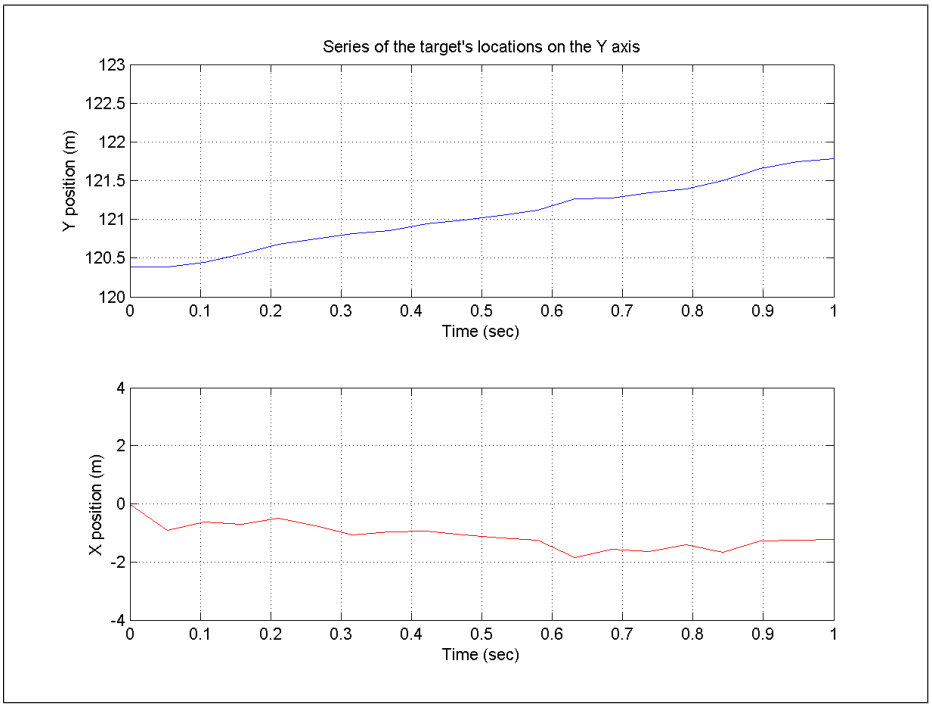

Figure 10.6: Localization results on buffers of 50 msec

$$\mathbf{BW} = \begin{pmatrix} b_{x,11} & b_{y,11} \\ b_{x,12} & b_{y,12} \\ b_{x,13} & b_{y,13} \\ b_{x,31} & b_{y,31} \\ b_{x,32} & b_{y,32} \\ b_{x,33} & b_{y,33} \end{pmatrix} \begin{pmatrix} w_x \\ w_y \end{pmatrix} = \begin{pmatrix} f_{D,11} \\ f_{D,12} \\ f_{D,13} \\ f_{D,31} \\ f_{D,32} \\ f_{D,33} \end{pmatrix} = \mathbf{F}_D, \tag{10.17}$$

where

$$b_{x,ik} = \frac{\cos\theta_{x,TX_i} + \cos\theta_{x,RX_k}}{\lambda}, \tag{10.18}$$

$$b_{y,ik} = \frac{\cos\phi_{y,TX_i} + \cos\phi_{y,RX_k}}{\lambda} \tag{10.19}$$

and $\theta_{x,TX_i/RX_k}$ and $\phi_{y,TX_i/RX_k}$ are, respectively, the angle between the x and y unit vectors in the grid and the vectors connecting the target to either the i^{th} tx or the k^{th} rx. The MLS solution $\hat{\mathbf{W}}_{MLS}$ of the system in equation (10.17)

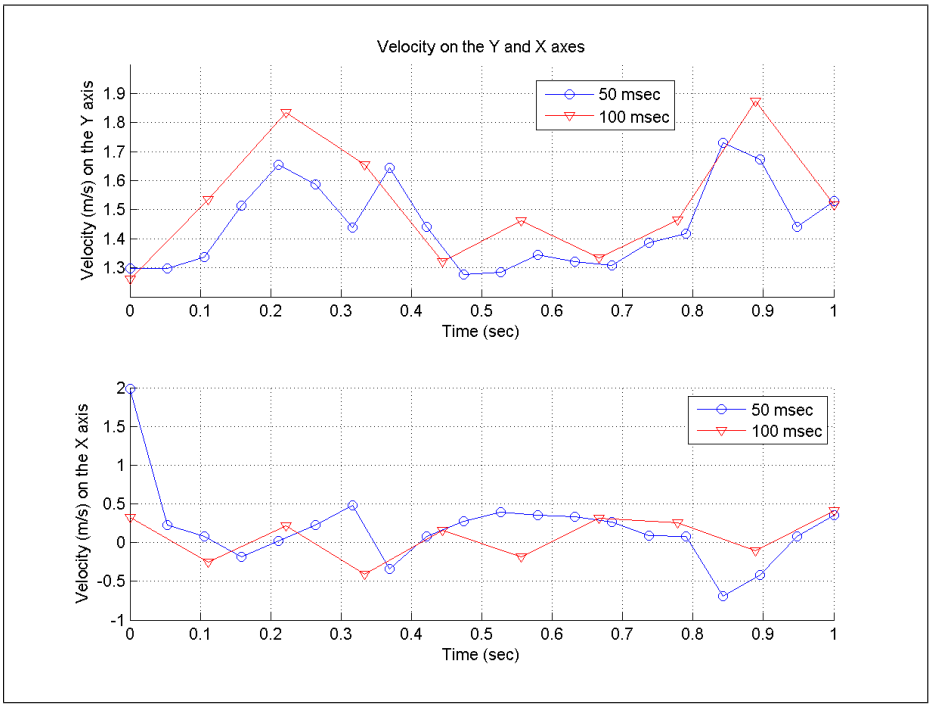

Figure 10.7: Velocity estimation on 50 amd 100 msec buffers

can be expressed as

$$\hat{\mathbf{W}}_{MLS} = \left(\mathbf{B}^T\mathbf{B}\right)^{-1}\mathbf{B}^T\mathbf{F}_D. \tag{10.20}$$

Figure 10.7 shows the estimated instantaneous velocity on both Y and X axes for buffers of 50 and 100 msec. From the experiment setup and the previous plots, it is possible to conclude that the target moves approximately with an average speed of 1.5 m/sec on the Y axis and 0 m/sec on the X axis. These values are confirmed by the results shown here.

Chapter 11

Frequency Diverse Array Radars

In this Chapter, manipulating the concept of the Frequency MIMO, the effects in transmission and propagation of a transmitted signal consisting of equally-spaced frequencies relatively close to one another are investigated. The system concept has been anticipated in Section 4.5.

11.1 The Frequency Diverse Array

In [76, 77] the pattern generated using an array of N antennas where each single element transmits a sinusoid $s_k(t)$:

$$s_k(t) = \exp\{-j2\pi f_k t\}, \tag{11.1}$$

whose frequency f_k differs from a starting frequency f_0 by a quantity $k\Delta f$, $k = 0, \ldots, N-1$ (Figure 4.7), i.e. $f_k = f_0 + k\Delta f$. For instance the number of array elements in this Chapter is fixed to $N = 9$. Frequencies are equally spaced by $\Delta f = 3$ KHz starting from $f_0 = 8$ GHz. The antenna elements comprising the array are mutually spaced by the quantity

$$\frac{1}{2}\min_k\{\lambda_k\} = \frac{1}{2}\lambda_{N-1} = \frac{1}{2}\frac{c}{f_0 + (N-1)\Delta f}, \tag{11.2}$$

i.e. the half wavelength spacing is maintained albeit now as a function of the maximum transmit frequency. The expression of the pattern $p(f, t, R_0, \theta)$ after coherent summation is as in equation (11.3):

$$
\begin{aligned}
p(f,t,R_0,\theta) &= \sum_{k=0}^{N-1} \frac{1}{R_k} \exp\left\{-j2\pi\left(f_k t - \frac{R_k}{\lambda_k}\right)\right\} \approx \\
&= \sum_{k=0}^{N-1} \frac{1}{R_k} \exp\left\{-j2\pi\left[(f_0 + k\Delta f)\left(t - \frac{R_k}{c}\right)\right]\right\} = \\
&= \exp\left\{j\phi_0\right\} \sum_{k=0}^{N-1} \frac{1}{R_k} \exp\left\{-j2\pi\left(k\Delta f t - k\frac{\Delta f R_0}{c} - k\frac{d\sin\theta}{\lambda_0} - k^2\frac{\Delta f d\sin\theta}{c}\right)\right\} \approx \\
&\approx \frac{\exp\left\{j\phi_0\right\}}{R_0} \sum_{k=0}^{N-1} \exp\left\{-j2\pi\left(k\Delta f t - k\frac{\Delta f R_0}{c} - k\frac{d\sin\theta}{\lambda_0} - k^2\frac{\Delta f d\sin\theta}{c}\right)\right\},
\end{aligned}
\tag{11.3}
$$

where $d_k = kd$ and $R_k = R_0 + kd\sin\theta$

$$
\phi_0 = -2\pi\left(f_0 t - \frac{R_0}{\lambda_0}\right) = -2\pi f_0\left(t - \frac{R_0}{c}\right) \tag{11.4}
$$

and the approximation is due to the fact that $R_k \approx R_0$.

In Figures 11.1 and 11.2 a numerical simulation of the beam pattern is computed. Whilst the first one reports the pattern as in equation (11.3) and it is useful to understand the regularity of the pattern as a function of range, in the second the dependance on the factor $\frac{1}{R_k}$ has been removed to show the recursiveness of the pattern. It is worth highlighting the 'S'-shaped pattern which assumes a varying gain in range. Replicas of this 'S'-shaped pattern occur at regularly intervals.

Although in general terms a closed form of the pattern in equation (11.3) cannot be written, a closed approximation exists when $(N-1)\frac{\Delta f}{c} << \frac{1}{\lambda_0}$, which is true as long as $(N-1)\Delta f << f_0$. In this case the term $k^2\frac{\Delta f d\sin\theta}{c}$ in equation (11.3) becomes negligible and the pattern can be written as

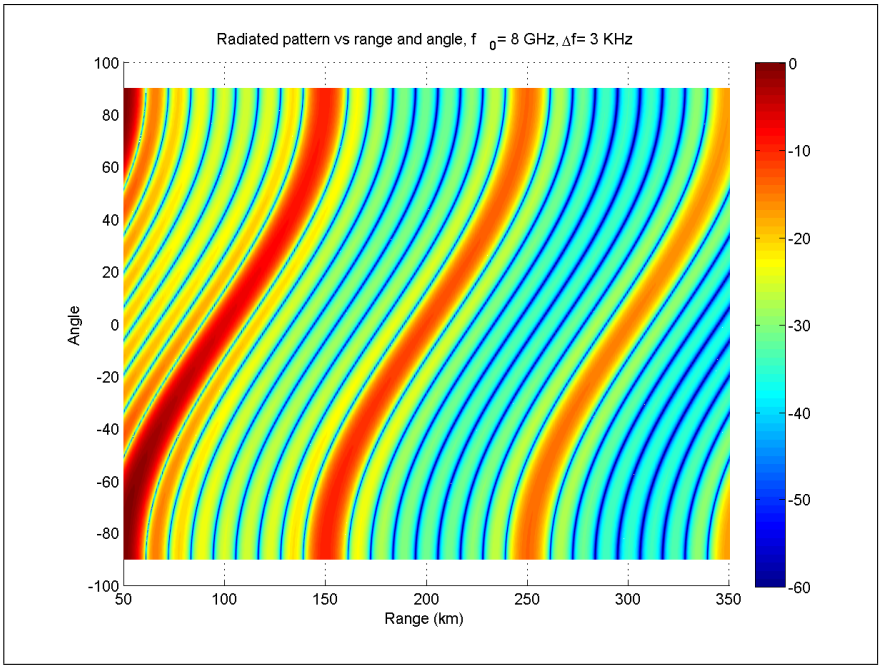

Figure 11.1: Frequency diverse array, pattern with range attenuation, minimum half-wavelength spacing

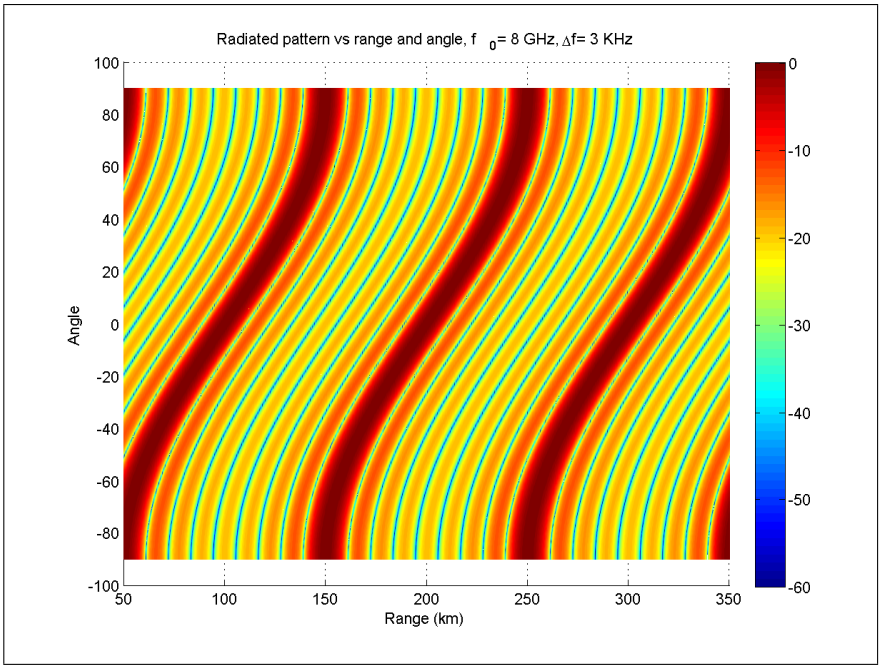

Figure 11.2: Frequency diverse array, pattern without range attenuation, minimum half-wavelength spacing

$$p(f,t,R_0,\theta) \approx \frac{\exp\left\{j\phi_0\right\}}{R_0} \cdot \sum_{k=0}^{N-1} \exp\left\{-j2\pi k\left(\Delta f t - \frac{\Delta f R_0}{c} - \frac{d\sin\theta}{\lambda_0}\right)\right\} =$$
$$= \frac{\exp\left\{j\left(\phi_c + \pi(N-1)\frac{d\sin\theta}{\lambda_0}\right)\right\}}{R_0} \frac{\sin\left[\pi N\left(\Delta f t - \frac{\Delta f R_0}{c} - \frac{d\sin\theta}{\lambda_0}\right)\right]}{\sin\left[\pi\left(\Delta f t - \frac{\Delta f R_0}{c} - \frac{d\sin\theta}{\lambda_0}\right)\right]}, \tag{11.5}$$

where

$$\phi_c = -2\pi f_c\left(t - \frac{R_0}{c}\right) \tag{11.6}$$

and

$$f_c = \frac{1}{N}\sum_{k=0}^{N-1} f_k = f_0 + \frac{N-1}{2}\Delta f. \tag{11.7}$$

Equation (11.5) provides further details on the behaviour of the pattern. In particular, fixing the angle θ:

(*i*) For a given instant of time the pattern is periodic in range and its peaks are spaced $\frac{c}{\Delta f}$ from one another and for a given range the pattern is periodic in time and its peaks are $\frac{1}{\Delta f}$ from one another;

(*ii*) The beamwidth at -3 dB is equal to $\frac{c}{N\Delta f}$ so the more elements comprising the array the sharper the peak and the greater the peak-to-sidelobe ratio and the time of illumination (width at -3 dB) of a target is $\frac{1}{N\Delta f}$;

(*iii*) Finally, the arguments in round brackets of the 'sin' functions can be rearranged as $\Delta f\left(t - \frac{R_0}{c} - \frac{1}{\Delta f}\frac{d}{\lambda_0}\sin\theta\right)$. The latter part of this expression explains clearly why the pattern is a function of angle as well. At the same time it shows that the distance between the peaks of the pattern at $\theta = 0$ and $\theta = \frac{\pi}{2}$ is $\frac{c}{\Delta f}\frac{d}{\lambda_0}$ in range and $\frac{1}{\Delta f}\frac{d}{\lambda_0}$ in

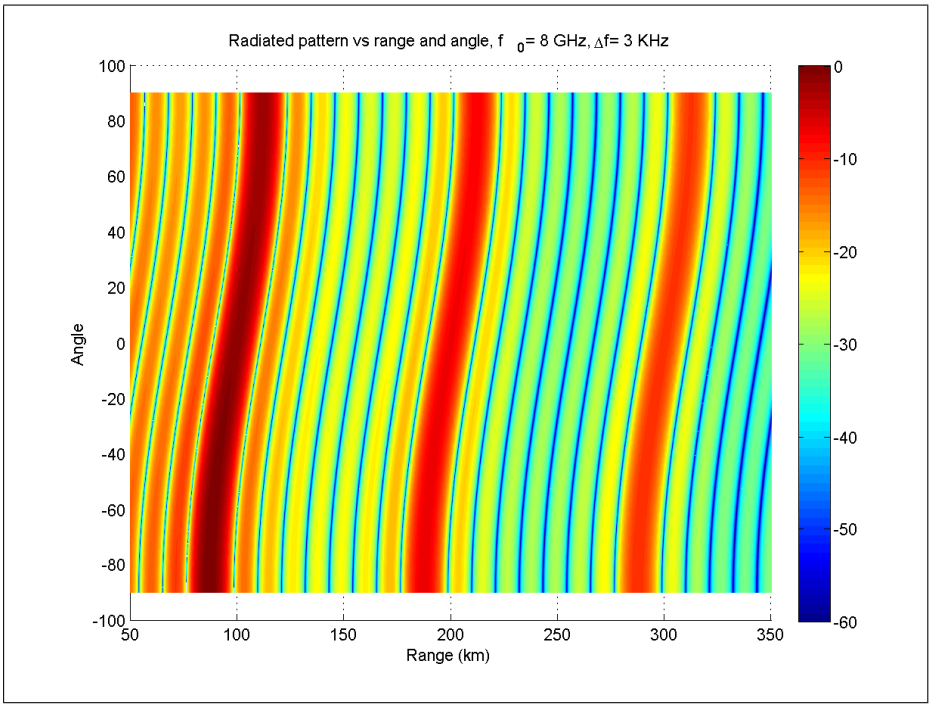

Figure 11.3: Frequency diverse array, pattern with range attenuation, octave-wavelength spacing

time. Therefore the 'S'-shape of the pattern is here shown clearly to be function of the ratio $\frac{d}{\lambda_0}$ and the frequency shift of the antenna elements Δf.

Figure 11.3 shows clearly the latter point, since the curvature in the 'S' shape of the pattern results to be dramatically reduced by diminishing the distance between the array elements. In this example the spacing has been taken equal to $\frac{\lambda_{N-1}}{8}$. Nevertheless, the distance between the peak at 0° and those in $\pm 90^\circ$ is in the order of tens of kilometers, with a challenging spacing between the elements.

11.2 The Wavelength Array

In order to avoid, or at least to lessen, the dependency of the range gain from angle gain, it was decided to rearrange the elements of the array

in a different configuration. This leads to what has been termed as the 'wavelength array'. The main idea is to separate the elements of the array from a reference point by a distance related to the transmitted wavelengths. In other words, here it assumed that the distances $d_k \propto \lambda_k$. It is important to highlight that the reference point is not active in transmission. This is shown schematically in Figure 11.4. Assuming $d_k = L\lambda_k$, the pattern $p(f, t, R_0, \theta)$ can be written as

$$\begin{aligned} p(f,t,R_0,\theta) &= \sum_{k=0}^{N-1} \frac{1}{R_k} \exp\left\{-j2\pi\left(f_k t - \frac{R_k}{\lambda_k}\right)\right\} = \\ &= \sum_{k=0}^{N-1} \frac{1}{R_k} \exp\left\{-j2\pi\left(f_k t - \frac{R_0 + L\lambda_k \sin\theta}{\lambda_k}\right)\right\} = \\ &= \sum_{k=0}^{N-1} \frac{1}{R_k} \exp\left\{-j2\pi L\sin\theta - j2\pi f_k\left(t - \frac{R_0}{c}\right)\right\} \approx \\ &\approx \frac{1}{R_0} \sum_{k=0}^{N-1} \exp\left\{-j2\pi L\sin\theta - j2\pi f_k\left(t - \frac{R_0}{c}\right)\right\} = \\ &= \frac{\exp\left\{j\left(\Phi + \phi_c\right)\right\}}{R_0} \frac{\sin\left(N\pi\Delta f\left(t - \frac{R_0}{c}\right)\right)}{\sin\left(\pi\Delta f\left(t - \frac{R_0}{c}\right)\right)} \end{aligned} \tag{11.8}$$

where

$$\Phi = -2\pi L \sin\theta. \tag{11.9}$$

The pattern derived here is shown in Figure 11.5. This is a most unusual beam pattern which exhibits constant peak gain with angle at a particular range, i.e. the beam pattern in the space is orthogonal to that produced by conventional fixed phased arrays. In this case it is worth highlighting clearly the following:

(*i*) The angle-dependency is found in the phase term only, whilst the amplitude depends on time, range and frequency shift only and not anymore on the angle;

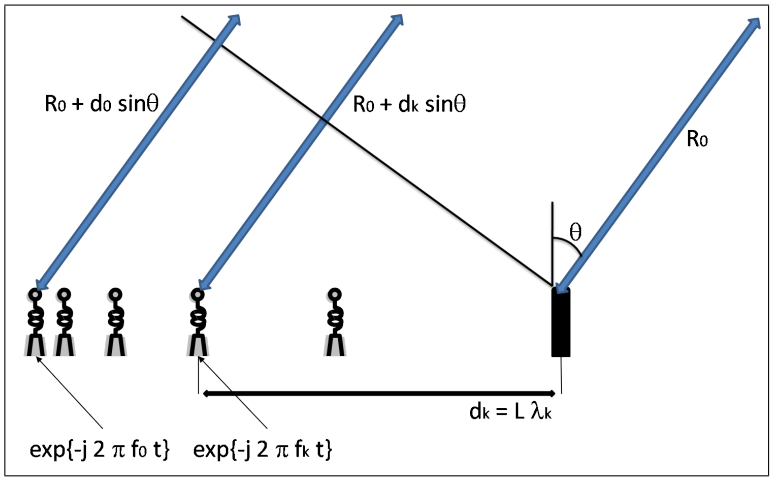

Figure 11.4: Frequency diverse array, pattern with range attenuation

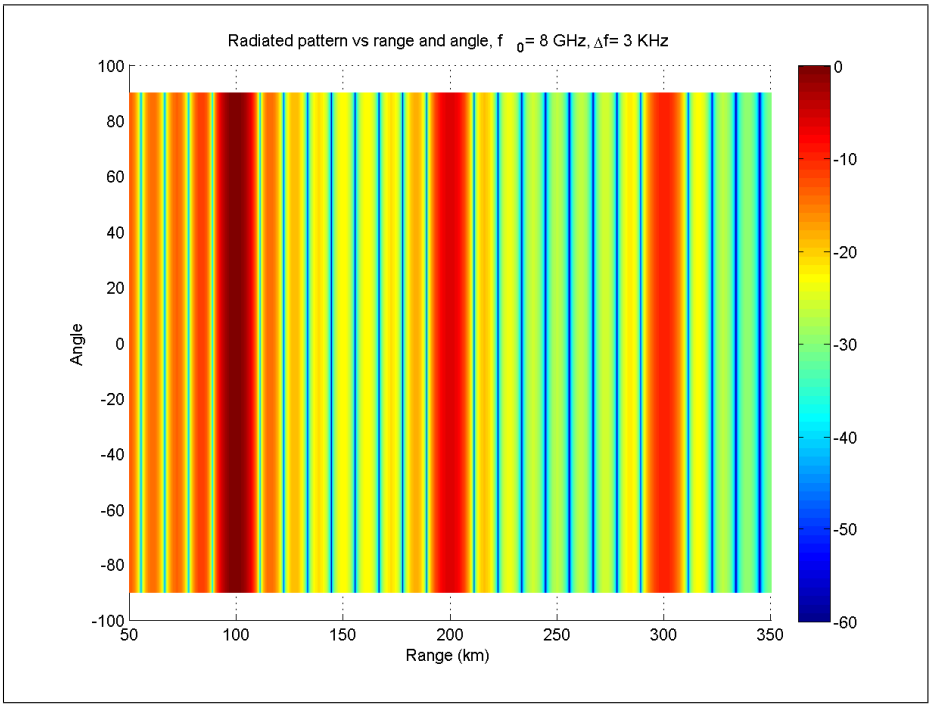

Figure 11.5: Wavelength array, pattern with range attenuation

(*ii*) As in the previous case, as the amplitude is function of time, this pattern slides in time across the ranges and the propagation velocity of the carrier;

(*iii*) L is a necessary additional parameter to achieve feasible distances between elements: in fact without L, the effective distance between two consecutive antennas would be equal to $\lambda_{k-1} - \lambda_k = \lambda_{k-1}\frac{\Delta f}{f_k} \approx 14$ nm!!

11.3 The Frequency Diverse Bistatic System

Starting from a wavelength array, we now consider L such that the wavelength array is actually feasible. For this purpose, assuming Δs the minimum feasible spacing between the antenna elements and

$$\Delta\lambda_{\min} = \min_k \{\lambda_{k-1} - \lambda_k\} = \lambda_{N-2} - \lambda_{N-1} \tag{11.10}$$

the minimum difference between two consecutive wavelengths, we write

$$L\Delta\lambda_{\min} \geq \Delta s, \tag{11.11}$$

which gives the requirement on the minimum L, i.e.

$$L \geq \frac{\Delta s}{\Delta\lambda_{\min}}. \tag{11.12}$$

For instance, let one set

$$\Delta s = \frac{1}{2}\lambda_{N-1} \tag{11.13}$$

in the rest of this Chapter.

After this assumption, the following considerations are required:

(*i*) The reference point is far $L\lambda_{N-1}$ from the closest element of the array. When equations (11.10), (11.12) and (11.13) apply, it can be demonstrated that the minimum distance D_L from the transmitting antenna and the reference point is

$$D_L \geq \frac{1}{2}\frac{f_{N-2}}{f_{N-1}}\frac{c}{\Delta f} \approx \frac{c}{2\Delta f}, \tag{11.14}$$

i.e. the receiver cannot be placed from the transmitter less than half the distance between two peaks (in the one-way pattern). Applying the numbers in this paper, $L \geq 1.33 \cdot 10^6$ and $D_L \geq 50$ km. For instance $L = 1.33 \cdot 10^6$ and $D_L = 50$ km are assumed.

(*ii*) Despite the high value of L, the spacing $\Delta d_k = L\,(\lambda_k - \lambda_{k+1})$ between two consecutive elements of the active array is in fact constant and equal to Δs. In other words, the difference $\Delta^2 d_k$ between the spacing of two consecutive active elements of the array is negligible. For instance, here $\Delta^2 d_k \approx 7.2$ nm.

(*iii*) From the previous two points, it is clear that the WA can be simplified into a standard array of antennas where each element is fed with a slight different carrier frequency. This is in fact a FDA. At an adequate distance from the active array, the so-termed reference point, it is possible to observe range-constant-periodic patterns. The reference point can be tens of kilometers far away from the active array, according to equation (11.14).

The reference geometry, then, has now to be reconsidered as in Figure 11.6. Whereas the distance between the FDA and the reference point is relevant, the angle under which the target is seen cannot be considered constant, the pattern in equation (11.8) should be rearranged according to the latter geometry. In particular, taking into account this geometry, the following can be demonstrated:

$$d_k = R_k - R_0 = L\lambda_k \frac{\cos\theta_2 - \cos\theta_1}{\sin(\theta_1 - \theta_2)}, \tag{11.15}$$

and

$$\begin{aligned} R_k = &\sqrt{R_0^2 + L^2\lambda_k^2 + 2L\lambda_k R_0 \sin\theta_2} \approx \\ \approx &\sqrt{R_0^2 + L^2\lambda_{N-1}^2 + 2L\lambda_{N-1} R_0 \sin\theta_2} = \hat{R}(L, \theta_2). \end{aligned} \tag{11.16}$$

The pattern p_{FDBS} of a FDBS can be therefore written as

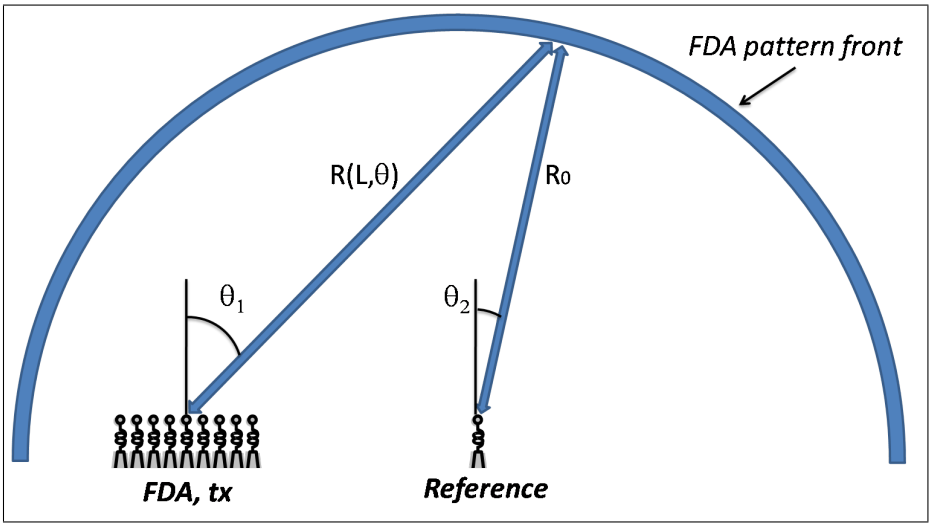

Figure 11.6: Frequency Diverse Bistatic System with an omnidirectional receiver

$$p_{FDBS}(f,t,R_0,\theta_1,\theta_2) = \frac{1}{R_0}\sum_{k=0}^{N-1}\frac{1}{R_k}\exp\left\{-j2\pi\left(f_k t - \frac{R_k + R_0}{\lambda_k}\right)\right\}. \quad (11.17)$$

Introducing equations (11.15) and (11.16) respectively in the phase and attenuation part of equation (11.17), the pattern p_{FDBS} can be written as

$$p_{FDBS}(f,t,R_0,\theta_1,\theta 2) \approx \frac{\exp\{j\Phi_3\}}{\hat{R}(L,\theta_2)R_0}\frac{\sin\left(N\pi\Delta f\left(t-\frac{2R_0}{c}\right)\right)}{\sin\left(\pi\Delta f\left(t-\frac{2R_0}{c}\right)\right)}, \quad (11.18)$$

where

$$\Phi_3 = -2\pi L\frac{\cos\theta_2 - \cos\theta_1}{\sin(\theta_1-\theta_2)} - 2\pi f_c\left(t-\frac{2R_0}{c}\right). \quad (11.19)$$

An immediate application of this concept consists in placing a passive phased array in the reference point. The overall pattern is the product of the 2-way FDBS pattern shown in Figure 11.7 with the typical passive phased array pattern in reception (Figure 11.8). The resulting pattern is reported

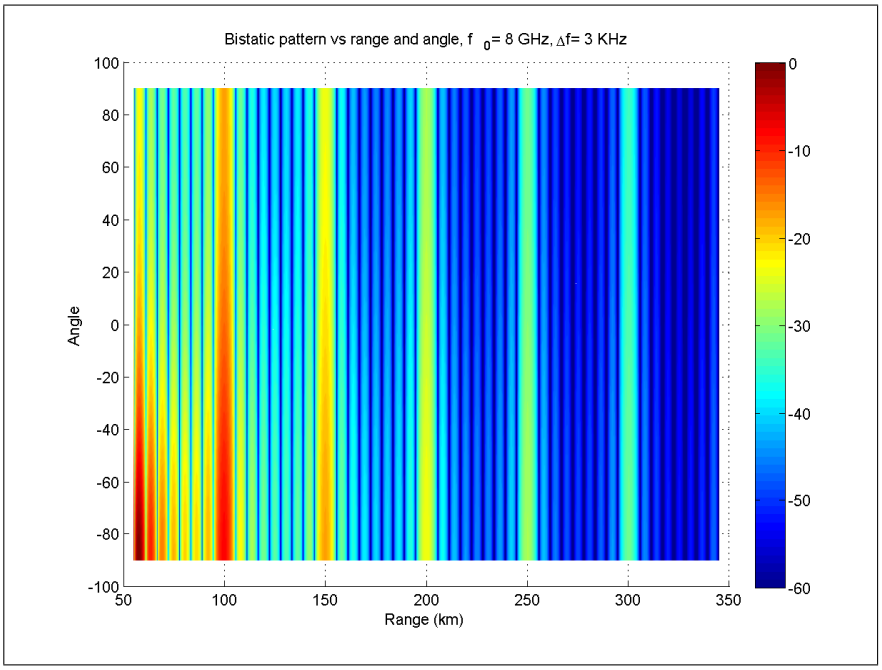

Figure 11.7: Frequency diverse bistatic system, normalized (2-way) pattern with range attenuation

in Figure 11.9 (where a 9-element passive phased array pointing at 0° has been considered in reception). Although this pattern exhibits asymmetrical peak-to-sidelobes levels in range and angle, especially evident for lower distances, it is clear that, instantly, most of the energy is concentrated in limited areas in range and angle. It is important to highlight clearly that, whilst at each angle the peak appears at specific ranges, the gain at each range varies in angle due to the difference in paths, as it can be inferred from Figure 11.6. This explains why the sidelobes in Figure 11.9 are much higher at $-90°$ than at $-20°$.

11.4 Windowing

As in standard arrays of antennas, windowing allows to modify the peak-to-sidelobe ratio, trading off on the resolution (in angle and range in this case). Figure 11.10 shows the pattern of a FDBS after the application

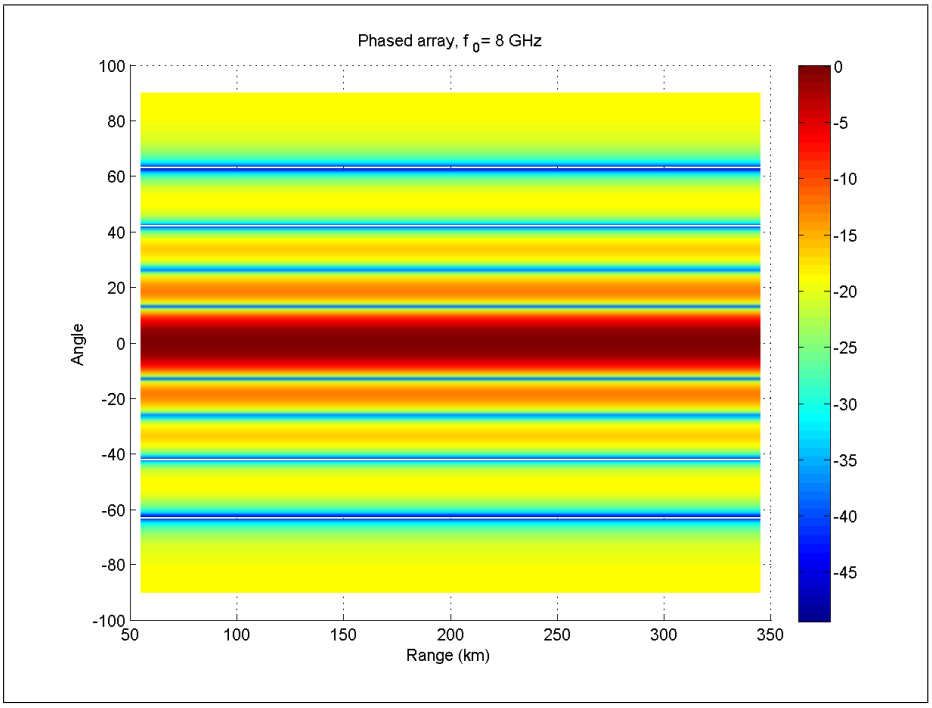

Figure 11.8: Phased array, pattern with range attenuation

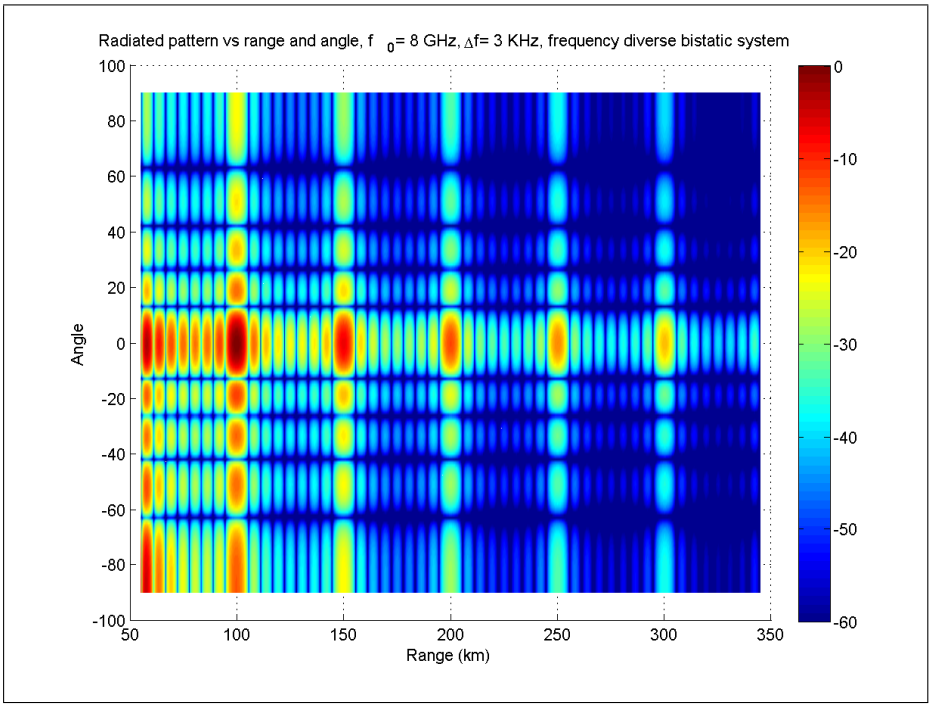

Figure 11.9: Pattern of a FDBS with an passive ESA

of a hann window in tx and rx. If compared to Figure 11.9, where no windowing is applied, it is here shown that the windowing enlarge the beamwidth not only in angle (rx), as in standard ESA, but also in range (tx). As a result, it is here shown that the $-90°$ sidelobes, which are highest in Figure 11.9 due to the reduced range attenuation, have been taken into control. However, it has to be pointed out that asymmetrical sidelobes are still present. This is clear observing, for instance, the pattern at 100 km.

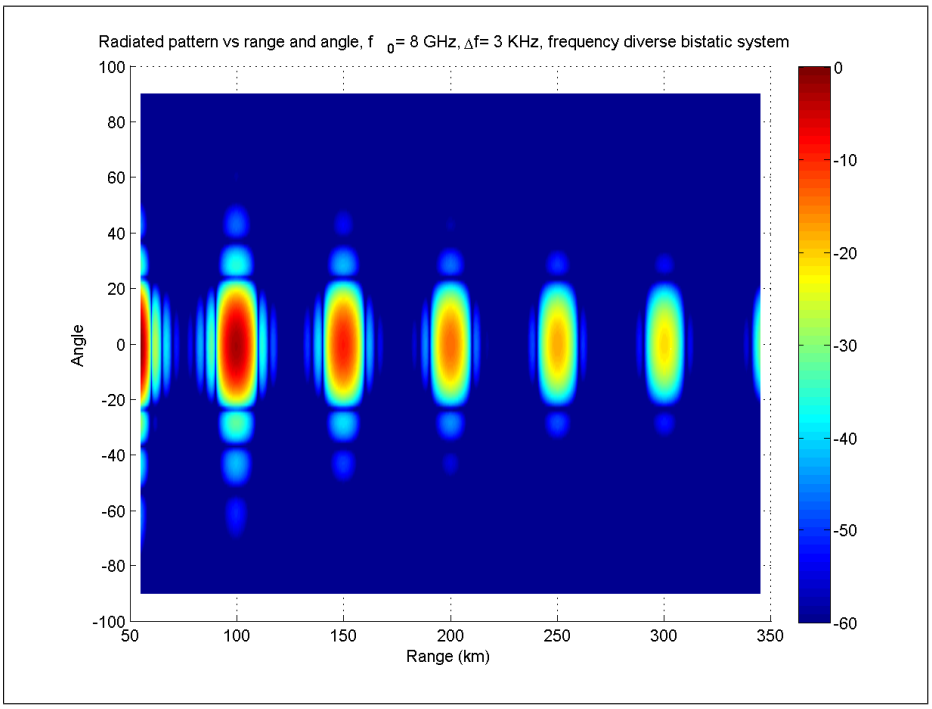

Figure 11.10: Pattern after applying a hann window in tx and rx, FDBS

11.5 Non-linear Frequency Shift

In this Section the application of non-linear frequency shifts to the active elements of the transmitting FDA is investigated. This allows to modify further the shape of the range beam, making possible to shift or reduce sidelobes. For instance, here the effects of applying frequency shifts which are no longer constant are examined. In particular these have been made

equal to $k\Delta f$, with $k = 0, 1, 2, \ldots 7, 9$. In other words, whilst the first 8 shifts are the same as in the previous case, the last one differs by an additional Δf.

Figure 11.11 shows the normalized pattern at $\theta_2 = 0^\circ$ of the beams formed with linear and non-linear shifts in blue and red respectively. It stands out clearly that the effect of the non-linear shift does not affect the mainlobe, as the signals are designed to cohere in that location, but produces different sidelobes at different positions. In this particular case it has to be pointed out that this configuration 'transforms' the nulls in the original pattern in sidelobes and viceversa.

As a means of quantitative comparison between these two patterns, the ISLR (Integrated SideLobe Ratio) is considered. This number is here evaluated by integrating the power of the sidelobes up to a the distance of $\frac{c}{4\Delta f}$ on the left and on the right of each peak and dividing it for the power of the mainlobe. The ISLR of the linear frequency spacing is ≈ -18.6 dB, whilst in the non-linear frequency spacing it is ≈ -13.8 dB. As a consequence there is an increase this ratio. However, the point of this shifting is not to decrease the ISLR but to provide the radar designer with an additional potential extra degree of control.

Further modifications to the frequency shift can lead to a pattern as in Figure 11.12. The pattern shown has been achieved applying to a FDBS (with an omnidirectional receiver) a linear shift equal to (0, 2, 4, 6, 8, 1, 3, 5, 7) Δf. The most evident drawback here is clearly that the linearity of the pattern across the same range, as in Figure 11.7, is lost. However this plot shows that nulls in range and angle can be created through this technique. The issue now concerns the best way of applying frequency shifts so to control in full the placement of the nulls.

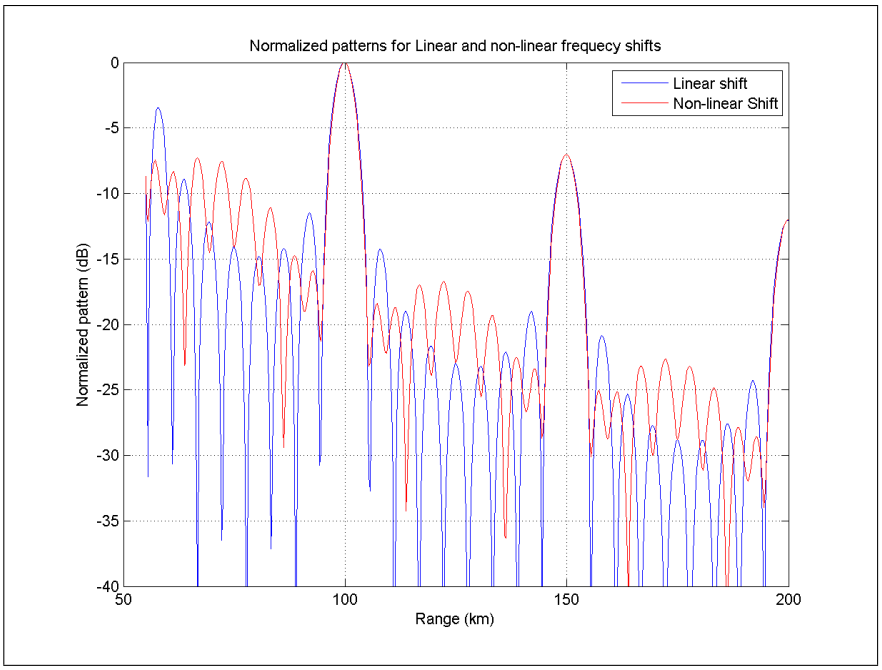

Figure 11.11: Comparison of main and sidelobes for linear and non-linear shifts

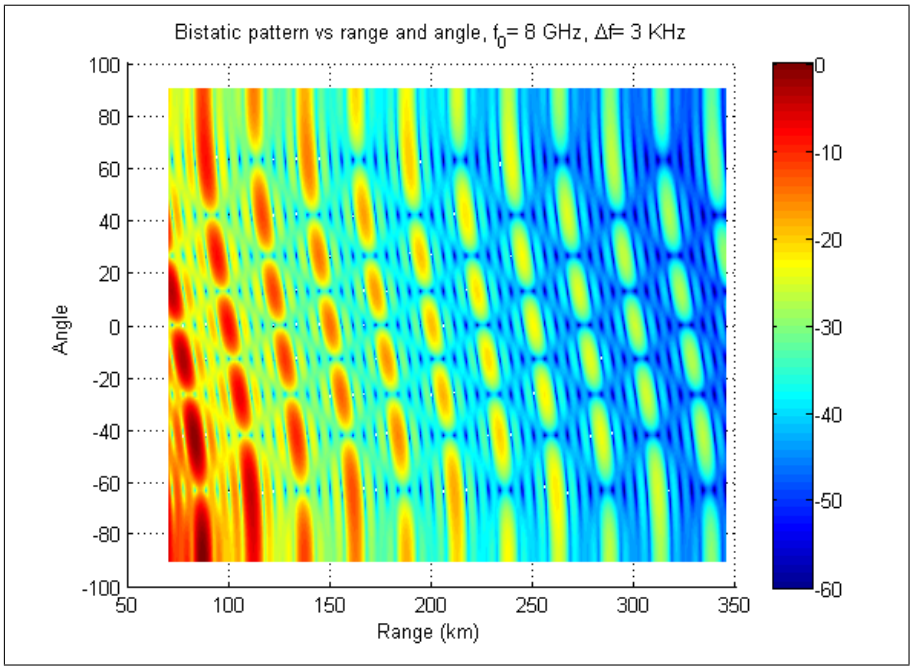

Figure 11.12: Additional example of the effects of non-linear frequency shift, FDBS

Chapter 12

Summary and conclusions

In this work a number of radar systems have been presented and compared under different scenarios. The main aim was to investigate the effects of spatial diversity together with distributing the energy and information processing in ways other than that of a conventional monostatic system.

In Chapter 2 background on MIMO radar and netted radars systems was introduced. It is important to highlight, once again, that in recent literature two kinds of MIMO are being developed. One exploits angular diversity to improve performance in terms of detection, parameters estimation, velocity and DOA, classification, etc. The other exploits waveform diversity over a conventional array of antennas to achieve a sharper beam through a synthetic array bigger than the original. Both these concepts require extra complexity (e.g. extra hardware, tight synchronization, appropriate waveform design) when compared to conventional monostatic systems or ESAs (Electronically Steered Arrays). However, the benefits to costs ratio can be profitable for specific applications, such as multiperspective classification, low-RCS target detection, through-the-wall sensing (angular diversity) or uniform illumination with multibeam in receive (waveform diversity). In Chapter 3 a description of the basic concepts of radar systems has been introduced. The information presented is a starting point to understand the basic concepts of the investigation of the rest of this work.

In Chapter 4 particular attention was focused on the processing approaches when data are collected from a radar network. In particular, systems exploiting angular (or spatial) diversity have been called NR, RPNR, MIMO and DRN. The differences between these systems lie in either the coherency in processing the data or the presence of a central collector of all the data. In addition, two additional cases have been examined to provide an insight of the effects of exchanging angular diversity with frequency diversity. These have been termed the Frequency MIMO and the Frequency Diverse Array. In Chapters 5 and 6 it has been shown that, given the limitations of the cases considered here that the MIMO and DRN provide a good compromise between a fully coherent system and the monostatic radar when noise only and noise and clutter are considered. They both have superior detection performance to (not-re-phased) NR. This is due to the fact that, since the phases of the incoming signals are totally uncorrelated, the coherent sum is statistically a disruptive event. This result has been confirmed also in other Chapters of this thesis (e.g. 7 and 10). On the contrary, for fully coherent systems (RPNR), the extra complexity required for re-aligning the phases to gain a factor L (where L is the number of summed signals) in SNR is difficult to implement, especially when the systems are working over broad frequency bandwidths and have high carrier frequencies. This has been confirmed not only for noise-like targets, such as the Swerling-modelled ones, but also for targets with a constant amplitude and random phase, as in the case of the sphere. In general terms, a loss of only few dB in terms of SNR has been observed, compared to the RPNR. A decentralized approach has also been shown to have a simplest structure of detector with moderate losses in SNR. Nonetheless, one of the greatest assets of this system is to allow an increased tolerance to jamming. Comparisons with the Frequency MIMO concept have shown that the exploitation of spatial diversity and frequency diversity leads to similar results for deterministic and fully random targets. This is not always the case in a practical scenario. It is important to highlight that in generic terms there is not a valid rule for deciding a-priori which kind of diversity has overall the greatest benefits. As it can be expected, this is strongly

dependent on the proposed application. For instance, whilst the angular diversity can be applied effectively to low-RCS target detection, frequency diversity can provide significant improvements in high-cluttered areas as it decorrelates the clutter samples. A quick comparison of the results of these Chapters show that just a few netted devices can provide an improvement on monostatic systems. This is a significant result as it means that it is possible to improve the sensing power keeping the complexity of the entire system moderate. In Chapter 7 it has been shown that the coverage of MIMO and DRN systems is roughly the same as a monostatic system, with the coherent systems providing, once again, the lower and upper limit.

Experiments have been carried to provide additional and practical knowledge on multistatic systems. At the same time the aim was to validate some of the assumptions made in evaluating the performance. Chapter 8 shows the setup of the experiment. In particular data were collected using UCL's radar network comprised of 2 transmitters and 3 receivers. Although the limitations of this system (reduced transmitted power, broad antenna beams, single waveform in transmission, direct feed of the antennas), the collected data allowed to analyze a number of characteristics of the RCS of the clutter and the target in multistatic systems. Multistatic correlation of target and clutter (Chapter 9) has been reported as a function of the different paths. It is important to highlight that this kind of study has not been investigated in literature so far. For this purpose, complex data, amplitude and phase correlations were analyzed to have a better insight. Particular attention was dedicated to the analysis of symmetrical paths as they should return the same signals and therefore any difference between these channels can be exploited as an indicator of issues in the network. Clutter PDFs have been reported as well. In this case the clutter was expected to have a Rayleigh-distributed amplitude, as most of the ground clutter. This has been confirmed by most of the plots reported. Nonetheless, it has been shown that for one node out of six the Gaussian behaviour was not matched. This provides a background for future research, as it has been shown that multistatic characteristics

cannot easily be predicted and this is a key point if radar networks are to be employed to maximize the gathered information.

Chapter 10 shows two possible ways of locating a target using the multistatic data acquired. The first method used a graphical approach summing on a screen all the gathered signals according to the strategies discussed in the performance analysis (i.e. NR, RPNR, spatial MIMO and DRN). Once again, similarities to the performance results have been shown: NR is the worst, RPNR is the best and the two incoherent approaches perform in the middle. In particular it has to be pointed out that whilst the MIMO approach keeps a degree of uncertainty in the position of the target, the DRN performs better. However, a visual approach to localization has not to be preferred in most of the applications where the target's position has to be tracked automatically. In addition, this approach does not allow to have a clear understanding of the movement of the target, as the Figures of the target position at the beginning and the end of the acquisition prove. As a consequence, a numerical method has been developed. After extracting the range-Doppler information from all the nodes, the position of the target and its velocity have been evaluated with a significant increase in performance. Actually, notwithstanding the ambiguity in range and Doppler measurements, the behaviour of the proposed algorithm for localizing and estimating the DOA and the velocity of the target has been shown to dramatically improve even coarse resolutions, achieving an accuracy below a tenth of the nominal. An additional benefit of merging numerically the multi-angle observations is in the extra information provided on the Doppler frequency. With spatially-different measurements of the Doppler it has been possible to reconstruct the full vector of the velocity of a target, whilst it is well known that with a monostatic case the only possible measurement is on the radial velocity.

Finally, in Chapter 11 an alternative way of beamforming has been presented. The results shown here differ from those in the rest of this work. Actually, whilst throughout this thesis the main aim was to investigate the effects of mismatching significantly (in either space or frequency) the

signals from/to each antenna, in this Chapter an insight on the potential of applying moderate alterations to the signals is reported. The results shown are a brand new topic of investigation which is progressively attracting the interest of the technical community. In this Chapter, after introducing the FDA, the FDBS has been developed, together with some immediate improvements. In particular, the use of non-linear frequency shifts has been demonstrated to allow the radar designer with an additional degree of freedom. Although only the CW case has been studied, the potential of generating (using a pulsed version of the FDBS) a pattern 'orthogonal' to that of a standard ESA is not only interesting for the development of LPI (Low Probability of Intercept) radars in range, but also for other applications such as controlling or at least mitigating echoes from unwanted ranges, as in low-grazing angle multipath.

In conclusion it has been shown that introducing a degree of diversity into radar systems enhances the performance and provides with new potential. This is true not only when devices are separated in space but also when a frequency diversity is applied. Most of the results obtained through real data processing are a starting point to further research to be developed. In addition, e.g. for localization, it has been shown that an appropriate processing of all the collected information can provide a result which is extremely more accurate than those of the single devices. In a second stage the data fusion can be extended to a full tracking algorithm and to multiangle classification. However, if full data have to be exchanged for allowing a joint processing and subsequently extracting as much information as possible, a tight cooperation between the devices of a radar network is required. This is still an issue as the synchronization schedules and communication channels are to be extremely robust and reliable.

Bibliography

[1] M.I. Skolnik, *Introduction to Radar Systems*, McGraw Hill, 1981.

[2] N. Levanon and E. Mozeson, *Radar Signals*, John Wiley & Sons, 2004.

[3] G. Picardi, *Elaborazione del segnale radar*, Franco Angeli, 2000.

[4] N. J. Willis, *Bistatic Radar*, SciTech Publishing, 2005.

[5] M. Cherniakov, *Bistatic Radars: Emerging Technology*, John Wiley & Sons, 2008.

[6] D.J. MacKay, *Information Theory, Inference and Learning Algorithms*, Cambridge University Press, 2003.

[7] S.M. Kay, *Fundamentals of Statistical Signal Processing: Estimation Theory*, Prentice Hall, 1993.

[8] S.M. Kay, *Fundamentals of Statistical Signal Processing: Detection Theory*, Prentice Hall, 1998.

[9] R.J.A. Tough K.D. Ward and S. Watts, *Sea Clutter: Scattering, The K Distribution And Radar Performance*, Institution of Engineering and Technology, April 2006.

[10] J.B. Billingsley, *Low-angle Radar Land Clutter*, Institution of Engineering and Technology, 2002.

[11] R.J.A. Tough, C.J. Baker, and J.M. Pink, "Radar performance in a maritime environment: single hit detection in the presence of multipath fading and non-Rayleigh sea clutter", *Radar and Signal Processing, IEE Proceedings*, vol. 137, no. 1, pp. 33–40, Feb 1990.

[12] A. Farina, F. Gini, M.V. Greco, and P. Lombardo, "Coherent radar detection of targets against a combination of K-distributed and gaussian clutter", *Radar Conference, 1995., Record of the IEEE 1995 International*, pp. 83–88, 8-11 May 1995.

[13] T. Bucciarelli, P. Lombardo, and S. Tamburrini, "Optimum CFAR detection against correlated K-distributed clutter", *Signals, Systems, and Electronics, 1995. ISSSE '95, Proceedings., 1995 URSI International Symposium on*, pp. 191–194, 25-27 Oct 1995.

[14] A. Farina and P. Lombardo, "Modelling of a mixture of K-distributed and gaussian clutter for coherent radar detection", *Electronics Letters*, vol. 30, no. 6, pp. 520–521, 17 Mar 1994.

[15] F. Gini, A. Farina, and M.V. Greco, "Detection of multidimensional Gaussian random signals in compound-Gaussian clutter plus thermal noise", *Signal Processing Proceedings, 1998. ICSP '98. 1998 Fourth International Conference on*, vol. 2, pp. 1650–1653 vol.2, 1998.

[16] P. Lombardo, D. Pastina, and T. Bucciarelli, "CFAR coherent radar detection against K-distributed clutter plus thermal noise", *Radar Conference, 1998. RADARCON 98. Proceedings of the 1998 IEEE*, pp. 129–134, 11-14 May 1998.

[17] S.D. Himonas and M. Barkat, "Adaptive CFAR detection in partially correlated clutter", *Radar and Signal Processing, IEE Proceedings*, vol. 137, no. 5, pp. 387–394, Oct 1990.

[18] C.J. Baker, "K-distributed coherent sea clutter", *Radar and Signal Processing, IEE Proceedings*, vol. 138, no. 2, pp. 89–92, Apr 1991.

[19] K.D. Ward, C.J. Baker, and S. Watts, "Maritime surveillance radar. I. radar scattering from the ocean surface", *Radar and Signal Processing, IEE Proceedings*, vol. 137, no. 2, pp. 51–62, Apr 1990.

[20] S. Watts, C.J. Baker, and K.D. Ward, "Maritime surveillance radar. II. detection performance prediction in sea clutter", *Radar and Signal Processing, IEE Proceedings F*, vol. 137, no. 2, pp. 63–72, Apr 1990.

[21] T. Hair, T. Lee, and C.J. Baker, "Statistical properties of multifrequency high-range-resolution sea reflections", *Radar and Signal Processing, IEE Proceedings F*, vol. 138, no. 2, pp. 75–79, Apr 1991.

[22] M.S. Greco and M.W. Long, "Sea and ground radar clutter modeling", Tutorial, Radarcon08, May, Rome, Italy 2008.

[23] E.J. Kelly, "Performance of an adaptive detection algorithm; rejection of unwanted signals", *Aerospace and Electronic Systems, IEEE Transactions on*, vol. 25, no. 2, pp. 122–133, Mar 1989.

[24] E.J. Kelly, "An adaptive detection algorithm", *Aerospace and Electronic Systems, IEEE Transactions on*, vol. AES-22, no. 2, pp. 115–127, March 1986.

[25] F.C. Robey, D.R. Fuhrmann, E.J. Kelly, and R. Nitzberg, "A CFAR adaptive matched filter detector", *Aerospace and Electronic Systems, IEEE Transactions on*, vol. 28, no. 1, pp. 208–216, Jan 1992.

[26] P. Monticciolo, E.J. Kelly, and J.G. Porakis, "A noncoherent adaptive detection technique", *Aerospace and Electronic Systems, IEEE Transactions on*, vol. 28, no. 1, pp. 115–124, Jan 1992.

[27] V.G. Hansen, "Constant false-alarm rate processing in search radars", *IEE 1973 International Radar Conference. Proceedings of*, pp. 325–332, 23-25 October 1973.

[28] M. Schwartz, "A coincidence procedure for signal detection", *Information Theory, IEEE Transactions on*, vol. 2, no. 4, pp. 135–139, Dec 1956.

[29] V.S. Chernyak, "Effective simplified decentralized target detection in multisensor systems", *Information Fusion. Proceedings of the Third International Conference on*, vol. 2, 10-13 July 2000.

[30] H.A. Khan, Y. Zhang, C. Ji, C.J. Stevens, D.J. Edwards, and D. O'Brien, "Optimizing polyphase sequences for orthogonal netted radar", *IEEE Signal Processing Letters*, vol. 13, no. 10, pp. 589–592, October 2006.

[31] H. Deng, "Polyphase code design for orthogonal netted radar systems", *Signal Processing, IEEE Transactions on*, vol. 52, no. 11, pp. 3126Ű3135, 2004.

[32] T. Johnsen, K. E. Olsen, S. Johnsrud, and R. Skjerpeng, "Simultaneous use of multiple pseudo random noise codes in multistatic cw radar", *the IEEE Radar Conference, Proceedings of*, 2004.

[33] E. Hanle, "Distance considerations for multistatic radar", *International Radar Conference*, pp. 100–105, Arlington, VA, April 28-30 1980.

[34] F. Verrazzani L. Gini, F. Lombardini, "Robust monoparametric multiradar CFAR detection againstnon-gaussian spiky clutter", in *Radar, Sonar and Navigation, IEE Proceedings*, Jun 1997, vol. 144.

[35] A. Farina and E. Hanle, "Position accuracy in netted monostatic and bistatic radar", *Aerospace and Electronic Systems, IEEE Transactions on*, vol. AES-19, no. 4, pp. 513–520, July 1983.

[36] C.J. Baker and A.L. Hume, "Netted radar sensing", *Aerospace and Electronic Systems Magazine, IEEE*, vol. 18, no. 2, pp. 3–6, Feb 2003.

[37] S. Miranda, C. Baker, K. Woodbridge, and H. Griffiths, "Knowledge-based resource management for multifunction radar: a look at scheduling and task prioritization", *Signal Processing Magazine, IEEE*, vol. 23, no. 1, pp. 66–76, Jan. 2006.

[38] S.L.C. Miranda, C.J. Baker, K. Woodbridge, and H.D. Griffiths, "Fuzzy logic approach for prioritisation of radar tasks and sectors

of surveillance in multifunction radar", *Radar, Sonar & Navigation, IET*, vol. 1, no. 2, pp. 131–141, April 2007.

[39] T.E. Derham, S. Doughty, K. Woodbridge, and C.J. Baker, "Design and evaluation of a low-cost multistatic netted radar system", *Radar, Sonar & Navigation, IET*, vol. 1, no. 5, pp. 362–368, October 2007.

[40] Y. Teng, H.D. Griffiths, C.J. Baker, and K. Woodbridge, "Netted radar sensitivity and ambiguity", *Radar, Sonar & Navigation, IET*, vol. 1, no. 6, pp. 479–486, Dec. 2007.

[41] N.D. Sidiropoulos A.B. Gershman, *Space-Time Processing for MIMO Communications*, John Wiley & Sons, 2005.

[42] W.G. Scanlon and K. Ziricastro, "Modelling of MIMO channels for the populated indoor environment", *MIMO: Communications Systems from Concept to Implementations, IEE Seminar on*, 12 Dec. 2001.

[43] K.I. Ziricastro, W.G. Scanlon, and N.E. Evans, "Prediction of variation in MIMO channel capacity for the populated indoor environment using a radar cross-section-based pedestrian model", *Wireless Communications, IEEE Transactions on*, vol. 4, no. 3, pp. 1186–1194, May 2005.

[44] Jeng-Shiann Jiang and M.A. Ingram, "Distributed source model for short-range MIMO", *Vehicular Technology Conference, 2003. VTC 2003-Fall. 2003 IEEE 58th*, vol. 1, pp. 357–362, 6-9 Oct. 2003.

[45] R. Venkataramani and Y. Bresler, "Multiple-input multiple-output sampling: necessary density conditions", *Information Theory, IEEE Transactions on*, vol. 50, no. 8, pp. 1754–1768, Aug. 2004.

[46] Hao Xu, D. Chizhik, H. Huang, and R. Valenzuela, "A generalized space-time multiple-input multiple-output (MIMO) channel model", *Wireless Communications, IEEE Transactions on*, vol. 3, no. 3, pp. 966–975, May 2004.

[47] G. Latsoudas and N.D. Sidiropoulos, "A hybrid probabilistic data association-sphere decoding detector for multiple-input-multiple-output systems", *Signal Processing Letters, IEEE*, vol. 12, no. 4, pp. 309–312, April 2005.

[48] A. Zanella, M. Chiani, and M.Z. Win, "MMSE reception and successive interference cancellation for MIMO systems with high spectral efficiency", *Wireless Communications, IEEE Transactions on*, vol. 4, no. 3, pp. 1244–1253, May 2005.

[49] P. Uthansakul and M.E. Bialkowski, "Multipath signal effect on the capacity of MIMO, MIMO-OFDM and spread MIMO-OFDM", *Microwaves, Radar and Wireless Communications, 2004. MIKON-2004. 15th International Conference on*, vol. 3, pp. 989–992, 17-19 May 2004.

[50] Y. Wang, M.I. Rahman, and S.S. Das, "Evaluation of mu-mimo based access techniques with fairness consideration", *2008 Annual IEEE Conference*, pp. 1–5, 15-26 Feb. 2008.

[51] S. Venkatesan, A. Lozano, and R. Valenzuela, "Network MIMO: Overcoming intercell interference in indoor wireless systems", *Signals, Systems and Computers, 2007. ACSSC 2007. Conference Record of the Forty-First Asilomar Conference on*, pp. 83–87, 4-7 Nov. 2007.

[52] S. Kozlowski, Y. Yashchyshyn, and J. Modelski, "Phased array antennas in MIMO receiver", *Microwaves, Radar & Wireless Communications, 2006. MIKON 2006. International Conference on*, pp. 473–476, 22-24 May 2006.

[53] E. Fishler, A. Haimovich, R. Blum, D. Chizhik, L. Cimini, and R. Valenzuela, "MIMO radar: an idea whose time has come", *Radar Conference, 2004. Proceedings of the IEEE*, pp. 71–78, 26-29 April 2004.

[54] E. Fishler, A. Haimovich, R. Blum, R. Cimini, D. Chizhik, and R. Valenzuela, "Performance of MIMO radar systems: advantages of angular diversity", *Signals, Systems and Computers, 2004. Conference*

Record of the Thirty-Eighth Asilomar Conference on, vol. 1, pp. 305–309, 7-10 Nov. 2004.

[55] E. Fishler, A. Haimovich, R.S. Blum, Jr. Cimini, L.J., D. Chizhik, and R.A. Valenzuela, "Spatial diversity in radars-models and detection performance", *Signal Processing, IEEE Transactions on [see also Acoustics, Speech, and Signal Processing, IEEE Transactions on]*, vol. 54, no. 3, pp. 823–838, March 2006.

[56] K.W. Forsythe, D.W. Bliss, and G.S. Fawcett, "Multiple-input multiple-output (MIMO) radar: performance issues", *Signals, Systems and Computers, 2004. Conference Record of the Thirty-Eighth Asilomar Conference on*, vol. 1, pp. 310–315, 7-10 Nov. 2004.

[57] A.M. Haimovich, R.S. Blum, and L.J. Cimini, "MIMO radar with widely separated antennas", *Signal Processing Magazine, IEEE*, vol. 25, no. 1, pp. 116–129, 2008.

[58] Nikolaus H. Lehmann, Alexander M. Haimovich, Rick S. Blum, and Len Cimini, "High resolution capabilities of MIMO radar", *Signals, Systems and Computers, 2006. ACSSC '06. Fortieth Asilomar Conference on*, pp. 25–30, Oct.-Nov. 2006.

[59] H.A. Khan, W.Q. Malik, D.J. Edwards, and C.J. Stevens, "Ultra wideband multiple-input multiple-output radar", *Radar Conference, 2005 IEEE International*, pp. 900–904, 9-12 May 2005.

[60] H.A. Khan and D.J. Edwards, "Doppler problems in orthogonal MIMO radars", *Radar, 2006 IEEE Conference on*, 24-27 April 2006.

[61] J. Li and P. Stoica, *MIMO radar signal processing*, John Wiley & Sons, 2008.

[62] D.W. Bliss and K.W. Forsythe, "Multiple-input multiple-output (MIMO) radar and imaging: degrees of freedom and resolution", *Signals, Systems and Computers, 2003. Conference Record of the Thirty-Seventh Asilomar Conference on*, vol. 1, pp. 54–59, 9-12 Nov. 2003.

[63] P. Bidigare, "MIMO capacity of radar as a communication channel", *Adaptive Sensor and Array Processing Workshop*, 11-13 March 2003.

[64] A. De Maio and M. Lops, "Design principles of MIMO radar detectors", *Aerospace and Electronic Systems, IEEE Transactions on*, vol. 43, no. 3, pp. 886–898, July 2007.

[65] D.J. Rabideau and P. Parker, "Ubiquitous MIMO multifunction digital array radar", *Signals, Systems and Computers, 2003. Conference Record of the Thirty-Seventh Asilomar Conference on*, vol. 1, pp. 1057–1064, 9-12 Nov. 2003.

[66] G. San Antonio and D.R. Fuhrmann, "Beampattern synthesis for wideband MIMO radar systems", *Computational Advances in Multi-Sensor Adaptive Processing, 2005 1st IEEE International Workshop on*, pp. 105–108, 13-15 Dec. 2005.

[67] F.C. Robey, S. Coutts, D. Weikle, J.C. McHarg, and K. Cuomo, "MIMO radar theory and experimental results", *Signals, Systems and Computers, 2004. Conference Record of the Thirty-Eighth Asilomar Conference on*, vol. 1, pp. 300–304, 7-10 Nov. 2004.

[68] D.R. Fuhrmann and G.S. Antonio, "Transmit beamforming for MIMO radar systems using partial signal correlation", *Signals, Systems and Computers, 2004. Conference Record of the Thirty-Eighth Asilomar Conference on*, vol. 1, pp. 295–299, 7-10 Nov. 2004.

[69] J. Li and P. Stoica, "Mimo radar with colocated antennas: Review of some recent work", *Signal Processing Magazine, IEEE*, vol. 24, no. 5, pp. 106–114, Sept. 2007.

[70] J. R. Guerci, M. C. Wicks, J. S. Bergin, P. M. Techau, and S. U. Pillai, "Theory and application of optimum and adaptive mimo radar", *Radarcon 2008. Conference Record of*, 26-30 May 2008.

[71] A. Farina, *Antenna-based signal processing techniques for radar systems*, Artech House, 1992.

[72] K.S. Kulpa and Z. Czekala, "Masking effect and its removal in PCL radar", *IEE Proceedings on Radar, Sonar and Navigation*, vol. 152, no. 3, pp. 174–178, 3 June 2005.

[73] R. Klemm and J. Ward, "Stap I – Architectures and algorithms", Tutorial Radarcon08, Rome, Italy, 26 May 2008.

[74] S. Goldstein and M. Picciolo, "Stap II – Advanced concepts", Tutorial Radarcon08, Rome, Italy, 26 May 2008.

[75] D.K. Barton, *Frequency Agility and Diversity*, Artech House, 1977.

[76] P. Antonik, M.C. Wicks, H.D. Griffiths, and C.J. Baker, "Frequency diverse array radars", *Radar, 2006 IEEE Conference on*, April 2006.

[77] M. Secmen, S. Demir, A. Hizal, and T. Eker, "Frequency diverse array antenna with periodic time modulated pattern in range and angle", *Radar Conference, 2007 IEEE*, pp. 427–430, April 2007.

[78] P. Antonik, M.C. Wicks, H.D. Griffiths, and C.J. Baker, "Multi-mission multi-mode waveform diversity", *Radar, 2006 IEEE Conference on*, April 2006.

[79] J. Farooq, M.A. Temple, and M.A. Saville, "Application of frequency diverse arrays to synthetic aperture radar imaging", *Electromagnetics in Advanced Applications, 2007. ICEAA 2007. International Conference on*, pp. 447–449, Sept. 2007.

[80] P. Baizert, T.B. Hale, M.A. Temple, and M.C. Wicks, "Forward-looking radar gmti benefits using a linear frequency diverse array", *Electronics Letters*, vol. 42, no. 22, pp. 1311–1312, 26 2006.

[81] P.F. Sammartino and C.J. Baker, "Frequency diverse array radars", Tech. Rep., SEA, Aug 2006.

[82] A. Papoulis, *Probability and Statistics*, Prentice Hall, 1990.